

Sílvia V. Conde · Rodrigo Iturriaga
Rodrigo del Rio · Estelle Gauda
Emília C. Monteiro *Editors*

Arterial Chemoreceptors

Mal(adaptive) Responses: O₂ Dependent and
Independent Mechanisms

Advances in Experimental Medicine and Biology

Volume 1427

Series Editors

Wim E. Crusio, Institut de Neurosciences Cognitives et Intégratives
d'Aquitaine, CNRS and University of Bordeaux, Pessac Cedex, France
Haidong Dong, Departments of Urology and Immunology, Mayo Clinic,
Rochester, MN, USA

Heinfried H. Radeke, Institute of Pharmacology and Toxicology,
Clinic of the Goethe University Frankfurt Main, Frankfurt am
Main, Hessen, Germany

Nima Rezaei, Research Center for Immunodeficiencies, Children's Medical
Center, Tehran University of Medical Sciences, Tehran, Iran

Ortrud Steinlein, Institute of Human Genetics, LMU University Hospital,
Munich, Germany

Junjie Xiao, Cardiac Regeneration and Ageing Lab, Institute of
Cardiovascular Sciences, School of Life Science, Shanghai University,
Shanghai, China

Advances in Experimental Medicine and Biology provides a platform for scientific contributions in the main disciplines of the biomedicine and the life sciences. This series publishes thematic volumes on contemporary research in the areas of microbiology, immunology, neurosciences, biochemistry, biomedical engineering, genetics, physiology, and cancer research. Covering emerging topics and techniques in basic and clinical science, it brings together clinicians and researchers from various fields.

Advances in Experimental Medicine and Biology has been publishing exceptional works in the field for over 40 years, and is indexed in SCOPUS, Medline (PubMed), EMBASE, BIOSIS, Reaxys, EMBiology, the Chemical Abstracts Service (CAS), and Pathway Studio.


2021 Impact Factor: 3.650 (no longer indexed in SCIE as of 2022).

Sílvia V. Conde • Rodrigo Iturriaga
Rodrigo del Rio • Estelle Gauda
Emília C. Monteiro
Editors


Arterial Chemoreceptors

Mal(adaptive) Responses: O₂
Dependent and Independent
Mechanisms

Editors

Sílvia V. Conde 
iNOVA4Health, NOVA Medical School
Faculdade de Ciências Médicas
Universidade Nova de Lisboa
Lisboa, Portugal

Rodrigo del Rio 
Departamento de Fisiología
Pontificia Universidad Católica de Chile
Santiago, Chile

Emília C. Monteiro 
NOVA Medical School, Faculdade de
Ciências Médicas
Universidade Nova de Lisboa
Lisboa, Portugal

Rodrigo Iturriaga 
Departamento de Fisiología
Universidad Católica de Chile
Santiago, Chile

Estelle Gauda
Division of Neonatology
Hospital for Sick Children
Toronto, ON, Canada

ISSN 0065-2598 ISSN 2214-8019 (electronic)
Advances in Experimental Medicine and Biology
ISBN 978-3-031-32370-6 ISBN 978-3-031-32371-3 (eBook)
<https://doi.org/10.1007/978-3-031-32371-3>

© The Editor(s) (if applicable) and The Author(s), under exclusive license to Springer Nature Switzerland AG 2023

This work is subject to copyright. All rights are solely and exclusively licensed by the Publisher, whether the whole or part of the material is concerned, specifically the rights of translation, reprinting, reuse of illustrations, recitation, broadcasting, reproduction on microfilms or in any other physical way, and transmission or information storage and retrieval, electronic adaptation, computer software, or by similar or dissimilar methodology now known or hereafter developed. The use of general descriptive names, registered names, trademarks, service marks, etc. in this publication does not imply, even in the absence of a specific statement, that such names are exempt from the relevant protective laws and regulations and therefore free for general use.

The publisher, the authors, and the editors are safe to assume that the advice and information in this book are believed to be true and accurate at the date of publication. Neither the publisher nor the authors or the editors give a warranty, expressed or implied, with respect to the material contained herein or for any errors or omissions that may have been made. The publisher remains neutral with regard to jurisdictional claims in published maps and institutional affiliations.

This Springer imprint is published by the registered company Springer Nature Switzerland AG
The registered company address is: Gewerbestrasse 11, 6330 Cham, Switzerland

Preface

This book continues the long tradition of leaving a written memory of each International Society of Arterial Chemoreception (ISAC) meeting. Recording part of the science presented at ISAC meetings in specific Proceedings Books for the purpose began at the II ISAC meeting held at Oxford in 1966 (Arterial Chemoreceptors, edited by R.W. Torrance, Blackwell Scientific Publications, 1968) and ran uninterrupted until the last meeting, ISAC XXI held at Nova Medical School, Universidade Nova de Lisboa, Portugal, from June 27 to 30, 2022.

The common denominator of these 21 meetings is obviously not only the quality of the science but also the success of its model, which brings together the world's leading experts in the field with PhD and post-doc students in a small-scale meeting (normally <200) with enough time for networking, benchmarking and to build relationships and new partnerships.

Despite this common denominator, all meetings are unique. The XXI ISAC meeting goes down in history for being postponed from 2020 to 2022 due to the pandemic, COVID-19, the infection by the SARS-CoV-2 virus. The aftermath of the pandemic still limited the participation of researchers from several countries. However, these circumstances created the opportunity to be preceded by a successful, one-day remote Kickoff Meeting on June 28, 2021, where three ISAC "Science in Pandemics" awards were given to the following young investigators: 1st – Ryan J Rokoczy (USA); 2nd – Lenise J. Kim (USA); Honorable Mention – Igor S.A. Felipe (New Zealand). Moreover, the experience in the use of remote communication platforms gained during the pandemics allowed extending the poster session in the XXI ISAC Meeting to participants who were not in person at the meeting. However, and despite XXI ISAC having been a hybrid event, the in-person participation of scientists in the field was remarkable, with an event with almost 100 people. Even more notable was the presence of a large community of young scientists, highlighting not only the growing interest in this field of research but also the enormous work that has been done by some researchers in promoting this field.

We would like to give our greatest thanks to Joana Sacramento, Fátima Martins, Bernardete Melo, Adriana Capucho, Dinis Pires and Joana Fernandes from Sílvia Conde's group for their amazing contributions to the organization in this unparalleled context. Teresa Bastos Lopes was definitive in managing

all the interaction with the Medical School, the attendees, the logistics and travel arrangements. Thanks, Teresa, for your unconditional assistance. A special thanks also to George Kim the ISAC website manager for his patience with the organizers.

Our thanks also go to everyone who, committed with the development of research, accepted the challenge of traveling to Lisbon in an early post-pandemic phase.

The introduction and welcome session paid tribute to the contributions of Chris Peers (1963–2018, Leeds, UK) and Robert Fitzgerald (1932–2022, Baltimore, USA) to the physiology of the carotid body.

The XXI ISAC meeting was organized around the topic (Mal)Adaptive responses of peripheral chemoreceptors: O₂ dependent and independent mechanisms. We had the privilege of a keynote lecture by Professor J. A. Ribeiro (Lisbon, Portugal, chairman of the VIII ISAC meeting in 1985) in the opening session. He framed the contributions of Portuguese researchers over time to the knowledge of arterial chemoreceptors. He highlighted the pioneering works of the histologist Celestino da Costa (1939–1940) in the designation of the carotid body as *metaneurogonia* and his subsequent personal contributions to the Physiology and Pharmacology of the carotid body as well as the recent work from Portuguese institutions in the field.

On the first day, there were three plenary sessions on carotid body and sleep apnea by Nanduri Prabhakar (Chicago, USA); adaptive responses to chronic intermittent hypoxia: contributions from the European Sleep Apnea Cohort (ESADA) by Maria Bonsignore (Palermo, Italy); and carotid body and inflammation: implications for anti-inflammatory reflex and chemosensory potentiation induced by sustained and intermittent hypoxia by Rodrigo Iturriaga (Santiago, Chile).

The following days were organized around symposia starting with invited lectures and followed by short oral presentations. Poster sessions were organized in the afternoons. The symposia were about chronic intermittent hypoxia and cardiorespiratory and metabolic dysfunction; chronic hypoxia and cancer; (mal)adaptive responses of chemoreceptor function; chemoreceptor function in the early life; and carotid body sensing and transduction. The invited speakers included Seva Polotsky (Baltimore, USA), Vincent Joseph (Quebec, Canada), Benedito Machado (São Paulo, Brazil), Claire Arnaud (Grenoble, France), Isaac Almendros (Barcelona, Spain), Rodrigo Del Rio (Santiago, Chile), Julian Paton (Auckland, New Zealand), Eduardo Colombari (São Paulo, Brazil), Ken O'Halloran (Cork, Ireland), Estelle Gauda (Toronto, Canada), Richard Kinkead (Quebec, Canada), José López-Barneo (Sevilha, Spain), Colin Nurse (Hamilton, Canada). Congratulations to all invited speakers for your outstanding science and thanks for sharing your achievements face-to-face with us and for the lively and fruitful discussions throughout the meeting.

The meeting was not possible without the generous sponsorship of Cambridge Electronics Design Limited; Oxford Optronics; Caltecnica/

Controltecnica; SICGEN Antibodies; FIDELIDADE; EGEAC; Águas de Portugal; FinePrint; Turismo de Lisboa; *Journal of Physiology*; Luso-American Development Foundation; and NOVA Medical School. We are extremely grateful to them.

Lisboa, Portugal

Silvia V. Conde

Lisboa, Portugal

Emilia C. Monteiro

Contents

1	Transcriptomics of the Carotid Body	1
	Audrys G. Pauza, David Murphy, and Julian F. R. Paton	
2	The Adult Carotid Body: A Germinal Niche at the Service of Physiology	13
	Ricardo Pardal	
3	Evidences That Sympathetic Overactivity and Neurogenic Hypertension Correlate with Changes in the Respiratory Pattern in Rodent Models of Experimental Hypoxia	23
	Benedito H. Machado	
4	Control of Arterial Hypertension by the AhR Blocker CH-223191: A Chronopharmacological Study in Chronic Intermittent Hypoxia Conditions	35
	António B. Pimpão, Cátia Sousa, Maria J. Correia, Nuno R. Coelho, Emília C. Monteiro, Antonio F. Melo Junior, and Sofia A. Pereira	
5	Three Days of Chronic Intermittent Hypoxia Induce β_1-Adrenoceptor Dependent Increases in Left Ventricular Contractility	43
	Anthony L. Marullo, Eric F. Lucking, Daniel Pender, Pardeep Dhaliwal, and Ken D. O'Halloran	
6	The Beneficial Effect of the Blockade of Stim-Activated TRPC-ORAI Channels on Vascular Remodeling and Pulmonary Hypertension Induced by Intermittent Hypoxia Is Independent of Oxidative Stress	53
	Rodrigo Iturriaga and Sebastián Castillo-Galán	
7	Intermittent Hypoxia and Weight Loss: Insights into the Etiology of the Sleep Apnea Phenotype	61
	Marianne Gagnon, Stéphanie Fournier, François Marcouiller, Loralie Guay, Vincent Joseph, Natalie J. Michael, and Richard Kinkead	

8	Effects of Gestational Intermittent Hypoxia on Placental Morphology and Fetal Development in a Murine Model of Sleep Apnea	73
	Esther Valverde-Pérez, Jesús Prieto-Lloret, Elvira Gonzalez-Obeso, María I. Cabero, Maria L. Nieto, Marta I. Pablos, Ana Obeso, Angela Gomez-Niño, Rosa M. Cárdbaba-García, Asunción Rocher, and Elena Olea	
9	Ventilatory Effects of Acute Intermittent Hypoxia in Conscious Dystrophic Mice	83
	Michael N. Maxwell, Anthony L. Marullo, Aoife D. Slyne, Eric F. Lucking, and Ken D. O'Halloran	
10	Intermittent Hypoxia and Diet-Induced Obesity on the Intestinal Wall Morphology in a Murine Model of Sleep Apnea	89
	Esther Valverde-Pérez, Elena Olea, Ana Obeso, Jesús Prieto-Lloret, Asunción Rocher, and Elvira Gonzalez-Obeso	
11	Enhanced Peripheral Chemoreflex Drive Is Associated with Cardiorespiratory Disorders in Mice with Coronary Heart Disease	99
	Liena Bravo, Katherin V. Pereyra, Hugo S. Diaz, Mariajosé Flores, Karla G. Schwarz, Camilo Toledo, Esteban Díaz-Jara, Leticia González, Marcelo E. Andia, and Rodrigo Del Rio	
12	Role of Peripheral Chemoreceptors on Enhanced Central Chemoreflex Drive in Nonischemic Heart Failure	107
	Katherin Pereyra, Esteban Díaz-Jara, Paulina Arias, Liena Bravo, Camilo Toledo, Karla Schwarz, and Rodrigo Del Rio	
13	Effect of Carotid Body Denervation on Systemic Endothelial Function in a Diabetic Animal Model	115
	Marlene D. Cabral, Fátima O. Martins, Inês B. Martins, Bernardete F. Melo, Joana F. Sacramento, Silvia V. Conde, and Jesus Prieto-Lloret	
14	Contribution of Carotid Bodies on Pulmonary Function During Normoxia and Acute Hypoxia	127
	Karla G. Schwarz, Maríajose Flores, Nicolas Voituron, and Rodrigo Del Rio	
15	Increased Abdominal Perimeter Differently Affects Respiratory Function in Men and Women	135
	Joana F. Sacramento, Iolanda Caires, Maria P. Guarino, Maria J. Ribeiro, João C. P. Santiago, Ana T. Timóteo, Mafalda Selas, Miguel Mota-Carmo, and Silvia V. Conde	

16 Carotid Body Resection Prevents Short-Term Spatial Memory Decline in Prediabetic Rats Without Changing Insulin Signaling in the Hippocampus and Prefrontal Cortex.	143
Adriana M. Capucho, Ana Chegão, Fátima O. Martins, Bernardete F. Melo, Natália Madeira, Joana F. Sacramento, Rosalina Fonseca, Hugo Vicente Miranda, and Sílvia V. Conde	
17 Constitutive Expression of Hif2α Confers Acute O₂ Sensitivity to Carotid Body Glomus Cells.	153
Olalla Colinas, Alejandro Moreno-Domínguez, Patricia Ortega-Sáenz, and José López-Barneo	
18 Of Mice and Men and Plethysmography Systems: Does LKB1 Determine the Set Point of Carotid Body Chemosensitivity and the Hypoxic Ventilatory Response?	163
A. Mark Evans	
19 Analyzing Angiotensin II Receptor Type 1 Clustering in PC12 Cells in Response to Hypoxia Using Direct Stochastic Optical Reconstruction Microscopy (dSTORM)	175
Hayyaf S. Aldossary, Daniel J. Nieves, Deirdre M. Kavanagh, Dylan Owen, Clare J. Ray, Prem Kumar, Andrew M. Coney, and Andrew P. Holmes	
20 The Carotid Body “Tripartite Synapse”: Role of Gliotransmission	185
Erin M. Leonard and Colin A. Nurse	
21 Carotid Body-Mediated Chemoreflex Function in Aging and the Role of Receptor-Interacting Protein Kinase	195
Esteban Díaz-Jara, Karla G. Schwarz, Angelica Ríos-Gallardo, Camilo Toledo, Julio A. Alcayaga, Felipe A. Court, and Rodrigo Del Rio	
22 Chronic Metformin Administration Does Not Alter Carotid Sinus Nerve Activity in Control Rats	203
Joana F. Sacramento, Bernardete F. Melo, Jesus Prieto-Lloret, and Silvia V. Conde	
Concluding Remarks	209

Contributors

Julio A. Alcayaga Laboratorio de Fisiología Celular, Facultad de Ciencias, Universidad de Chile, Santiago, Chile

Hayyaf S. Aldossary School of Biomedical Sciences, Institute of Clinical Sciences, University of Birmingham, Birmingham, UK
College of Medicine, Basic Medical Sciences, King Saud bin Abdulaziz University for Health Sciences, Riyadh, Saudi Arabia

Marcelo E. Andia Radiology Department & ANID – Millennium Institute for Intelligent Healthcare Engineering – iHEALTH, Pontificia Universidad Católica de Chile, Santiago, Chile

Paulina Arias Laboratory of Cardiorespiratory Control, Pontificia Universidad Católica de Chile, Santiago, Chile

Liena Bravo Laboratory of Cardiorespiratory Control, Pontificia Universidad Católica de Chile, Santiago, Chile

María I. Cabero Instituto de Biomedicina y Genética Molecular (IBGM), UVa-CSIC, Valladolid, Spain

Marlene D. Cabral NOVA Medical School|Faculdade de Ciências Médicas, NMSIFCM, Universidade Nova de Lisboa, Lisboa, Portugal

Iolanda Caires NOVA Medical School|Faculdade de Ciências Médicas, NMSIFCM, Universidade Nova de Lisboa, Lisboa, Portugal

Adriana M. Capucho iNOVA4Health, NOVA Medical School, Faculdade de Ciências Médicas, Universidade Nova de Lisboa, Lisboa, Portugal

Rosa M. Cárdaba-García Departamento de Enfermería, Grupo de Investigación en Cuidados Enfermeros (GICE), Facultad de Enfermería, Universidad de Valladolid, Valladolid, Spain

Sebastián Castillo-Galán Lab Neurobiología, Facultad de Ciencias Biológicas, Pontificia Universidad Católica de Chile, Santiago, Chile
Laboratory of Nano-Regenerative Medicine, Centro de Investigación e Innovación Biomédica (CIIB), Faculty of Medicine, Universidad de los Andes, Santiago, Chile

IMPACT, Center of Interventional Medicine for Precision and Advanced Cellular Therapy, Santiago, Chile

Ana Chegão iNOVA4Health, NOVA Medical School, Faculdade de Ciências Médicas, Universidade Nova de Lisboa, Lisboa, Portugal

Nuno R. Coelho iNOVA4Health, NOVA Medical School, Faculdade de Ciências Médicas, NMS, FCM, Universidade Nova de Lisboa, Lisboa, Portugal

Egas Moniz Center for Interdisciplinary Research, Egas Moniz School of Health and Science, Caparica, Portugal

Olalla Colinas Instituto de Biomedicina de Sevilla (IBiS), Hospital Universitario Virgen del Rocío/CSIC/Universidad de Sevilla, Seville, Spain
Departamento de Fisiología Médica y Biofísica, Facultad de Medicina, Universidad de Sevilla, Seville, Spain

Centro de Investigación Biomédica en Red sobre Enfermedades Neurodegenerativas (CIBERNED), Madrid, Spain

Silvia V. Conde iNOVA4Health, NOVA Medical School, Faculdade de Ciências Médicas, Universidade NOVA de Lisboa, Lisbon, Portugal

Andrew M. Coney School of Biomedical Sciences, Institute of Clinical Sciences, University of Birmingham, Birmingham, UK

Maria J. Correia iNOVA4Health, NOVA Medical School, Faculdade de Ciências Médicas, NMS, FCM, Universidade Nova de Lisboa, Lisboa, Portugal

Felipe A. Court Center for Integrative Biology, Faculty of Sciences, Universidad Mayor, Santiago, Chile

FONDAP Geroscience Center for Brain Health and Metabolism, Santiago, Chile

Buck Institute for Research on Aging, Novato, CA, USA

Rodrigo Del Rio Laboratory of Cardiorespiratory Control, Pontificia Universidad Católica de Chile, Santiago, Chile

Centro de Excelencia en Biomedicina de Magallanes (CEBIMA), Universidad de Magallanes, Punta Arenas, Chile

Pardeep Dhaliwal Department of Physiology, School of Medicine, College of Medicine & Health, University College Cork, Cork, Ireland

Hugo S. Diaz Laboratory of Cardiorespiratory Control, Pontificia Universidad Católica de Chile, Santiago, Chile

Esteban Díaz-Jara Laboratory of Cardiorespiratory Control, Pontificia Universidad Católica de Chile, Santiago, Chile

A. Mark Evans Centre for Discovery Brain Sciences, Hugh Robson Building, University of Edinburgh, Edinburgh, UK

Mariajosé Flores Laboratory of Cardiorespiratory Control, Pontificia Universidad Católica de Chile, Santiago, Chile

Rosalina Fonseca iNOVA4Health, NOVA Medical School, Faculdade de Ciências Médicas, Universidade Nova de Lisboa, Lisboa, Portugal

Stéphanie Fournier Centre de Recherche de l'Institut Universitaire de Cardiologie et Pneumologie de Québec, Québec City, QC, Canada

Marianne Gagnon Centre de Recherche de l'Institut Universitaire de Cardiologie et Pneumologie de Québec, Québec City, QC, Canada
Faculty of Pharmacy, Université Laval, Québec City, QC, Canada

Angela Gomez-Niño Instituto de Biomedicina y Genética Molecular (IBGM), UVa-CSIC, Valladolid, Spain
Departamento de Biología Celular, Genética, Histología y Farmacología, Universidad de Valladolid, Valladolid, Spain

Leticia González Radiology Department & ANID – Millennium Institute for Intelligent Healthcare Engineering – iHEALTH, Pontificia Universidad Católica de Chile, Santiago, Chile

Elvira Gonzalez-Obeso Instituto de Biomedicina y Genética Molecular (IBGM), UVa-CSIC, Valladolid, Spain
Servicio de Anatomía Patológica, Hospital Clínico Universitario de Valladolid, Valladolid, Spain

Maria P. Guarino ciTechCare, Escola Superior de Saúde de Leiria, Instituto Politécnico de Leiria, Leiria, Portugal

Loralie Guay Centre de Recherche de l'Institut Universitaire de Cardiologie et Pneumologie de Québec, Québec City, QC, Canada

Andrew P. Holmes School of Biomedical Sciences, Institute of Clinical Sciences, University of Birmingham, Birmingham, UK

Rodrigo Iturriaga Facultad de Ciencias Biológicas, Pontificia Universidad Católica de Chile, Santiago, Chile
Centro de Investigación en Fisiología y Medicina de Altura (FIMEDALT), Facultad de Ciencias de la Salud, Universidad de Antofagasta, Antofagasta, Chile

Vincent Joseph Faculty of Pharmacy, Université Laval, Québec City, QC, Canada
Department of Pediatrics, Faculty of Medicine, Université Laval, Québec City, QC, Canada

Deirdre M. Kavanagh Micron Bioimaging Facility, University of Oxford, Oxford, UK

Richard Kinkead Faculty of Pharmacy, Université Laval, Québec City, QC, Canada
Department of Pediatrics, Faculty of Medicine, Université Laval, Québec City, QC, Canada

Prem Kumar School of Biomedical Sciences, Institute of Clinical Sciences, University of Birmingham, Birmingham, UK

Erin M. Leonard Department of Biology, Wilfrid Laurier University, Waterloo, Canada

José López-Barneo Instituto de Biomedicina de Sevilla (IBiS), Hospital Universitario Virgen del Rocío/CSIC/Universidad de Sevilla, Seville, Spain
Departamento de Fisiología Médica y Biofísica, Facultad de Medicina, Universidad de Sevilla, Seville, Spain
Centro de Investigación Biomédica en Red sobre Enfermedades Neurodegenerativas (CIBERNED), Madrid, Spain

Eric F. Lucking Department of Physiology, School of Medicine, College of Medicine & Health, University College Cork, Cork, Ireland

Benedito H. Machado Department of Physiology, School of Medicine of Ribeirão Preto, University of São Paulo, Ribeirão Preto, São Paulo, Brazil

Natalia Madeira iNOVA4Health, NOVA Medical School, Faculdade de Ciências Médicas, Universidade Nova de Lisboa, Lisboa, Portugal

François Marcouiller Centre de Recherche de l'Institut Universitaire de Cardiologie et Pneumologie de Québec, Québec City, QC, Canada

Fatima O. Martins iNOVA4Health, NOVA Medical School, Faculdade de Ciências Médicas, Universidade Nova de Lisboa, Lisboa, Portugal

Ines B. Martins iNOVA4Health, NOVA Medical School/Faculdade de Ciências Médicas, NMSIFCM, Universidade Nova de Lisboa, Lisboa, Portugal

Anthony L. Marullo Department of Physiology, School of Medicine, College of Medicine & Health, University College Cork, Cork, Ireland

Michael N. Maxwell Department of Physiology, School of Medicine, College of Medicine & Health, University College Cork, Cork, Ireland

António F. Melo Júnior iNOVA4Health, NOVA Medical School, Faculdade de Ciências Médicas, NMS, FCM, Universidade Nova de Lisboa, Lisboa, Portugal

Bernardete F. Melo iNOVA4Health NOVA Medical School/Faculdade de Ciências Médicas, NMSIFCM, Universidade Nova de Lisboa, Lisboa, Portugal

Natalie J. Michael Centre de Recherche de l'Institut Universitaire de Cardiologie et Pneumologie de Québec, Québec City, QC, Canada
Faculty of Pharmacy, Université Laval, Québec City, QC, Canada

Emilia C. Monteiro iNOVA4Health, NOVA Medical School, Faculdade de Ciências Médicas, NMS, FCM, Universidade Nova de Lisboa, Lisboa, Portugal

Alejandro Moreno-Domínguez Instituto de Biomedicina de Sevilla (IBiS), Hospital Universitario Virgen del Rocío/CSIC/Universidad de Sevilla, Seville, Spain
Departamento de Fisiología Médica y Biofísica, Facultad de Medicina, Universidad de Sevilla, Seville, Spain

Centro de Investigación Biomédica en Red sobre Enfermedades Neurodegenerativas (CIBERNED), Madrid, Spain

Miguel Mota-Carmo NOVA Medical School/Faculdade de Ciências Médicas, NMS/FCM, Universidade Nova de Lisboa, Lisbon, Portugal
Serviço de Cardiologia, Hospital Santa Marta, Centro Hospital Lisboa Central, EPE, Lisboa, Portugal

David Murphy Molecular Neuroendocrinology Research Group, Bristol Medical School, Translational Health Sciences, University of Bristol, Bristol, UK

Maria L. Nieto Instituto de Biomedicina y Genética Molecular (IBGM), UVa-CSIC, Valladolid, Spain

Daniel J. Nieves Institute of Immunology and Immunotherapy and Centre of Membrane Proteins and Receptors (COMPARE), University of Birmingham, Birmingham, UK

Colin A. Nurse Department of Biology, McMaster University, Hamilton, ON, Canada

Ken D. O'Halloran Department of Physiology, School of Medicine, College of Medicine & Health, University College Cork, Cork, Ireland

Ana Obeso Departamento de Bioquímica y Biología Molecular y Fisiología, Facultad de Medicina, Universidad de Valladolid, Valladolid, Spain
Instituto de Biomedicina y Genética Molecular (IBGM), UVa-CSIC, Valladolid, Spain

Elena Olea Instituto de Biomedicina y Genética Molecular (IBGM), UVa-CSIC, Valladolid, Spain
Departamento de Enfermería, Grupo de Investigación en Cuidados Enfermeros (GICE), Facultad de Enfermería, Universidad de Valladolid, Valladolid, Spain

Patricia Ortega-Sáenz Instituto de Biomedicina de Sevilla (IBiS), Hospital Universitario Virgen del Rocío/CSIC/Universidad de Sevilla, Seville, Spain
Departamento de Fisiología Médica y Biofísica, Facultad de Medicina, Universidad de Sevilla, Seville, Spain
Centro de Investigación Biomédica en Red sobre Enfermedades Neurodegenerativas (CIBERNED), Madrid, Spain

Dylan Owen School of Mathematics, University of Birmingham, Birmingham, UK

Marta I. Pablos Departamento de Bioquímica y Biología Molecular y Fisiología, Facultad de Medicina, Universidad de Valladolid, Valladolid, Spain

Ricardo Pardal Dpto. de Fisiología Médica y Biofísica, Instituto de Biomedicina de Sevilla (IBiS), Hospital Universitario Virgen del Rocío/CSIC/Universidad de Sevilla, Sevilla, Spain

Julian F. R. Paton Manaaki Manawa – The Centre for Heart Research, Department of Physiology, Faculty of Medical & Health Sciences, University of Auckland, Auckland, New Zealand

Audrys G. Pauza Manaaki Manawa – The Centre for Heart Research, Department of Physiology, Faculty of Medical & Health Sciences, University of Auckland, Auckland, New Zealand

Daniel Pender Department of Physiology, School of Medicine, College of Medicine & Health, University College Cork, Cork, Ireland

Sofia A. Pereira iNOVA4Health, NOVA Medical School, Faculdade de Ciências Médicas, NMS, FCM, Universidade Nova de Lisboa, Lisboa, Portugal

Katherin V. Pereyra Laboratory of Cardiorespiratory Control, Pontificia Universidad Católica de Chile, Santiago, Chile

António B. Pimpão iNOVA4Health, NOVA Medical School, Faculdade de Ciências Médicas, NMS, FCM, Universidade Nova de Lisboa, Lisboa, Portugal

Jesús Prieto-Lloret Departamento de Bioquímica y Biología Molecular y Fisiología, Facultad de Medicina, Universidad de Valladolid, Valladolid, Spain

Instituto de Biomedicina y Genética Molecular (IBGM), UVa-CSIC, Valladolid, Spain

NOVA Medical School/Faculdade de Ciências Médicas, NMS/FCM, Universidade Nova de Lisboa, Lisboa, Portugal

Clare J. Ray School of Biomedical Sciences, Institute of Clinical Sciences, University of Birmingham, Birmingham, UK

Maria J. Ribeiro iNOVA4Health, NOVA Medical School/Faculdade de Ciências Médicas, NMS/FCM, Universidade Nova de Lisboa, Lisboa, Portugal

Angelica Ríos-Gallardo Laboratory of Cardiorespiratory Control, Pontificia Universidad Católica de Chile, Santiago, Chile

Centro de Excelencia en Biomedicina de Magallanes (CEBIMA), Universidad de Magallanes, Punta Arenas, Chile

Asunción Rocher Departamento de Bioquímica y Biología Molecular y Fisiología, Facultad de Medicina, Universidad de Valladolid, Valladolid, Spain

Instituto de Biomedicina y Genética Molecular (IBGM), UVa-CSIC, Valladolid, Spain

Joana F. Sacramento iNOVA4Health, NOVA Medical School, Faculdade de Ciências Médicas, Universidade Nova de Lisboa, Lisboa, Portugal

João C. P. Santiago iNOVA4Health, NOVA Medical School/Faculdade de Ciências Médicas, NMS/FCM, Universidade Nova de Lisboa, Lisboa, Portugal

Karla G. Schwarz Laboratory of Cardiorespiratory Control, Pontificia Universidad Católica de Chile, Santiago, Chile

Mafalda Selas Serviço de Cardiologia, Hospital Santa Marta, Centro Hospital Lisboa Central, EPE, Lisbon, Portugal

Aoife D. Slyne Department of Physiology, School of Medicine, College of Medicine & Health, University College Cork, Cork, Ireland

Cátia Sousa iNOVA4Health, NOVA Medical School, Faculdade de Ciências Médicas, NMS, FCM, Universidade Nova de Lisboa, Lisboa, Portugal

Ana T. Timóteo NOVA Medical School/Faculdade de Ciências Médicas, NMS/FCM, Universidade Nova de Lisboa, Lisbon, Portugal
Serviço de Cardiologia, Hospital Santa Marta, Centro Hospital Lisboa Central, EPE, Lisbon, Portugal

Camilo Toledo Laboratory of Cardiorespiratory Control, Pontificia Universidad Católica de Chile, Santiago, Chile

Esther Valverde-Pérez Departamento de Bioquímica y Biología Molecular y Fisiología, Facultad de Medicina, Universidad de Valladolid, Valladolid, Spain
Instituto de Biomedicina y Genética Molecular (IBGM), UVa-CSIC, Valladolid, Spain

Hugo Vicente Miranda iNOVA4Health, NOVA Medical School, Faculdade de Ciências Médicas, Universidade Nova de Lisboa, Lisboa, Portugal

Nicolas Voituron Laboratoire Hypoxie & Poumon UMR INSERM U1272, Université Sorbonne Paris Nord, Paris, France



Transcriptomics of the Carotid Body

1

Audrys G. Pauza, David Murphy,
and Julian F. R. Paton

Abstract

The carotid body (CB) has emerged as a potential therapeutic target for treating sympathetically mediated cardiovascular, respiratory, and metabolic diseases. In adjunct to its classical role as an arterial O₂ sensor, the CB is a multimodal sensor activated by a range of stimuli in the circulation. However, consensus on how CB multimodality is achieved is lacking; even the best studied O₂-sensing appears to involve multiple convergent mechanisms. A strategy to understand multimodal sensing is to adopt a hypothesis-free, high-throughput transcriptomic approach. This has proven instrumental for understanding fundamental mechanisms of CB response to hypoxia and other stimulants, its developmental niche, cellular heterogeneity, laterality, and pathophysiological remodeling in disease states. Herein, we review this published work that reveals novel molecular mechanisms underpinning multimodal sensing

and reveals numerous gaps in knowledge that require experimental testing.

Keywords

RNA sequencing · Microarrays · Gene expression · Novel therapeutic targets · Sympathetic · Cardiovascular · Respiratory disease

1.1 Introduction

Transcriptomics refers to the study of biological systems where complexity is explored through the lens of gene expression. In its essence, transcriptomics is a set of methodologies designed to study the transcriptome, defined as the steady-state sum of all single-stranded RNA molecules within a biological system at any one time. An informational intermediate between genome and proteome, transcriptomics is central for understanding the environment-genome-communication and phenotypic plasticity that occurs in disease states.

The aim of this focused review is to summarize what is currently known about the carotid body (CB) transcriptome and to identify gaps in knowledge informed by these investigations. Although transcriptomics incorporates many different aspects of RNA biology, this chapter focuses solely on steady-state gene expression at the high-throughput (hundreds of genes at the time) scale.

A. G. Pauza (✉) · J. F. R. Paton
Manaaki Manawa – The Centre for Heart Research,
Department of Physiology, Faculty of Medical &
Health Sciences, University of Auckland,
Auckland, New Zealand
e-mail: audrys.pauza@auckland.ac.nz

D. Murphy
Molecular Neuroendocrinology Research Group,
Bristol Medical School, Translational Health
Sciences, University of Bristol, Bristol, UK

1.1.1 Notes of Caution

It is important to note that studying RNA is technically challenging and caution should be exercised when interpreting gene expression results.

- It has been shown that ~30% of variation in gene expression levels is strongly associated with the sample RNA quality where a high degree of RNA degradation can become the predominant source of differential gene expression between samples (Gallego Romero et al. 2014). For this, we draw attention to the RNA integrity number (RIN) (Schroeder et al. 2006). RIN is an effort to standardize RNA quality reporting where a single score is calculated based on 18S–28S ribosomal RNA (rRNA) subunit abundance ratio and the presence of small RNA species that rise in abundance as RNA decay progresses (Schroeder et al. 2006). RIN ranges from 0 to 10 where it represents completely degraded and intact RNA, respectively.
- Power to detect differential expression between samples scales depending on the number of biological replicates included in the study and the sequencing depth achieved in RNA-seq studies (Baccarella et al. 2018; Ching et al. 2014). Benchmarking indicates that a minimum of $n = 6$ biological replicates per experimental group are required to accurately detect large differences in expression, rising to $n \geq 12$ to identify differential expression for all fold changes (Ching et al. 2014; Schurch et al. 2016). This means that in underpowered studies, physiologically relevant but small deviations in gene expression may be missed. This is especially important in the context of investigating the functional significance of gene networks.
- Pioneering microarray studies have been largely replaced by the RNA-sequencing technology offering greater flexibility and scaling. Microarrays are limited by dependency on known, predefined nucleotide sequences. As genome annotations continue to develop, raw microarray data cannot be readily reanalyzed based on newer, updated iterations of the genome. Commercial microarrays consist of preset, well-characterized genes and may not include all critical genes involved in a systemic response under investigation. In practice, microarrays are less sensitive at detecting low-expression fold changes (Pauža et al. 2021; Zhao et al. 2014) and provide a relative measure of gene expression between samples that cannot be easily compared between experiments and platforms (Campain and Yang 2010; Tarca et al. 2006). For this, it is important to consider limitations associated with each technology the study is based on.
- Another critical consideration is the chemistry used to generate sequencing libraries. While a variety of methods are available, they all share a critical step to remove rRNA content making up >80% of the total RNA mass. This is achieved either by rRNA depletion or poly-A selection procedures. While rRNA depletion is attractive as it permits an analysis of all transcribed elements of the genome, it requires greater sequencing depth to achieve the same level of exonic coverage compared to poly-A selected libraries (Zhao et al. 2018). This is important to consider as detection of transcripts with low, class-dependent expression (Fig. 1.1b) may be missed in underpowered studies.
- Transcriptomics results can be heavily influenced by bioinformatic analysis that turns raw sequence/microarray data into differential expression results (Van den Berge et al. 2019). Esoteric at times, performance differences between bioinformatic tools may translate to discrepancies observed between studies (Schurch et al. 2016).

1.2 Overview of Carotid Body Transcriptomic Studies

Key studies describing the CB transcriptome are summarized in Table 1.1. Henceforth, studies are discussed in chronological order based on the technology employed.

A pioneering microarray study investigated the transcriptional CB response following 24-h exposure of 12-week-old C57BL/6J mice to hypoxia (10% O₂) (Ganforina et al. 2005). The

Table 1.1 Key studies describing the carotid body transcriptome

References	Sp	Samples; background	Technology	Data availability	Comparison
Ganfomina et al. (2005)	Mm	CB and AM; C57BL/6J $n = 1$; RIN = NA	Microarray	NA	CB response to 24-h exposure to hypoxic vs. normoxic conditions
Balbir et al. (2007)	Mm	CB; DBA/2J and A/J $n = 3$; RIN = NA	Microarray	Public. NCBI GEO: GSE5313	CB transcriptome comparison between hypoxia-susceptible vs. hypoxia-resistant mice strains
Gao et al. (2017)	Mm	CB, AM, SCG; C57/B6 ^{WT} $n = 1$; RIN ≥ 7.8	Microarray	Public. NCBI GEO: GSE99593	Transcriptomic comparison of three organs of common neural-crest origin
Fagerlund et al. (2010)	Hs	CB; $n = 5$; RIN ≥ 5.5 Patients underwent oncosurgery	Microarray	Upon request	Human CB analysis focusing on O ₂ -sensing and signaling genes
Mkrtchian et al. (2012)	Hs	Same as in Fagerlund et al. (2010)	Microarray	NA	Basal human of human CB cross-tissue and cross-species analysis
Chang et al. (2015)	Mm	CB and AM; C57BL/6J $n = 3$; RIN 7.2 avg	RNA-seq microarray	Public. NCBI GEO: GSE72166	CB vs. AM
Zhou et al. (2016)	Mm	CB; C57B16/J $n = 8$ cells	RNA-seq	Public. NCBI GEO: GSE76579	Basal transcriptome of isolated chemosensory glomus cells
Mkrtchian et al. (2020)	Rn	CB; $n = 5-10$ Sprague-Dawley RIN 6.2-7.5	RNA-seq	Upon request	Effects of DAMPs on CB transcriptome
Pauza et al. (2022)	Rn	CB; SHR and WKY $n = 12$; RIN ≥ 7	RNA-seq	Public. NCBI GEO: GSE178504	CB remodeling in hypertension
Mkrtchian et al. (2018)	Hs	CB; Ex vivo $n = 5$; RIN = NA	microRNA ready-to-use PCR human panel I + II	NA	Basal miRNA expression profile; miRNA transcriptional response to acute hypoxia ex vivo
Navarro-Guerrero et al. (2016)	Rn	CB neurospheres in vitro RIN = NA	Microarray	Public. NCBI GEO: GSE67429	Undifferentiated neurospheres vs. differentiated neurospheres

AM adrenal medulla, CB carotid body, DAMPs endogenous danger-associated molecular patterns, Hs Homo sapiens, Mm Mus musculus, NA not available, Rn Rattus norvegicus, SCG superior cervical ganglion, SD Sprague-Dawley, SHR spontaneously hypertensive rat, Sp species, WKY Wistar-Kyoto rat

CB gene expression profile obtained was compared to that of the adrenal medulla (AM) from matched samples to identify 800 transcripts uniquely expressed in the CB out of the 9286 transcripts detected in total. Seven hundred fifty-one CB genes were found to respond to reduced O₂ levels with significant expression change. Hypoxia led to transcriptional remodeling of K⁺ channels (*Kcnj8*, *Kcnk4*, *Kcnab1*) and activation of gene pathways linked to nucleotide

binding, encoding ribosomal proteins, and transferase activity. This study included a single biological replicate ($n = 1$) per tissue type in each group where bilateral CBs from five animals were pooled to obtain sufficient RNA yield required for the analysis. Notably, the integrity (quality) of the isolated CB RNA was not reported.

A second microarray study explored the differences in the CB transcriptomes between mice

displaying divergent responses to hypoxia, i.e., hypoxia-susceptible DBA/2J and hypoxia-resistant A/J mice (Balbir et al. 2007). 1361 genes were found differentially expressed between the strains with divergent expression mostly linked to ion channels (*Cacna1b*, *Cacna2d3*, *Kcnmb2*, *Scnn1b*, *Scn8a*, *Trpc5*, *Trpm2*), metabolism of neurotransmitters (*Th*, *Adm*), neurotransmitter receptors (*Agtr1*, *P2ry12*), transporters (*Slc18a1*, *Slc18a2*), and a chemosensor protein (*Hif1a*). The authors do not report the total number of detected transcripts. This study incorporated 3 replicates per group where each replicate corresponded to 2 bilateral CBs pooled from 17 to 21 animals. The quality of RNA used in the study was not reported (Balbir et al. 2007).

The latest microarray study performed in the C57/B6^{WT} background compared the transcriptomes of three TH containing organs: a classical chemosensor (CB), an endocrine gland (AM), and superior cervical ganglion (SCG) that all share common neural crest-derived developmental origin (Gao et al. 2017).¹ The study revealed CB to have a “signature metabolic profile.” For example, the expression of Hypoxia-inducible factor-2a (*Epas1*), NADH dehydrogenase (ubiquinone) 1 alpha subcomplex, 4-like 2 (*Ndufa4l2*), and pyruvate carboxylase (*Pcx*), genes critical for cellular respiration, was markedly higher in the CB compared to postganglionic SCG neurons. This study incorporated three biological replicates per group where each CB sample corresponded to bilateral CBs pooled from ten mice. The study reports to use high-integrity RNA samples (RIN ≥ 7.8) for microarray hybridization.

Further two microarray studies are invaluable for being the only high-throughput works describing human CB transcriptome, offering thus far unmatched translational perspective (Fagerlund et al. 2010; Mkrtchian et al. 2012). Both studies used RNA derived from the same five patients

that underwent unilateral neck surgery for cancer. Both studies identified ~13,500 expressed genes in total and reiterated the previous finding from animal models of a unique gene expression profile distinct from other tissue types. Comparison of the human CB transcriptome with that of the C57BL/6J and DBA/2J mice (Balbir et al. 2007; Ganfornina et al. 2005) revealed a similar pattern of expression between the species but also highlighted a number of important differences for genes encoding O₂-sensing proteins (*NOX2*, *CTH*, *CBS*, *PRKAA1*, *EPAS1*, *NOS1*) and K⁺ channels (Kv1.1, Kv3.3, Kv4.1, Kv4.2, Kv4.3, TREK-1, TASK-1). Likely related to challenges of obtaining CB clinical samples, the authors report that RNA used to hybridize microarrays exhibited a degree of degradation (RIN ≥ 5.5) likely impacting the result reported. RNA degradation and limitations related to microarray technology may explain some paradoxical results. For example, tyrosine hydroxylase (*TH*), a marker of chemosensory glomus cells, was not detected in any of the samples using microarrays but was subsequently detected using the same samples by RT-PCR (Fagerlund et al. 2010). Similarly, nicotinic acetylcholine receptor alpha 3 subunit (*CHRNA3*) and the purinergic ionotropic P2X2 receptor (*P2RX2*) were detected in 2/5 and 0/5 human CB samples analyzed using microarrays. Meanwhile, subsequently the expression of *CHRNA3* and *P2RX2* was detected in all five samples using RT-qPCR (Fagerlund et al. 2010). These results indicate that some important regulatory/signaling genes with class-dependent low-expression levels (Fig. 1.2b) might have been missed in the study. Thus, a better-powered deep sequencing of the human CB transcriptome is warranted to provide a more accurate translational perspective (confirming gene expression in humans) about the mechanistic models generated in animal studies.

The first study to use RNA-seq technology to profile the CB transcriptome was conducted in C57/BL6 mice (Chang et al. 2015). This experiment has led to the initial discovery of the olfactory receptor 78 (*Olfir78*) in the CB, the identification of which has formed the basis for the lactate-based theory of acute O₂-sensing in the chemosensory glomus cells. Parallel to previ-

¹Study claims to compare the transcriptomes of O₂-sensitive organs (CB, AM) to those insensitive to O₂ (SCG) (Gao et al. 2017). However, more recently, it was shown that SCG neurons modulate ventilatory responses to hypoxia independently of preganglionic input in mice with bilateral transection of the cervical sympathetic chain (Getsy et al. 2021). This shows that SCG cannot be regarded as O₂-insensitive.

ous microarray studies, the authors compared the CB transcriptome to that of the embryologically similar AM. This study illustrated the residual potential for de novo gene discovery using a more scalable and sensitive RNA-seq approach even in an organism and experimental paradigm previously studied using microarrays (Ganformina et al. 2005; Gao et al. 2017). The study used $n = 3$ biological replicates where each corresponded to 18 CBs pooled from 10 adult mice. Authors report the average RIN of 7.2 used for sequencing which suggests that some RNA samples included in the analysis may have displayed a degree of degradation (RIN < 7). Notably, the study spares a detailed description of the RNA-seq results; however, sequencing data is publicly available for mining (Table 1.1).

A landmark study using single-cell RNA-seq technology investigated gene expression profiles of isolated CB chemosensory glomus cells in C57Bl6/J mice (Zhou et al. 2016). This study comprehensively characterized the transcriptomes of eight dissociated chemosensory glomus cells, details the most abundantly expressed transcripts, and catalogs highly expressed G protein-coupled receptors (GPCR), ion channels, and O₂-sensing genes. To this day, this study offers cellular resolution unmatched by all other CB transcriptomic studies (Table 1.1). However, to obtain isolated cells, the CB had to undergo harsh enzymatic digestion followed by mechanical trituration; both have been recently shown to significantly alter gene expression and initiate apoptotic cell reprogramming (Denisenko et al. 2020; Massoni-Badosa et al. 2020; O’Flanagan et al. 2019). This raises concerns about the translatability of the data reported. For example, stress response related genes (*Jun*, *Junb*, *Jund*) display much higher levels of expression in dissociated glomus cells compared to bulk-tissue RNA-seq in identical genetic background (Chang et al. 2015). Immediate-early activation genes *Fos* and *Egr1* were the top 14 and top 7 most abundant transcripts in dissociated cells and the 6876 and 2794 most abundant transcript detected in intact organ RNA-seq, respectively. Moreover, the gene encoding dual-specificity phosphatase 1 (*Dusp1*), previously shown to augment cell apoptosis rate, was the top 97 most abundantly expressed tran-

script in dissociated cells and the 3429 most abundant transcript in whole-organ RNA-seq. At the extremes of 8 cells sequenced, “cell 2” had 10, 124,445, and 305,336 times greater expression of *Th*, *Olfir78*, *Epas1* (established glomus cell markers), respectively, compared to “cell 4.” This again indicates that the transcriptomes of isolated glomus cells might be confounded by sample preparation related artifacts and this revelation may possibly be applied to any experimental setting involving CB dissociation.

More recently, RNA-seq was used to profile CB response to endogenous damage-/danger-associated molecular patterns (DAMPs) and humoral signals of tissue injury (ex vivo) in Sprague-Dawley rats (Mkrtchian et al. 2020). Here, explanted CBs were maintained as an organotypic culture for 16–18 h and exposed to individual DAMPs or condition plasma from a model of aseptic tibia injury. RNA-seq was used as a functional readout of the CB response and demonstrated a transcriptional remodeling linked to the immune response. Reported RNA quality ranges from 6.2 to 7.5 RIN indicating that some samples displayed a degree of RNA decay influencing the results. The study includes $n = 10$ control and $n = 5$ replicates for each treatment group.

The most recent study used RNA-seq to compare the CB transcriptomes between the spontaneously hypertensive (SH) and the normotensive Wistar-Kyoto (WKY) rats (Pauza et al. 2022). The principal finding is the identification of novel target genes related to G protein-coupled receptor signaling and ion channel activity linked to CB sensitization in cardiometabolic disease (Abdala et al. 2012; Pijacka et al. 2016). Interestingly, the study identified little overlap between genes associated with CB sensitization in hypertension and genes linked to augmented CB response to hypoxia (Balbir et al. 2007). This suggests divergent molecular mechanisms to underlie hyperreflexia at the end-organ level. Notably, deep sequencing of the CB transcriptomes has led to the discovery of Glucagon like-peptide 1 receptor (*Glp1r*) expression in the CB where it was shown to suppress the arterial chemoreflex (Pauza et al. 2022). This once again demonstrated the residual potential for de novo discovery using a hypothesis-free transcriptomic

approach. The study uses a conservative RNA quality cutoff ($RIN > 7$) and includes $n = 12$ replicates per group where each sample represented a unilateral CB.

An analysis of unilateral CB for the first time revealed differences between bilateral CBs within the same individual. Although no differences in gene expression were detected in the “left vs. right” comparison, transcriptomics revealed 57 genes differentially expressed between the bilateral CBs consistent across multiple animals (unpublished data). For example, Transient receptor potential cation channel, subfamily V, member 3 (*Trpv3*), consistently had higher expression in one CB compared to the other (Fig. 1.1). Interestingly, higher *Trpv3* expression occurred in either one of the CBs and was not linked to a specific side (Fig. 1.1). This suggests the existence of intraindividual lateral differences between the CBs that can occur on either side. Previously, the existence of a “dominant” CB side was proposed to explain divergent responses to unilateral CB removal (Narkiewicz et al. 2016). This is supported by the fact that

contralateral CB sizes show weak or no correlation to each other (Nair et al. 2013; Nguyen et al. 2011). Detection of lateral differences in gene expression further substantiates the existence of a “dominant CB.” However, further work is required to demonstrate any detectable functional differences between sides.

Mkrtchian et al. investigated the noncoding elements of the human CB transcriptome (Mkrtchian et al. 2018). Here, surgically removed human CB slices were exposed to conditions of acute hypoxia ex vivo and studied using a preset miRNA qPCR array. Human CB was found to express 224 out of 752 miRNAs included in the array. Exposure of the CB slices to hypoxia has led to altered expression of 39 miRNAs estimated to have 550 possible mRNA targets linked to cell proliferation, cell differentiation, and apoptosis. It must be noted that the human miRNAome is estimated to consist 2300 mature miRNAs with most exhibiting organ-specific expression (Alles et al. 2019). This suggests that the noncoding components of the CB transcriptome remain largely unexplored.

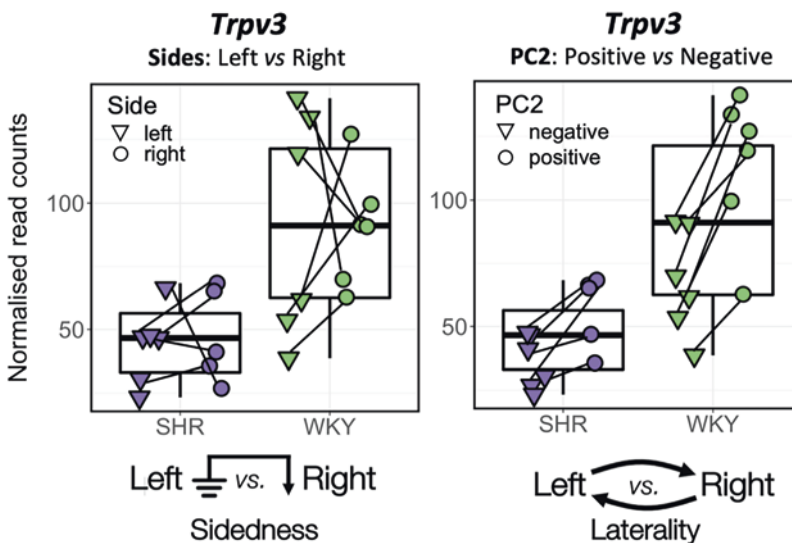


Fig. 1.1 Intraindividual lateral differences between carotid bodies. Data points represent expression of *Trpv3* in individual rat CB samples as reported in Pauza et al. (2022). Lines connect bilateral CB samples of the same animal. *Trpv3* was downregulated in CBs of SH rats compared to WKY (fold change = 0.5, $p_{\text{adj}} = 6.3E-05$). Data points shown in the right represents the same data points shown in the left but assigned a different group based on

Trpv3 expression having higher (positive) or lower (negative) expression in relation to the contralateral side of the same animal. No differences in *Trpv3* expression was detected comparing the left versus the right CB (sidedness comparison; left panel). However, *Trpv3* always had higher expression (fold change = 1.64, $p_{\text{adj}} = 0.015$) in one of the two CBs (laterality comparison; right panel)

Lastly, Navarro-Guerrero et al. used microarrays to study molecular messengers driving stem cell differentiation in neurosphere cultures derived from CB progenitor cells (Navarro-Guerrero et al. 2016; Pardal et al. 2007). The authors provide a detailed description of genes underlying neurosphere differentiation; however, being the parallels between the in vitro system and the intact CB transcriptome remains to be detailed.

1.3 The Known Unknowns of the Carotid Body's Transcriptome

Publicly available CB transcriptome datasets serve as a powerful resource to investigate arterial chemoreception (Table 1.1). To illustrate this point, we compared published mouse and rat CB transcriptomes and the top 20 most abundant transcripts encoding pharmacological targets in those datasets (Fig. 1.2). This highlights a few important aspects about gene expression in the CB. First, comparison of the mouse and the rat CB transcriptomes indicated a highly concordant pattern of gene expression between the organisms (Fig. 1.2a, d). Consistent with previous cross-species comparisons (Mkrtchian et al. 2012), transcriptomics indicates that core genes underlying CB arterial chemoreceptor function are evolutionary conserved across the mammalian taxa (Milsom and Bureson 2007). This is an important consideration for translational studies linking mechanistic models generated in animals to human disease. Next, it shows that steady-state gene expression in the CB is gene class dependent (Fig. 1.2b). In general, genes encoding proteins associated with housekeeping roles (enzymes, transporters) are more abundantly expressed compared to gene families associated with regulatory/signaling roles (ion channels, receptors).

Figure 1.2c illustrates that lowly expressed transcripts usually display much higher expression fold changes in contrast to abundant transcripts that display only marginal deviation from the baseline. However, even a small expression change of an abundant gene may have a powerful effect at the end-organ level. Similarly, genes encoding crucial signaling components and dis-

playing marked expression fold changes in response to treatment can have barely detectable steady-state expression at baseline. This is important to consider when assessing biological relevance of any particular candidate gene based on steady-state and differential expression levels.

Browsing the list of most abundantly expressed transcripts quickly leads to the identification of genes with established arterial chemoreceptor roles (Fig. 1.2d). Tyrosine hydroxylase (Th), DOPA decarboxylase (Ddc), and carboxypeptidase E (Cpe) are among the most highly expressed enzymes illustrating the neurosecretory function of the chemosensory glomus cells. Genes encoding Task-1 background channels (Kcnk3) and Transient Receptor Potential Cation Channel Subfamily M Member 7 (Trpm7) are among the mostly highly expressed voltage-gated ion channels, while cholinergic and purinergic channels (Chrna3, Chrna7, Chrn2, Chrn4, P2rx4, P2rx7) dominate the highly expressed ligand-gated ion channels in rodent CB at baseline.

There is a sparsity of information available regarding the majority of pharmacological targets (as defined by IUPHAR/BPS classification) abundantly expressed in the CB (Fig. 1.2d). However, this is not unique to the study of CBs and applies to all life science disciplines. The human genome is estimated to contain 20,352 protein-coding genes (Pertea et al. 2018). A mere 5% of those genes dominate 70% of neuroscience publications, while the remaining 95% have been defined as the ignomine (Pandey et al. 2014; Stoeger et al. 2018). In our view, such convergence hinders progress and impedes advances in medicine. Transcriptomics can be used to highlight patches in our understanding of arterial chemoreception function and to encourage the arterial chemoreception community to pursue new investigation into the “known unknowns” of the CBs.

One such example is adrenomedullin. Two studies (Balbir et al. 2007; Gao et al. 2017) identified proadrenomedullin (*Adm*) as a principal component of the CB response to hypoxia. Prior studies have demonstrated the presence of adrenomedullin in the CB of humans and showed adrenomedullin synthesis to increase in isolated

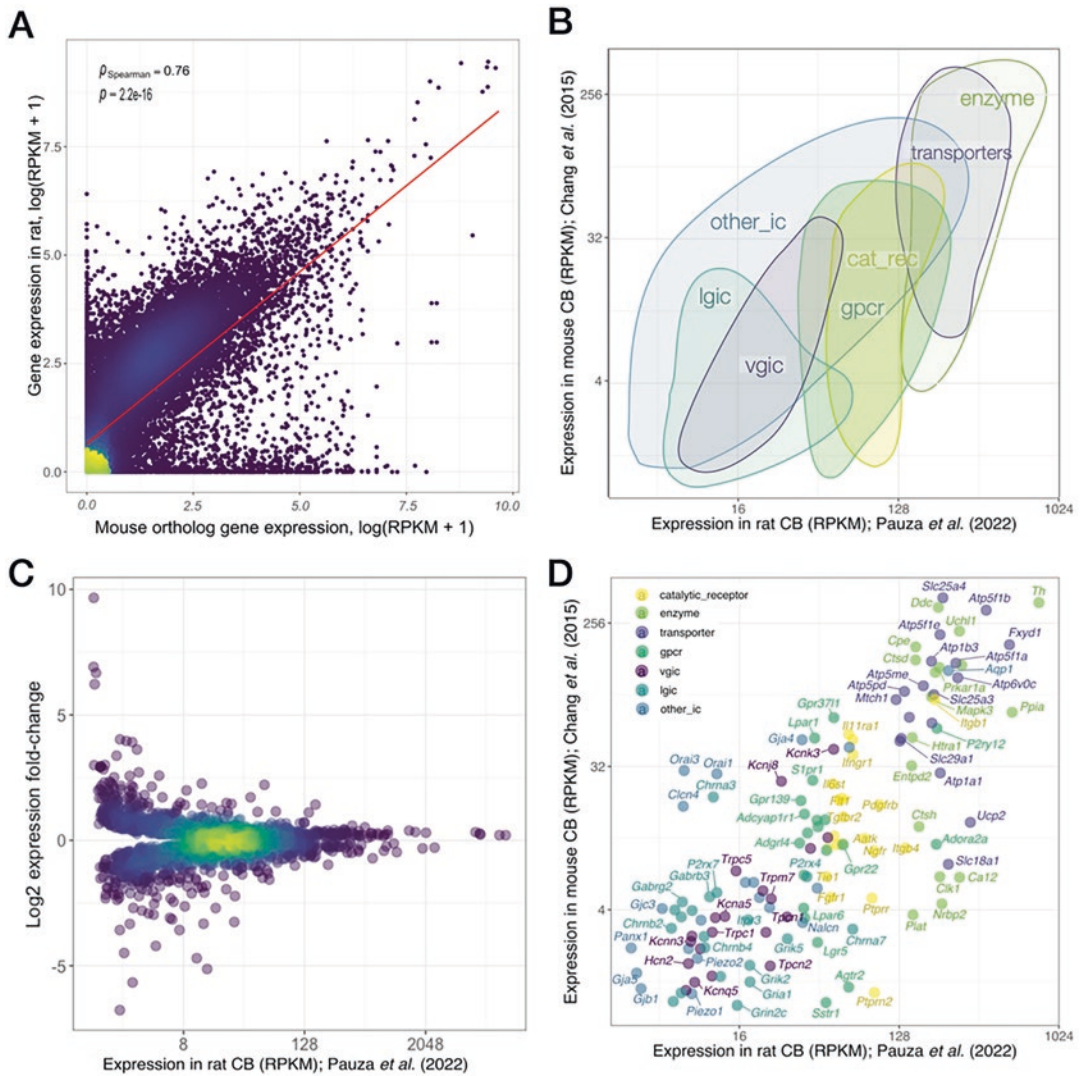


Fig. 1.2 Comparison of published rat and mouse carotid body RNA-seq datasets (Chang et al. 2015; Pauza et al. 2022). Gene expression is presented as log normalized reads per kilobase of transcript, per million mapped reads (RPKM). +1 pseudocount was added to the calculated RPKM values to eliminate negative expression values following log transformation. (a) Density scatterplot depicting steady-state gene expression levels for all detected transcripts in the rat CB and matched expression of their ortholog genes in the mouse CB. Overlap between dots is represented by a color gradient (hot color indicating amount of overlap). Red line represents fitted linear regression model. Numbers indicate derived Spearman's

rank correlation ρ (rho) coefficient and associated p value. (b) Convex hull for each gene family shown in (d). (c) Relationship between basal level of gene expression (x-axis) and detected expression fold changes for differentially expressed genes ($p_{\text{adj}} \leq 0.05$) detected in SHR CBs (Pauza et al. 2022). (d) Comparison of 20 most abundantly expressed genes in mouse and rat CB based on IUPHAR/BPS target categories (Alexander et al. 2019). (b) the convex hull for each gene family shown in (c). *Cat_rec* catalytic receptor, *Gpcr* G protein-coupled receptors, *Other_ic* other ion channels, *vgic* voltage-gated ion channels, *lgic* ligand-gated ion channels

rat glomus cells following exposure to chronic hypoxia (Liu et al. 2013; Martinez et al. 2003; Porzionato et al. 2006). RNA-seq studies found high expression of calcitonin receptor-like

(*Calcrl*) and Receptor activity modifying protein 2 (*Ramp2*) and 3 (*Ramp3*) suggesting the presence of functional adrenomedullin receptors in the rodent CB (Chang et al. 2015; Pauza et al.

2022). Mining of scRNA-seq data shows high expression of *Adm* and the absence of *Calcr1*, *Ramp2*, and *Ramp3* in the chemosensory glomus cells (Zhou et al. 2016). This suggests that adrenomedullin may be released from glomus cells in a paracrine manner to dilate the CB vasculature following hypoxia. However, Martinez et al. (2003) report application of adrenomedullin to evoke a dose-dependent dopamine release from an isolated rat CB (Martinez et al. 2003). Provided glomus cells do not express adrenomedullin receptors, and their activation must be indirect and involve secondary messengers. Despite a well-documented transcriptional signature, little is known about the end-organ effect and the mechanism of action of adrenomedullin in the CB in health or disease.

ATP is the principal excitatory neurotransmitter released by the glomus cells to activate the chemosensory petrosal afferents acting via P2X3 receptors (Bardsley et al. 2021; Pijacka et al. 2016). Transcriptomics indicates P2Y12 purinergic receptor (*P2ry12*) as the most highly expressed GPCR in the rat CB (Fig. 1.2c). However, little is known about its action in the CB besides a single pilot report showing ATP to inhibit Ca²⁺ response to anoxia in isolated glomus cells blocked by MRS2395, a specific P2Y12 receptor antagonist (Carroll et al. 2012). Despite a well-documented P2Y2R-[Ca²⁺]_i-Panx-1 pathway in the tripartite synapse of the CB (Leonard et al. 2018), the mechanisms of negative feedback autoregulation of glomus cells involving P2Y12 receptors remain under researched. Notably, higher expression of *P2ry12* in the CB was linked to strain susceptibility to hypoxia (Balbir et al. 2007). Another crucial component of purinergic signaling in the CB is the extracellular enzymes that metabolize ATP following its release from the glomus cells (Conde et al. 2017; Holmes et al. 2018). Transcriptomics indicates NTPDase 2 (*Entpd2*) as the most highly expressed ectonucleoside triphosphate diphosphohydrolase in the CB (Fig. 1.2c), however, no expression of *Entpd2* was detected in isolated glomus cells (Zhou et al. 2016). This is in line with previous reports locating NTPDase 2 to type II cells and showing *Entpd2* expression to be strongly reduced in the rat CB following chronic hypoxia (Salman et al. 2017) and its downregula-

tion in hypertensive CB (Pauza et al. 2022). *P2ry12* and *Entpd2* being the most highly expressed purinergic metabotropic receptor and ATP hydrolyzing enzyme in a rodent CB, respectively, warrant further investigation into their involvement in peripheral chemoreceptor sensitization in disease states.

Transcriptomics further pinpoints to a number of orphan GPCRs (*Gpr3711*, *Gpr22*, *Gpr139*) highly expressed in the CB (Fig. 1.2d). CB is a highly specialized peripheral chemosensor with an array of established and accessible functional readouts. These properties may thus be exploited to explore endogenous ligands of the orphan GPCRs present in the CB. Similarly, transcriptomics highlights an array of transient receptor potential (TRP) channels (*Trpc1*, *Trpc5*, *Trpm2*, *Trpm3*, *Trpm4*, *Trps1*, *Trp11*, *Trpv2*, *Trpv3*, *Trpv4*, and *Trpv6*) about which little is known in comparison with *Trpv1* (Jendzjowsky et al. 2018, 2021) and *Trpm7* (Kim et al. 2022; Shin et al. 2019) with established roles in arterial chemosensory transduction.

1.4 Summary: Future Directions

In summary, only a handful of published studies focused on the CB transcriptome (Table 1.1). These have demonstrated CB to possess a unique gene expression profile linked to its specialized arterial chemosensory role. Transcriptomics indicate that the CBs of model organisms closely parallel that of humans and can be used to better understand the mechanisms of acute O₂-sensing and other chemosensory modalities of the CB. Most importantly, data made publicly available by these studies serve as a powerful hypothesis-generating resource for future scientific inquiries and a higher fidelity understanding of carotid body function.

References

- Abdala AP, McBryde FD, Marina N, Hendy EB, Engelman ZJ, Fudim M, Sobotka PA, Gourine AV, Paton JFR (2012) Hypertension is critically dependent on the carotid body input in the spontaneously hypertensive rat. *J Physiol* 590:4269–4277

- Alexander SPH, Kelly E, Mathie A, Peters JA, Veale EL, Armstrong JF, Faccenda E, Harding SD, Pawson AJ, Sharman JL, Al E (2019) The concise guide to pharmacology 2019/20: introduction and other protein targets. *Br J Pharmacol* 176:S1–S20
- Alles J, Fehlmann T, Fischer U, Backes C, Galata V, Minet M, Hart M, Abu-Halima M, Grässer FA, Lenhof HP, Keller A, Meese E (2019) An estimate of the total number of true human miRNAs. *Nucleic Acids Res* 47:3353–3364
- Baccarella A, Williams CR, Parrish JZ, Kim CC (2018) Empirical assessment of the impact of sample number and read depth on RNA-Seq analysis workflow performance. *BMC Bioinf* 19:1–12
- Balbir A, Lee H, Okumura M, Biswal S, Fitzgerald RS, Shirahata M (2007) A search for genes that may confer divergent morphology and function in the carotid body between two strains of mice. *Am J Phys Lung Cell Mol Phys* 292:L704–L715
- Bardsley EN, Pen DK, McBryde FD, Ford AP, Paton JFR (2021) The inevitability of ATP as a transmitter in the carotid body. *Auton Neurosci* 234:102815
- Campaign A, Yang YH (2010) Comparison study of microarray meta-analysis methods. *BMC Bioinf* 11:408
- Carroll JL, Agarwal A, Donnelly DF, Kim I (2012) Purinergic modulation of carotid body glomus cell hypoxia response during postnatal maturation in rats. In: Nurse CA, Gonzalez C, Peers C, Prabhakar N (eds) *Arterial chemoreception, advances in experimental medicine and biology*. Springer Netherlands, Dordrecht, pp 249–253
- Chang AJ, Ortega FE, Riegler J, Madison DV, Krasnow MA (2015) Oxygen regulation of breathing through an olfactory receptor activated by lactate. *Nature* 527:240–244
- Ching T, Huang S, Garmire LX (2014) Power analysis and sample size estimation for RNA-Seq differential expression. *RNA* 20:1684
- Conde SV, Monteiro EC, Sacramento JF (2017) Purines and carotid body: new roles in pathological conditions. *Front Pharmacol* 8:913
- Denisenko E, Guo BB, Jones M, Hou R, de Kock L, Lassmann T, Poppe D, Clément O, Simmons RK, Lister R, Forrest ARR (2020) Systematic assessment of tissue dissociation and storage biases in single-cell and single-nucleus RNA-seq workflows. *Genome Biol* 21:21–25
- Fagerlund MJ, Kåhlin J, Ebberyd A, Schulte G, Mkrtchian S, Eriksson LI (2010) The human carotid body: expression of oxygen sensing and signaling genes of relevance for anesthesia. *Anesthesiology* 113:1270–1279
- Gallego Romero I, Pai AA, Tung J, Gilad Y (2014) RNA-seq: impact of RNA degradation on transcript quantification. *BMC Biol* 12:1–13
- Ganformina MD, Pérez-García MT, Gutiérrez G, Miguel-Velado E, Lopez-Lopez JR, Marín A, Sánchez D, González C (2005) Comparative gene expression profile of mouse carotid body and adrenal medulla under physiological hypoxia. *J Physiol* 566:491–503
- Gao L, Bonilla-Henao V, García-Flores P, Arias-Mayenco I, Ortega-Sáenz P, López-Barneo J (2017) Gene expression analyses reveal metabolic specifications in acute O₂-sensing chemoreceptor cells. *J Physiol* 595:6091
- Getsy PM, Coffee GA, Hsieh Y-H, Lewis SJ (2021) The superior cervical ganglia modulate ventilatory responses to hypoxia independently of preganglionic drive from the cervical sympathetic chain. *J Appl Physiol* 131:836–857
- Holmes AP, Ray CJ, Pearson SA, Coney AM, Kumar P (2018) Ecto-5'-nucleotidase (CD73) regulates peripheral chemoreceptor activity and cardiorespiratory responses to hypoxia. *J Physiol* 596:3137–3148
- Jendzjowsky NG, Roy A, Barioni NO, Kelly MM, Green FHY, Wyatt CN, Pye RL, Tenorio-Lopes L, Wilson RJA (2018) Preventing acute asthmatic symptoms by targeting a neuronal mechanism involving carotid body lysophosphatidic acid receptors. *Nat Commun* 9:1–15
- Jendzjowsky NG, Roy A, Iftinca M, Barioni NO, Kelly MM, Herrington BA, Visser F, Altier C, Wilson RJA (2021) PKC ϵ stimulation of TRPV1 orchestrates carotid body responses to asthmakines. *J Physiol* 599:1335–1354
- Kim LJ, Shin M-K, Pho H, Tang W-Y, Hosamane N, Anokye-Danso F, Ahima RS, Sham JSK, Pham LV, Polotsky VY (2022) TRPM7 channels regulate breathing during sleep in obesity by acting peripherally in the carotid bodies. *J Physiol* 600:5145
- Leonard EM, Salman S, Nurse CA (2018) Sensory processing and integration at the carotid body tripartite synapse: neurotransmitter functions and effects of chronic hypoxia. *Front Physiol* 9:1–14
- Liu X, He L, Dinger B, Stensaa L, Fidone S (2013) Sustained exposure to cytokines and hypoxia enhances excitability of oxygen-sensitive type I cells in rat carotid body: correlation with the expression of HIF-1 α protein and adrenomedullin. *High Alt Med Biol* 14:53–60
- Martinez A, Saldise L, Ramirez MJ, Belzunegui S, Zudaire E, Luquin MR, Cuttitta F (2003) Adrenomedullin expression and function in the rat carotid body. *J Endocrinol* 176:95–102
- Massoni-Badosa R, Iacono G, Moutinho C, Kulis M, Palau N, Marchese D, Rodríguez-Ubrea J, Ballestar E, Rodríguez-Esteban G, Marsal S, Aymerich M, Colomer D, Campo E, Julià A, Martín-Subero JI, Heyn H (2020) Sampling time-dependent artifacts in single-cell genomics studies. *Genome Biol* 21:1–16
- Milsom WK, Burleson ML (2007) Peripheral arterial chemoreceptors and the evolution of the carotid body. *Respir Physiol Neurobiol* 157:4–11
- Mkrtchian S, Kåhlin J, Ebberyd A, Gonzalez C, Sanchez D, Balbir A, Kostuk EW, Shirahata M, Fagerlund MJ, Eriksson LI (2012) The human carotid body transcriptome with focus on oxygen sensing and inflammation – a comparative analysis. *J Physiol* 590:3807–3819

- Mkrtchian S, Lee KL, Kåhlin J, Ebberyd A, Poellinger L, Fagerlund MJ, Eriksson LI (2018) Hypoxia regulates MicroRNA expression in the human carotid body. *Adv Exp Med Biol* 1071:25–33
- Mkrtchian S, Kåhlin J, Gómez-Galán M, Ebberyd A, Yoshitake T, Schmidt S, Kehr J, Hildenborg M, Jonsson Fagerlund M, Erlandsson Harris H, Eriksson LI (2020) The impact of damage-associated molecular patterns on the neurotransmitter release and gene expression in the ex vivo rat carotid body. *Exp Physiol* 105:1634–1647
- Nair S, Gupta A, Fudim M, Robinson C, Ravi V, Hurtado-Rua S, Engelman Z, Lee KS, Phillips CD, Sista AK (2013) CT angiography in the detection of carotid body enlargement in patients with hypertension and heart failure. *Neuroradiology* 55:1319–1322
- Narkiewicz K, Ratcliffe LEK, Hart EC, Briant LJB, Chrostowska M, Wolf J, Szyndler A, Hering D, Abdala AP, Manghat N, Burchell AE, Durant C, Lobo MD, Sobotka PA, Patel NK, Leiter JC, Engelman ZJ, Nightingale AK, Paton JFR (2016) Unilateral carotid body resection in resistant hypertension: a safety and feasibility trial. *JACC Basic Transl Sci* 1:313–324
- Navarro-Guerrero E, Platero-Luengo A, Linares-Clemente P, Cases I, López-Barneo J, Pardal R (2016) Gene expression profiling supports the neural crest origin of adult rodent carotid body stem cells and identifies CD10 as a marker for mesectoderm-committed progenitors. *Stem Cells* 34:1637–1650
- Nguyen RP, Shah LM, Quigley EP, Harnsberger HR, Wiggins RH (2011) Carotid body detection on CT angiography. *AJNR Am J Neuroradiol* 32:1096–1099
- O’Flanagan CH, Campbell KR, Zhang AW, Kabeer F, Lim JLP, Biele J, Eirew P, Lai D, McPherson A, Kong E, Bates C, Borkowski K, Wiens M, Hewitson B, Hopkins J, Pham J, Ceglia N, Moore R, Mungall AJ, McAlpine JN, Shah SP, Aparicio S (2019) Dissociation of solid tumor tissues with cold active protease for single-cell RNA-seq minimizes conserved collagenase-associated stress responses. *Genome Biol* 20:1–13
- Pandey AK, Lu L, Wang X, Homayouni R, Williams RW (2014) Functionally enigmatic genes: a case study of the brain ignorome. *PLoS One* 9:e88889
- Pardal R, Ortega-Sáenz P, Durán R, López-Barneo J (2007) Glia-like stem cells sustain physiologic neurogenesis in the adult mammalian carotid body. *Cell* 131:364–377
- Pauza AG, Mecawi AS, Paterson A, Hindmarch CCT, Greenwood M, Murphy D, Greenwood MP (2021) Osmoregulation of the transcriptome of the hypothalamic supraoptic nucleus: a resource for the community. *J Neuroendocrinol* 33:e13007
- Pauza AG, Thakkar P, Tasic T, Felipe I, Bishop P, Greenwood MP, Rysevaite-Kyguoliene K, Ast J, Broichhagen J, Hodson DJ, Salgado HC, Pauza DH, Japundzic-Zigon N, Paton JFR, Murphy D (2022) GLPIR attenuates sympathetic response to high glucose via carotid body inhibition. *Circ Res* 130:694–707
- Pertea M, Shumate A, Pertea G, Varabyou A, Breitwieser FP, Chang YC, Madugundu AK, Pandey A, Salzberg SL (2018) CHESSE: a new human gene catalog curated from thousands of large-scale RNA sequencing experiments reveals extensive transcriptional noise. *Genome Biol* 19:1–14
- Pijacka W, Moraes DJA, Ratcliffe LEK, Nightingale AK, Hart EC, da Silva MP, Machado BH, McBryde FD, Abdala AP, Ford AP, Paton JFR (2016) Purinergic receptors in the carotid body as a new drug target for controlling hypertension. *Nat Med* 22:1151–1159
- Porzionato A, Macchi V, Sandra Belloni A, Parenti A, De Caro R (2006) Adrenomedullin immunoreactivity in the human carotid body. *Peptides* 27:69–73
- Salman S, Vollmer C, McClelland GB, Nurse CA (2017) Characterization of ectionucleotidase expression in the rat carotid body: regulation by chronic hypoxia. *Am J Phys Cell Phys* 313:C274–C284
- Schroeder A, Mueller O, Stocker S, Salowsky R, Leiber M, Gassmann M, Lightfoot S, Menzel W, Granzow M, Ragg T (2006) The RIN: an RNA integrity number for assigning integrity values to RNA measurements. *BMC Mol Biol* 7:3
- Schurch NJ, Schofield P, Gierliński M, Cole C, Sherstnev A, Singh V, Wrobel N, Gharbi K, Simpson G, Owen-Hughes T, Blaxter M, Barton GJ (2016) How many biological replicates are needed in an RNA-seq experiment and which differential expression tool should you use? *RNA* 22:839–851
- Shin M, Eraso CC, Mu Y, Gu C, Yeung BHY, Lenise J, Sham JSK, Polotsky VY (2019) Leptin induces hypertension acting on transient receptor potential melastatin 7 channel in the carotid body. *Circ Res* 125:989–1002
- Stoeger T, Gerlach M, Morimoto RI, Nunes Amaral LA (2018) Large-scale investigation of the reasons why potentially important genes are ignored. *PLoS Biol* 16:e2006643
- Tarca AL, Romero R, Draghici S (2006) Analysis of microarray experiments of gene expression profiling. *Am J Obstet Gynecol* 195:373
- Van den Berge K, Hembach KM, Sonesson C, Tiberi S, Clement L, Love MI, Patro R, Robinson MD (2019) RNA sequencing data: Hitchhiker’s guide to expression analysis. *Ann Rev Biomed Data Sci* 2:139–173
- Zhao S, Fung-Leung WP, Bittner A, Ngo K, Liu X (2014) Comparison of RNA-Seq and microarray in transcriptome profiling of activated T cells. *PLoS One* 9:78644
- Zhao S, Zhang Y, Gamini R, Zhang B, von Schack D (2018) Evaluation of two main RNA-seq approaches for gene quantification in clinical RNA sequencing: polyA+ selection versus rRNA depletion. *Sci Rep* 8:4781
- Zhou T, Chien M-S, Kaleem S, Matsunami H (2016) Single cell transcriptome analysis of mouse carotid body glomus cells. *J Physiol* 594:4225–4251



The Adult Carotid Body: A Germinal Niche at the Service of Physiology

2

Ricardo Pardal

Abstract

The carotid body is the most relevant oxygen sensor in mammalian organisms. This organ helps to detect acute changes in PO_2 , but it is also crucial for the organismal adaptation to a maintained hypoxemia. Profound angiogenic and neurogenic processes take place in the carotid body to facilitate this adaptation process. We have described a plethora of multipotent stem cells and restricted progenitors, from both vascular and neuronal lineages, existing in the quiescent normoxic carotid body, ready to contribute to organ growth and adaptation upon the arrival of the hypoxic stimulus. Our deep understanding of the functioning of this stunning germinal niche will very likely facilitate the management and treatment of an important group of diseases that course with carotid body over-activation and malfunction.

Keywords

Neural crest-derived stem cell niche ·
Neurogenesis and angiogenesis · Neuroblasts

and mesectoderm-restricted progenitors ·
Sympathetic activation · Hypoxia

2.1 Introduction

The carotid body (CB) is a paired organ situated in the bifurcation of the carotid artery. The CB represents the main arterial chemoreceptor in mammals, and it patrols for any significant discrepancies in diverse chemical variables within the blood, such as oxygen or CO_2 levels, pH, glucose concentration, etc. Remarkably important is the sensing of oxygen levels (PO_2), since this element is essential for the subsistence of every single cell in mammalian pluricellular systems (Weir et al. 2005). The capital role of oxygen as the final acceptor of electrons in the mitochondrial respiratory chain, thus making achievable the fabrication of energy by oxidative phosphorylation, has allowed the evolutionary radiation of aerobes. As an outcome, complex aerobic organisms, such as mammals, have evolved integrating a homeostatic oxygen-sensing system, including accurate sensors of environmental oxygen levels and operative effectors, to ensure proper amounts of the element to every single cell (Weir et al. 2005). The carotid body is an ultimate constituent of this system and represents the most relevant oxygen detector in mammalian organisms (Lopez-Barneo et al. 2016a). This organ identifies subtle reductions in blood PO_2 and warns the

R. Pardal (✉)
Dpto. de Fisiología Médica y Biofísica, Instituto de
Biomedicina de Sevilla (IBiS), Hospital Universitario
Virgen del Rocío/CSIC/Universidad de Sevilla,
Sevilla, Spain
e-mail: rpardal@us.es

central nervous system throughout the glossopharyngeal nerve. This sensory data stimulates the cardiorespiratory centers within the brain stem, which in turn will rise breath and heart rates to recover oxygen levels reaching the cells (López-Barneo et al. 2001).

The cellular organization of the carotid body has been under study since the beginning of the twentieth century (De Castro 1926). Glomus or type I cells were rapidly identified as the chemoreceptor elements in the carotid body parenchyma (Heymans et al. 1930). These cells are organized in glomeruli and establish sensory synapses with afferent nerve fibers. Carotid body glomus cells are neuron-like excitable cells that express voltage-dependent channels in their membranes and have abundant exocytotic vesicles. A reduction in blood O₂ levels inhibits potassium channels in the glomus cell membrane, inducing a depolarization that provokes voltage-dependent calcium channel opening, calcium entry, and exocytotic liberation of neurotransmitters to the chemoreceptive synapse (Lopez-Barneo et al. 1988; Urena et al. 1994). The mechanism by which potassium channels in glomus cells are inhibited by hypoxia has only recently been elucidated, with the description of the role of mitochondria in the process (Arias-Mayenco et al. 2018; Fernandez-Aguera et al. 2015; Moreno-Domínguez et al. 2020). According to those recent findings, the mechanism by which carotid body glomus cells detect an acute hypoxemic situation involves special metabolic cellular properties and redox signaling from mitochondria to ion channels in the membrane (Gao et al. 2017).

In addition to acute oxygen sensing, the CB is crucial in the adaptation of the organism during chronic exposures to the lack of oxygen, as it happens in high-altitude residents or in patients with problems with O₂ homeostasis (sleep apnea, chronic obstructive pulmonary disease, etc.). When the human organism is exposed to a maintained low level of oxygen, the carotid body suffers intense histochemical changes to augment the oxygen-sensing parenchyma, which in turn permits strengthening of

the respiratory drive from the brain stem and physiological adaptation (Arias-Stella and Valcarcel 1976; Wang and Bisgard 2002). Therefore, the carotid body is able to lead the respiratory and cardiovascular adjustments necessary to ensure survival in a maintained hypoxemic situation (Lopez-Barneo et al. 2016b). Histochemical changes occurring in the carotid body during chronic hypoxia include a profound angiogenic process and a clear production of new chemoresponsive glomus cells (Wang and Bisgard 2002). This formation of new neuronal cells or neurogenesis constitutes a capital feature of the adult carotid body, denotes an impressive capacity for cellular plasticity, and is absolutely necessary to overcome the physiological adaptation of the organism to the new hypoxemic situation.

The cellular events taking place in the carotid body growing parenchyma under chronic hypoxia have only recently been thoroughly studied. The organ contains a cell type, classically known as sustentacular or type II cell, that expresses the glial fibrillary acidic protein (GFAP), has cellular protrusions enveloping type I cells, and was originally described as supportive for glomus cells (Kameda 1996). We have shown that these type II cells in the organ are truly neural crest-derived multipotent stem cells with the capacity to participate in both neurogenesis and angiogenesis by converting into new glomus and vascular cells in response to hypoxia (Annese et al. 2017; Pardal et al. 2007). GFAP+ sustentacular cells are quiescent in normoxic conditions and become activated under hypoxia, changing their phenotype to nestin+/GFAP- proliferative progenitors, which in turn will differentiate into new glomus or vascular cells (Fig. 2.1) (Pardal et al. 2007). CB stem cells (CBSCs) therefore display a glial phenotype, similar to other populations of adult neural stem cells in both peripheral and central nervous systems. The discovery of these tissue-specific stem cells has allowed a better comprehension of the cellular events taking place in the CB during chronic hypoxia, thus permitting an improved understanding of organismal adaptation to low oxygen.

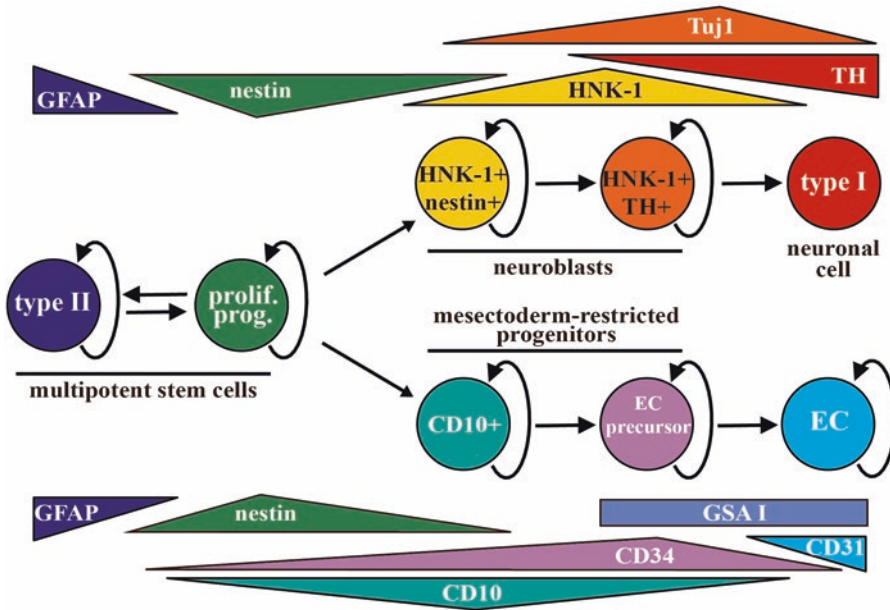


Fig. 2.1 Balls and arrows diagram of CB cell lineages. Balls represent the identified cell types within the adult CB germinal niche, and arrows represent their lineage relationships. Expression of diverse markers spanning the different cells is represented in triangles near to the corresponding cells. Cells with proliferative potential have bowed arrows indicating to themselves. The neuronal lin-

eage gives rise to TH+ mature glomus cells (type I), going through different types of neuroblasts, while the mesodermal lineage produces either CD31+ endothelial cells (EC) or SMA+ smooth muscle cells and pericytes (not included in the diagram). (Figure adapted from Sobrino et al. (2019a), by permission from Springer Nature)

2.2 The CB Contains Intermediate Restricted Progenitors from Both Vascular and Neuronal Lineages, to Accelerate Adaptation to Chronic Hypoxia

During CB adaptation to chronic hypoxia, an intense angiogenesis occurs, in addition to the growth of neuronal parenchyma (Chen et al. 2007; Wang and Bisgard 2002). The new vessels guarantee appropriate supply to the developing neuronal glomeruli and ensure the chemoreceptive function of the organ. Since CBSCs are derived from the neural crest, and neural crest stem cells have mesodermal differentiation potential (Le Douarin et al. 2008), the question rapidly arose as to whether stem cells in the CB could also fuel angiogenesis by differentiating into new vascular cells. We therefore examined

the possibility of CBSCs being able to differentiate into vascular cells, by using cell fate mapping approaches with transgenic mice (Annese et al. 2017). We discovered that these tissue-specific stem cells do preserve multipotent differentiation capability *in vivo*, contributing to both neurogenesis and angiogenesis in response to the hypoxic stimulus. Conversion of CBSCs into endothelial cells is facilitated by diverse vascular cytokines such as erythropoietin or VEGF, and it is also triggered by hypoxia itself in a HIF2 α -dependent way (Annese et al. 2017). Moreover, we even recognized a subpopulation of mesodermal-committed intermediate progenitor cells, positive for the membrane protein CD10, present in quiescence in the normoxic CB and ready for rapid transformation into vascular cells upon the arrival of the hypoxic stimulus (Fig. 2.1) (Navarro-Guerrero et al. 2016). We found that these committed progenitors really include a somehow heterogeneous population of

cells, distributed from those more resembling multipotent cells (nestin+ and CD10+) to those more resembling endothelial cells (CD34+, CD31+, CD10+) (Fig. 2.1), all along the same specification progression line. To the best of our knowledge, CBSCs seem to be the only neural stem cells studied so far as capable of differentiating into both neuronal and vascular cell types in an adult physiological situation *in vivo*. Our results underline the importance of this germinal niche for the correct homeostasis of oxygen and hence for the subsistence of the organism in varying environmental circumstances.

Regarding the neuronal lineage, during the past century, different morphometric studies discriminated two types of glomus cells in the CB, classically termed type A and type B glomus cells. This categorization was made attending to ultrastructural considerations, such as the diameter of exocytotic vesicles, the number of mitochondria, or the size of the nucleus, among others (Hellström 1975). Type A glomus cells showed more copious dense-core vesicles and with greater diameter. These cells were commonly in contact with nerve terminals and sinusoidal capillaries, displaying the anticipated aspect of chemoreceptor glomus cells. The proportion between both types of cells appeared to be equal, but type B cells were typically in the margin of type A cell glomeruli and with cytoplasmic expansions surrounding type A cells (Chen and Yates 1984). We have lately demonstrated that type B glomus cells appear to be immature neuroblast-like cells, ready to transform into fully mature glomus cells (type A) in response to the hypoxic stimulus (Sobrino et al. 2018).

CB neuroblasts (CBNBs), or type B glomus cells, share numerous properties with mature glomus cells (type A neuronal cells), such as the expression of dopaminergic markers like tyrosine hydroxylase (TH) or dopamine decarboxylase (DDC). Nevertheless, they also exhibit proper characteristics of immature cells (Sobrino et al. 2018), such as expression of immature cell markers typical of sympathoadrenal progenitor cells, like HNK-1 (Langley and Grant 1999) or the transcription factor *Ascl1* (Kameda 2005), and expression of neuroblast markers like *Tuj1* or

Ncam2 (Bonfanti et al. 1992; Menezes and Luskin 1994). Furthermore, we have revealed that CBNBs do not yet enclose a mature hypoxia-responsive apparatus, since they are not able to respond to acute exposures to hypoxia, the way mature glomus cells do, despite their membrane expression of ion channels and their sensitivity to other chemical stimuli (Sobrino et al. 2018). In addition, we have also described that CBNBs are smaller in size than mature glomus cells, they have less mitochondria and vesicles and smaller vesicle size, and their location in the glomeruli is marginal (Sobrino et al. 2018). All these ultrastructural characteristics are in consonance with the traditional morphometric studies accomplished in type B glomus cells (Chen and Yates 1984; Hellström 1975).

In normoxic resting situation, CBNBs remain quiescent within the CB neural parenchyma. However, the hypoxic stimulus incites these cells to enter the cell cycle, performing one or two cell divisions and promptly maturing into glomus cells (Sobrino et al. 2018). This recent depiction of CBNB proliferation in response to hypoxia provides understanding to the process of CB growth-mediated adaptation during chronic hypoxemia (Arias-Stella and Valcarcel 1976; McGregor et al. 1984). But it also assists to resolve a traditional discussion about the observation of cell cycle protein expression in CB TH+ dopaminergic cells (Chen et al. 2007; Wang et al. 2008). We have exposed by time-lapse microscopy that mature glomus cells are postmitotic and that neuroblasts are capable of dividing once or twice speedily under the hypoxic stimulus (Sobrino et al. 2018). Additionally, we have detected *in vivo* that neuroblast proliferation takes much less time (3–4 days) than the stem cell production of new glomus cells, which takes 7–10 days to be accomplished (Pardal et al. 2007; Sobrino et al. 2018). Therefore, the existence of quiescent immature neuronal cells within the CB neural parenchyma may have evolved to allow a speedier neurogenesis and hence faster adjustment to the hypoxic environment. Remarkably, the fact that we find some neuroblasts still expressing nestin (see Fig. 2.1), and that we also observe neuroblasts dividing only once while

others divide twice, might denote the presence of different grades of specification among neuroblasts, which could somehow increase duration and effectiveness of this fast neurogenesis.

An interesting question that arises in the CB, regarding the different neural crest-derived cell lineages present in the organ, is whether multipotent stem cells dedicate themselves preferentially to a particular lineage upon activation or they rather differentiate into all of them with similar rates. Although we do not count with definitive data to answer this question, we have studied the movements of nestin+ activated progenitors, in order to try to envision their destination. By combining electron microscopy with immunodetection of GFAP and nestin, using gold particle-associated antibodies, we have analyzed the shape and position of multipotent, quiescent (GFAP+) or proliferative (nestin+), stem cells within the CB parenchyma (Sobrino et al. 2019b). We used different developmental times during silver enhancement method, in order to procure a different gold particle diameter for the recognition of GFAP or nestin with ultrasmall gold particle-conjugated antibodies, permitting us to achieve both labeling procedures at the same time (Sobrino et al. 2019b). The position of nestin+ progenitors, compared to GFAP+ cells, is noticeably more disconnected from neuronal glomeruli and closer to blood vessels, which suggests a movement process. We even found some cells in transition, positive for both GFAP and nestin, getting detached from glomus cells (Sobrino et al. 2019b). Hence, these preliminary data suggest that CBSCs are generally dedicated to angiogenesis and the formation of vascular cells upon the arrival of the stimulus, while neurogenesis might mostly depend on the activity of CBNBs.

In summary, GFAP+ and nestin+ stem cells are the quiescent and proliferative versions, respectively, of CB multipotent progenitors (CBSCs), and we have discovered specified progenitors from both neuronal and vascular cell lineages, with quiescent phenotype, within the normoxic CB parenchyma *in vivo*. The existence of these restricted progenitors might confer a clear evolutionary benefit to this niche since these

cells are able to transform into differentiated cells under hypoxia much faster than multipotent stem cells. We have found specific markers for these restricted progenitors and have studied their biology and their intersecting marker expression with other cell types (Fig. 2.1).

2.3 Mature Glomus Cells as Master Regulators of the Adult Carotid Body Germinal Niche

Since mature glomus cells in the CB are capable of detecting and responding to the hypoxic stimulus in the course of seconds or minutes, it is attractive to think that the rest of the germinal niche events depend on this fast activation by glomus cells. In the last few years, we have tried to respond to this question by analyzing whether multipotent progenitor cells, mesectoderm-restricted progenitors, and CBNBs are able to react to specific glomus cell-released molecules during chronic hypoxia.

Traditional ultrastructural analyses on the carotid body have described sustentacular cells physically surrounding neuronal cells within the glomus parenchyma (Kameda 1996; Wang et al. 2005). Glomeruli of glomus cells are typically shielded by sustentacular cell elongations that closely attach to the membrane, causing an apposition of the two cells with an intermembrane space no thicker than a synaptic cleft (Platero-Luengo et al. 2014). This structure clearly reveals its function, since glomus cells are specialized neurons with synaptic vesicles disseminated all across their membranes, with no synaptic specialization regions. Hence, this anatomical association between neuronal cells and stem cells within the carotid body is indicative of an intimate cross talk between the two cell types. We confirmed this hypothesis by exposing neurosphere-forming sustentacular cells to culture media including different neurotransmitters and neuromodulators defined as plentiful in glomus cell vesicles. From all substances tested, endothelin-1 (ET-1) revealed the strongest augmenting effect on neurosphere progression and

diameter (Platero-Luengo et al. 2014). Although ET-1 is a cytokine typically associated to secretion from vascular cells (Faller 1999), in the case of carotid body, glomus cells have been shown to release ET-1 in response to the hypoxic stimulus (Chen et al. 2002; McQueen et al. 1995; Paciga et al. 1999; Platero-Luengo et al. 2014). Additionally, we have disclosed that CB progenitor cells express receptors for ET-1 both during quiescence and upon activation (Platero-Luengo et al. 2014). Abolition of glomus cell exocytosis, by means of genetic maneuvering or throughout pharmacological inhibition *in vivo*, declines the proportion of CBSCs stimulated by hypoxia (Platero-Luengo et al. 2014), corroborating the importance of neuronal cell activity as a boost for stem cell proliferation and organ growth. ET-1 is an effective proliferative agent, able to regulate the behavior of neural crest progenitors during development (Bonano et al. 2008; Hosoda et al. 1994; Shin et al. 1999). Therefore, these results fit well with the neural crest origin of CBSCs and propose a new molecular and cellular mechanism by which neuronal activity controls the activation process of multipotent progenitors within the adult CB niche.

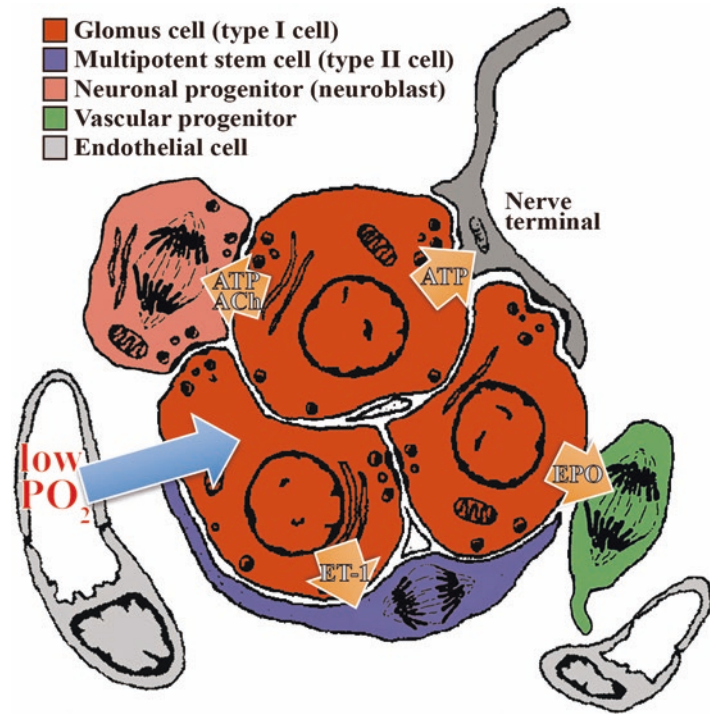
CBNBs are also susceptible to detect glomus cell activity, since they are also located at the periphery of neuronal glomeruli and in close apposition to mature cells. In fact, we have observed that CBNBs are able to mature in response to different niche signaling (Sobrinho et al. 2018). Incubation of these neuroblasts with purinergic molecules (ATP or UTP) or with acetylcholine (ACh) for 48 h produces a very comparable maturation process than exposure to low oxygen. Furthermore, we have revealed the expression of purinergic receptors by CBNBs (Sobrinho et al. 2018), and classical morphometric analyses showed the existence of nicotinic receptors for ACh in the membrane of type B glomus cells (neuroblasts) (Chen and Yates 1984). These whole data together corroborate that CBNBs have the capability to mature into entirely responsive glomus cells in response to purinergic and cholinergic signals being liberated mostly by mature neuronal cells.

Ultimately, *in vitro* studies proposed that vascular differentiation from CBSCs might be potentiated by hypoxia itself (via HIF2 α) and by the liberation of pro-angiogenic cytokines during the hypoxic stimulus (Annese et al. 2017). Although the classical source for these cytokines is the vessels, in the case of CB, some of these cytokines, such as EPO or endothelin-1 (ET-1), have been exposed to be liberated by neuronal cells (Lam et al. 2009; Platero-Luengo et al. 2014), constituting a nice example of neuronal activity-dependent modulation of multipotent stem cell decisions. The role of ET-1 is especially attractive since we exhibited that this cytokine triggers stem cell proliferation after being liberated by neuronal cells (see above and Platero-Luengo et al. 2014), and it also inculcates proliferative progenitors to differentiate into the vascular lineage (Annese et al. 2017; Navarro-Guerrero et al. 2016). Taken together, these results corroborate that glomus cells stimulate angiogenesis through the induction of multipotent stem cells into the vascular lineage and through the complete specification of mesectoderm-restricted progenitors. Our data place mature glomus cells in the center of the niche functioning, designating them as master regulators of the cellular events taking place in the organ in response to the hypoxic stimulus (Fig. 2.2).

2.4 Clinical Implications and Concluding Remarks

The carotid body has been involved in the pathophysiology of numerous illnesses that course with sympathetic overstimulation, normally distressing the cardiorespiratory system. In some of these pathologies, like in hypertension, sleep apnea, chronic heart failure, or some types of chronic kidney disease, an over-activation of the CB has been recognized (Gao et al. 2014; Paton et al. 2013). In some others, like in asthma, metabolic syndrome, obesity, obstructive pulmonary disease, and diabetes mellitus, the CB is in the focus because of playing some non-illuminated role (Cramer et al. 2014; Gao et al. 2014; Lopez-

Fig. 2.2 Cellular scheme of the adult CB germinal niche. Drawing displaying the most relevant cell types existing in an adult carotid body glomerulus. Cells with the capacity to proliferate are depicted with metaphasic separating chromosomes. Arrows show the direction of communication upon the arrival of the hypoxic stimulus (low PO_2), indicating the different molecules involved. Mature glomus cells are depicted as master regulators of the adult CB germinal niche functioning. (Figure adapted from Sobrino et al. (2019a), by permission from Springer Nature)



Barneo et al. 2016b; McBryde et al. 2013; Paton et al. 2013). In the majority of these conditions, an increase in the extension of the CB has been informed (Cramer et al. 2014), very likely related to its over-activation and to disease advancement. Nonetheless, in some circumstances, over-activation does not unavoidably involve parenchyma growth, but possibly just maturation of neuroblasts without proliferation (Sobrino et al. 2018). Currently, the CB constitutes a principal objective during the handling of most of these diseases. In fact, in the case of chronic heart failure and hypertension, resection and denervation of the CB is being experienced to try to improve the symptoms (Del Rio et al. 2013; Narkiewicz et al. 2016; Ribeiro et al. 2013). Nevertheless, clinical research in these pathologies is recently focusing on trying to find drugs that would reduce over-activation of the CB, in order to prevent the direct surgical resection of the organ (McBryde et al. 2013; Pijacka et al. 2016). Our work suggests multiple possibilities to try to cease this over-activation of the organ. We have depicted the existence of various multipotent and restricted progenitor cells within the CB parenchyma and

have illuminated the mechanisms by which all these cells proliferate and differentiate to contribute to the organ growth. By pharmacologically obstructing these processes, we should be capable of avoiding CB growth and hence of inhibiting CB over-activation.

Regarding a very distinct type of illness, a stimulating concern is whether the proliferative potential of the CB germinal niche is related to the manifestation of paragangliomas in the organ. These tumors are normally benign and resemble the CB of individuals exposed to chronic hypoxemia (Arias-Stella and Valcarcel 1976; Kliever et al. 1989). Furthermore, the frequency of CB paragangliomas rises in high-altitude residents (Arias-Stella and Bustos 1976; Astrom et al. 2003; Saldana et al. 1973). Nevertheless, it has not been demonstrated whether there is a connection between CB stem cell niche and tumorigenesis within the organ. Mitochondrial mutations shown as the most frequent reason for congenital paraganglioma (Baysal 2008; Rustin et al. 2002) do not provoke any type of growth when analyzed in animal models (Diaz-Castro et al. 2012; Piruat et al. 2004). Moreover, a recent work has

established that inactivation of PHD2 in dopaminergic cells produces paraganglioma-like growth in the mouse CB (Fielding et al. 2018). Expression of HIF2 α in dopaminergic cells seems to stimulate substantial proliferation of TH $^+$ cells, escorted by robust vascularization. These data propose that there could be an association between the cellular mechanisms for CB hypertrophy and the development of paragangliomas. In any case, our comprehension of the CB niche functioning will very likely improve our ability to treat paraganglioma tumors.

In conclusion, the CB has developed as a noteworthy oxygen sensor in mammals, comprising an impressive germinal niche within the adult peripheral nervous system, essential for a precise physiological adjustment to a changing environment. Our recent data on the description of various stem and progenitor cells existing within the CB parenchyma is augmenting our comprehension of the organ physiology and pathology and will very likely facilitate the treatment of a diversity of diseases related to CB malfunction.

Acknowledgments This work was supported by grants from the Spanish Ministry of Economy and Competitiveness (PID2019-110817R, co-funded by FEDER funds) and the Andalusian Government (P18-RT-3151; US-1262985).

References

- Annese V, Navarro-Guerrero E, Rodriguez-Prieto I et al (2017) Physiological plasticity of neural-crest-derived stem cells in the adult mammalian carotid body. *Cell Rep* 19:471–478
- Arias-Mayenco I, Gonzalez-Rodriguez P, Torres-Torrel H et al (2018) Acute O₂ sensing: role of coenzyme QH₂/Q ratio and mitochondrial ROS compartmentalization. *Cell Metab* 28:145–158
- Arias-Stella J, Bustos F (1976) Chronic hypoxia and chemodectomas in bovines at high altitudes. *Arch Pathol Lab Med* 100:636–639
- Arias-Stella J, Valcarcel J (1976) Chief cell hyperplasia in the human carotid body at high altitudes; physiologic and pathologic significance. *Hum Pathol* 7:361–373
- Astrom K, Cohen JE, Willett-Brozick JE et al (2003) Altitude is a phenotypic modifier in hereditary paraganglioma type 1: evidence for an oxygen-sensing defect. *Hum Genet* 113:228–237
- Baysal BE (2008) Clinical and molecular progress in hereditary paraganglioma. *J Med Genet* 45:689–694
- Bonano M, Tribulo C, De Calisto J et al (2008) A new role for the Endothelin-1/Endothelin-A receptor signaling during early neural crest specification. *Dev Biol* 323:114–129
- Bonfanti L, Olive S, Poulain DA et al (1992) Mapping of the distribution of polysialylated neural cell adhesion molecule throughout the central nervous system of the adult rat: an immunohistochemical study. *Neuroscience* 49:419–436
- Chen IL, Yates RD (1984) Two types of glomus cell in the rat carotid body as revealed by alpha-bungarotoxin binding. *J Neurocytol* 13:281–302
- Chen J, He L, Dinger B et al (2002) Role of endothelin and endothelin A-type receptor in adaptation of the carotid body to chronic hypoxia. *Am J Phys Lung Cell Mol Phys* 282:L1314–L1323
- Chen J, He L, Liu X et al (2007) Effect of the endothelin receptor antagonist bosentan on chronic hypoxia-induced morphological and physiological changes in rat carotid body. *Am J Phys Lung Cell Mol Phys* 292:L1257–L1262
- Cramer JA, Wiggins RH, Fudim M et al (2014) Carotid body size on CTA: correlation with comorbidities. *Clin Radiol* 69:e33–e36
- De Castro F (1926) Sur la structure et l'innervation de la glande intercarotidienne (glomus caroticum) de l'homme et des mammifères, et sur un nouveau système d'innervation autonome du nerf glossopharyngien. *Trab Lab Invest Biol Univ Madrid* 24:13
- Del Rio R, Marcus NJ, Schultz HD (2013) Carotid chemoreceptor ablation improves survival in heart failure: rescuing autonomic control of cardiorespiratory function. *J Am Coll Cardiol* 62:2422–2430
- Diaz-Castro B, Pintado CO, Garcia-Flores P et al (2012) Differential impairment of catecholaminergic cell maturation and survival by genetic mitochondrial complex II dysfunction. *Mol Cell Biol* 32:3347–3357
- Faller DV (1999) Endothelial cell responses to hypoxic stress. *Clin Exp Pharmacol Physiol* 26:74–84
- Fernandez-Aguera MC, Gao L, Gonzalez-Rodriguez P et al (2015) Oxygen sensing by arterial chemoreceptors depends on mitochondrial complex I signaling. *Cell Metab* 22:825–837
- Fielding JW, Hodson EJ, Cheng X et al (2018) PHD2 inactivation in Type I cells drives HIF-2 α dependent multi-lineage hyperplasia and the formation of paraganglioma-like carotid bodies. *J Physiol* 596:4393–4412
- Gao L, Ortega-Sáenz P, García-Fernández M et al (2014) Glucose sensing by carotid body glomus cells: potential implications in disease. *Front Physiol* 5:398
- Gao L, Bonilla-Henao V, Garcia-Flores P et al (2017) Gene expression analyses reveal metabolic specifications in acute O₂-sensing chemoreceptor cells. *J Physiol* 595:6091–6120
- Hellström S (1975) Morphometric studies of dense-cored vesicles in Type I cells of rat carotid body. *J Neurocytol* 4:77–86

- Heymans C, Bouckaert J, Dautrebande L (1930) Sinus carotidien et réflexes respiratoires. II. Influences respiratoires reflexes de l'acidose, de l'alcalose, de l'anhydride carbonique, de l'ion hydrogene et de l'anoxémie: sinus carotidiens et échanges respiratoires dans les poumons et au dela des poumons. *Arch Int Pharmacodyn Ther* 39:400–408
- Hosoda K, Hammer RE, Richardson JA et al (1994) Targeted and natural (piebald-lethal) mutations of endothelin-B receptor gene produce megacolon associated with spotted coat color in mice. *Cell* 79:1267–1276
- Kameda Y (1996) Immunoelectron microscopic localization of vimentin in sustentacular cells of the carotid body and the adrenal medulla of guinea pigs. *J Histochem Cytochem* 44:1439–1449
- Kameda Y (2005) Mash1 is required for glomus cell formation in the mouse carotid body. *Dev Biol* 283:128–139
- Kliwer KE, Wen DR, Cancilla PA et al (1989) Parangliomas: assessment of prognosis by histologic, immunohistochemical, and ultrastructural techniques. *Hum Pathol* 20:29–39
- Lam SY, Tipoe GL, Fung ML (2009) Upregulation of erythropoietin and its receptor expression in the rat carotid body during chronic and intermittent hypoxia. *Adv Exp Med Biol* 648:207–214
- Langley K, Grant NJ (1999) Molecular markers of sympathoadrenal cells. *Cell Tissue Res* 298:185–206
- Le Douarin NM, Calloni GW, Dupin E (2008) The stem cells of the neural crest. *Cell Cycle* 7:1013–1019
- Lopez-Barneo J, Lopez-Lopez JR, Urena J et al (1988) Chemotransduction in the carotid body: K⁺ current modulated by PO₂ in type I chemoreceptor cells. *Science* 241:580–582
- López-Barneo J, Pardo R, Ortega-Sáenz P (2001) Cellular mechanisms of oxygen sensing. *Annu Rev Physiol* 63:259–287
- Lopez-Barneo J, Gonzalez-Rodriguez P, Gao L et al (2016a) Oxygen sensing by the carotid body: mechanisms and role in adaptation to hypoxia. *Am J Phys Cell Phys* 310:C629–C642
- Lopez-Barneo J, Ortega-Saenz P, Gonzalez-Rodriguez P et al (2016b) Oxygen-sensing by arterial chemoreceptors: mechanisms and medical translation. *Mol Asp Med* 47–48:90–108
- McBryde FD, Abdala AP, Hendy EB et al (2013) The carotid body as a putative therapeutic target for the treatment of neurogenic hypertension. *Nat Commun* 4:2395
- McGregor KH, Gil J, Lahiri S (1984) A morphometric study of the carotid body in chronically hypoxic rats. *J Appl Physiol* 57:1430–1438
- McQueen DS, Dashwood MR, Cobb VJ et al (1995) Endothelins and rat carotid body: autoradiographic and functional pharmacological studies. *J Auton Nerv Syst* 53:115–125
- Menezes JR, Luskin MB (1994) Expression of neuron-specific tubulin defines a novel population in the proliferative layers of the developing telencephalon. *J Neurosci* 14:5399–5416
- Moreno-Domínguez A, Ortega-Sáenz P, Gao L et al (2020) Acute O₂ sensing through HIF2 α -dependent expression of atypical cytochrome oxidase subunits in arterial chemoreceptors. *Sci Signal* 13:eaay9452
- Narkiewicz K, Ratcliffe LE, Hart EC et al (2016) Unilateral carotid body resection in resistant hypertension: a safety and feasibility trial. *JACC Basic Transl Sci* 1:313–324
- Navarro-Guerrero E, Platero-Luengo A, Linares-Clemente P et al (2016) Gene expression profiling supports the neural crest origin of adult rodent carotid body stem cells and identifies CD10 as a marker for mesectoderm-committed progenitors. *Stem Cells* 34:1637–1650
- Paciga M, Vollmer C, Nurse C (1999) Role of ET-1 in hypoxia-induced mitosis of cultured rat carotid body chemoreceptors. *Neuroreport* 10:3739–3744
- Pardo R, Ortega-Saenz P, Duran R et al (2007) Glia-like stem cells sustain physiological neurogenesis in the adult mammalian carotid body. *Cell* 131:364–377
- Paton JFR, Sobotka PA, Fudim M et al (2013) The carotid body as a therapeutic target for the treatment of sympathetically mediated diseases. *Hypertension* 61:5–13
- Pijacka W, Moraes DJA, Ratcliffe LEK et al (2016) Purinergic receptors in the carotid body as a new drug target for controlling hypertension. *Nat Med* 22(10):1151–1159
- Piruat JI, Pintado CO, Ortega-Saenz P et al (2004) The mitochondrial SDHD gene is required for early embryogenesis, and its partial deficiency results in persistent carotid body glomus cell activation with full responsiveness to hypoxia. *Mol Cell Biol* 24:10933–10940
- Platero-Luengo A, Gonzalez-Granero S, Duran R et al (2014) An O₂-sensitive glomus cell-stem cell synapse induces carotid body growth in chronic hypoxia. *Cell* 156:291–303
- Ribeiro MJ, Sacramento JF, Gonzalez C et al (2013) Carotid body denervation prevents the development of insulin resistance and hypertension induced by hypercaloric diets. *Diabetes* 62:2905–2916
- Rustin P, Munnich A, Rotig A (2002) Succinate dehydrogenase and human diseases: new insights into a well-known enzyme. *Eur J Hum Genet* 10:289–291
- Saldana MJ, Salem LE, Travezan R (1973) High altitude hypoxia and chemodectomas. *Hum Pathol* 4:251–263
- Shin MK, Levorse JM, Ingram RS et al (1999) The temporal requirement for endothelin receptor-B signalling during neural crest development. *Nature* 402:496–501
- Sobrinho V, Gonzalez-Rodriguez P, Anese V et al (2018) Fast neurogenesis from carotid body quiescent neuroblasts accelerates adaptation to hypoxia. *EMBO Rep* 19:e44598
- Sobrinho V, Anese V, Navarro-Guerrero E et al (2019a) The carotid body: a physiologically relevant germinal niche in the adult peripheral nervous system. *Cell Mol Life Sci* 76:1027–1039

- Sobrino V, Annese V, Pardal R (2019b) Progenitor cell heterogeneity in the adult carotid body germinal niche. *Adv Exp Med Biol* 1123:19–38
- Urena J, Fernandez-Chacon R, Benot AR et al (1994) Hypoxia induces voltage-dependent Ca²⁺ entry and quantal dopamine secretion in carotid body glomus cells. *Proc Natl Acad Sci U S A* 91:10208–10211
- Wang ZY, Bisgard GE (2002) Chronic hypoxia-induced morphological and neurochemical changes in the carotid body. *Microsc Res Tech* 59:168–177
- Wang LP, Kempermann G, Kettenmann H (2005) A subpopulation of precursor cells in the mouse dentate gyrus receives synaptic GABAergic input. *Mol Cell Neurosci* 29:181–189
- Wang Z, Olson EBJ, Bjorling DE et al (2008) Sustained hypoxia-induced proliferation of carotid body type I cells in rats. *J Appl Physiol* 104:803–808
- Weir EK, Lopez-Barneo J, Buckler KJ et al (2005) Acute oxygen-sensing mechanisms. *N Engl J Med* 353:2042–2055



Evidences That Sympathetic Overactivity and Neurogenic Hypertension Correlate with Changes in the Respiratory Pattern in Rodent Models of Experimental Hypoxia

Benedito H. Machado

Abstract

The main question of this chapter is as follows: What is the contribution of changes in the sympathetic-respiratory coupling to the hypertension observed in some experimental models of hypoxia? Although there is evidence supporting the concept that sympathetic-respiratory coupling is increased in different models of experimental hypoxia [chronic intermittent hypoxia (CIH) and sustained hypoxia (SH)], it was also observed that in some strains of rats and in mice, these experimental models of hypoxia do not affect the sympathetic-respiratory coupling and the baseline arterial pressure. The data from studies performed in rats (different strains, male and female, and in the natural sleep cycle) and mice submitted to chronic CIH or SH are critically discussed. The main message from these studies performed in freely moving rodents and in the *in situ* working heart-brainstem preparation is that experimental hypoxia changes the respiratory pattern, which correlates with increased sympathetic activity and

may explain the hypertension observed in male and female rats previously submitted to CIH or SH.

Keywords

Sympathetic-respiratory coupling · Sustained hypoxia · Chronic intermittent hypoxia · Rodents models of hypoxia · Neurogenic hypertension · Peripheral chemoreflex

3.1 Introduction

On the last few years, our laboratory explored the sympathetic-respiratory coupling from different perspectives in order to understand how this phenomena impact on the sympathetic overactivity and consequently to neurogenic hypertension in rodent experimental models of hypoxia. This has not been a simple task, and the body of experimental evidence presented below is pointing out that we must take care in the characterization of the sympathetic-respiratory coupling, which is a very precise and dynamic process dependent on several factors and experimental conditions, which are presented below. In spite of all faced limitations to reach a better picture of the role of sympathetic-respiratory coupling in the genesis of neurogenic hypertension, our findings are indi-

B. H. Machado (✉)
Department of Physiology, School of Medicine of
Ribeirão Preto, University of São Paulo,
Ribeirão Preto, São Paulo, Brazil
e-mail: bhmachad@fmrp.usp.br

cating that the sympathetic-respiratory coupling is associated with the increase in the sympathetic drive and consequently in the neurogenic hypertension. But the main message from this chapter is as follows: Be aware because the sympathetic and respiratory activities may be coupled in most but not in all experimental models and conditions. This apparent conflict may bring the following question: Is the sympathetic-respiratory coupling just a mirage or it has a real physiological meaning?

The purpose of this chapter is to discuss some experimental data obtained under different experimental conditions in studies performed in our laboratory to bring ideas and new contributions for better understanding the functional relevance of changes in the sympathetic-respiratory coupling to the neurogenic hypertension. In order to organize our view and try to present at the end some lights about this complex issue, we need to take into consideration several different factors that might contribute to the final outcome of changes in the sympathetic-respiratory coupling in different experimental models under different physiological conditions. The main factors to be considered are the following: (1) models of hypoxia (chronic intermittent hypoxia (CIH) and sustained hypoxia (SH)), (2) strain of rats (Wistar Ribeirão Preto (RP)-Wistar Hannover-Sprague-Dawley), (3) sex (male and female Wistar RP submitted to hypoxia), (4) experimental approach (in situ preparation – freely moving rats – sleep-wake cycle), and (5) species (rats and mice).

To study the sympathetic-respiratory coupling, two models of experimental hypoxia were used and are described here:

- (a) Chronic intermittent hypoxia: characterized by cycles in which the FI O₂ is reduced from 21% to 6% for few seconds; these cycles are repeated during 8 h a day for 10 days, while the controls are maintained in a normoxic chamber for 24 h for 10 days (Zoccal et al. 2007, 2008).
- (b) Sustained hypoxia: The FI O₂ is reduced from 21% to 10% and maintained at this level for 24 h, while the control rats are maintained under normoxia for the same period of time (Moraes et al. 2014a, b).

3.2 Wistar Ribeirão Preto Rats Submitted to Chronic Intermittent Hypoxia

3.2.1 Male Rats Submitted to Chronic Intermittent Hypoxia

At the end of the experimental protocol of 10 days, CIH rats presented a significant increase in baseline MAP (Zoccal et al. 2007, 2008). It is important to emphasize that this increase in MAP is mediated by a sympathetic overactivity, which in whole animals was indirectly evaluated by intravenous injection of hexamethonium, a ganglionic blocker, and a major fall in arterial pressure was observed in CIH when compared to control rats (Zoccal et al. 2007). Therefore, Wistar RP rats submitted to CIH develops neurogenic hypertension.

Using the in situ working heart-brainstem preparation (WHBP), the activities of several nerves were recorded simultaneously, including the phrenic, sympathetic, and abdominal nerves (Paton 1996; Paton et al. 2022). Using this approach, the most interesting finding was an increase in the sympathetic nerve activity at the end of expiratory phase of the respiratory cycle, which is identified as Late-E events. A careful evaluation of the sympathetic and abdominal nerve recordings in CIH rats showed that at this phase, the abdominal nerves presented a large increase in its activity, indicating that expiration became an active process. It is important to highlight that the increase in sympathetic nerve activity correlated very well with the Late-E in the abdominal nerve, which is not observed in control rats (Zoccal et al. 2008; Moraes et al. 2013; Machado et al. 2017). Therefore, in CIH rats, there is a correlation between the increase in thoracic sympathetic nerve activity (tSNA) and increase in the abdominal nerve activity (Abd) in the Late-E (Fig. 3.1). In this case, the major issue remaining for further discussion is related to the contribution of this increase in sympathetic nerve activity coupled to changes in the pattern of respiration [active expiration] to the hypertension observed in this experimental model of hypoxia.

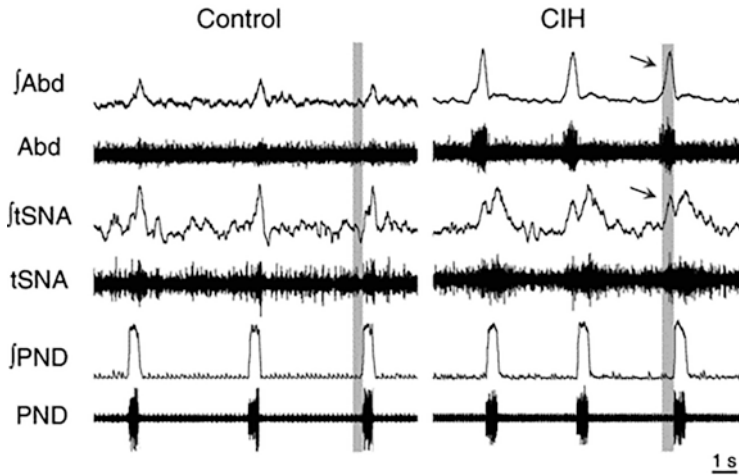


Fig. 3.1 Simultaneous recordings of raw and integrated (\int) abdominal (Abd), thoracic sympathetic (tSNA) and phrenic nerve activities (PND) in a representative control and CIH-treated WHBP (CIH). The shaded gray area in

the recordings represents the late expiratory phase of the respiratory cycle. Note the emergence of late expiratory discharges in both the Abd and tSNA (arrowed) of CIH-treated rats. (Reproduced from Zoccal et al. 2008)

After the characterization of the active expiration (Late-E) in CIH rats using the in situ WHBP, the next question was about the presence of this event in conscious freely moving rats. To answer this question, microelectrodes were previously implanted in the diaphragm and in the abdominal muscles for EMG recordings. The recordings showed that conscious freely moving CIH, but not control rats, exhibited active expiration, i.e., a large increase in the activity of the abdominal muscle in the Late-E (Bazilio et al. 2019). It was also important to answer the following questions: Are changes in the respiratory pattern observed in all phases of the sleep-wake cycle? Or it is restricted to some specific phase of the cycle? The recordings of the cardiovascular and respiratory parameters in control and CIH rats were obtained in a time window of 3 h during the day. For this purpose, the rats received previously, under anesthesia, implantation of microelectrodes in the skull for electrocorticogram and in the neck for electromyogram [for characterization of the different phase of the natural sleep cycle], a catheter in the femoral artery for recording the arterial pressure, and microelectrodes for recording diaphragm and abdominal muscle activities.

During the wakefulness in CIH rats, it was observed a significant increase in baseline MAP, diastolic and systolic pressure, as well as baseline heart rate in comparison with control rats. Similar increases were observed in these cardiovascular parameters in CIH rats during NREM as well as in REM sleep phases. However, when we looked at all phases of the sleep-wake cycle, the abdominal muscle activity was observed only during wakefulness in both control and CIH rats, but the frequency and amplitude of the activity of this muscle was greater in CIH (Fig. 3.2). Important to note that during NREM and REM sleep phases, the abdominal muscle presented no activity in both CIH and control rats. The questions for further discussions are the following: (a) Why the abdominal muscle presented activity only during the wakefulness? (b) Is this activity related to the behavior of sniffing or smelling the environment?

In this context, another important issue is the incidence of the active expiration of CIH and control rats in the wakefulness. When these events were recorded in a time frame of 3 h, it was verified that the percentage of incidence of active expiration in CIH was 11% while in control rats it was in the range of 3% (Bazilio et al. 2019). Therefore, the incidence of active expira-

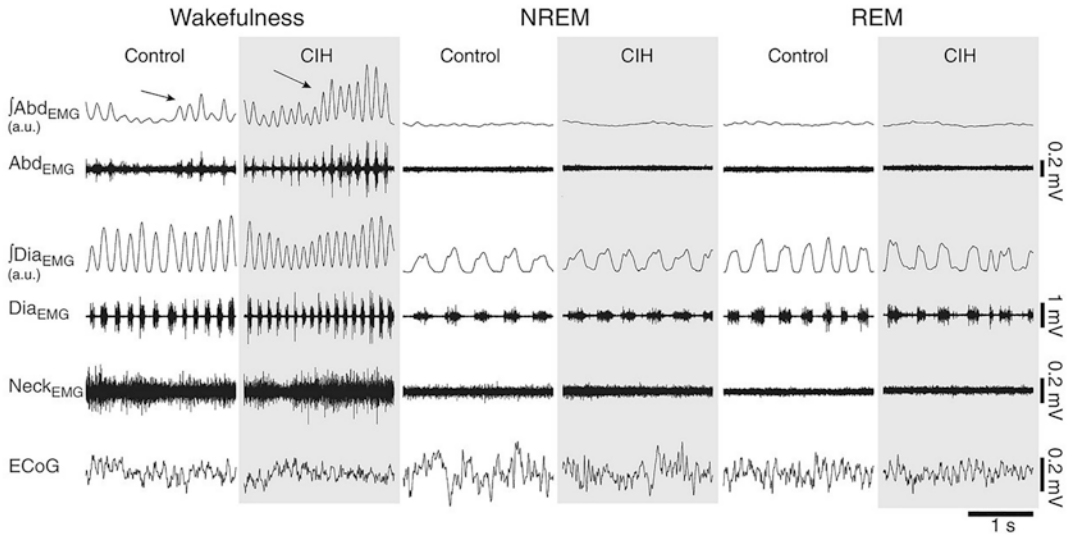


Fig. 3.2 Representative traces from the EMG activities of respiratory and cervical muscles and electrocorticographic activity of a control rat and a CIH rat during the different phases of the sleep-wake cycle. The figure shows EMG activities of the diaphragm (Dia_{EMG}), oblique abdominal muscles (Abd_{EMG}), cervical muscles (Neck_{EMG}),

and electrocorticographic activity (ECoG) during wakefulness and NREM and REM sleep. Note that active expiration events (arrows) occurred only during wakefulness in both groups, and the incidence of these events was higher in rats submitted to CIH than in control rats. (Reproduced from Bazilio et al. 2019)

tion was almost four times higher than in control rats. Nonetheless, the incidence of active expiration even in awake CIH rats is relatively small, and the question for further discussion is related to the strength of this incidence in the overall increased sympathetic activity during the natural sleep-wake cycle and in what extension it may contribute to the development of neurogenic hypertension in CIH rats.

In summary, we observed that male Wistar RP submitted to CIH presented hypertension (freely moving rats) and in the *in situ* WHBP it was documented, by analysis of cross correlation, that the increase in the thoracic sympathetic nerve activity during Late-E correlated with the Late-E peak of abdominal nerve activity in CIH but not in controls (Zoccal et al. 2007). With respect to the active expiration during the sleep-wake cycle, it was observed only in the wakefulness and the incidence is higher in CIH than in control rats (11% vs. 3%), but much lower than that observed in the *in situ* WHBP (~100%). The findings that the active expiration was not observed in NREM and REM sleep phases also highlight that chronic intermittent hypoxia in rats might not be the most

representative experimental model for the obstructive sleep apnea in humans, in which the changes in the respiratory pattern occur during the sleep.

3.2.2 Female Rats Submitted to Chronic Intermittent Hypoxia

In order to evaluate whether the impact of CIH protocol in the autonomic function to the cardiovascular system is similar in both sexes, juvenile female rats were submitted to CIH, and the data were compared to those obtained in male rats (Souza et al. 2015, 2016). In this case, both sexes were from the Wistar RP strain of rats. It was observed a significant increase in the baseline mean arterial pressure in female rats (freely moving) submitted to CIH and also an increase in the sympathetic activity in the *in situ* WHBP. However, the increase of the sympathetic activity was observed during the inspiration phase of the respiratory cycle, but not in the Late-E (Fig. 3.3). These findings indicated that in spite of the fact

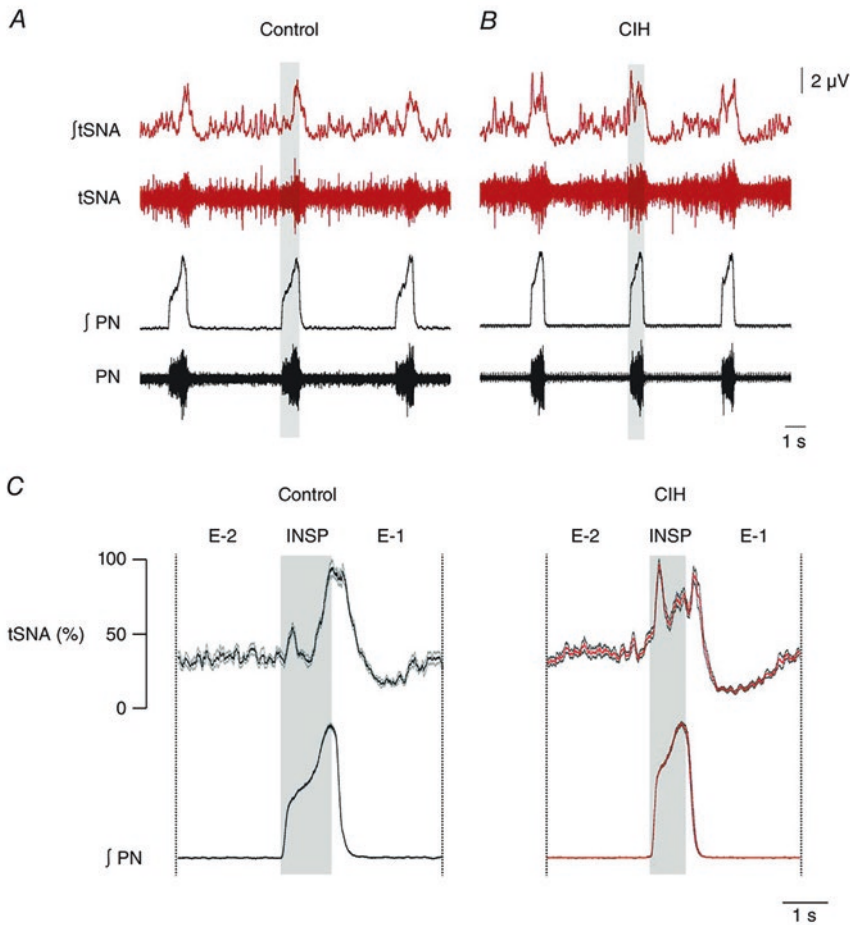


Fig. 3.3 Respiratory modulation of sympathetic activity shown during the respiratory cycles in female rats exposed to CIH or control conditions. Recordings of thoracic sympathetic nerve (tSNA) and phrenic nerve (PN) activities from representative female rats of the CIH and control groups. (a) representative recordings of tSNA and PN activity from one female control rat. (b) representative recordings of tSNA and PN activity from one CIH-

exposed female rat. (c) waveform neurograms of ten respiratory cycles (means \pm SEM) of one representative female rat from the control group and another from the CIH group. Note that CIH-exposed female rats presented an abnormal increase in inspiratory-related tSNA compared with control rats. (Reproduced from Souza et al. 2016)

that female rats are hypertensive after CIH, the changes in the sympathetic-respiratory coupling are different when compared to male rats, in which the increase in the sympathetic activity occurred in the Late-E (Souza et al. 2015). Therefore, male and female rats submitted to CIH present increase in the sympathetic activity and hypertension, but the changes in the sympathetic-respiratory coupling occurred in different phases of the respiratory cycle. Although

changes in the sympathetic-respiratory coupling in response to CIH is also contributing to the increase in arterial pressure in female rats, the mechanisms underlying these changes is specific to this sex.

These findings indicating that female submitted to a hypoxic challenge presents different pattern of respiratory response in comparison with male rats also suggest that the neural pathways in the brainstem affected by hypoxia are different

among sex, but the impact on the arterial pressure is similar since hypertension was observed in both sexes. It is important to note that similar pattern of the sympathetic-respiratory coupling was observed in spontaneously hypertensive rats (SHR). In a study by Simms et al. (2009) using the in situ WHBP to evaluate the sympathetic-respiratory coupling in neonates and 3- and 5-week-old SHR [a development period in which these rats are not yet hypertensive], they documented that the burst amplitude of the tSNA during inspiration was significantly larger in SHR than in Wistar Kyoto rats (control, Simms et al. 2009). In that study, the authors also observed that the larger burster of the tSNA during inspiration impacts on the amplitude of the Traube-Hering waves and consequently in higher perfusion pressure, which may contribute to the development of hypertension in these animals when they become young adults. It is important to highlight that the sympathetic bursting in SHR occurs earlier in the respiratory cycle with the peak during the inspiration (Simms et al. 2009), with an increase in the frequency discharge of action potentials of post inspiratory modulated RVLM pre-sympathetic neurons, recorded by whole cell patch clamp, in pre-hypertensive spontaneously hypertensive rats (Moraes et al. 2014b). In the case of SHR, it is also important to note that the increase in the sympathetic tSNA in the inspiration is similar to that observed in female rats submitted to CIH, as described above.

3.3 Wistar Ribeirão Preto Rats Submitted to Sustained Hypoxia

Another important experimental model of hypoxia for rodents is the SH, which was used in several studies from our laboratory. In this model, the animals are maintained inside of the chamber for periods of 24 h with a $Fi O_2$ of 10%. We documented that similarly to the model of CIH, Wistar RP rats when submitted to SH also presented a significant increase in the baseline arterial pressure (Moraes et al. 2014a). Therefore, 24 h of SH produced hypertension in Wistar RP rats.

Using the in situ WHBP, we also observed that Wistar RP rats submitted to SH presented a large and significant increase in the activity of the abdominal nerve during the Late-E, which correlates very well with a large and significant increase in the sympathetic nerve activity (Moraes et al. 2014a). As mentioned before, these rats presented a significant increase in the baseline mean arterial pressure after SH, and the neurogenic mechanisms underlying hypertension seems to be similar to that observed in CIH rats.

3.4 Wistar Hannover Rats Submitted to Sustained Hypoxia

Due to changes in the strain of rats provided by our institutional animal care facility, our laboratory was induced to use rats from the Wistar Hannover strain. When we started the transition from Wistar RP to Wistar Hannover rats, we were not aware about possible differences among strains in relation to their responses to the experimental protocol of SH, which was successfully used previously with the Wistar RP strain, as described above.

Initially, we observed that the Wistar Hannover rats submitted to SH and recorded in the in situ WHBP presented no major changes in the Late-E and no changes in the sympathetic nerve activity when compared with rats from the Sprague-Dawley, as will be discussed below (Fig. 3.4). Therefore, differently of the data described for Wistar RP rats, no major changes were observed in the sympathetic-respiratory coupling in Wistar Hannover rats. When the cardiovascular parameters were recorded in these freely moving rats, we verified that Wistar Hannover rats submitted to SH presented no significant changes in the baseline mean arterial pressure. Therefore, the same protocol of SH in Wistar Hannover rats produced no changes in the sympathetic-respiratory coupling nor increase in the baseline arterial pressure. Therefore, SH in this strain produced no hypertension (Bazilio et al. 2021).

In the in situ WHBP of Wistar Hannover rats, we verified that the baseline tSNA in SH rats was

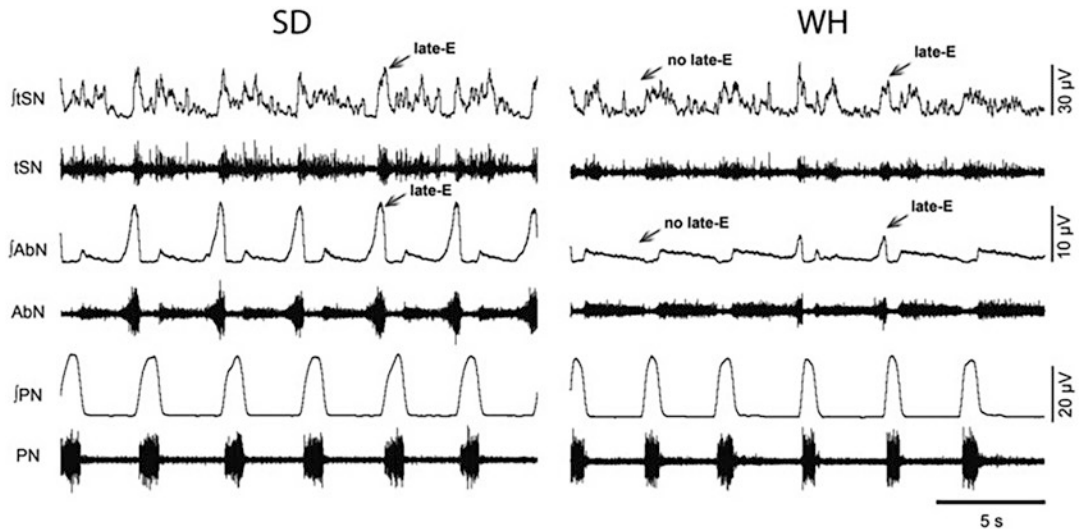


Fig. 3.4 Sympathetic and respiratory activities in situ preparations of Sprague-Dawley (SD) and Wistar Hannover (WH) rats previously submitted to 24-h SH. Representative traces from in situ recordings of an SD rat and a WH rat after exposure to 24-h SH showing raw and integrated (\int) activities of thoracic sympathetic nerve

(tSN), abdominal nerve (AbN), and phrenic nerve (PN). Note that Late-E bursts in AbN and tSN were not observed in several respiratory cycles in WH rats, indicating lower incidence of Late-E events in this rat strain in comparison with SD rats after exposure to SH. (Reproduced from Bazilio et al. 2021)

similar to that recorded in control rats. However, the incidence of Late-E in Wistar Hannover rats submitted to SH (~23%) was higher than in control (0%) rats, but it was much smaller than the incidence observed in Sprague-Dawley rats submitted to the same experimental protocol of hypoxia (~97%). This observation brings the following question: How high should be the incidence of Late-E and the coupled increase in the sympathetic activity to produce a sustained increase in the overall baseline sympathetic activity and consequently neurogenic hypertension?

These unexpected findings allow us to discuss the following several important issues: (a) Are the rats of this Hannover strain less sensitive to hypoxia? (b) In case that these rats are maintained in the SH protocol for periods longer than 24 h, should they present similar changes in the sympathetic-respiratory coupling to that observed in rats of the Wistar RP strain? (c) Considering that the rats of this strain presented either no changes in the sympathetic-respiratory coupling nor increase in baseline mean arterial, is it possible to establish a correlation between the appearance of the changes in the sympathetic-respiratory

couplings and the increase in arterial pressure? Important to highlight that in Wistar RP rats, as described above, the changes in the sympathetic-respiratory coupling were correlated with a significant increase in baseline mean arterial pressure, while in the Wistar Hannover rats, there was a minor increase in the incidence of Late-E when compared to Wistar RP (~20% vs. 100%) and no increase in the baseline mean arterial pressure.

3.5 Sprague-Dawley Rats Submitted to Sustained Hypoxia

Due to the fact that the effects of the protocol of SH in Hannover rats were different in relation to Wistar RP and considering that the rats of Wistar RP strain were not available anymore in the institutional animal care facility, we start to evaluate the effects of SH on rats from the Sprague-Dawley strain. Rats of this strain submitted to SH ($\text{FiO}_2 - 0.1 - 24 \text{ h}$) presented a significant increase in the baseline systolic, diastolic, and mean arte-

rial pressure but no significant change in the baseline heart rate (Bazilio et al. 2021). The rats of this strain in response to sustained hypoxia also presented a significant increase in the baseline respiratory parameters, including the respiratory frequency, tidal volume, and volume minute (VE). Therefore, the changes in baseline cardiovascular and respiratory parameters in rats from the Sprague-Dawley strain were similar to the changes previously observed in rats from the Wistar RP strain submitted to the same experimental protocol of SH (Bazilio et al. 2021).

Using the *in situ* WHBP, we also verified that Sprague-Dawley rats previously submitted to SH presented a consistent increase in the incidence of AbN Late-E during the E2 (Fig. 3.4), which highly correlates (~100%) with the increase in the tSN. These changes in AbN Late-E and in tSN were not observed in the Sprague-Dawley control rats. Sprague-Dawley rats when submitted to SH presented high incidence of AbN Late-E (~100%) and a significant increase in the overall baseline sympathetic activity, which may explain why awake rats of this strain are hypertensive similarly to the rats from the Wistar RP strain while Wistar Hannover rats submitted to the same hypoxia protocol presented no change in the sympathetic-respiratory coupling nor hypertension (Bazilio et al. 2021). As mentioned above, the incidence of AbN Late-E in Wistar Hannover rats submitted to SH (~20%) was much smaller than in Sprague-Dawley (~100%), and we suggest that the incidence of AbN Late-E in response to SH represents a reliable index to be considered in the determination of hypertension. Therefore, the index of correlation in between the AbN Late-E and the increase in tSN activity should be considered among several factors contributing to determine neurogenic hypertension, at least in rats.

3.6 Mice Submitted to Sustained Hypoxia

In accordance with the description above, the pattern of the changes in the sympathetic-respiratory coupling in response to the experimental model

of SH is dependent of the strain of rats. Considering the availability of transgenic models of mice is useful for studies on the central neural control of autonomic and respiratory functions, we recently started a transition from the use of rats to mice in order to evaluate changes in the synaptic transmission in the brainstem nuclei involved with the processing of the cardiovascular and respiratory reflexes in response to hypoxic challenges. In this scenario, the major question in these studies was about the changes or not in the sympathetic-respiratory coupling in mice submitted to SH. At this point, it is important to highlight that our goal was not just to replace rats by mice and to compare the results obtained. Neither was part of our original plan to check the sensitivity of rats and mice to the protocols of experimental hypoxia. Rather, we start to use mice because this rodent is part of the contemporary strategic plan in our as well as in several laboratories involved with the central neural control of autonomic and respiratory functions. The possibility of genetic modifications and the standardized approaches to use opto- and pharmacogenetics in mice these days are compelling us to use this rodent to perform fine and complex experiments in order to answer fundamental questions such as the neuronal and astrocytic changes in response to experimental hypoxia. Therefore, before any further complex experiments, it was a basic requirement to characterize the pattern of autonomic and respiratory changes in mice submitted to SH.

Mice of the strain C57BL/6 (7–8-week-old, ~25 g) were submitted to the same experimental protocol of SH used for rats (FI O₂ 0.1 – 24 h), and the recordings of the cardiovascular parameters in conscious freely moving mice showed no significant changes in systolic, diastolic, and MAP but a significant reduction in the baseline heart rate (Rodrigues et al. 2021; Souza et al. 2022). Therefore, the first important observation is that, at least in this strain of mice, SH produced no increase in baseline MAP, but a significant decrease in the baseline heart rate, indicating a different pattern of response compared to the data obtained from Wistar RP and Sprague-Dawley, described above. In addition, SH mice *in vivo*

presented a significant increase in the baseline respiratory frequency. At least in terms of the cardiovascular parameters, the changes observed in mice in response to sustained hypoxia resemble more the pattern observed in Wistar Hannover than in rats from the Wistar RP and Sprague-Dawley strain.

In the *in situ* WHBP of mice previously submitted to SH presented a high incidence of AbN Late-E (~80%), which was not observed in the control group (Fig. 3.5; Rodrigues et al. 2021). With respect to the respiratory parameters, SH mice presented a significant decrease in the frequency of the phrenic nerve discharge (PND) with the correspondent increase in the time of expiration. It is really important to note that the tSN activity in mice submitted to SH was significantly reduced during E2 (Fig. 3.5). Therefore, in spite of the high incidence of AbN Late-E in SH in mice, it does not correlate with increase in the sympathetic nerve activity. In fact, during E2, it was observed a significant reduction in the sympathetic nerve activity, which may explain, at least in part, why mice of the C57BL strain, when submitted to SH, did not present increase in the baseline MAP. With respect to the vagus nerve activity, there is a significant increase during the post-I, which is probably related to the motor

innervation of the upper airways. In relation to the parasympathetic component to the heart, there is data showing that it is also increased because the baseline heart rate in *in vivo* SH mice is significantly reduced when compared to control and after the treatment with methyl-atropine (a muscarinic antagonist) the heart rate presented a significant increase. The blockade of the sympathetic and parasympathetic tone to the heart using sequential injections of methyl-atropine and propranolol and vice versa in mice submitted to SH documented that the parasympathetic tone to the heart is really increased (Souza et al. 2022).

In summary, mice of the strain C57BL/6 when submitted to SH present an increase in the AbN Late-E, but it was not correlated with an increase in the thoracic sympathetic nerve activity. Therefore, the increase in the sympathetic activity during Late-E seems to be restricted to some strains of rats submitted to CIH or SH, but it was not observed in C57BL/6 mice submitted to SH. Apparently, we cannot establish a direct correlation between increase in incidence of Late-E and an overall increase in the sympathetic nerve activity and consequently in MAP, i.e., hypertension, at least in mice. However, these findings support the concept that the increase in the sympathetic-respiratory coupling observed in

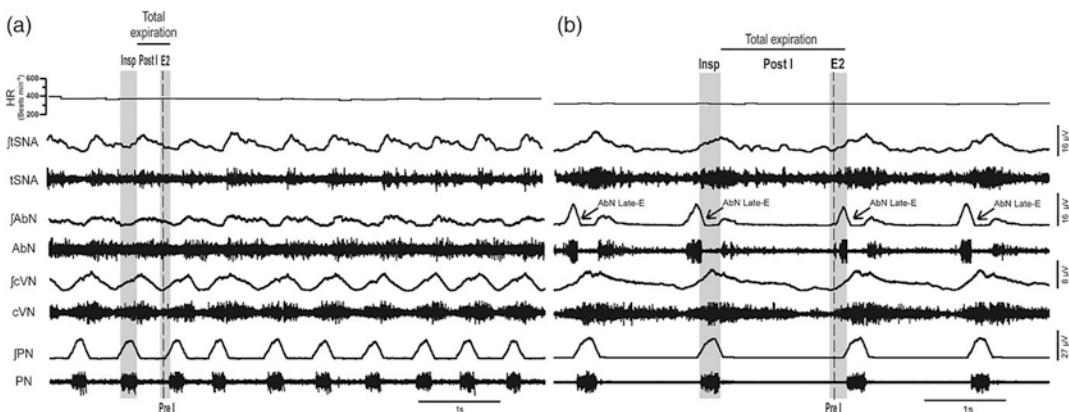


Fig. 3.5 Tracings of baseline heart rate and autonomic and respiratory recordings in *in situ* preparations representative of control (a) and SH (b) mice. Tracings from representative *in situ* preparations of a control (a) and a SH (b) mouse showing baseline heart rate (HR) and raw and integrated (\int) activities of thoracic sympathetic nerve (tSN),

abdominal nerve (AbN), and phrenic nerve (PN). The dashed black line marks the beginning of the Pre-I phase, which ends at PN burst onset. Insp, inspiratory; Post-I, stage 1 expiration; E2, stage 2 expiration. Black arrows indicate Late-E events in AbN activity. (Reproduced from Rodrigues et al. 2021)

Wistar RP and Sprague-Dawley rats correlates very well with the presence of hypertension in these experimental models, because in the absence of changes in the sympathetic-respiratory coupling such as in Wistar Hannover rats and C57BL/6 mice, increase in the baseline MAP was not observed. It is also important to discuss that the increase in the incidence of the Late-E alone, as observed in mice, is not enough to produce changes either in the sympathetic activity nor in the baseline mean arterial pressure. Therefore, the changes in the respiratory pattern in response to hypoxia challenge must be coupled to changes in the sympathetic nerve activity to produce increase in baseline mean arterial pressure, i.e., hypertension.

3.7 Summary

The high incidence of AbN Late-E and increased SNA correlated with hypertension in Wistar RP and Sprague-Dawley rats, while in Wistar Hannover rats, the incidence of AbN Late-E was very low, the sympathetic nerve activity was not increased, and no hypertension was observed in rats of this strain. Therefore, in rats, there is a positive correlation between changes in the sympathetic-respiratory coupling and neurogenic hypertension, which is clearly documented in Wistar RP and Sprague-Dawley rats.

In C57BL/6 mice, the incidence of AbN Late-E was high, but the sympathetic nerve activity was reduced, and no correlation was observed with changes in the baseline mean arterial pressure. Therefore, in mice apparently there is no correlation between changes in the respiratory pattern and increase in the sympathetic activity, and consequently there is no hypertension in mice submitted to SH.

It is important to note that the increase in the sympathetic-respiratory coupling is not a general profile and it is dependent on the strain of rats and the physiological condition of the recordings (in situ preparation, awake freely moving, and natural sleep cycle), and it is different in mice, in female rats, and in spontaneously hypertensive rats.

In spite of all the evidence presented above, it is difficult to determine in what extension the changes in the respiratory pattern (Late-E) and simultaneous increase in the sympathetic nerve activity are affecting the long-term baseline SNA and contributing to neurogenic hypertension. However, the experimental data described here strongly support the concept that increase in the sympathetic-respiratory coupling contributes to neurogenic hypertension, because in the lack of this evidence in Wistar Hannover rats and C57BL/6 mice, neurogenic hypertension was not observed.

It is also true that the changes in the sympathetic-respiratory coupling and its correlation with neurogenic hypertension are not restricted to changes in the AbN Late-E because in female rats (Wistar RP) and juvenile SHR, the increase in the sympathetic activity was observed during the inspiration and no changes were observed in the respiratory pattern, i.e., AbN Late-E.

The overall description of the findings in this chapter emphasizes that the positive correlation between the incidence of AbN Late-E and increased SNA in some experimental models as well as increased SNA during inspiration in other experimental models contribute to neurogenic hypertension. This concept implies that changes in the sympathetic activity driven by changes in the respiratory pattern are another important factor to be considered among others contributing to the generation of the neurogenic hypertension.

Acknowledgments The studies performed in our laboratory were supported by FAPESP (2018/15957-2) and CNPq (309338/2020-4). The author thanks Dr. Lusiane M. Bendhack for her comments and suggestions and all collaborators involved with the studies cited in this chapter.

References

- Bazilio DS, Bonagamba LGH, Moraes DJA, Machado BH (2019) Cardiovascular and respiratory profiles during the sleep-wake cycle of rats previously submitted to chronic intermittent hypoxia. *Exp Physiol* 104(9):1408–1419. <https://doi.org/10.1113/EP087784>

- Bazilio DS, Rodrigues KL, Moraes DJA, Machado BH (2021) Distinct cardiovascular and respiratory responses to short-term sustained hypoxia in juvenile Sprague Dawley and Wistar Hannover rats. *Auton Neurosci* 230:102746. <https://doi.org/10.1016/j.autneu.2020.102746>. Epub 2020 Nov 14
- Machado BH, Zoccal DB, Moraes DJA (2017) Neurogenic hypertension and the secrets of respiration. *Am J Phys Regul Integr Comp Phys* 312(6):R864–R872
- Moraes DJ, da Silva MP, Bonagamba LG, Mecawi AS, Zoccal DB, Antunes-Rodrigues J, Varanda WA, Machado BH (2013) Electrophysiological properties of rostral ventrolateral medulla presympathetic neurons modulated by the respiratory network in rats. *J Neurosci* 33(49):19223–19237. <https://doi.org/10.1523/JNEUROSCI.3041-13.2013>
- Moraes DJ, Bonagamba LG, Costa KM, Costa-Silva JH, Zoccal DB, Machado BH (2014a) Short-term sustained hypoxia induces changes in the coupling of sympathetic and respiratory activities in rats. *J Physiol* 592(9):2013–2033. <https://doi.org/10.1113/jphysiol.2013.262212>
- Moraes DJ, Machado BH, Paton JF (2014b) Specific respiratory neuron types have increased excitability that drive presympathetic neurones in neurogenic hypertension. *Hypertension* 63(6):1309–1318. <https://doi.org/10.1161/HYPERTENSIONAHA.113.02283>
- Paton JFR (1996) A working heart-brainstem preparation of the mouse. *J Neurosci Methods* 65(1):63–68
- Paton JFR, Machado BH, Moraes DJA, Zoccal DB, Abdala AP, Smith JC, Antunes VR, Murphy D, Dutschmann M, Dhingra RR, McAllen R, Pickering AE, Wilson RJA, Day TA, Barioni NO, Allen AM, Menuet C, Donnelly J, Felipe I, St-John WM (2022) Advancing respiratory-cardiovascular physiology with the working heart-brainstem preparation over 25 years. *J Physiol* 600(9):2049–2075. <https://doi.org/10.1113/JP281953>
- Rodrigues KL, Souza JR, Bazilio DS, de Oliveira M, Moraes MPS, Moraes DJA, Machado BH (2021) Changes in the autonomic and respiratory patterns in mice submitted to short-term sustained hypoxia. *Exp Physiol* 106(3):759–770. <https://doi.org/10.1113/EP089323>. Epub 2021 Feb 6
- Simms AE, Paton JF, Pickering AE, Allen AM (2009) Amplified respiratory-sympathetic coupling in the spontaneously hypertensive rat: does it contribute to hypertension? *J Physiol* 587(3):597–610. <https://doi.org/10.1113/jphysiol.2008.165902>
- Souza GM, Bonagamba LG, Amorim MR, Moraes DJ, Machado BH (2015) Cardiovascular and respiratory responses to chronic intermittent hypoxia in adult female rats. *Exp Physiol* 100(3):249–258. <https://doi.org/10.1113/expphysiol.2014.082990>
- Souza GM, Bonagamba LG, Amorim MR, Moraes DJ, Machado BH (2016) Inspiratory modulation of sympathetic activity is increased in female rats exposed to chronic intermittent hypoxia. *Exp Physiol* 101(11):1345–1358. <https://doi.org/10.1113/EP085850>
- Souza JR, Oliveira M, Machado BH (2022) Sustained hypoxia in mice increases parasympathetic but not sympathetic tone. *Curr Res Physiol* 5:361–368. <https://doi.org/10.1016/j.crphys.2022.09.006>
- Zoccal DB, Bonagamba LGH, Oliveira FRT, Antunes-Rodrigues J, Machado BH (2007) Increased sympathetic activity in rats submitted to chronic intermittent hypoxia. *Exp Physiol* 92(1):79–85. <https://doi.org/10.1113/expphysiol.2006.035501>
- Zoccal DB, Simms AE, Bonagamba LGH, Braga VA, Pickering AE, Paton JFR, Machado BH (2008) Increased sympathetic outflow in juvenile rats submitted to chronic intermittent hypoxia correlates with enhanced expiratory activity. *J Physiol* 586(13):3253–3265. <https://doi.org/10.1113/jphysiol.2008.154187>



Control of Arterial Hypertension by the AhR Blocker CH-223191: A Chronopharmacological Study in Chronic Intermittent Hypoxia Conditions

António B. Pimpão, Cátia Sousa, Maria J. Correia, Nuno R. Coelho, Emília C. Monteiro, Antonio F. Melo Junior, and Sofia A. Pereira

Abstract

Chronic intermittent hypoxia (CIH) is a major contributor to the development of hypertension (HTN) in obstructive sleep apnea (OSA). OSA subjects frequently display a non-dipping pattern of blood pressure (BP) and resistant HTN. After discovering that AHR-CYP1A1 axis is a druggable target in CIH-HTN, we hypothesized that CH-223191 could control BP in both active and inactive periods

Authors Antonio F. Melo Junior and Sofia A. Pereira have equally contributed to this chapter.

A. B. Pimpão · C. Sousa · M. J. Correia · E. C. Monteiro
A. F. Melo Junior · S. A. Pereira (✉)
iNOVA4Health, NOVA Medical School, Faculdade de Ciências Médicas, NMS, FCM, Universidade Nova de Lisboa, Lisboa, Portugal
e-mail: sofia.pereira@nms.unl.pt

N. R. Coelho
iNOVA4Health, NOVA Medical School, Faculdade de Ciências Médicas, NMS, FCM, Universidade Nova de Lisboa, Lisboa, Portugal

Egas Moniz Center for Interdisciplinary Research, Egas Moniz School of Health and Science, Caparica, Portugal

of the animals, recovering the BP dipping profile in CIH conditions.

We evaluated the chronopharmacology of the antihypertensive efficacy of the AhR blocker CH-223191 in CIH conditions (21% to 5% of O₂, 5.6 cycles/h, 10.5 h/day, in inactive period of Wistar rats). BP was measured by radiotelemetry, at 8 am (active phase) and at 6 pm (inactive phase) of the animals. The circadian variation of AhR activation in the kidney in normoxia was also assessed, measuring the CYP1A1 (hallmark of AhR activation) protein levels.

Despite drug administration before starting the inactive period of the animals, CH-223191 was not able to decrease BP during the inactive phase, in CIH conditions, therefore not reverting the non-dipping profile. These results suggest that a higher dose or different time of administration of CH-223191 might be needed for an antihypertensive effect throughout the 24-h cycle.

Keywords

Aryl hydrocarbon receptor · CYP1A1 · Circadian rhythmicity · Blood pressure

4.1 Introduction

We have previously demonstrated that along with increased blood pressure (BP), chronic intermittent hypoxia (CIH) activates the aryl hydrocarbon receptor (AhR) pathway, particularly in the kidney (Coelho et al. 2020). These results were obtained by submitting *Wistar* Hannover rats to a paradigm of CIH that mimics mild obstructive sleep apnea (OSA) (Diogo et al. 2015; Coelho et al. 2020; Correia et al. 2021). We reported that the AhR antagonist CH-223191 decreased CIH-induced BP during the animal's active period. Moreover, in the kidney tissue, the AhR antagonist reduced the level of CYP1A1 (a hallmark protein of AhR activation) in a time frame where hypertension (HTN) is already established (21–35 days) (Correia et al. 2021).

The AhR constitutes an exposome receptor activated by xenobiotics, microbiome metabolites, and endogenous molecules and is the hub of a network that integrates these signals and regulates the human metabolome (Coelho et al. 2021, 2022). The AhR physiological role may help individuals to survive in changing environments or promote self-recovery during the early stages of disease, but, upon chronic exposures, these AhR-associated adaptive responses may switch to become harmful and/or to increase the severity of the disease (Coelho et al. 2021). In addition, the AhR activation interferes with circadian clock by forming a heterodimer with BMAL1 [a “core” clock gene (Takahashi 2017)] and disrupting the transcription of *Per* (Tischkau et al. 2011; Xu et al. 2013), providing a link between CIH and the circadian variation of the blood pressure (Coelho et al. 2020). The loss of BP dipper profile is well known in OSA, as well as the prevalence of resistant HTN among non-dipper patients (Marrone and Bonsignore 2018). Therefore, and supported by our previous data, the aim of this work was to evaluate the effect of CIH in the BP circadian variation and whether the antihypertensive effect of CH-223191 was also maintained in the animal's inactive period (during CIH stimuli).

4.2 Material and Methods

4.2.1 In Vivo Experiments

4.2.1.1 Ethics

All applicable institutional and governmental regulations concerning the ethical use of animals in research were followed, according to the NIH Principles of Laboratory Animal Care (NIH Publication 85-23, revised 1985), the European guidelines for the protection of animals used for scientific purposes (European Union Directive 2010/63/EU), and the Portuguese regulation and laws on the protection of animals used for scientific purposes (Law n° 113/2013). All experimental procedures were approved by the Ethical Committee of the NOVA Medical School for the animal care and use in research (protocol n° 15/2017/CEFCM) and by the Portuguese National Authority for Animal Health (DGAV – Direcção-Geral de Alimentação e Veterinária).

4.2.1.2 Animals

Male *Wistar* Hannover rats [CrI:WI (Han)] (*Rattus norvegicus* L.) were obtained from the NOVA Medical School animal facility and maintained under standard laboratory conditions: artificial 12-h light/dark cycles (9 am to 9 pm), at room temperature (22 ± 2.0 °C), and a relative humidity of $60 \pm 10\%$. The rats were maintained on a standard laboratory diet, in the form of dried pellets (SDS diets RM1, Special Diets Services) and reverse osmosis water, given ad libitum. Corncob bedding (Probiológica, Lisbon, Portugal) was used and changed weekly. The animals were specific pathogen-free, according to the Federation for Laboratory Animal Science Associations (FELASA) recommendations (Mähler (Convenor) et al. 2014). The 3Rs policy was employed to minimize the number of animals used.

Two sets of animals were used: one to evaluate the chronopharmacology of the antihypertensive efficacy of the AhR blocker CH-223191 in CIH conditions (Sect. 4.2.1.4.1) and the other to

ascertain the physiological (normoxia) circadian variation of AhR activation in the kidney cortex (Sect. 4.2.1.4.2).

4.2.1.3 Chronic Intermittent Hypoxia Paradigm

We used a CIH paradigm that is well established in the laboratory and mimics mild OSA (Diogo et al. 2015; Coelho et al. 2020; Correia et al. 2021). Briefly, rats were kept in a eucapnic atmosphere inside medium A-chambers (76 × 51 × 51 cm, A-60274-P, Biospherix Ltd, NY, USA). The chambers were equipped with gas injectors and sensors of O₂ and CO₂ levels to ensure the accuracy of CIH cycles. The sensors of O₂ and CO₂, along with the gas injectors, were regulated through the OxyCycler system. In addition, accumulation of CO₂ was prevented by the continuous flow of the gas mixtures, by the circulation of the gases inside the chambers through vent holes, and by the presence of soda lime (AnalaR Normapur[®], VWR International BVBA, Leuven, Belgium), which absorbs the expired CO₂. The CO₂ levels inside the chambers never exceeded 1%. A silica gel (Chameleon[®] C 2–6 mm, VWR International BVBA, Leuven, Belgium) container was also placed inside the chambers to absorb water. Oxygen concentration inside the chambers was regulated by electronically regulated solenoid switches that controlled 100% N₂ and 100% O₂

gas input in a three-channel gas mixer and gradually lowered the oxygen in the chamber from 21% to 5% O₂ (OxyCycler AT series, Biospherix Ltd). The chambers were infused with 100% N₂ for 3.5 min to briefly reduce the O₂ concentration to 5%; afterward, the chambers were infused with 100% O₂ for 7 min to restore O₂ to ambient levels of 21% until the start of the next CIH cycle. Each CIH cycle had a duration of 10.5 min (5.6 CIH cycles/h). Animals were exposed to IH for 10.5 h per day, i.e., during the animal's sleep period (inactive period or light phase of light/dark cycle, 9.30 am to 8 pm). During the remaining hours of the day, the chambers were ventilated with a constant flow of room air (21% of O₂).

4.2.1.4 Study Design

4.2.1.4.1 Evaluation of the Chronopharmacology of the Antihypertensive Efficacy of the AhR Blocker CH-223191 in CIH Conditions

Five male Wistar rats (mean age 12.80 ± 0.73 weeks and mean weight 290.0 ± 7.29 g) were subjected to CIH for 21 days, and on the 22nd day the daily administration of CH-223191 (5 mg/kg in vegetable oil) was started and maintained in CIH condition for the following 14 days (Fig. 4.1).

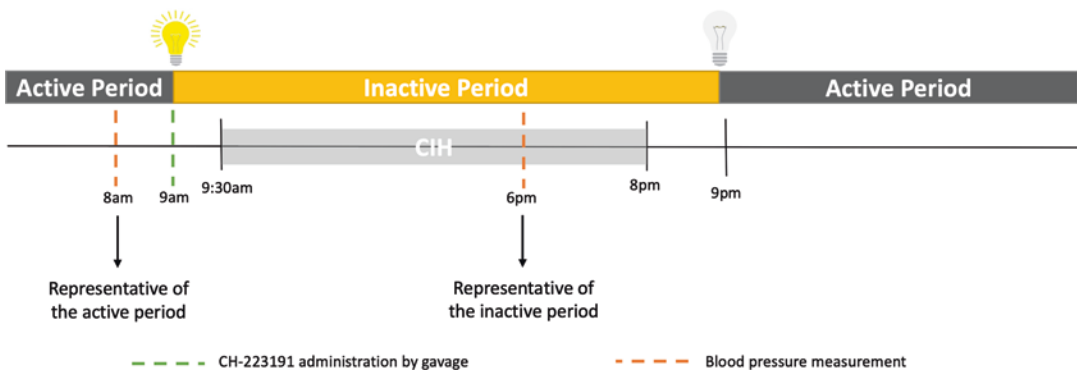


Fig. 4.1 Experimental design. The animals were subjected to CIH for 21 days until established HTN and further daily administered the AhR antagonist CH-223191

(5 mg/kg in vegetable, by gavage) for 14 days, concomitantly with the CIH stimuli to assess its antihypertensive effect

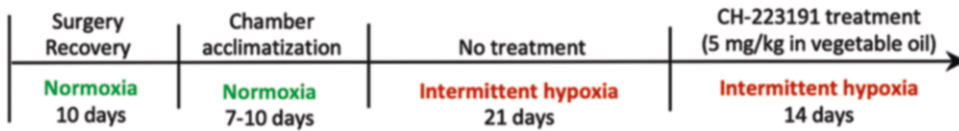


Fig. 4.2 Daily time schedule of the study. The AhR antagonist CH- 223191 was administered just before the inactive period, and the cardiovascular parameters (BP and HR) were measured two times a day, one in the active

and other in the inactive period, to assess their circadian variation and the chronopharmacological properties of the AhR antagonist

The CH-223191 was administered daily at 9 am. The systolic BP (SBP), diastolic BP (DBP), and heart rate (HR) were recorded every day, twice a day, during 35 days in two time points:

- Active period (cardiovascular (CV) parameters measured at 8 am, lights-off phase, chosen to mimic the diurnal HTN in OSA patients) by radiotelemetry (Fig. 4.2).
- Inactive period (CV parameters measured at 6 pm, lights-on phase, chosen to mimic nocturnal HTN under CIH stimuli in the sleeping period of the animals) by radiotelemetry (Fig. 4.2).

4.2.1.4.2 Circadian Variation of AhR Activation in the Kidney Cortex Under Normoxic Conditions

Ten male rats (mean age 18.40 ± 0.16 weeks and mean weight 339.0 ± 10.11 g) were randomly selected and divided into two groups and maintained under normoxic conditions, and then sacrificed at 2 different time-points (9 am and 6 pm) in order to characterize the circadian variation of CYP1A1 expression in renal cortex tissue.

4.2.1.5 Terminal Surgeries

At the end of experiments, rats were anesthetized by intraperitoneal injection with a solution of medetomidine (0.5 mg/kg body weight; Domitor[®], Pfizer Animal Health, Auckland, New Zealand) and ketamine (75 mg/kg body weight; Imalgene 1000[®], Merial, Lyon, France), and cardiac puncture was performed. Death was confirmed by cervical dislocation. Renal cortex tissue was collected and stored at -80 °C for Western blot analysis for study described in Sect. 4.2.2.

4.2.2 Assessment of AhR Activation Through Western Blot Analysis of CYP1A1 Levels

The kidney CYP1A1 protein levels were evaluated by Western blot as previously described (Correia et al. 2021). Briefly, kidney cortex samples were submitted to electrophoresis in 10% SDS-PAGE. Nitrocellulose membranes were blocked with 5% bovine serum albumin and incubated with the following primary antibodies: CYP1A1 (1:1000, E-AB-13483, ElabScience Biotechnology Inc., Houston, TX, USA) and β -actin (1:10,000, 8H10D10, Cell Signaling Technology Inc., Danvers, MA, USA). Then, the membranes were incubated with horseradish peroxidase (HRP)-conjugated anti-rabbit (1:5000, sc-2357, Santa Cruz Biotechnology Inc., Dallas, TX, USA) and HRP-conjugated anti-mouse (1:5000, sc-516102, Santa Cruz Biotechnology Inc., Dallas, TX, USA) for CYP1A1 and β -actin detection, respectively. Western blot signals were quantified using Bio-Rad Image Lab 5.2.1 software, and protein expression levels were normalized to β -actin expression.

4.2.3 Statistical Analysis

Statistical analysis was performed using GraphPad Prism[®] version 8.0 (GraphPad Software Inc., San Diego, CA, USA). The median value per week of each animal was used to obtain SBS, DBP, and HR. Data are expressed as mean \pm SEM. Statistical significance for all tests was set at the level of $p < 0.05$. t-test or one-way ANOVA was used whenever applicable.

4.3 Results

Firstly, we evaluated the effect of CIH in circadian variation of BP. In the active period (Fig. 4.3), after 2 weeks of CIH, both SBP and DBP were increased in 14 ± 3 mmHg and 12 ± 3 mmHg, respectively. Similarly, in the inactive period, an increase was observed for the SBP and DBP, of 16 ± 2 mmHg and 11 ± 2 mmHg, respectively.

The administration of CH-223191 reduced the SPB and DBP in the animal's active period, whereas no impact was found in the inactive period. Thus, the AhR antagonist was not capable of restoring the dipper profile in both SBP and DBP.

Taking these results into account, we further investigated the circadian variation of AhR activation in normoxic conditions by measuring the protein levels of CYP1A1, the hallmark of AhR activation by Western blot. Figure 4.4 shows that CYP1A1 protein levels in the kidney cortex were higher in the animal's inactive period, suggesting that in this tissue AhR activation follows a circadian pattern of expression.

4.4 Discussion

Our data demonstrated that CIH induced an increase of SBP and DBP in both active and inactive periods of the animals. In addition, the physiological decrease of BP during the inactive period (i.e., the dipping profile of BP) is lost with the CIH. Overall, we observed that CIH disturbs the circadian variation of BP. Furthermore, the renal activation of AhR underlies the pathophysiologic mechanisms of CIH-HTN, at least in the active period. Finally, we also described for the first time that the AhR-CYP1A1 signaling has a circadian variation, being more activated during the inactive period (lights-on phase) and less activated in the active period (lights-off phase).

We focused our AhR analysis in the kidney for several reasons. Firstly, due to the pivotal involvement of the kidney in the control of BP, the AhR becomes a druggable target in CIH-HTN (Coelho et al. 2020). Second, because in comparison with

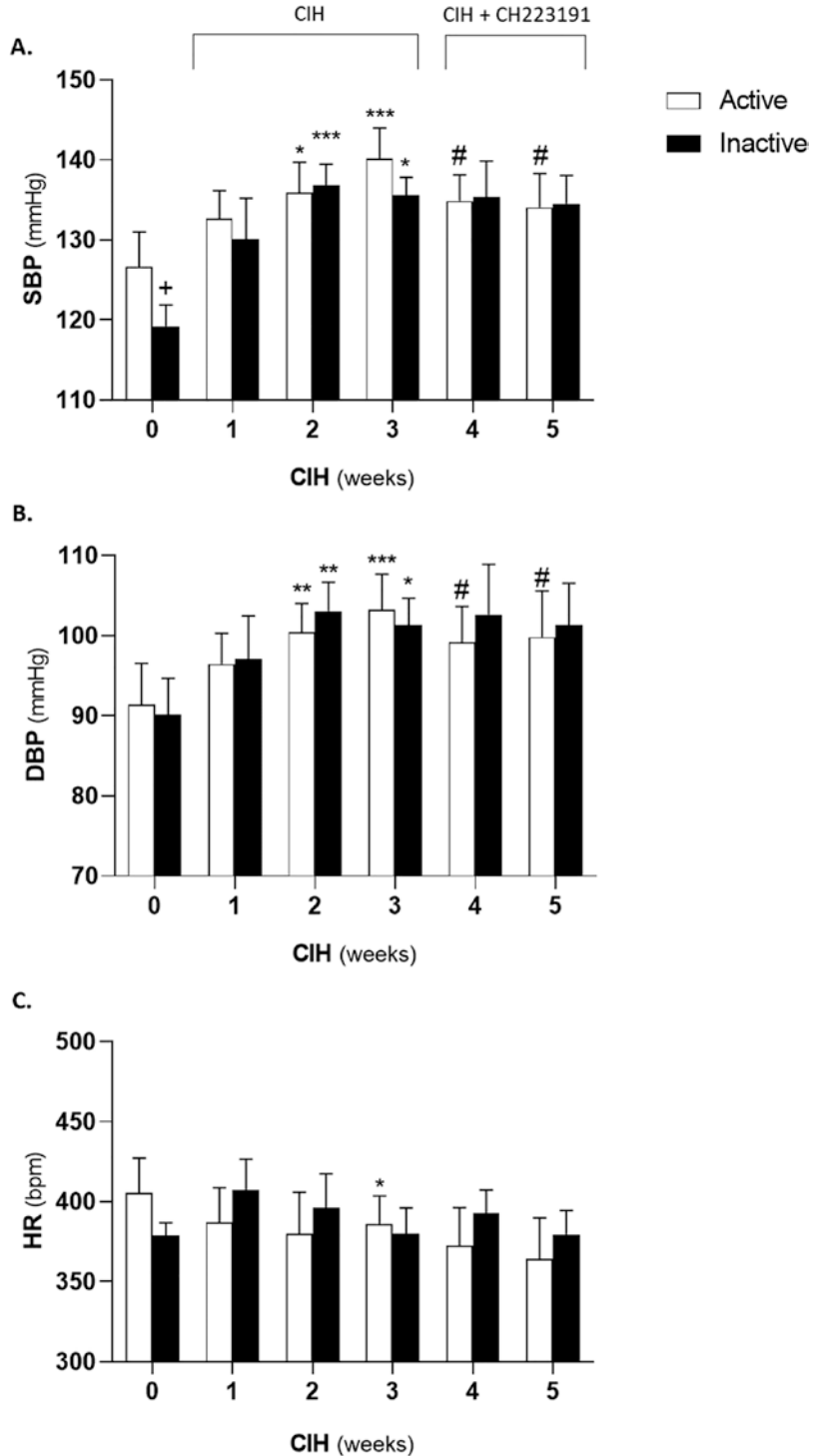
other organs, the kidney has more clock-regulated genes (Gumz 2016), and several renal genes with circadian expression have been identified (Solocinski and Gumz 2015), which might be putative drug targets. Also, the interaction of AhR and BMAL-1 is well known (Jaeger and Tischkau 2016). Finally, and despite having no data concerning the active period, there is an overactivation of AhR by long-term CIH (established HTN) in the kidney during inactive period (Correia et al. 2021).

The relationship between AhR and the circadian variation of BP is bidirectional. On one hand, the rhythmicity of the AhR expression is under the control of Clock (Tanimura et al. 2011). On the other hand, the AhR might control the expression of clock genes (Jaeger and Tischkau 2016). While the responsible for CIH-dependent AhR overactivation is still to be identified, rodent (Gentner and Weber 2011) studies have been demonstrating the association between AhR agonists and the loss of dipper profile of BP and sodium excretion. Therefore, we hypothesize a role for renal AhR activation in the circadian control of BP.

This motivated us to investigate if the antihypertensive effect of CH-223191 observed at 8 am – lights-off (active period) – was also observed in another period of the day. Our data show that the blockage of AhR was present at the end of the active period of the animals, precisely at 23 h after CH-223191 administration (13 h after the end of CIH). However, during the inactive period, 6 pm – lights-on (while the rats were being subjected to the CIH period) – and only 7 h after CH-223191 administration, no effect was observed. This observation might be justified by a convergence of factors.

One of them is the renal pO₂ level that attains its lower levels during the inactive period (Emans et al. 2017). This small variation in O₂ is associated with the decreased BP pressure (dipper profile) (Emans et al. 2017) and has been described as necessary to reset the clocks in a hypoxia-induced factor (HIF)-1 α dependent manner (Adamovich et al. 2017). It is therefore plausible that the kidney is more vulnerable to CIH during the inactive period and might blunt the reset of

Fig. 4.3 Impact of CH-223191 on blood pressure, heart rate, and their circadian variation in established HTN induced by CIH. (+) Comparison between the active and inactive period of the animals in normoxia (week 0) for (a) SBP, (b) DBP, and (c) HR. (*) Effect of the chronicity of intermittent hypoxia in cardiovascular parameters until the development of established arterial hypertension (each week vs. week 0). (#) Effect of AhR antagonist in the cardiovascular parameters in established arterial hypertension (each week vs. week 3). CIH: chronic intermittent hypoxia; DBP: diastolic blood pressure. *HR* heart rate, *Nx* normoxia, *SBP* systolic blood pressure, *W* week. * $p < 0.05$, ** $p < 0.01$, *** $p < 0.001$ relative to week 0. # $p < 0.05$ relative to week 3



clocks. A higher stabilization of HIF interferes with AhR-CYP1A1 pathway as they compete for the dimerization partner ARNT (Vorrink and Domann 2014). This might imply that AhR binds

to other binding partners, namely, Bmal-1, impacting AhR circadian variation (Jaeger and Tischkau 2016). CYP1A1 in the inactive period in the kidney is overactivated after 21 days of

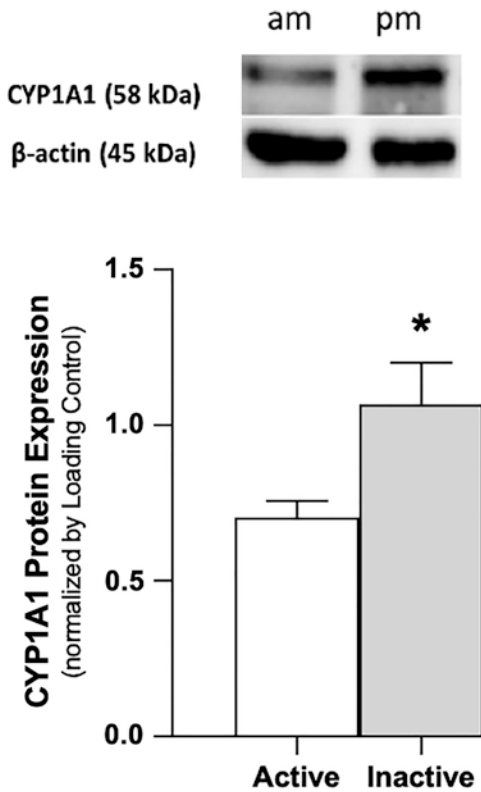


Fig. 4.4 Circadian variation of CYP1A1 expression. CYP1A1 expression is compared between renal cortex tissue of male animals sacrificed during their active (9 am) or inactive (6 pm) period. The quantification is presented as the mean of two replicates of each sample. Expression values are presented in arbitrary units (AU). Data are represented as mean \pm SEM ($n = 5$). Data were analyzed by *Mann-Whitney's U-test* (* p -value < 0.05). CYP1A1 cytochrome P450 family 1, subfamily A, polypeptide 1

CIH comparatively to normoxic conditions (Correia et al. 2021), and we herein show that, physiologically, CYP1A1 is more expressed in inactive than in the active period. This circadian pattern might be related to CYP1A1 substrates like the sleep hormone melatonin (Lu et al. 2020), which also lowers the blood pressure (Baker and Kimpinski 2018). Overall, a higher dose of CH-223191 or another time of administration of the antagonist might be necessary to counteract the overactivation of this signaling pathway.

The precise mechanism underlying the rationale for the timing of administration requires further clarification but might also be related to pharmacokinetic (PK) properties of the drug and

its metabolites. That represents another plausible factor to explain our results, namely, that the responsible for the decrease in BP in the active period is a CH-223191 metabolite. While the knowledge on PK properties of the CH-223191 is scarce, this hypothesis is sustained by predicted PK data obtained in a publicly accessible platform, SwissADME. According to that, CH-223191 is predicted to be a lipophilic compound with a higher gastrointestinal absorption, which permeates the blood-brain barrier and does not inhibit glycoprotein-P.

This work supports a role for AhR in the pathophysiological mechanisms of HTN and in the circadian variation of BP in OSA. Our study has several limitations, including the use of only one dose and the assessment of BP only two times per day. As a final consideration, experimental chronopharmacological studies might allow to ascertain mechanisms of non-dipping profile of BP, a common feature in OSA and resistant HTN. The knowledge of these mechanisms might aid to find new targets, assist in drug design, and support guidelines for optimal timed antihypertensive administration in OSA, justifying the pertinence of this study.

Acknowledgments This work was supported by Fundação para Ciência e Tecnologia [PTDC/MED-TOX/30418/2017] and iNOVA4Health [UID/Multi/04462/2013]. A.B.P., M.J.C., and N.R.C. are supported by FCT grants [2022.11188.BD, SFRH/BD/131331/2017, and PD/BD/114257/2016, respectively].

References

- Adamovich Y et al (2017) Rhythmic oxygen levels reset Circadian clocks through HIF1 α . *Cell Metab* 25(1):93–101. <https://doi.org/10.1016/j.cmet.2016.09.014>
- Baker J, Kimpinski K (2018) Role of melatonin in blood pressure regulation: an adjunct anti-hypertensive agent. *Clin Exp Pharmacol Physiol* 45(8):755–766. <https://doi.org/10.1111/1440-1681.12942>
- Coelho NR et al (2020) First evidence of aryl hydrocarbon receptor as a druggable target in hypertension induced by chronic intermittent hypoxia. *Pharmacol Res* 159:104869. <https://doi.org/10.1016/j.phrs.2020.104869>
- Coelho NR et al (2021) AHR canonical pathway: in vivo findings to support novel antihypertensive strategies.

- Pharmacol Res 165:105407. <https://doi.org/10.1016/j.phrs.2020.105407>
- Coelho NR et al (2022) Pharmacological blockage of the AHR-CYP1A1 axis: a call for in vivo evidence. *J Mol Med* 100(2):215–243. <https://doi.org/10.1007/s00109-021-02163-2>
- Correia MJ et al (2021) Aryl hydrocarbon receptor and cysteine redox dynamics underlie (Mal)adaptive mechanisms to chronic intermittent hypoxia in kidney cortex. *Antioxidants* 10(9):1484. <https://doi.org/10.3390/antiox10091484>
- Diogo LN et al (2015) The association between antihypertensive medication and blood pressure control in patients with obstructive sleep apnea, pp. 201–209. https://doi.org/10.1007/978-3-319-18440-1_22
- Emans TW et al (2017) Circadian rhythm in kidney tissue oxygenation in the rat. *Front Physiol* 8. <https://doi.org/10.3389/fphys.2017.00205>
- Gentner NJ, Weber LP (2011) Intranasal benzo[a]pyrene alters circadian blood pressure patterns and causes lung inflammation in rats. *Arch Toxicol* 85(4):337–346. <https://doi.org/10.1007/s00204-010-0589-6>
- Gumz ML (2016) Molecular basis of circadian rhythmicity in renal physiology and pathophysiology. *Exp Physiol* 101(8):1025–1029. <https://doi.org/10.1113/EP085781>
- Jaeger C, Tischkau SA (2016) Role of aryl hydrocarbon receptor in circadian clock disruption and metabolic dysfunction. *Environ Health Insights* 10:EHI.S38343. <https://doi.org/10.4137/EHI.S38343>
- Lu J et al (2020) New insights of CYP1A in endogenous metabolism: a focus on single nucleotide polymorphisms and diseases. *Acta Pharm Sin B* 10(1):91–104. <https://doi.org/10.1016/j.apsb.2019.11.016>
- Mähler (Convenor) M et al (2014) FELASA recommendations for the health monitoring of mouse, rat, hamster, guinea pig and rabbit colonies in breeding and experimental units. *Lab Anim* 48(3):178–192. <https://doi.org/10.1177/0023677213516312>
- Marrone O, Bonsignore MR (2018) Blood-pressure variability in patients with obstructive sleep apnea: current perspectives. *Nature Sci Sleep* 10:229–242. <https://doi.org/10.2147/NSS.S148543>
- Solocinski K, Gumz ML (2015) The Circadian clock in the regulation of renal rhythms. *J Biol Rhythm* 30(6):470–486. <https://doi.org/10.1177/0748730415610879>
- Takahashi JS (2017) Transcriptional architecture of the mammalian circadian clock. *Nat Rev Genet* 18(3):164–179. <https://doi.org/10.1038/nrg.2016.150>
- Tanimura N et al (2011) Aryl hydrocarbon receptor-mediated Cyp1a1 expression is modulated in a CLOCK-dependent circadian manner. *Toxicology* 290(2–3):203–207. <https://doi.org/10.1016/j.tox.2011.09.007>
- Tischkau SA, Jaeger CD, Krager SL (2011) Circadian clock disruption in the mouse ovary in response to 2,3,7,8-tetrachlorodibenzo-p-dioxin. *Toxicol Lett* 201(2):116–122. <https://doi.org/10.1016/j.toxlet.2010.12.013>
- Vorrink SU, Domann FE (2014) Regulatory crosstalk and interference between the xenobiotic and hypoxia sensing pathways at the AhR-ARNT-HIF1 α signaling node. *Chem Biol Interact* 218:82–88. <https://doi.org/10.1016/j.cbi.2014.05.001>
- Xu C-X et al (2013) Aryl hydrocarbon receptor activation attenuates Per1 gene induction and influences circadian clock resetting. *Toxicol Sci* 132(2):368–378. <https://doi.org/10.1093/toxsci/kfs345>



Three Days of Chronic Intermittent Hypoxia Induce β_1 -Adrenoceptor Dependent Increases in Left Ventricular Contractility

Anthony L. Marullo, Eric F. Lucking, Daniel Pender, Pardeep Dhaliwal, and Ken D. O'Halloran

Abstract

Sleep apnea is characterized by bouts of chronic intermittent hypoxia (CIH) that elicit sympathetic hyperactivity resulting in residual hypertension. We previously demonstrated that exposure to CIH increases cardiac output and sought to determine if enhanced cardiac contractility manifests prior to hypertension.

Male Wistar rats were exposed to cyclical bouts of hypoxia ($\text{FiO}_2 = 0.05$ nadir; 90 s) and normoxia ($\text{FiO}_2 = 0.21$; 210 s) 8 h/day for 3 days (CIH; $n = 6$). Control animals ($n = 7$) were exposed to room air. Data are presented as mean \pm SD and were analyzed using unpaired Student *t*-tests.

Three-day exposure to CIH did not elicit changes in heart rate and blood pressure ($p > 0.05$). However, baseline left ventricular contractility ($\text{dP}/\text{dt}_{\text{MAX}}$) was significantly increased in CIH-exposed animals compared with control (15300 ± 2002 vs. 12320 ± 2725 mmHg/s; $p = 0.025$), despite no difference in catecholamine concentrations. Acute β_1 -adrenoceptor inhibition reduced contractility in CIH-exposed animals

(-7604 ± 1298 vs. -4747 ± 2080 mmHg/s; $p = 0.014$), to levels equivalent to control, while preserving cardiovascular parameters. Sympathetic ganglion blockade (hexamethonium 25 mg/kg; i.v.) produced equivalent cardiovascular responses suggesting similar global sympathetic activity between groups. Interestingly, gene expression of the β_1 -adrenoceptor pathway in cardiac tissue was unchanged.

Our results suggest that CIH increases cardiac contractility via β_1 -adrenoceptor dependent mechanisms prior to development of global sympathetic hyperactivity suggesting that positive cardiac inotropy contributes to the development of hypertension in CIH-exposed rats.

Keywords

Intermittent hypoxia · β_1 -adrenoceptor · Obstructive sleep apnea · Cardiac contractility · Hypertension

A. L. Marullo · E. F. Lucking · D. Pender
P. Dhaliwal · K. D. O'Halloran (✉)
Department of Physiology, School of Medicine,
College of Medicine & Health, University College
Cork, Cork, Ireland
e-mail: k.ohalloran@ucc.ie

5.1 Introduction

Obstructive sleep apnea (OSA) is characterized by chronic intermittent bouts of hypoxia (CIH) due to repetitive obstruction of the upper airway resulting in transient cessation of breathing (Flemons et al. 1999). Individuals with long-term

OSA express deleterious cardiovascular consequences (i.e., nocturnal and diurnal hypertension, stroke, and cardiac failure) driven by sympathetic hyperactivity (Shahar et al. 2001). Animal models that recapitulate the recurrent oxygen desaturation of OSA by exposure to chronic intermittent hypoxia (CIH) consistently develop hypertension (e.g., mouse (Peng et al. 2021), rat (Zoccal et al. 2007), and canine models (Brooks et al. 1997)). The late-stage hypertensive phenotype is primarily driven by elevated peripheral vasoconstriction; however, studies indicate that cardiac output is increased before the onset of peripheral vasoconstriction suggesting that CIH-induced positive cardiac inotropy may contribute to the development of hypertension (Lucking et al. 2014).

Catecholamines function as ligands binding to β_1 -adrenoceptors located specifically in the heart, kidney, and adipocytes. Thus, β_1 -adrenoceptors may play a pivotal role in elevating cardiac work in CIH-exposed animal models. Therefore, in this study, we sought to test the hypothesis that exposure to CIH elicits a β_1 -adrenoceptor dependent increase in left ventricular contractility, which is established before the development of CIH-induced hypertension.

5.2 Methods

5.2.1 Ethical Approval

All procedures on live animals were performed under license from the Government of Ireland Department of Health (B100/4498) in accordance with national and European Union legislation. Experiments were performed conforming with guidelines provided by the University College Cork Animal Welfare Body with prior ethical approval granted by the University College Cork animal ethics committee (AEEC #2013/035).

5.2.2 Chronic Intermittent Hypoxia Protocol

Adult male Wistar rats (10 weeks old; $n = 16$) were randomly assigned to control or chronic

intermittent hypoxia groups. Using a dynamic O_2/N_2 controller (Oxycycler™; Biospherix, New York, NY, USA), animals assigned to the CIH group were exposed to 5-min cycles of 90s hypoxia (nadir, 5% O_2) and 210s of normoxia, for 8 h per day for 3 days during the light phase of the light-dark cycle. This normoxic period allowed for complete recovery from each hypoxic episode, ensuring the hypoxic stimulus was intermittent. Control animals were exposed to the same environmental cues, with normoxia maintained over the 3-day period; however, control animals were not exposed to the high airflows generated during CIH. Room humidity, temperature, O_2 , and light-dark cycle control were all monitored. Each hypoxic cycle resulted in an arterial oxygen desaturation ($SpO_2 \sim 70\%$) followed by subsequent reoxygenation to normoxic levels. This oxygen desaturation-resaturation profile was chosen because nadirs of 70% SpO_2 are commonly found in severe OSA patients (Guilleminault et al. 1986).

5.2.3 Anesthetized In Vivo Preparation

After 3 days of CIH, animals were anesthetized with urethane (1.5 g/kg i.p., 20% w/v) following induction with isoflurane. The depth of anesthesia was monitored throughout by assessment of the reflex response to tail/paw pinch, with supplemental doses (10% of the loading dose) administered i.v. as required. Core body temperature was maintained at 37 °C using a homeothermic blanket system (Harvard Apparatus, Holliston, MA, USA). The right jugular vein was cannulated for i.v. infusion and the right carotid artery cannulated for the insertion of a pressure catheter, which was advanced into the left ventricle (LV). The left femoral artery was also cannulated for recording of arterial blood pressure and analysis of blood gas chemistry. A tracheotomy was performed to ensure patent breathing and to measure tracheal flow and $ETCO_2$. Once surgical preparations were concluded, a 45-min recovery was observed. Thereafter, arterial blood gases were evaluated, and a 10-min period of

baseline cardiorespiratory indices was sampled for assessment.

Cardiorespiratory responsiveness to the manipulation of inspired gases was then evaluated in 5-min epochs, with a 10-min recovery period provided after each gas manipulation. Animals were successively challenged with hypoxia ($FiO_2 = 0.10$, balance N_2), hypercapnia ($FiCO_2 = 0.05$, $FiO_2 = 0.21$, balance N_2), and asphyxia ($FiCO_2 = 0.05$, $FiO_2 = 0.10$, balance N_2).

Subsequently, the cardiovascular response to β -adrenoceptor antagonism was assessed. β_1 -Adrenoceptor inhibition was achieved via atenolol (5 mg/kg; i.v.), β_2 -adrenoceptors were inhibited with ICI-118,551 (2 μ g/kg), and global sympathetic activity was suppressed using the ganglion blocker, hexamethonium (25 mg/kg; i.v.). Washout periods of 10–20 min were provided after each drug administration. Prior to euthanasia, a blood sample was taken for molecular analysis. The animal was then euthanized via anesthetic overdose and the heart removed. The right ventricle (RV) was sectioned away from the rest of the heart and weighed. The left ventricle (LV) and interventricular septum were weighed as a single entity and rapidly frozen in liquid nitrogen and stored at -80°C for later use. Blood samples were centrifuged at 10,000 g for 10 min with 10 μ l heparin saline with plasma aspirated into a clean Eppendorf. Plasma and urine samples were also rapidly frozen in liquid nitrogen and stored at -80°C for later use. Adrenaline and noradrenaline in the plasma and urine of control and CIH-exposed rats were analyzed using a commercially available ELISA kit (KA1877, Abnova).

5.2.4 Gene Expression

RNA was extracted from frozen LV samples (25–50 mg) that were homogenized in Tripure Isolation Reagent (Roche Diagnostics, West Sussex, UK). Reverse Transcription RNA was treated with TURBO DNA-free kit (Life Technologies, Bio-Sciences, Dun Laoghaire, Ireland). A Nanodrop 1000 was utilized to deter-

mine the quantity and purity of the RNA isolated (Thermo Scientific, Wilmington, DE). The integrity of the RNA was also assessed using a gel electrophoresis system (E-gel, Life Technologies, Carlsbad, CA). RNA was reverse transcribed using Transcriptor First-Strand cDNA Synthesis Kit (Roche Diagnostics). cDNA was amplified using RealTime assays and Fast Start Essential DNA Probe Master Mix as per the manufacturer's instructions, using the LightCycler 96 (Roche Diagnostics). All samples were amplified in duplicate alongside RNA negatives, reverse transcriptase negatives, cDNA negatives, and plate calibrator controls. All data were normalized to a housekeeping reference gene, *hprt1*. Several candidate genes were screened, and *hprt1* was found to be the most stable reference gene. Relative expression of genes associated with the β_1 -adrenoceptor pathway was calculated using the $\Delta\Delta\text{CT}$ method to normalize expression to the reference gene with changes in expression displayed as a fold change over the control group.

5.2.5 Data and Statistical Analysis

Statistical analysis was performed using GraphPad Prism (GraphPad Software Inc., USA). Following tests for normality and equal variance in the data sets, unpaired Student t-tests were used for statistical comparisons; absolute p values are reported and $p < 0.05$ was taken as significant. Data are reported in the text as the mean \pm SD (control vs. CIH). Graphical results are presented as box plots showing individual data points, with the median, interquartile range, and maximum and minimum (whiskers) values shown.

5.3 Results

5.3.1 Baseline Cardiovascular Parameters

Three days of CIH exposure were not sufficient to elicit changes in systolic blood pressure (Fig. 5.1a; 124 ± 9 vs. 123 ± 15 mmHg;

$p = 0.4393$), mean arterial blood pressure (Fig. 5.1b; 81 ± 11 vs. 77 ± 11 mmHg; $p = 0.2669$), or heart rate (Fig. 5.1c; 445 ± 47 vs. 468 ± 22 bpm; $p = 0.1493$) in control and CIH-exposed rats, respectively. However, the 3 days of CIH exposure increased left ventricular contractility (Fig. 5.1d; LV dP/dt_{MAX} ; 12321 ± 2725 vs. 15301 ± 2002 mmHg/s; $p = 0.026$), while left ventricular relaxation was similar between groups (Fig. 5.1e; LV dP/dt_{MIN} ; -7977 ± 1081 vs. -7940 ± 1695 mmHg/s; $p = 0.223$). No change was observed in respiratory rate (98 ± 13 vs. 106 ± 11 bpm; $p = 0.135$), tidal volume (Fig. 5.1f; V_T 0.45 ± 0.04 vs. 0.46 ± 0.04 ml/100 g; $p = 0.337$), and minute ventilation (Fig. 5.1g; V_E 43.3 ± 6.5 vs. 48.6 ± 5.0 ml/min/100 g).

5.3.2 Left Ventricular Contractility in Response to Chemostimulation

Interestingly, during 10% O_2 exposure, the hypoxic-induced reduction in left ventricular contractility was larger in control rats compared with CIH-exposed rats (Fig. 5.2a; -34.7 ± 19.8 vs. $-17.8 \pm 18.9\%$; $p = 0.051$) indicating preserved positive inotropy in CIH-exposed rats during hypoxia. However, changes in contractility were similar in control and CIH-exposed rats in response to hypercapnia (Fig. 5.2b; 4.9 ± 4.0 vs. $6.4 \pm 5.6\%$; $p = 0.584$) and asphyxia (Fig. 5.2c; -9.3 ± 15.6 vs. $-8.5 \pm 10.5\%$; $p = 0.918$).

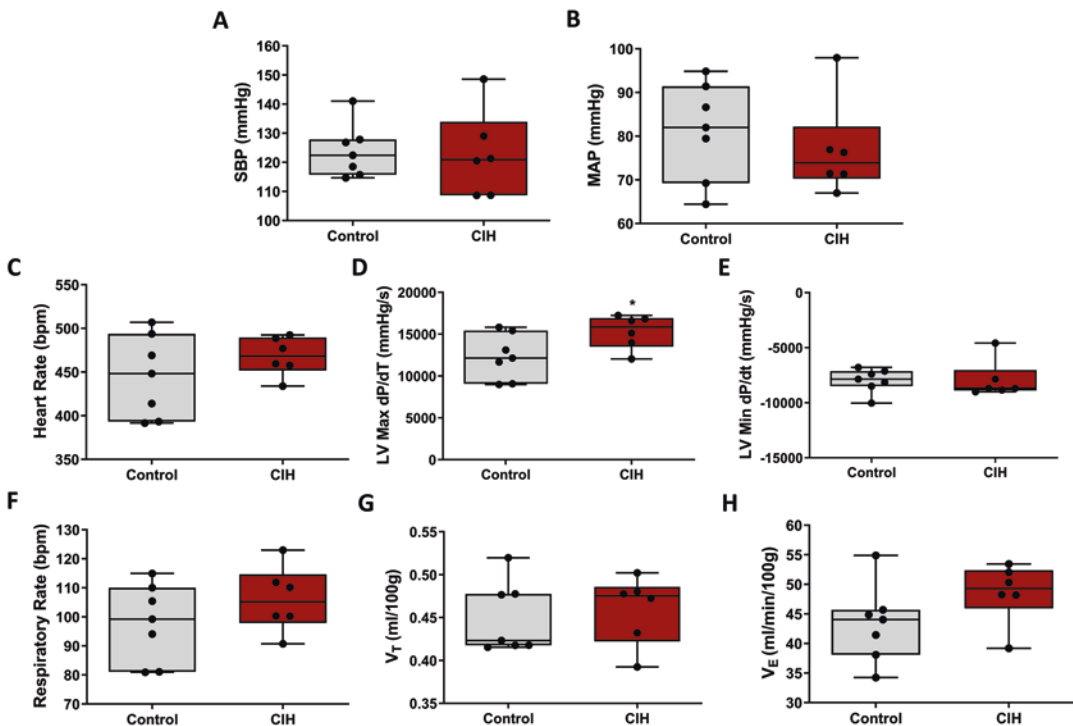


Fig. 5.1 Baseline cardiorespiratory parameters in control and CIH-exposed rats. (a) Systolic blood pressure (SBP; mmHg). (b) Mean arterial pressure (MAP; mmHg). (c) Heart rate (bpm). (d) Left ventricular contractility (LV dP/dt_{MAX} ; mmHg/s).

(e) Left ventricular relaxation (LV dP/dt_{MIN} ; mmHg/s). (f) Respiratory rate (bpm). (g) Tidal volume (V_T ; ml/100 g). (h) Minute ventilation (V_E ; ml/min/100 g).

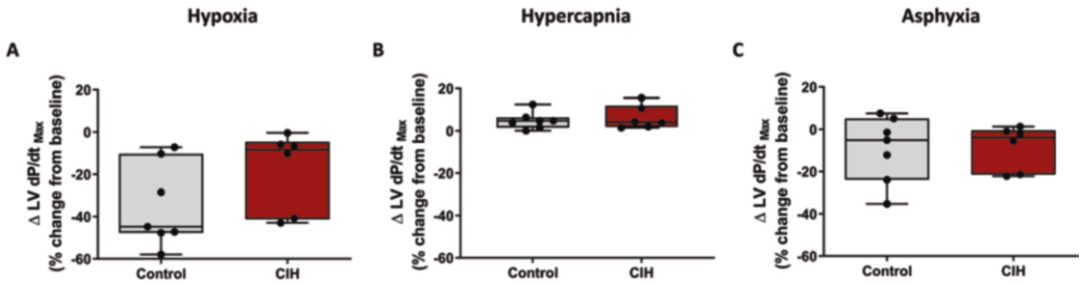


Fig. 5.2 Left ventricular contractility in response to chemostimulation in control and CIH-exposed rats. Left ventricular contractility expressed as a % change from baseline in response to varying chemostimulation. (a) Change in left ventricular contractility (Δ LV dP/dt_{MAX}, %)

during exposure to hypoxia ($\text{FiO}_2 = 0.10$). (b) Change in left ventricular contractility during exposure to hypercapnia ($\text{FiCO}_2 = 0.05$). (c) Change in left ventricular contractility during exposure to asphyxia ($\text{FiCO}_2 = 0.05$; $\text{FiO}_2 = 0.10$)

5.3.3 Cardiovascular Response to β_1 -Adrenoceptor Blockade

Measured as a change from baseline, the response of the following cardiovascular parameters to β_2 -adrenoceptor inhibitor ICI-118,551 (2 $\mu\text{g}/\text{kg}$) remained unchanged both in control and CIH-exposed animals: systolic blood pressure (Fig. 5.3a; -14.0 ± 11.3 vs. $-10.2 \pm 12.3\%$; $p = 0.595$), heart rate (Fig. 5.3b; -7.6 ± 3.3 vs. $-9.9 \pm 4.5\%$; $p = 0.342$), and left ventricular contractility (Fig. 5.3c; -9.5 ± 6.7 vs. $-5.1 \pm 4.5\%$, $p = 0.214$). However, upon administration of the β_1 -adrenoceptor antagonist atenolol (5 mg/kg), CIH-exposed rats demonstrated a greater loss of inotropy compared to control animals (Fig. 5.3f; -45.0 ± 3.5 vs. $-55.3 \pm 2.9\%$; $p < 0.05$), while the change in systolic blood pressure (Fig. 5.3d; -30.7 ± 14.2 vs. $-29.0 \pm 14.4\%$; $p = 0.836$) and heart rate (Fig. 5.3e; -14.3 ± 4.2 vs. $-16.9 \pm 2.8\%$; $p = 0.0241$) was equivalent.

5.3.4 Sympathetic Nervous System Inhibition

Global sympathetic nervous system inhibition via hexamethonium administration (25 $\mu\text{g}/\text{kg}$) in control and CIH-exposed animals yielded similar reductions in systolic blood pressure (Fig. 5.4a:

-51.0 ± 11.6 vs. $-45.0 \pm 12.3\%$; $p = 0.482$), heart rate (Fig. 5.4b: -9.7 ± 13.1 vs. $-12.8 \pm 18.8\%$; $p = 0.786$), and LV contractility (Fig. 5.4c: -38.3 ± 11.3 vs. $-39.1 \pm 15.0\%$; $p = 0.910$).

5.3.5 Gene Expression of the β_1 -Adrenoceptor Pathway

Relative gene expression of *Adrb1* (Fig. 5.5a; 1.11 ± 0.56 vs. 1.04 ± 0.32 ; $p = 0.828$), *Gnas* (Fig. 5.5b; 1.38 ± 0.99 vs. 1.08 ± 0.46 ; $p = 0.590$), *Adcy6* (Fig. 5.5c; 1.11 ± 0.54 vs. 1.10 ± 0.57 ; $p = 0.965$), *Prkaca* (Fig. 5.5d; 1.03 ± 0.26 vs. 1.11 ± 0.65 ; $p = 0.795$), *Pde4b* (Fig. 5.5e; 1.06 ± 0.39 vs. 1.05 ± 0.37 ; $p = 0.976$), *Ryr2* (Fig. 5.5f; 1.01 ± 0.14 vs. 1.09 ± 0.47 ; $p = 0.768$), *Pln* (Fig. 5.5g; 1.05 ± 0.38 vs. 1.03 ± 0.28 ; $p = 0.914$), and *Cacnac1c* (Fig. 5.5h; 1.06 ± 0.39 vs. 1.05 ± 0.37 ; $p = 0.976$) were similar in control ($n = 5$) compared to CIH-exposed left ventricles ($n = 4$).

5.3.6 Catecholamine Concentrations

Plasma concentrations of adrenaline (Fig. 5.6a; 20.5 ± 10.9 vs. 14.5 ± 7.4 $\mu\text{g}/\text{ml}$; $p = 0.296$) and

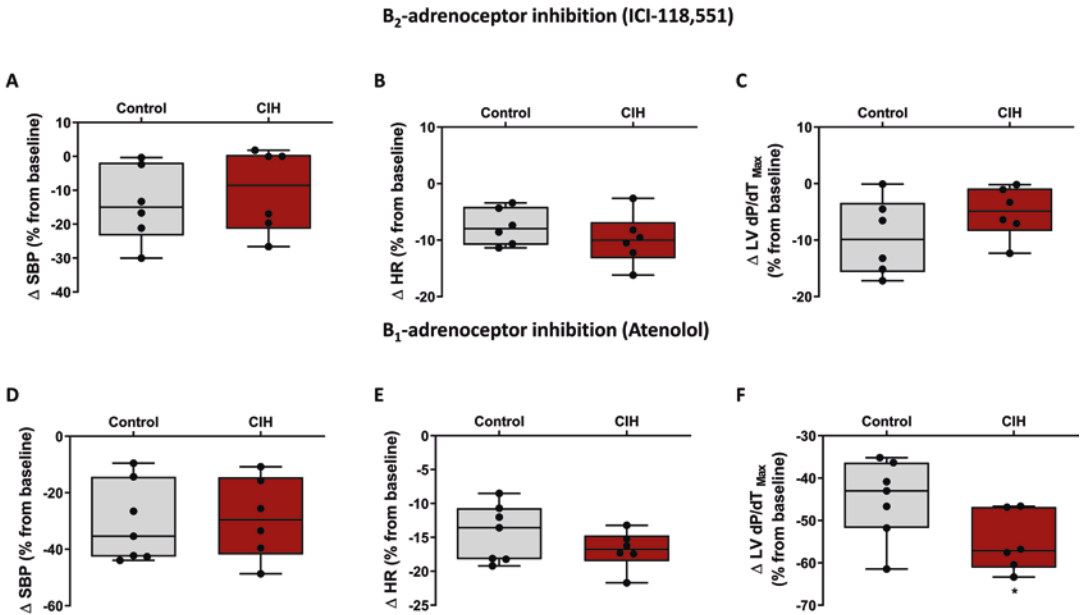


Fig. 5.3 Cardiovascular response to β -adrenoceptor blockade in control and CIH-exposed rats. Changes in cardiovascular parameters in response to the β_2 -adrenoceptor antagonist ICI-118,551 (2 μ g/kg) in control and CIH-exposed rats. (a) Change in systolic blood pressure (Δ SBP, %). (b) Change in heart rate (Δ HR, %). (c)

Change in left ventricular contractility (Δ LV dP/dT_{MAX}, %). Changes in cardiovascular parameters in response to the β_1 -adrenoceptor antagonist atenolol (5 mg/kg). (d) Change in systolic blood pressure (Δ SBP, %). (e) Change in heart rate (Δ HR, %). (f) Change in left ventricular contractility (Δ LV dP/dT_{MAX}, %; * $p < 0.05$)

Hexamethonium sympathetic blockade

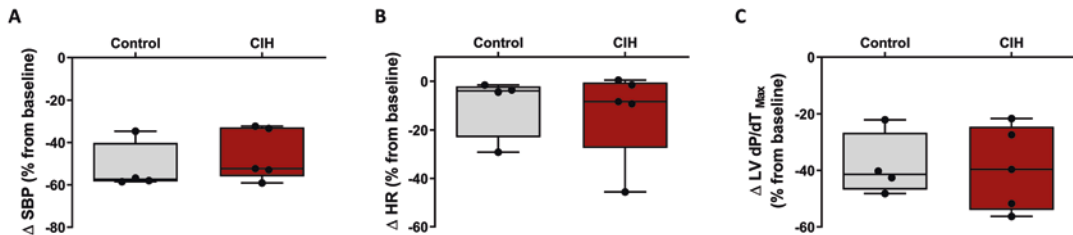


Fig. 5.4 Sympathetic nervous system inhibition in control and CIH-exposed rats. Cardiovascular responses to the sympathetic nervous system blocker hexamethonium (25 μ g/kg) in control and CIH-exposed rats. (a) Change in

systolic blood pressure (Δ SBP, %). (b) Change in heart rate (Δ HR, %). (c) Change in left ventricular contractility (Δ LV dP/dT_{MAX}, %)

noradrenaline (Fig. 5.6b; 37.8 ± 11.1 vs. 24.7 ± 19.2 pg/ml; $p = 0.294$) were equivalent in control and CIH-exposed animals. Urinary concentrations of adrenaline (Fig. 5.6c; 16.26 ± 8.49 vs. 21.66 ± 10.86 ng/mg creatinine; $p = 0.150$) and noradrenaline (Fig. 5.6d; 10.05 ± 6.89 vs. 7.39 ± 4.97 ng/mg creatinine; $p = 0.201$) were also similar in control and CIH-exposed animals.

5.4 Discussion

We sought to determine the mechanisms responsible for the manifestation of increased cardiac output after short-term exposure to CIH. Compared to control, CIH-exposed rats did not show evidence of enhanced global sympathetic activation as catecholamine concentrations

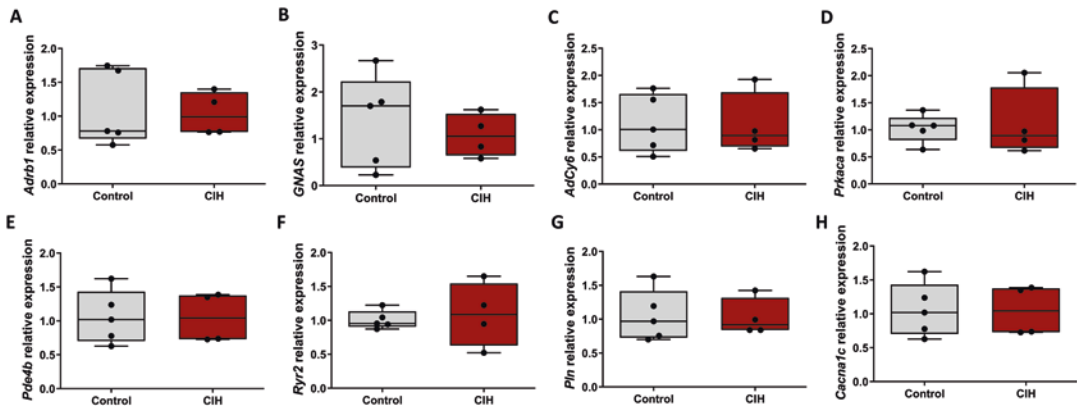


Fig. 5.5 Gene expression of the β_1 -adrenoceptor pathway in control and CIH-exposed rats. Relative expression of key genes associated with the β_1 -adrenoceptor pathway in control and CIH-exposed rats

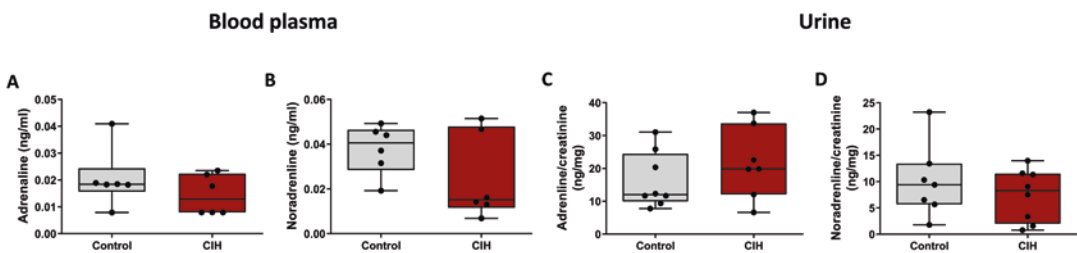


Fig. 5.6 Plasma and urinary catecholamine concentrations in control and CIH-exposed rats. (a, b) Plasma adrenaline (ng/ml) and noradrenaline (ng/ml) concentra-

tions. (c, d) Urine adrenaline and noradrenaline concentrations normalized to creatinine (ng/mg creatinine) in control vs. CIH-exposed rats

were similar and global inhibition of the sympathetic nervous system yielded similar cardiovascular responses. This was consistent with the observation that both systolic blood pressure and mean arterial blood pressure did not change after 3 days of exposure to CIH. However, in support of our hypothesis, cardiac contractility was significantly elevated after 3 days of exposure to CIH. Moreover, the CIH-induced increase in cardiac contractility was reversed after administration of the β_1 -adrenoceptor blocker atenolol, reducing LV contractility to levels comparable to control animals. These data suggest that β_1 -adrenoceptor activation is wholly responsible for driving the CIH-induced positive cardiac inotropy. However, we did not observe an upregulation of genes associated with the β_1 -adrenoceptor pathway. This suggests that β_1 -adrenoceptors are not overexpressed; however, analysis via Western blot would be required to confirm the abundance of β_1 -adrenoceptors in CIH-exposed cardiac tis-

sue. A plausible explanation for β_1 -adrenoceptor-mediated increased ventricular contractility includes an increase in adrenoceptor efficacy, that is, the adrenoceptors effect a greater response for a given stimulus. Alternatively, sympathetic nervous system hyperactivity specific to the cardiac branch would induce increased cardiac work without influencing peripheral resistance via α -adrenoceptors. Further experiments are warranted to evaluate the molecular mechanisms of β_1 -adrenoceptor-mediated LV hypercontractility in CIH-exposed animals.

5.4.1 Hypoxia and the Cardiovascular System

Hypoxia is a profound stressor on the cardiovascular system affecting multiple regions in unique ways. Acute hypoxia results in localized vasodila-

tion (Carrier et al. 1964), dropping blood pressure, which in turn activates the baroreflex causing an increase in sympathetic activity (Mancia et al. 1984), while also eliciting a localized response on the heart, resulting in bradycardia and myocardial depression (van Beek 1998). Hypoxia also activates O_2 -sensing glomus cells within the carotid bodies that result in further downstream activation of the sympathetic nervous system, resulting in peripheral vasoconstriction, hyperventilation, as well as vagally mediated bradycardia (de Burgh et al. 1979). Repetitive exposure to intermittent hypoxia augments carotid body sensitivity, a phenomenon partially caused by enhanced ROS production that manifests from recurrent deoxygenation-reoxygenation cycles (Semenza and Prabhakar 2018). Increased peripheral chemoreceptor sensitivity enhances sympathetic activation perpetuating the hypertensive phenotype associated with OSA.

Hypertension associated with OSA is primarily driven by peripheral vasoconstriction. Whereas CIH-induced hypertension can present as early as 1–2 days into CIH exposure (Marcus et al. 2009), it is also reported to be relatively delayed between 12 and 21 days in rats, preceded by enhanced chemosensory function and autonomic imbalance (Iturriaga et al. 2009). Mean arterial pressure is the product of total peripheral resistance and cardiac output. Previous studies have observed a decrease in cardiac output in long-term CIH animal models (Chen et al. 2005), but others have

observed tachycardia and increased left ventricular function (Marcus et al. 2009). The apparently conflicting findings may relate to the experimental model and magnitude of the hypoxic exposure but most likely are a result of differences in the cumulative duration of exposure to CIH, that is, short term (days to weeks) compared with long term (weeks to months).

Interestingly, hypoxia can also directly activate β_1 -adrenoceptors, which may be essential to hypoxia inducible factor-1 (HIF-1) accumulation (Cheong et al. 2016). HIF-1 functions to increase erythrocyte production and angiogenesis during hypoxia to allow for adequate oxygenation of tissues (Gleadle and Ratcliffe 1997). A study assessing the relationship between β_1 -adrenoceptors and HIF-1 observed a significant decrease in HIF-1 levels in mice treated with beta blockers (Cheong et al. 2016). Additionally, other work suggests that reduced contractility in HIF-1 α null mice could be associated with hypovascularity, modified energy metabolism, or calcium signaling (Huang et al. 2004).

Our model of short-term exposure to CIH was not associated with hypertension or elevations in plasma and urine catecholamine levels; however, we did observe an increase in left ventricular contractility. The positive cardiac inotropy was returned to control levels upon administration of the β_1 -adrenoceptor antagonist atenolol, as shown in Fig. 5.7. The CIH-induced increase in contractility may relate to combined β_1 -adrenoreceptor

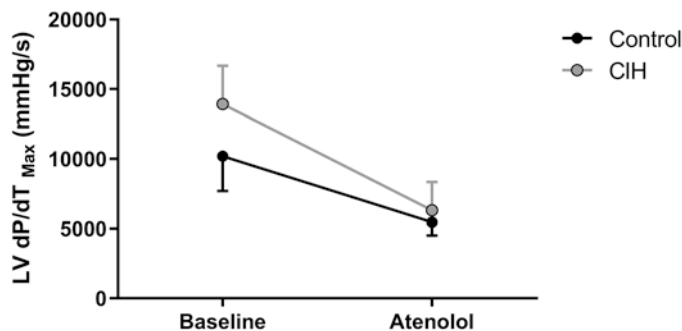


Fig. 5.7 Left ventricular contractility in control and CIH-exposed rats before and after atenolol. Left ventricular contractility (LV dP/dT_{MAX} ; mmHg/s) before (baseline) and after β_1 -adrenoceptor blockade with atenolol. Two-

way ANOVA with Sidak's multiple comparison tests revealed $p = 0.010$ for control vs. CIH at baseline and $p = 0.727$ for control vs. CIH following atenolol

activation and HIF-1 associated transcriptional changes in cardiomyocytes in response to episodic hypoxia.

5.5 Conclusion

Our study was designed to assess the cardiovascular effects of short-term (3 days) exposure to CIH in rats to elucidate early physiological responses that may contribute to the elaboration of the well-recognized CIH-induced hypertension. Our findings indicate that 3 days of exposure to CIH increases left ventricular contractility without evidence of an increase in sympathetic activation based on similar catecholamine concentrations and cardiovascular responses to sympathetic ganglion blockade in control and CIH-exposed rats. Elevated LV contractility in CIH-exposed rats was acutely reversed by atenolol administration implicating β_1 -adrenoceptor dependent signaling. While the molecular mechanism remains unclear, our findings are supportive of the hypothesis that increased cardiac work drives the manifestation of the hypertensive phenotype during early exposure to CIH.

References

- Brooks D, Horner RL, Kozar LF, Render-Teixeira CL, Phillipson EA (1997) Obstructive sleep apnea as a cause of systemic hypertension. Evidence from a canine model. *J Clin Invest* 99(1):106–109
- Carrier O, Walker JR, Guyton AC (1964) Role of oxygen in autoregulation of blood flow in isolated vessels. *Am J Physiol* 206(5):951–954 [Internet]. Available from: www.physiology.org/journal/ajplegacy
- Chen L, Einbinder E, Zhang Q, Hasday J, Balke CW, Scharf SM (2005) Oxidative stress and left ventricular function with chronic intermittent hypoxia in rats. *Am J Respir Crit Care Med* 172(7):915–920
- Cheong HI, Asosingh K, Stephens OR, Queisser KA, Xu W, Willard B et al (2016) Hypoxia sensing through β -adrenergic receptors. *Ref Inf JCI Insight* 1(21):90240
- de Burgh DM, Angell-James JE, Elsner R (1979) Role of carotid-body chemoreceptors and their reflex interactions in bradycardia and cardiac arrest. *Lancet* 313(8119):764–767
- Flemons WW, Buysse D, Redline S, Oack A, Strohl K, Wheatley J et al (1999) Sleep-related breathing disorders in adults: recommendations for syndrome definition and measurement techniques in clinical research. *Sleep* 22(5):667–689
- Gleadle JM, Ratcliffe PJ (1997) Induction of hypoxia-inducible factor-1, erythropoietin, vascular endothelial growth factor, and glucose transporter-1 by hypoxia: evidence against a regulatory role for Src kinase. *Blood* 89(2):503–509
- Guilleminault C, Motta J, Mihm F, Melvin K (1986) Obstructive sleep apnea and cardiac index. *Chest* 89:331–334
- Huang Y, Hickey RP, Yeh JL, Liu D, Dadak A, Young LH et al (2004) Cardiac myocyte-specific HIF-1 α deletion alters vascularization, energy availability, calcium flux, and contractility in the normoxic heart. *The FASEB Journal* [Internet]. Available from: <https://faseb.onlinelibrary.wiley.com/doi/10.1096/fj.04-1510fj>
- Iturriaga R, Rey S, del Rio R, Moya EA, Alcayaga J (2009) Arterial chemoreceptors. In: Gonzalez C, Nurse CA, Peers C (eds) *Adv Exp Med Biol* 648:329–335 [Internet]. Available from: <http://link.springer.com/10.1007/978-90-481-2259-2>
- Lucking EF, O'Halloran KD, Jones JFX (2014) Increased cardiac output contributes to the development of chronic intermittent hypoxia-induced hypertension. *Exp Physiol* 99(10):1312–1324
- Mancia G, Grassi G, Bertinieri G, Ferrari A, Zanchetti A (1984) Arterial baroreceptor control of blood pressure in man. *J Auton Nerv Syst* 11:115–124
- Marcus NJ, Olson EB, Bird CE, Philippi NR, Morgan BJ (2009) Time-dependent adaptation in the hemodynamic response to hypoxia. *Respir Physiol Neurobiol* 165(1):90–96
- Peng YJ, Su X, Wang B, Matthews T, Nanduri J, Prabhakar NR (2021) Role of olfactory receptor78 in carotid body-dependent sympathetic activation and hypertension in murine models of chronic intermittent hypoxia. *J Neurophysiol* 126(6):2054–2067
- Semenza GL, Prabhakar NR (2018) The role of hypoxia-inducible factors in carotid body (patho) physiology. *J Physiol* 596(15):2977–2983
- Shahar E, Whitney CW, Redline S, Lee ET, Newman AB, Javier Nieto F et al (2001) Sleep-disordered breathing and cardiovascular disease cross-sectional results of the Sleep Heart Health Study. *Am J Respir Crit Care Med* 163:19–25 [Internet]. Available from: www.ats-journals.org
- van Beek JHGM (1998) Effects of hypoxia and hypercapnia on cardiac contractility and energetics. *Physiol Pharmacol Cardio-Resp Control*:19–24
- Zoccal DB, Bonagamba LGH, Antunes-Rodrigues J, Machado BH (2007) Plasma corticosterone levels is elevated in rats submitted to chronic intermittent hypoxia. *Auton Neurosci* 134(1–2):115–117



The Beneficial Effect of the Blockade of Stim-Activated TRPC-ORAI Channels on Vascular Remodeling and Pulmonary Hypertension Induced by Intermittent Hypoxia Is Independent of Oxidative Stress

Rodrigo Iturriaga  and Sebastián Castillo-Galán

Abstract

Obstructive sleep apnea (OSA), a sleep breathing disorder featured by chronic intermittent hypoxia (CIH), is associated with pulmonary hypertension (PH). Rats exposed to CIH develop systemic and lung oxidative stress, pulmonary vascular remodeling, and PH and overexpress Stim-activated TRPC-ORAI chan-

nels (STOC) in the lung. Previously, we demonstrated that 2-aminoethyl-diphenylborinate (2-APB)-treatment, a STOC-blocker, prevents PH and the overexpression of STOC induced by CIH. However, 2-APB did not prevent systemic and pulmonary oxidative stress. Accordingly, we hypothesize that the contribution of STOC in the development of PH induced by CIH is independent of oxidative stress. We measured the correlation between right ventricular systolic pressure (RVSP) and lung malondialdehyde (MDA) with the gene expression of STOC and morphological parameters in the lung from control, CIH-treated, and 2-APB-treated rats. We found correlations between RVSP and increased medial layer and STOC pulmonary levels. 2-APB-treated rats showed a correlation between RVSP and the medial layer thickness, α -actin-ir, and STOC, whereas RVSP did not correlate with MDA levels in CIH and 2-APB-treated rats. CIH rats showed correlations between lung MDA levels and the gene expression of *TRPC1* and *TRPC4*. These results suggest that STOC channels play a key role in developing CIH-induced PH that is independent from lung oxidative stress.

R. Iturriaga

Facultad de Ciencias Biológicas, Pontificia Universidad Católica de Chile, Santiago, Chile

Centro de Investigación en Fisiología y Medicina de Altura (FIMEDALT), Facultad de Ciencias de la Salud, Universidad de Antofagasta, Antofagasta, Chile

S. Castillo-Galán (✉)

Lab, Neurobiología, Facultad de Ciencias Biológicas, Pontificia Universidad Católica de Chile, Santiago, Chile

Centro de Investigación en Fisiología y Medicina de Altura (FIMEDALT), Facultad de Ciencias de la Salud, Universidad de Antofagasta, Antofagasta, Chile

Laboratory of Nano-Regenerative Medicine, Centro de Investigación e Innovación Biomédica (CIIB), Faculty of Medicine, Universidad de los Andes, Santiago, Chile

Keywords

Obstructive sleep apnea · Stim-activated TRPC-ORAI channels · Pulmonary hypertension · 2-APB · Chronic intermittent hypoxia · Oxidative stress

6.1 Introduction

Obstructive sleep apnea (OSA) is a sleep breathing disorder characterized by chronic intermittent hypoxia (CIH). OSA is associated with mild pulmonary hypertension characterized by a right ventricular systolic pressure (RVSP) higher than 25 mm Hg. Indeed, 20–50% of OSA patients developed mild pulmonary hypertension (Sajkov and McEvoy 2009; Floras 2018). Hypoxia-inducible factors (HIFs), oxidative stress, and calcium dysregulation have been proposed to contribute to the CIH-induced vascular remodeling and pulmonary hypertension (Nisbet et al. 2009; Jin et al. 2014, 2016; Iturriaga and Castillo-Galán 2019; Castillo-Galán et al. 2020). The calcium entry via Stim-activated TRPC-ORAI channels (STOC) plays a significant role in the physiology and pathophysiology of pulmonary circulation (Reyes et al. 2018). Previously, we found that CIH induces overexpression of STOC subunits in the lung (Castillo-Galan et al. 2020). The blockade of STOC with 2-aminoethyl-diphenyl borinate (2-APB) abolishes the development of pulmonary hypertension without affecting the systemic and lung oxidative stress induced by CIH (Castillo-Galan et al. 2022).

It is well known that CIH induces oxidative stress at the systemic and lung levels, which can alter calcium homeostasis and contribute to the pulmonary vascular remodeling (Del Rio et al. 2010; Jin et al. 2016). Previous studies in pre-clinical models of pulmonary hypertension induced by CIH have shown that treatment with antioxidants such as procyanidin and melatonin reduces oxidative stress and pulmonary hypertension (Jin et al. 2014, 2016).

Our previous results showed that 2-APB treatment abolished the development of pulmonary hypertension but did not prevent the increase of systemic and lung oxidative stress levels. These

results suggested that the effects of 2-APB on the pulmonary vasculature are related to the inhibitory action of STOC. Therefore, we hypothesize that the development of vascular alterations and the pulmonary hypertension induced by CIH are related to the increased expression of the STOC subunits but not oxidative stress itself. Accordingly, we measured the correlation of the RVSP and the oxidative stress marker, malondialdehyde (MDA), with the morphologic variables and the gene expression of STOC subunits in the lung of control, CIH-treated rats, and CIH-treated rats plus 2-APB.

6.2 Methods

6.2.1 Animals and Intermittent Hypoxia Protocol

The Scientific Ethical Committee approved the experimental protocols for Animal and Environment Care from the Pontificia Universidad Católica de Chile, Santiago, Chile (ID:180803006), which were performed according to the National Institutes of Health Guide (NIH, USA) for the care and use of animals.

The experiments were performed in 18 male Sprague-Dawley rats (~200 g) from the Center for Innovation in Biomedical Experimental Models (CIBEM) of the Pontificia Universidad Católica de Chile. Rats were fed with a standard diet and access to water ad libitum, and the room temperature was maintained between 23 and 25 °C. Rats were exposed to CIH 5% O₂ for 20 s, followed by 290 s of normoxia, 12 times for 8 h/day, from 9:00 am to 5:00 pm for 28 days. The O₂ levels in the chambers were regulated with a computerized system, which opens and closes solenoid valves that control the entry of N₂ and its removal by a fan (Del Rio et al. 2012, Castillo-Galán et al. 2020, 2022).

6.2.1.1 2-APB Treatment

Rats were randomized and divided into three groups: control normoxic rats (control), CIH-treated rats plus 2-APB (2-APB), and CIH-treated rats + vehicle (vehicle). At 14 days of CIH, rats were anesthetized with isoflurane 2% in

oxygen, and osmotic pumps (2ML4, Alzet Scientific Products, MD, USA) were implanted subcutaneously in the back. Pumps were loaded with 2-APB (Sigma-Aldrich, USA) to produce a continuous release of 10 mg/kg/day or its vehicle (dimethyl sulfoxide/ETOH/saline: 1:5:4). After surgery, both groups were exposed to CIH for 14 more days. The results were compared with the control group of rats exposed to normoxia.

6.2.2 Right Ventricular Systolic Pressure Measurement

At the end of 28 days of CIH, rats were anesthetized with urethane/ α -chloralose (40/800 mg/kg, i.p.) and tracheostomized and artificially ventilated with a RoVent Jr. ventilator (Kent Scientific, Torrington, CT, USA). A thoracotomy was performed to expose the heart. The RVSP was recorded with a heparinized catheter inserted into the right ventricle connected to a Statham P23 transducer (Hato Rey, Puerto Rico, USA). The heart rate was measured from the pressure signal recorded with a PowerLab 16 channels acquisition system (ADInstruments, Castle Hill, Australia) (Castillo-Galán et al. 2022).

6.2.3 STOC Pulmonary Gene Expression

Frozen left lung samples (~100 mg) were homogenized in TRIzol (Thermo Fisher, Waltham, MA, USA). The gene expression of *TRPC1*, *TRPC4*, *TRPC6*, *ORAI1*, *ORAI2*, and *I8S* was determined by real-time PCR (qPCR) in a StepOne Plus equipment (Applied Biosystems, Foster City, CA, USA) with the sequence of the primers used by Castillo-Galán et al. (2020). Relative gene expression was calculated with the 2^{-Ct} method using the *I8S* gene.

6.2.4 Systemic and Pulmonary Oxidative Stress Measurement

The systemic and pulmonary oxidative stress levels were expressed as malondialdehyde (MDA)

concentration. MDA was measured using a specific enzyme immunoassay thiobarbituric acid reactive substance (TBARS) kit (Cayman Chemical, Ann Arbor, MI, USA) in the lung tissue and the plasma following the manufacturer's instruction (Castillo-Galán et al. 2022).

6.2.5 Vascular Remodeling and Immunohistochemistry

Samples of ~1 cm of the external portion of the medium lobe from the left lung were fixed by immersion in paraformaldehyde 4%, included in paraffin blocks, and cut in 3–5 μ m slides. For the morphological analysis, the slides were deparaffinized, dehydrated, and stained with Van Gieson. The percentage of muscle layer (%Muscle layer) was determined using the following formula: muscle area – lumen area/muscle area * 100 (Castillo-Galán et al. 2020).

Immunohistochemical detection of α -actin (Clone RM253, Sigma-Aldrich, Missouri, USA, dilution: 1:400) and Ki-67 (Clone MIB-1, Dako, Glostrup, Denmark, dilution 1:100) was performed. The α -actin-ir in the muscle layer of small pulmonary arteries was measured as pixel count per area. The percentage of KI-67-ir positive nuclei in the medial layer of pulmonary arterial smooth muscle cells (PASMC) was calculated as the percentage of positive KI-67 nuclei (Castillo-Galán et al. 2016, 2022).

6.2.6 Data Analysis, Pearson Correlation, and Statistical Analyses

We performed a new analysis of our previously published results (Castillo-Galan et al. 2022). We performed a correlational analysis using the Pearson correlation coefficient (Williams et al. 2020) between RVSP with the levels of medial layer, α -actin-ir, KI-67, lung MDA, plasma MDA, *TRPC1*, *TRPC4*, *TRPC6*, *ORAI1*, and *ORAI2* (Fig. 6.1a–j) and between the lung MDA levels with RVSP, medial layer, α -actin-ir, KI-67, plasma MDA, *TRPC1*, *TRPC4*, *TRPC6*, *ORAI1*, and *ORAI2* (Fig 6.2a–j). The results were analyzed

and plotted in GraphPad Prism6.01 (GraphPad Software Inc., CA, USA). Statistically differences were considered significant at $P < 0.05$.

6.3 Results

6.3.1 Pearson's Correlation of Physiological Variables Related to Right Ventricle Systolic Pressure

In the control animals, RVSP did not show any significant correlation with all variables studied (Fig. 6.1a-j). Rats exposed for 28 days to CIH plus vehicle showed a direct significant correlation with the %Muscle layer ($r = 0.936$, $r^2 = 0.878$, $P = 0.006$) and the pulmonary expression of the STOC subunits *TRPC1* ($r = 0.913$, $r^2 = 0.834$, $P = 0.01$), *TRPC4* ($r = 0.8418$, $r^2 = 0.71$, $P = 0.035$), and *TRPC6* ($r = 0.894$, $r^2 = 0.764$, $P = 0.049$) (Fig. 6.1a, f-h). The rats exposed to CIH plus 2-APB showed a significant correlations between RVSP and the %Muscle layer ($r = 0.964$, $r^2 = 0.930$, $P = 0.001$), α -actin-ir ($r = 0.965$, $r^2 = 0.921$, $P = 0.002$), and the STOC subunits *TRPC1* ($r = 0.921$, $r^2 = 0.847$, $P = 0.004$), *TRPC4* ($r = 0.987$, $r^2 = 0.974$, $P = 0.0001$), and *Orai1* ($r = 0.874$, $r^2 = 0.763$, $P = 0.015$) (Fig. 6.1a, b, f-h).

6.3.2 Pearson's Correlation of Physiological Variables Related to MDA Concentrations at the Pulmonary Level

In control rats, we did not find significant correlations between lung MDA levels and all the variables. Similarly, CIH-treated rats with 2-APB did not show significant correlations to all variables. On the other hand, rats exposed to CIH plus vehicle treated rats showed a significant correlation between the pulmonary MDA levels and the pulmonary gene expression of *TRPC1* ($r = 0.923$, $r^2 = 0.862$, $P = 0.007$) and *TRPC4* ($r = 0.833$, $r^2 = 0.695$, $P = 0.039$) (Fig. 6.2f, g).

6.4 Discussion

The main findings of this study showed that CIH-increased RVPS was correlated with the pulmonary vascular remodeling and the increased gene expression of *TRPC1*, *TRPC4*, and *TRPC6*. The rats exposed to CIH plus 2-APB presented significant correlations between RVSP and pulmonary vascular remodeling and pulmonary gene expression of *TRPC1* and *TRPC4*. No correlation was found between lung MDA with RVPS, vascular remodeling variables, and STOC subunits. These results suggest that the effects of 2-APB on RVPS is due to its anti-remodeling effects of 2-APB, which directly correlated to the reduction of the gene expression of STOC subunits, suggesting a main role for STOC, specifically for the subunits *TRPC1*, *TRPC4*, and *TRPC6* in the development of CIH-induced pulmonary hypertension. When analyzing the correlations regarding the oxidative stress levels at the pulmonary level (MDA concentration), we found that the animals exposed to 28 days of CIH presented significant correlations with the gene expression of *TRPC1* and *TRPC4*. On the contrary, the animals exposed to CIH that received 2-APB did not show significant correlations between RVPS and the analyzed variables. These results suggest that STOC subunits play a crucial role in the development of pulmonary hypertension induced by exposure to CIH and that the antihypertensive effect did not correlate with the oxidative stress at the pulmonary level measured as MDA. Although an antioxidant action of 2-APB has been suggested in a model of damage by ischemia/reperfusion in mouse cardiomyocytes (Moriyama et al. 2017), present results did support any antioxidant effect for 2-APB, which may reduce the pulmonary hypertension.

It is known that oxidative stress increases the expression of STOC and STOC-dependent calcium entry. Indeed, in rat PSMC, the activation of *TRPC1* and *TRPC6* channels by the transcription factor BMP4 depends on the NOX4-mediated increase in ROS (Jiang et al. 2014). It has been proposed that ROS induced by hypoxia activates the RyR receptors, depleting calcium from the reticulum and activating STIM1, which in turn

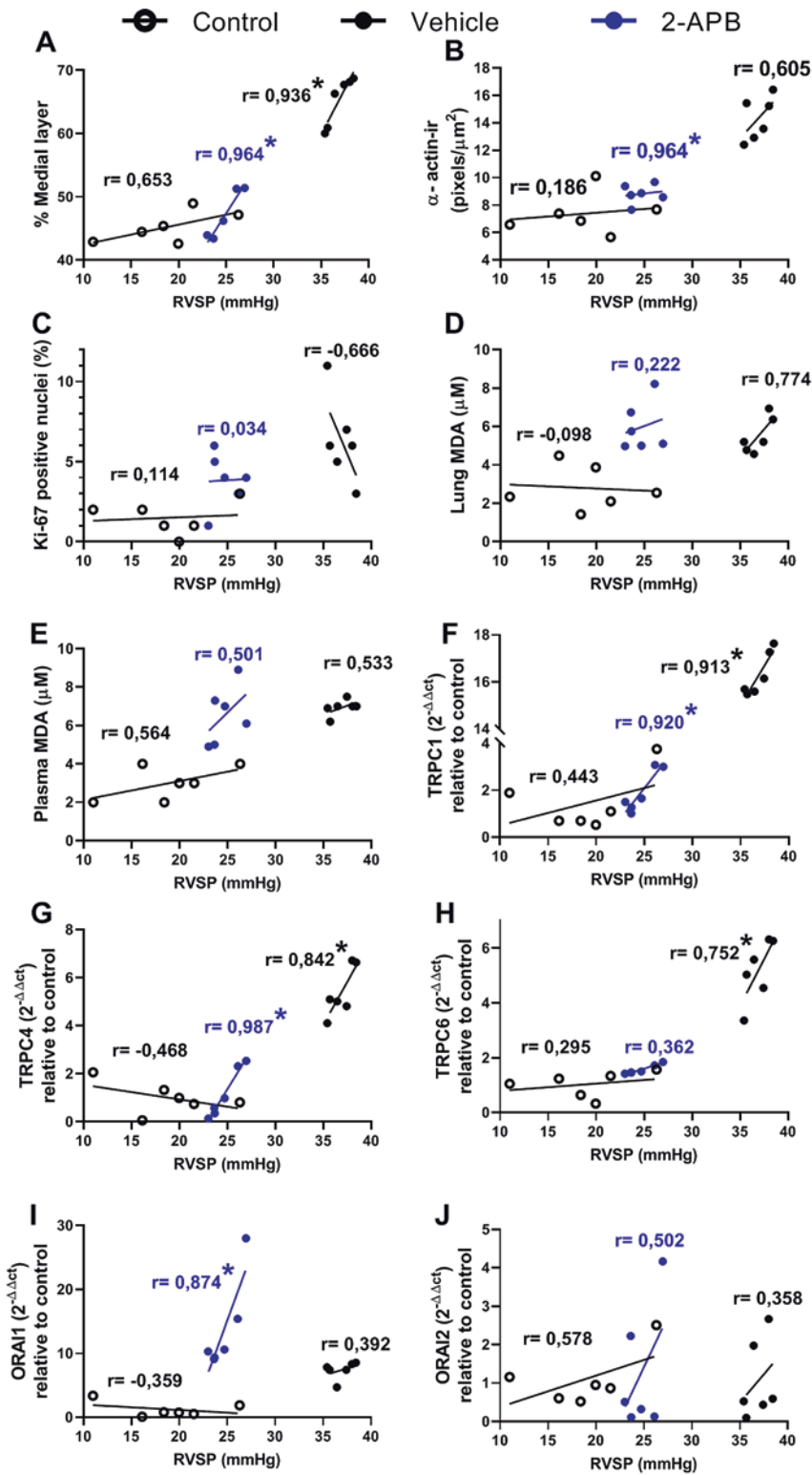


Fig. 6.1 Pearson's correlation of physiological variables related to right ventricle systolic pressure. Pearson's correlation in control animals (open circles, $n = 6$), 2-APB-vehicle treated animals (black circles, $n = 6$), and animals treated with 2-APB (blue circles = 6). $r = 1$: perfect correlation;

$r = 0$: there is no change in the variables; $0 > r > 0$: one variable increases and the other decreases. $r > 0$: the variables tend to increase or decrease together; $r = 1$: perfect correlation; $1 > r > 0$: the variables tend to increase or decrease together; $r = 0$: there is no change in the variables; $0 > r$: one variable increases and the other decreases. Data expressed as X/Y correlation. *, $P < 0.05$

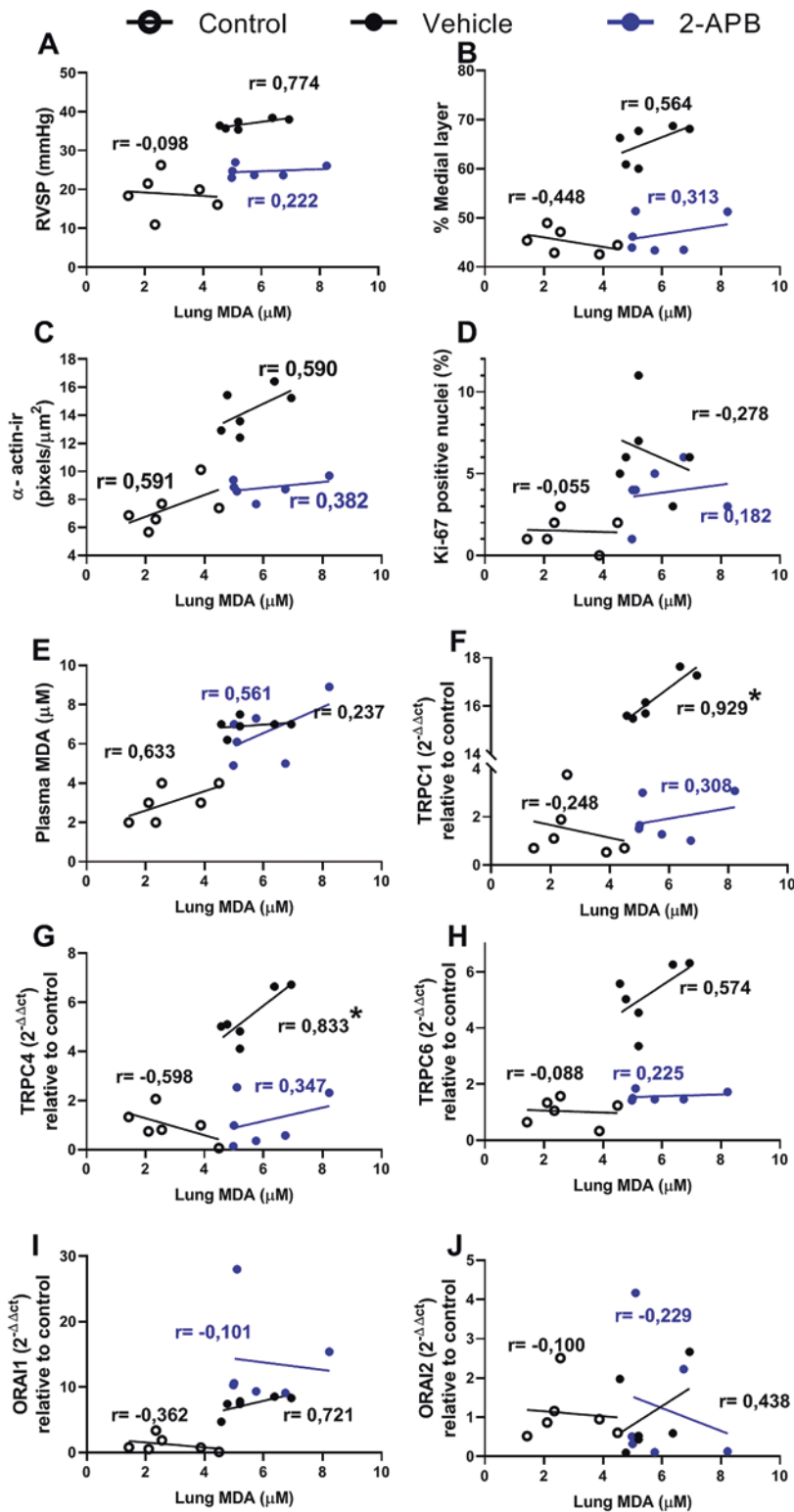


Fig. 6.2 Pearson's correlation of physiological variables related to MDA concentrations at the pulmonary level. Pearson's correlation in control animals ($n = 6$), 2-APB-vehicle treated animals (black circles, $n = 6$), and animals treated with 2-APB (blue circles = 6).

$r = 1$: perfect correlation; $1 > r > 0$: the variables tend to increase or decrease together; $r = 0$: there is no change in the variables; $0 > r$: one variable increases and the other decreases. Data expressed as X/Y correlation. *, $P < 0.05$

allows the interaction with ORAI in the plasma membrane producing the subsequent activation of STOCs (Sommer et al. 2016; Reyes et al. 2018). On the other hand, it has been shown in PASMC isolated from rats that the increase of H2O2 resulting from exposure to hypoxia for 24 and 48 h of increases the expression gene and protein TRPC1, STIM1, and ORAI1, promotes the activation of STIM1 and sub-sequent interaction with ORAI1 and TRPC1, inducing an increase in SOCE (Chen et al. 2017). Finally, it was found in COS 7 cells transfected with STIM1 that H2O2 promotes the activation of STIM1 in an independent way of reticular calcium depletion (Hawkins et al. 2010).

These results suggested that oxidative stress may contribute to the overexpression and activation of STOC subunits but not the pulmonary pathology itself. Present results indicate that the STOC is the main factor for inducing and establishing pulmonary hypertension, but not the oxidative itself.

Acknowledgments Supported by FONDECYT #1211443 from ANID, Fondecyt Postdoctorado N° 3230447 from ANID, and Basal Funding for Scientific and Technological Center of Excellence, IMPACT, #FB210024 from ANID.

References

- Castillo-Galan S, Quezada S, Moraga F et al (2016) 2-Aminoethylidiphenylborinate modifies the pulmonary circulation in pulmonary hypertensive newborn lambs partially gestated at high altitude. *Am J Phys Lung Cell Mol Phys* 311:L788–L799. <https://doi.org/10.1152/ajplung.00230.2016>
- Castillo-Galán S, Arenas GA, Reyes RV et al (2020) Stim-activated TRPC-ORAI channels in pulmonary hypertension induced by chronic intermittent hypoxia. *Pulm Circ* 10:13–22. <https://doi.org/10.1177/2045894020941484>
- Castillo-Galán S, Riquelme B, Iturriaga R (2022) Crucial role of stromal interaction molecule-activated TRPC-ORAI channels in vascular remodeling and pulmonary hypertension induced by intermittent hypoxia. *Front Physiol* 17(13):841828. <https://doi.org/10.3389/fphys.2022.841828>
- Chen TX, Xu XY, Zhao Z, Zhao FY et al (2017) Hydrogen peroxide is a critical regulator of the hypoxia-induced alterations of store-operated Ca²⁺ entry into rat pulmonary arterial smooth muscle cells. *Am J Phys Lung Cell Mol Phys* 312(4):L477–L487. <https://doi.org/10.1152/ajplung.00138.2016>
- Del Rio R, Moya EA, Iturriaga R (2010) Carotid body and cardiorespiratory alterations in intermittent hypoxia: the oxidative link. *Eur Respir J* 36:143–150. <https://doi.org/10.1183/09031936.00158109>
- Del Rio R, Moya EA, Parga MJ et al (2012) Carotid body inflammation and cardiorespiratory alterations in intermittent hypoxia. *Eur Respir J* 39:1492–1500. <https://doi.org/10.1183/09031936.00141511>
- Floras JS (2018) Sleep apnea and cardiovascular disease: an enigmatic risk factor. *Circ Res* 122(12):1741–1764. <https://doi.org/10.1161/CIRCRESAHA.118.310783>
- Hawkins BJ, Irrinki KM, Mallilankaraman K, Lien et al (2010) S-glutathionylation activates STIM1 and alters mitochondrial homeostasis. *J Cell Biol* 190(3):391–405. <https://doi.org/10.1083/jcb.201004152>
- Iturriaga R, Castillo-Galán S (2019) Potential contribution of carotid body-induced sympathetic and renin-angiotensin system overflow to pulmonary hypertension in intermittent hypoxia. *Curr Hypertens Rep* 21(11):89. <https://doi.org/10.1007/s11906-019-0995-y>
- Jiang Q, Fu X, Tian L, Chen Y, Yang K, Chen X, Zhang J, Lu W, Wang J (2014) NOX4 Mediates BMP4-induced upregulation of TRPC1 and 6 protein expressions in distal pulmonary arterial smooth muscle cells. *PLoS One* 9(9):e107135. <https://doi.org/10.1371/journal.pone.0107135>
- Jin H, Wang Y, Zhou L, Liu L et al (2014) Melatonin attenuates hypoxic pulmonary hypertension by inhibiting the inflammation and the proliferation of pulmonary arterial smooth muscle cells. *J Pineal Res* 57:442–450. <https://doi.org/10.1111/jpi.12184>
- Jin H, Liu M, Zhang X et al (2016) Grape seed procyanidin extract attenuates hypoxic pulmonary hypertension by inhibiting oxidative stress and pulmonary arterial smooth muscle cells proliferation. *J Nutr Biochem Elsevier BV* 36:81–88. <https://doi.org/10.1016/j.jnutbio.2016.07.006>
- Morihara H, Obana M, Tanaka S et al (2017) 2-aminoethoxydiphenyl borate provides an anti-oxidative effect and mediates cardioprotection during ischemia reperfusion in mice. *PLoS One* 12:1–20. <https://doi.org/10.1371/journal.pone.0189948>
- Nisbet RE, Graves AS, Kleinhenz DJ et al (2009) The role of NADPH oxidase in chronic intermittent hypoxia-induced pulmonary hypertension in mice. *Am J Respir Cell Mol Biol* 40:601. <https://doi.org/10.1165/2008-0145OC>
- Reyes RV, Castillo-Galán S, Hernandez I et al (2018) Revisiting the role of TRP, Orai, and ASIC channels in the pulmonary arterial response to hypoxia. *Front Physiol* 9:1–9. <https://doi.org/10.3389/fphys.2018.00486>
- Sajkov D, McEvoy RD (2009) Obstructive sleep apnea and pulmonary hypertension. *Prog Cardiovasc Dis* 51(5):363–370. <https://doi.org/10.1016/j.pcad.2008.06.001>
- Salnikow K, Kluz T, Costa M et al (2002) The regulation of hypoxic genes by calcium involves c-Jun/AP-1, which cooperates with hypoxia-inducible factor 1 in

- response to hypoxia. *Mol Cell Biol* 22:1734–1741. <https://doi.org/10.1128/MCB.22.6.1734-1741.2002>
- Somers VK, White DP, Amin R et al (2008) Sleep apnea and cardiovascular disease. An American Heart Association/American College of Cardiology foundation scientific statement from the American Heart Association Council for High Blood Pressure Research Professional Education Committee, Council on. *J Am Coll Cardiol* 52:686–717. <https://doi.org/10.1016/j.jacc.2008.05.002>
- Sommer N, Strielkov I, Pak O, Weissmann N (2016) Oxygen sensing and signal transduction in hypoxic pulmonary vasoconstriction. *Eur Respir J* 47(1):288–303. <https://doi.org/10.1183/13993003.00945-2015>
- Williams B, Halloin C, Löbel W, Finklea F, Lipke E, Zweigerdt R, Cremaschi S (2020) Data-driven model development for cardiomyocyte production experimental failure prediction. In: *Computer aided chemical engineering*, vol 48. Elsevier, Amsterdam, pp 1639–1644



Intermittent Hypoxia and Weight Loss: Insights into the Etiology of the Sleep Apnea Phenotype

7

Marianne Gagnon, Stéphanie Fournier,
François Marcouiller, Loralie Guay,
Vincent Joseph, Natalie J. Michael,
and Richard Kinkead

Abstract

Sleep apnea (SA) is a major respiratory disorder with increased risk for hypertension and obesity; however, our understanding of the origins of this complex disorder remains limited. Because apneas lead to recurrent drops in O_2 during sleep, intermittent hypoxia (IH) is the main animal model to explore the pathophysiology of SA. Here, we assessed the impacts of IH on metabolic function and related signals. Adult male rats were exposed to 1 week of moderate IH ($FiO_2 = 0.10\text{--}30$ s, ten cycles/hour, 8 h/day). Using whole-body plethysmography, we measured respiratory variability and apnea index during sleep.

Blood pressure and heart rate were measured by the tail-cuff method; blood samples were taken for multiplex assay. At rest, IH augmented arterial blood pressure, respiratory instability, but not apnea index. IH induced weight, fat, and fluid loss. IH also reduced food intake and plasma leptin, adrenocorticotrophic hormone (ACTH), and testosterone levels but increased inflammatory cytokines. We conclude that IH does not replicate the metabolic clinical features of SA patient, thus raising our awareness of the limitations of the IH model. The fact that the risk for hypertension occurs before the appearance of apneas provides new insights into the progression of the disease.

M. Gagnon (✉) · N. J. Michael
Centre de Recherche de l'Institut Universitaire de
Cardiologie et Pneumologie de Québec, Québec City,
QC, Canada

Faculty of Pharmacy, Université Laval, Québec City,
QC, Canada
e-mail: marianne.gagnon.15@ulaval.ca

S. Fournier · F. Marcouiller · L. Guay
Centre de Recherche de l'Institut Universitaire de
Cardiologie et Pneumologie de Québec, Québec City,
QC, Canada

V. Joseph · R. Kinkead
Centre de Recherche de l'Institut Universitaire de
Cardiologie et Pneumologie de Québec, Québec City,
QC, Canada

Department of Pediatrics, Faculty of Medicine,
Université Laval, Québec City, QC, Canada

Keywords

Intermittent hypoxia · Sleep apnea · Control
of breathing · Metabolism · Inflammation ·
Whole-body plethysmography

7.1 Introduction

Sleep apnea (SA) is a common respiratory disorder characterized by cyclical cessations (apneas) or reductions (hypopneas) in breathing rate during sleep (Gastaut et al. 1966; Dempsey et al. 2010; Benjafield et al. 2019). The origins of these events can be central (no respiratory effort),

obstructive (upper airway obstruction with inspiratory efforts), or mixed (American Academy of Sleep Medicine 1999). A narrow or collapsible upper airway is a main cause of SA, and obesity is an aggravating factor as the body mass index (BMI) is positively correlated with the severity of SA (Young et al. 2005; Dempsey et al. 2010; White and Younes 2012). Fluid retention, which is common in hypertension and obesity (Miller and Borlaug 2020), can exacerbate the overnight rostral fluid shift and therefore amplify the propensity for airway collapse by increasing tissue pressure in the neck area (White and Bradley 2013).

The fact that SA patients breathe normally during daytime indicates that SA is more than an anatomical problem (Eckert et al. 2013; Eckert and Younes 2014; Eckert 2018). Anomalies in respiratory control become apparent when the respiratory drive associated with wakefulness is lost. In fact, “nonanatomic traits” are estimated to play an important role in 56% of SA patients (Eckert et al. 2013; Eckert 2018). An excessive ventilatory response to hypoxia (high loop gain) is a common “nonanatomical trait”; in SA patients, modest blood gas disturbances during sleep trigger strong responses that lead to arousal and/or transient and cyclical loss of CO₂-related respiratory drive. This, in turn, promotes further respiratory instability and apneas (Dempsey et al. 2010; White and Younes 2012).

Regardless of their origins, apneas generally lead to bouts of hypoxemia that repetitively activate the carotid bodies during the night (Iturriaga et al. 2021). Once it reaches the central nervous system, this chemoafferent signal is widely distributed within the medulla and hypothalamus, and with time, it can contribute to multiple SA-related problems reported in humans, including sleep fragmentation, depression, and cardiovascular and metabolic morbidity (Shamsuzza-man et al. 2003; Alam et al. 2007). As it mimics those repeated drops in arterial O₂, intermittent hypoxia (IH) is the most common animal model for mechanistic studies of SA.

In summary, SA is a complex respiratory disorder that affects multiple physiological systems, and because metabolic disturbance is a common

problem, many endocrine factors such as leptin, hypogonadism, stress, and inflammation have been evoked to explain its pathogenesis. However, there is limited information pertaining to the role of these different hormones to the disease process. In fact, data supporting this hypothesis originates from several studies, and the lack of consistency in the duration and severity of IH protocols used makes it difficult to reach a clear conclusion. To address this issue and gain insights into the progressive development of the key aspects of the SA phenotype, we subjected adult male rats to a moderate IH protocol for 1 week. We then evaluated its impacts on cardiorespiratory function and body composition before taking terminal blood samples to perform a broad evaluation of the hormonal profile of these rats by measuring hormones related to metabolism (leptin, stress hormones), reproduction (sex steroids), and inflammation.

7.2 Methods

7.2.1 Animals and Experimental Groups

All experimental procedures were approved by the Laval University Animal Care Committee in accordance with the Canadian Council on Animal Care. The experiments were carried out on 27 Sprague-Dawley male rats (8 weeks old). Because the prevalence of SA is greater in men than in women prior to menopause (Sunwoo et al. 2018), we chose to focus on male rats. All rats were born and raised in our animal care facility. Animals were given food (chow) and water ad libitum and were kept under standard care conditions (21 °C, 12/12 h light/dark cycle: lights on at 06.00 h and off at 18.00 h).

7.2.1.1 Intermittent Hypoxia Protocol

The animals were randomly assigned to either room air (control) or to a 7-day IH protocol. The ventilated cages that house the animals were connected to an oxy-cycler (Biospherix, Redfield, NY, USA). Within their cage (internal volume

0.05 m³), rats intermittently received a nitrogen-enriched hypoxic mixture, followed by room air for reoxygenation. Each bout of hypoxia lasted 30 s, reached a nadir FIO₂ of 0.10, and was followed by 5-min reoxygenation. Rats were exposed to ten cycles per hour, for 8 h between 10.00 h and 18.00 h. This protocol is based on the original study of Fletcher et al. (1992) and aims to replicate the repeated desaturations and reoxygenation seen in human with sleep apnea; a 1-week protocol is sufficient to increase in blood pressure (Hinojosa-Laborde and Mifflin 2005). Moreover, the moderate depth of hypoxia chosen is more clinically applicable compared to other severe protocols (Dematteis et al. 2009; Toth and Bhargava 2013). The controls were kept in the normoxic condition of the housing room.

7.2.2 Animal Monitoring and Experimental Measurements

Body weight, body composition, blood pressure, and food intake were assessed before the IH protocol and at the end of the experiments (day 7). Body composition of the animals was evaluated using preclinical magnetic resonance imaging (MRI) (Minispec LF90, Bruker Corporation, Massachusetts, USA). Arterial blood pressure was measured by the tail-cuff method by volume pressure recording (CODA system; Kent Scientific, Torrington, CT, USA). The rats were previously acclimatized for 1 h to cylindrical acrylic support and warming mat. The mean blood pressure and heart rate values reported reflect the mean of ten consecutive data points (Feng et al. 2008). These measurement experiments were performed between 08.00 h and 11.00 h to minimize variability related to the circadian rhythm. For food intake, all rats were housed in pairs with a known amount of food. At the end of the experiments, the amount of remaining food was weighed and divided by 2 to calculate the intake for each animal. Ventilatory measurements were performed after the IH protocol (day 7).

7.2.2.1 Ventilatory Measurements

Ventilatory measurements were performed by whole-body flow through plethysmography system (EMKA technologies, Paris, France) according to standard laboratory procedures (Laouafa et al. 2017). Briefly, the rats were placed in a 4.5-l plexiglass plethysmography chamber in which they could move freely. The airflow through the chamber was maintained between 1.5 and 2.0 L/min. Rats acclimatize to the chamber for 1 h before experiments began by recording respiratory activity at rest (normoxia). The respiratory signals were all recorded using Spike2 data acquisition software (version 7.20, Micro 1401 data acquisition system; Cambridge Electronic Design, Cambridge, England). Water pressure, O₂ (RH-300, FC-2 Sable Systems, Las Vegas, NV, USA), and CO₂ (CD-3A, Ametek, Berwyn, PA, USA) levels were continuously measured using gas analyzers. Body temperature was measured with a rectal probe before and after plethysmography recording and reported as mean. Experiments were performed between 09:00 h and 13:00 h, when rats normally sleep.

7.2.2.2 Assessment of Respiratory Reflexes

Following 2 hours of baseline recording, the acute responses to respiratory stimuli were measured. We first induced hypoxia by changing the incoming gas to pure nitrogen for 120 s. A nadir of 10% O₂ was reached within 180 s, and FiO₂ then progressively returned to 0.21 within 10 min. The rats recovered for 1 h before being exposed to hypercapnia by introducing a gas mixture of 21% O₂ and 5% CO₂ for 10 min. This was followed by a period of 1 h to return to normal with ambient air.

7.2.2.3 Data Analysis

Basal respiratory rate (fR), tidal volume (V_T), and minute ventilation (V_E) were obtained during non-rapid eye movement (non-REM) sleep; this sleep/wake state was easily identified based on the stability of the respiratory signals as described by Bastianini et al. (2017). Sighs were defined by a large inspiration with at least twice the normal V_T and followed by a rapid expiration. Apneas

were defined as two missed breaths, after a sigh (post sigh apnea) or without preceding sigh (spontaneous apnea) (Nakamura et al. 2003; Bastianini et al. 2019). During data analysis, the software parameters were adjusted to eliminate non-respiratory signals related to animal movement or sniffing. Body temperature, barometric pressure, room temperature, and humidity were measured to express V_T in milliliters per 100 g according to the equations of Drorbaugh (1955). V_E and oxygen consumption were also corrected for body weight and expressed in BTPS. The respiratory exchange ratio (RER) was reported as V_{CO_2}/V_{O_2} . We expressed the rate of O_2 consumption and CO_2 production as volume (mL) per minute and 100 g of body weight.

Breathing variability was calculated by the nonlinear geometric analysis Poincaré plot, and variability indexes SD1 and SD2 were determined as described by Brennan et al. (2001). SD1 indicates the level of short-term breathing variability and SD2 in long-term records. Variability indexes were assessed for three periods lasting about 400 breaths on stable portions of the respiratory trace and were expressed as the mean (Brennan et al. 2001).

Analysis of the hypoxic ventilatory response focused on the rapid increase of breathing frequency at the onset of hypoxia; this acute phase reflects carotid body activation (Powell et al. 1998). The peak frequency increase measured at 3 min was expressed as a percent change from baseline. Because the ventilatory response to hypercapnia typically reaches “steady state” within 5 min and involves V_T , we measured V_E during the last 3 min of CO_2 exposure; the rat’s response was then expressed as a percent change from baseline.

7.2.2.4 Blood Sampling and Biochemical Analyses

After ventilatory recording, animals were deeply anesthetized with ketamine/xylazine 80–10 mg/ml, and terminal blood samples were obtained by intracardiac puncture. The samples were placed in a serum-gel clotting activator microtube for analysis of sex hormones and in a plasma-gel clotting activator microtube to assess levels of

stress hormones, cytokines and leptin (Sarstedt, Nümbrecht, Germany). The serum and plasma were separated by centrifugation at 9000 rpm for 10 min at 4 °C and stored at –80 °C until assayed. Estradiol, progesterone, testosterone (Millipore MSHMAG-21K), cytokines, and leptin (Millipore RECYTMAG-65K) were measured by a multiplex assay, according to the manufacturer assay protocol (Milliplex, USA). Bead complexes were read on a run plate on Luminex 200 and analyzed by MAGPIX with xPONENT software. Corticosterone and adrenocorticotrophic hormone (ACTH) plasma levels were also measured by a bead-based multiplex assay (Millipore RSHMAG-69K, Milliplex, USA) but were performed by Eve Technologies, Calgary, AB, Canada. Results below the test’s sensitivity (out of range) were eliminated from the analyses, thus explaining why the number of replicates is not the same for each test. Out of range data were observed only for cytokine assays and did not differ between groups: (TNF- α : Ctrl: 9; IH: 5) (IL-10: Ctrl: 3; IH: 2) (IL-1 β : Ctrl: 3; IH: 2).

7.2.3 Statistical Analysis

Data are expressed as means \pm standard deviations of the mean (SD). The effects of exposition (room air vs. IH) on respiratory parameters, metabolic data, as well as hormones analysis were assessed using a one-way ANOVA. For body weight, we used a two-way ANOVA for repeated measures (IH as independent variables and time as the repeated variable). $P < 0.05$ was considered significant. All P-values are indicated in the figures. Statistical analyses were performed using JASP (JASP Team (2022) JASP (Version 0.16.3) [Computer software]). All figures were obtained using SigmaPlot 14.5 (SPSS Inc. and IBM Company, USA).

7.3 Results

Table 7.1 reports baseline values for respiratory variables; IH did not influence those measurements. Body temperature (T_b), measured during

Table 7.1 Respiratory parameters and hormone levels measured under resting conditions at the end of the protocol

	Normoxia	Intermittent hypoxia
Body temperature (T_b : °C)	35.3 ± 0.5 (15)	35.7 ± 0.8 (12)
Breathing frequency (fR: breaths/min)	95.6 ± 10.6 (15)	92.2 ± 9.7 (10)
Tidal volume (V_T : mL/100 g)	0.52 ± 0.10 (15)	0.53 ± 0.11 (10)
Minute ventilation (V_E : mL/min/100 g)	49.7 ± 13.6 (15)	48.8 ± 11.0 (10)
Oxygen consumption rate ($\dot{V}O_2$: mL/min/100 g)	1.19 ± 0.35 (15)	1.41 ± 0.48 (8)
CO ₂ production rate ($\dot{V}CO_2$: mL/min/100 g)	1.27 ± 0.32 (15)	1.21 ± 0.33 (8)
Corticosterone (ng/mL)	108 ± 19 (10)	123 ± 41 (8)
Estradiol (pmol/L)	0.14 ± 0.04 (6)	0.11 ± 0.04 (6)
Progesterone (pmol/L)	2.12 ± 1.81 (7)	0.79 ± 0.61 (6)

Animals were exposed to normoxia (control) or to a FiO_2 of 0.10–30 s, ten cycles/hour, 8 h/day for 7 days

respiratory recordings, was also similar in all groups: 35.3–35.7 °C.

All values are means ± SD. The number of animals for each mean is indicated in parentheses.

7.3.1 Moderate IH Augments Respiratory Instability During Sleep and “Basal” Arterial Blood Pressure

By comparison with normoxic controls, rats subjected to moderate IH showed a decreased apnea frequency during non-REM sleep (Fig. 7.1a) but had a less stable breathing pattern as indicated by the Poincaré plot (Fig. 7.1b, d). Compared to controls, the variability indexes SD1 and SD2 were higher in IH rats (Fig. 7.1c), thus indicating that both the short- and long-term breathing variability was augmented. IH exposure also augmented the mean arterial blood pressure and heart rate (Fig. 7.1e, f, respectively).

7.3.2 IH Increases the Chemoreflex Response

Hypoxia triggered a rapid increase in breathing frequency in all groups, but the response of rodents previously exposed to IH was significantly higher than controls; IH also prolonged the time to recover and return to baseline values (8 min after the onset of the challenge in control, compared to 13 min in IH rats; Fig. 7.2a). On average, the peak response of IH rats was 30% greater than controls (Fig. 7.2b). Conversely, IH reduced the minute ventilation response to CO₂ by 30% (Fig. 7.2c). This effect was mainly due to a reduced V_T response (data not shown).

7.3.3 IH Induces Weight and Fat Loss

While body weights were similar prior to the experiments (day 0), 1-week IH exposure led to significant weight loss, whereas control rats gained weight over the same period (Fig. 7.3a). Analysis of body composition showed that IH decreased the relative body fat and fluids (Fig. 7.3b, c, respectively) and reduced food intake (Fig. 7.3d). Additionally, IH rats showed a reduced leptinemia compared to controls (Fig. 7.3e). Interestingly, leptin levels were positively correlated to the apnea index for the entire population (Fig. 7.3f). Rats subjected to IH had lower respiratory quotient at rest than nonexposed rats (Fig. 7.3g).

7.3.4 IH Reduces ACTH and Testosterone Levels and Promotes Inflammation

IH decreased plasma ACTH and serum testosterone concentrations (Fig. 7.4a, b). IH exposure altered the cytokine profile with higher levels in interleukin-10 (IL-10) and interleukin-1 β (IL-1 β) (Fig. 7.4c, d). Tumor necrosis factor- α (TNF- α) concentrations were unaffected by IH (Fig. 7.4e). IH did not affect corticosterone levels (Table 7.1).

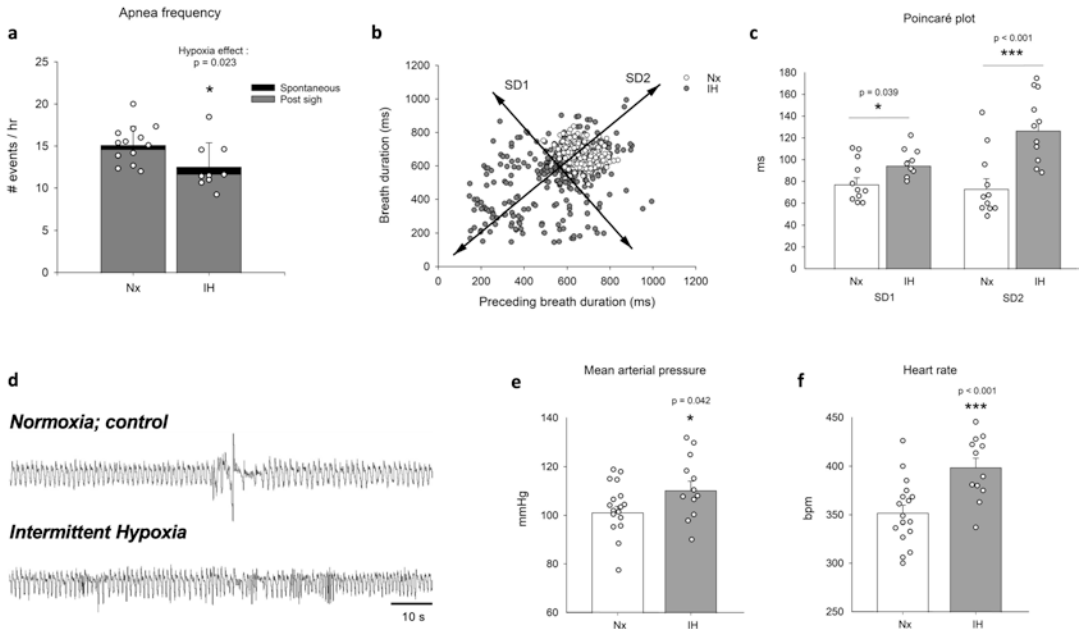


Fig. 7.1 Comparison of respiratory variability in non-REM sleep and cardiovascular variables, between adult male rats exposed to room air (Nx; control) or intermittent hypoxia (IH; $FiO_2 = 0.10\text{--}30$ s, ten cycles/hour, 8 h/day, 7 days). Apnea frequency at rest (a), Poincaré plot showing individual breath duration as a function of the duration of the preceding breath (b), and measures of the dispersion of the points of the Poincaré plot: SD1 and SD2 (c). SD1 indicates the level of short-term breathing variability

and SD2 the long-term. Plethysmographic recordings at rest (d) comparing control rat (top trace) and an IH-exposed rat (bottom trace). Mean arterial pressure (e) and heart rate (f) measured by the tail-cuff method in conscious rats. Sleep states were indirectly according to variability of respiratory signal (Bastianini et al., 2017). All values mean \pm SD. ANOVA results are reported in figures. * $P < 0.05$, *** $P < 0.001$ vs. corresponding groups (as indicated)

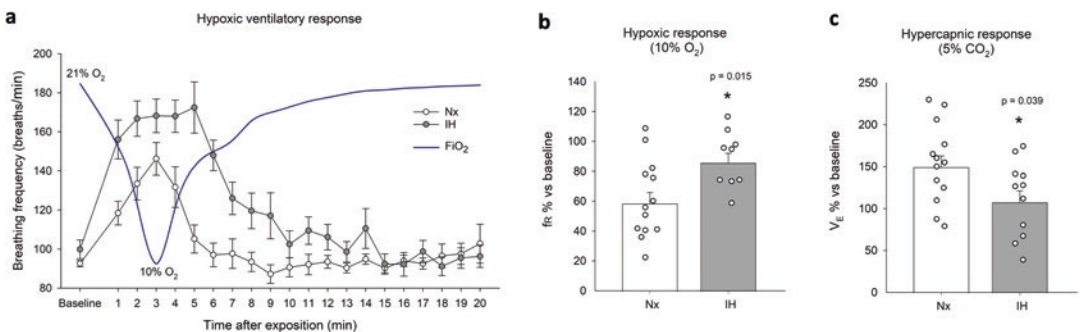


Fig. 7.2 Test of chemoreflex function in adult male rats, exposed to room air (Nx; control) or intermittent hypoxia (IH). Dynamics of the breathing frequency response to hypoxia ($10\% O_2$, 2 min); the dark line illustrates the O_2 level within the chamber over the course of the challenge (a). Peak frequency response measured during the third

minute of hypoxic exposure; values are expressed as percent change from baseline (b). Minute ventilation response to hypercapnia ($5\% CO_2$; 10 min). Values were obtained over the last 3 min of exposure and expressed as a percent change from baseline (c). All values mean \pm SD. ANOVA results are reported in figures. * $P < 0.05$

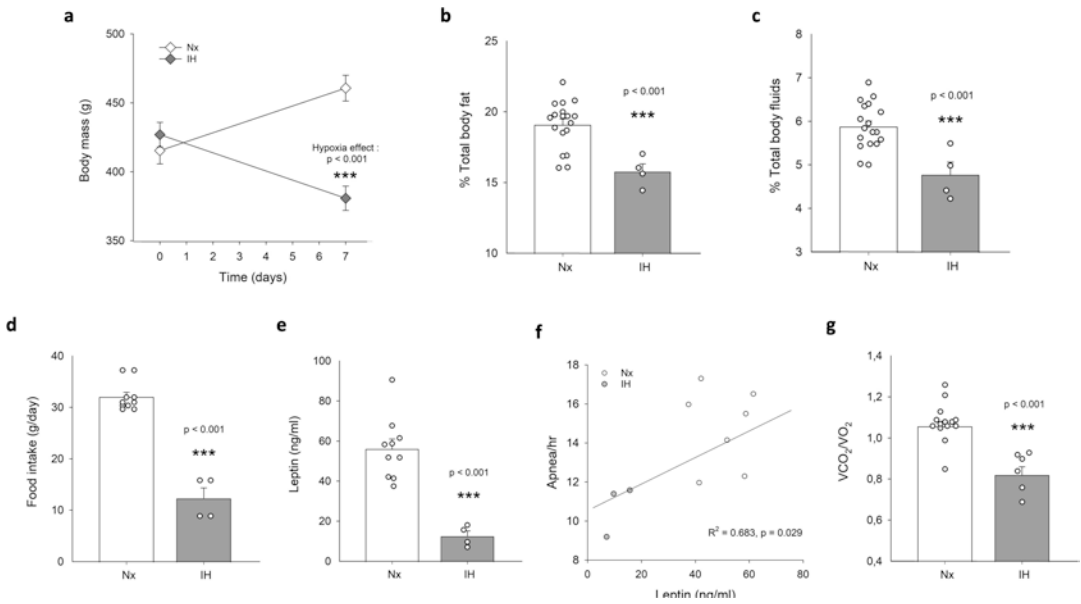


Fig. 7.3 Effect of 1-week exposure to intermittent hypoxia on body weight (a) and indicators of metabolic function. Body fat (b) and fluids (c) were obtained at the end by preclinical MRI. Food intake was calculated over the 7 days of the protocol (d) and plasma leptin levels were analyzed by a multiplex assay on samples taken at the end of the protocol (e). Regression analysis of the rela-

tionship between apnea index and leptin levels in normoxia (white circles) and IH-exposed rats (gray circles) over the course of the protocol. All values mean \pm SD. ANOVA results are reported in figures. *** $P < 0.001$

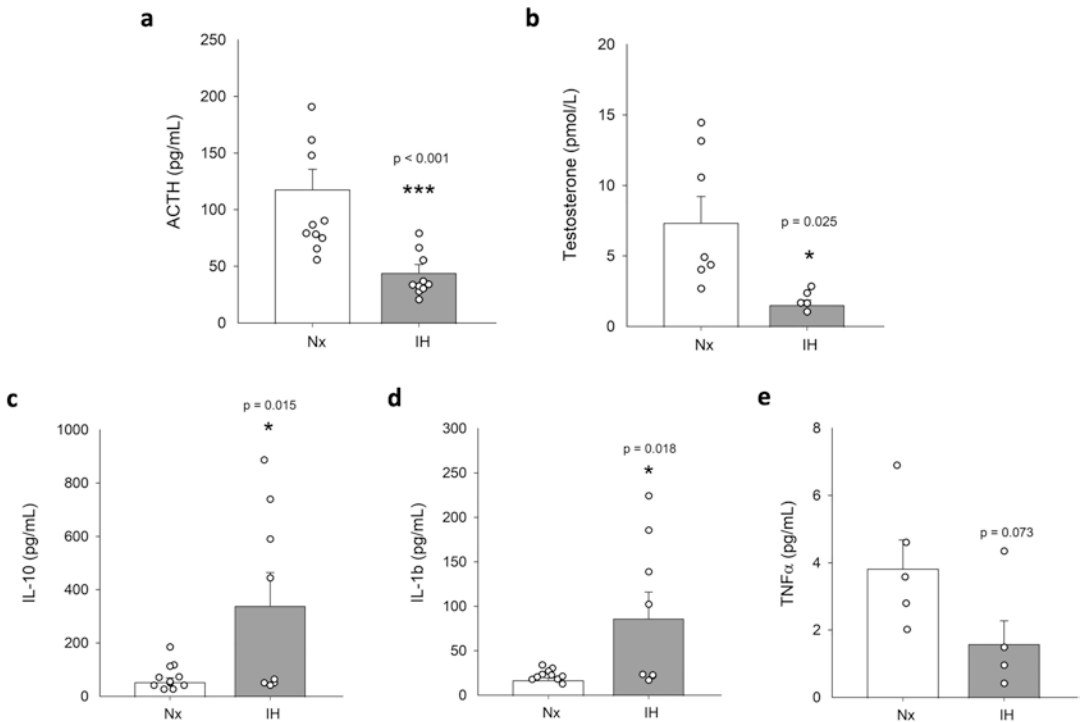


Fig. 7.4 Concentrations of ACTH (a), testosterone (b), and pro- and anti-inflammatory cytokines in rats previously exposed to IH. Testosterone levels were measured in serum and ACTH, IL-10 (c), IL-1 β (d), and TNF- α (e) in

plasma. Blood samples were taken at the end of the protocol and analyzed by a multiplex assay. All values mean \pm SD. ANOVA results are reported in figures. * $P < 0.05$, *** $P < 0.001$

No difference was observed for estradiol and progesterone levels in serum (Table 7.1).

7.4 Discussion

Sleep apnea (SA) is a complex respiratory disorder in which anomalies of respiratory control during sleep are an important part of the pathophysiology. The evidence indicating that with time, intermittent hypoxia exacerbates this problem by enhancing carotid body function is compelling. Keeping in mind that IH is a consequence, not a cause of SA, this effect of IH is nonetheless important because excessive responsiveness to hypoxia leads to respiratory instability during sleep and disrupts autonomic balance by favoring sympathetic activation. Owing to its robust ability to induce these cardiorespiratory anomalies, IH has emerged as a powerful model to investigate SA and related health issues. However, SA is multifactorial disease in which metabolic dysfunction, obesity, and fluid retention are common comorbidities that also contribute to respiratory disturbance by favoring hypoventilation and airway collapse during sleep. Considering that the pathophysiology of SA involves multiple physiological systems, we explored the metabolic and endocrine disturbances induced by IH.

7.4.1 Efficiency of the Intermittent Hypoxia Protocol

The use of IH in SA research has grown exponentially over the past 20 years and has led to a broad range of protocols varying in severity and duration. The 1-week protocol used here is relatively modest, yet as reported previously, it was sufficient to disrupt respiratory control as indicated by the greater respiratory instability during sleep, augmented hypoxic ventilatory response (Prabhakar et al. 2015). Furthermore, arterial blood pressure and heart rate were augmented which is indicative of augmented sympathetic activation. Pro- and anti-inflammatory cytokine release from macrophages is another key sympathetic response, and cell culture studies indicate

that the cytokine release profile varies according to catecholamine concentrations. Though the cytokine profile reported here perfectly matches the response of macrophages exposed to high noradrenaline concentration (10^{-6} M) (Martinez-Sanchez et al. 2022), these data differ from the “low-grade inflammation” commonly reported in SA patients and obese subjects in which levels of TNF- α are elevated and the anti-inflammatory cytokine (IL-10) is reduced (Lavie and Polotsky 2009; Sahlman et al. 2009; Kheirandish-Gozal and Gozal 2019). The fact that this clinical profile matches the macrophage response to low (10^{-6} M) noradrenaline concentration raises the possibility that our protocol induced a very strong sympathetic response. Considering the limitations inherent to our multiplex analyses, the challenges of comparing in vivo and in vitro studies, and that cytokines originate from multiple sources (e.g., adipocytes), this interpretation requires caution. However, other results tend to support it.

7.4.2 Intermittent Hypoxia Reduces ACTH and Favors Weight Loss

Because IH is a systemic stress, the lower ACTH values and lack of rise in corticosterone following IH treatment were not anticipated. These results could suggest that our protocol was not sufficiently severe to activate the stress pathways, but the rise in blood pressure and heart rate does not support this view. In fact, the stress hormone data likely reflect a condition of chronic stress which disrupts feedback mechanisms and dissociates ACTH and corticosterone secretion. The physiological symptoms of IH treated rats (weight, fat, and fluid loss with reduced food intake) support this interpretation as they are consistent with stress-induced adrenal insufficiency (Aguilera 1994; Russell and Lightman 2019). Since body fat composition reflects food intake and cellular metabolic regulation, the origin of weight loss is difficult to identify, but it has been shown that increased sympathetic signaling to the adipose tissues favors lipolysis and thus reduces plasma leptin (Martinez-Sanchez et al. 2022). Furthermore, the reduced respiratory quo-

tient following IH supports this point as a value near 0.75 reflects a greater utilization of lipids over carbohydrates.

7.4.3 Intermittent Hypoxia and Leptin

The leptin measurements obtained following IH contrast with what was expected based on the clinical literature and the strong link between SA and obesity (Ciriello et al. 2022). In humans, hyperleptinemia is associated with both low-grade systemic inflammation and metabolic dysfunction in obese subjects. Moreover, obesity and SA are associated with low testosterone in men, which correlates with high body fat. While IH reduced testosterone, the impact on body fat did not match the clinical profile.

In addition to its actions on metabolism and appetite, leptin has a strong influence on respiratory control as leptin receptors are expressed in the carotid bodies and key brain structures regulating breathing. While the current consensus indicates that leptin stimulates breathing (Amorim et al. 2022), the lower leptin levels observed following IH were not associated with a change ventilatory activity at rest. That being said, the positive correlation between leptin and apnea frequency is intriguing as it seems to dissociate respiratory variability from apneic events. Although interesting, this relationship should be interpreted cautiously because the range of values (both leptin and apnea index) is relatively narrow by comparison with pathological states.

7.5 Conclusions

Intermittent hypoxia is the main experimental model to investigate the pathophysiology of SA. While our results reproduced important aspects and disease such as increased sympathetic activity and hypogonadism, the impacts on body weight metabolic signals do not match the clinical reality; such limitation of the model requires consideration. While the duration of the protocol was relatively short, the intense

responses observed suggest that the intensity and/or frequency of hypoxic events is quite strong. However, other studies using more severe protocols (6.5% O₂, 80 s, 8 h/day) over longer period (96 days) have reported gains in body weight and fat by the end of their protocol (Ciriello et al. 2022). Thus, with time, rats may become “desensitized” and/or “adapt” to the intense stimulus and may ultimately develop a phenotype that is more in line with clinical observations. Such differences suggest that problems related to sympathetic overactivation such as high blood pressure appear before obesity. Whether this trajectory matches clinical observations is uncertain.

Acknowledgments This research is supported by operating grants from the Canadian Institutes of Health Research (CIRH, RK, and VJ). N.J.M. was supported by a Sentinel North Partnered Research Chair in Sleep Pharmacometabolism (Canada First Research Excellence Fund) and a Fonds de Recherche du Québec-Santé (FRQS) Research Scholar J1 award. MG is the recipient of a doctoral scholarship from the FRQS.

References

- Aguilera G (1994) Regulation of pituitary ACTH secretion during chronic stress. *Front Neuroendocrinol* 15(4):321–350. <https://doi.org/10.1006/frne.1994.1013>
- Alam I, Lewis K, Stephens JW, Baxter JN (2007) Obesity, metabolic syndrome and sleep apnoea: all pro-inflammatory states. *Obes Rev* 8(2):119–127. <https://doi.org/10.1111/j.1467-789X.2006.00269.x>
- American Academy of Sleep Medicine (1999) Sleep-related breathing disorders in adults: recommendations for syndrome definition and measurement techniques in clinical research. *Sleep* 22(5):667–689. <https://doi.org/10.1093/sleep/22.5.667>
- Amorim MR, Aung O, Mokhlesi B, Polotsky VY (2022) Leptin-mediated neural targets in obesity hypoventilation syndrome. *Sleep* 45(9):zsac153. <https://doi.org/10.1093/sleep/zsac153>
- Bastianini S, Alvente S, Berteotti C, Lo Martire V, Silvani A, Swoap SJ, Valli A, Zoccoli G, Cohen G (2017) Accurate discrimination of the wake-sleep states of mice using non-invasive whole-body plethysmography. *Sci Rep* 7:41698. <https://doi.org/10.1038/srep41698>
- Bastianini S, Alvente S, Berteotti C, Bosi M, Lo Martire V, Silvani A, Valli A, Zoccoli G (2019) Post-sigh sleep apneas in mice: systematic review and data-driven

- definition. *J Sleep Res* 28(6). <https://doi.org/10.1111/jsr.12845>
- Benjafield AV, Ayas NT, Eastwood PR, Heinzer R, Ip MSM, Morrell MJ, Nunez CM, Patel SR, Penzel T, Pépin J-L, Peppard PE, Sinha S, Tufik S, Valentine K, Malhotra A (2019) Estimation of the global prevalence and burden of obstructive sleep apnoea: a literature-based analysis. *Lancet Respir Med* 7(8):687–698. [https://doi.org/10.1016/S2213-2600\(19\)30198-5](https://doi.org/10.1016/S2213-2600(19)30198-5)
- Brennan M, Palaniswami M, Kamen P (2001). Do existing measures of Poincaré plot geometry reflect nonlinear features of heart rate variability? *IEEE Trans Biomed Eng* 48(11):1342–1347. <https://doi.org/10.1109/10.959330>
- Ciriello J, Moreau JM, Caverson MM, Moranis R (2022) Leptin: a potential link between obstructive sleep apnea and obesity. *Front Physiol* 12:767318. <https://doi.org/10.3389/fphys.2021.767318>
- Dematteis M, Godin-Ribuot D, Arnaud C, Ribuot C, Stanke-Labesque F, Pépin J-L, Lévy P (2009) Cardiovascular consequences of sleep-disordered breathing: contribution of animal models to understanding the human disease. *ILAR J* 50(3):262–281. <https://doi.org/10.1093/ilar.50.3.262>
- Dempsey JA, Veasey SC, Morgan BJ, O'Donnell CP (2010) Pathophysiology of sleep apnea. *Physiol Rev* 90(1):47–112. <https://doi.org/10.1152/physrev.00043.2008>
- Drorbaugh E (1955) Method for measuring in newborn infants. 9
- Eckert DJ (2018) Phenotypic approaches to obstructive sleep apnoea – new pathways for targeted therapy. *Sleep Med Rev* 37:45–59. <https://doi.org/10.1016/j.smrv.2016.12.003>
- Eckert DJ, Younes MK (2014) Arousal from sleep: implications for obstructive sleep apnea pathogenesis and treatment. *J Appl Physiol* (Bethesda, Md: 1985) 116(3):302–313. <https://doi.org/10.1152/jappphysiol.00649.2013>
- Eckert DJ, White DP, Jordan AS, Malhotra A, Wellman A (2013) Defining phenotypic causes of obstructive sleep apnea. Identification of novel therapeutic targets. *Am J Respir Crit Care Med* 188(8):996–1004. <https://doi.org/10.1164/rccm.201303-0448OC>
- Feng M, Whitesall S, Zhang Y, Beibel M, Alecy LD, DiPetrillo K (2008) Validation of volume-pressure recording tail-cuff blood pressure measurements. *Am J Hypertens* 21(12):1288–1291. <https://doi.org/10.1038/ajh.2008.301>
- Fletcher EC, Lesske J, Behm R, Miller CC, Stauss H, Unger T (1992) Carotid chemoreceptors, systemic blood pressure, and chronic episodic hypoxia mimicking sleep apnea. *J Appl Physiol* 72(5):1978–1984. <https://doi.org/10.1152/jappl.1992.72.5.1978>
- Gastaut H, Tassinari CA, Duron B (1966) Polygraphic study of the episodic diurnal and nocturnal (hypnic and respiratory) manifestations of the pickwick syndrome. *Brain Res* 1(2):167–186. [https://doi.org/10.1016/0006-8993\(66\)90117-X](https://doi.org/10.1016/0006-8993(66)90117-X)
- Hinojosa-Laborde C, Mifflin SW (2005) Sex differences in blood pressure response to intermittent hypoxia in rats. *Hypertension* 46(4):1016–1021. <https://doi.org/10.1161/01.HYP.0000175477.33816.f3>
- Iturriaga R, Alcayaga J, Chappelle MW, Somers VK (2021) Carotid body chemoreceptors: physiology, pathology, and implications for health and disease. *Physiol Rev* 101(3):1177–1235. <https://doi.org/10.1152/physrev.00039.2019>
- Kheirandish-Goza L, Gozal D (2019) Obstructive sleep apnea and inflammation: proof of concept based on two illustrative cytokines. *Int J Mol Sci* 20(3):459. <https://doi.org/10.3390/ijms20030459>
- Laouafa S, Ribon-Demars A, Marcouiller F, Roussel D, Bairam A, Pialoux V, Joseph V (2017) Estradiol protects against cardiorespiratory dysfunctions and oxidative stress in intermittent hypoxia. *Sleep* 40(8):zsx104. <https://doi.org/10.1093/sleep/zsx104>
- Lavie L, Polotsky V (2009) Cardiovascular aspects in obstructive sleep apnea syndrome – molecular issues, hypoxia and cytokine profiles. *Respiration* 78(4):361–370. <https://doi.org/10.1159/000243552>
- Martinez-Sanchez N, Sweeney O, Sidarta-Oliveira D, Caron A, Stanley SA, Domingos AI (2022) The sympathetic nervous system in the 21st century: neuro-immune interactions in metabolic homeostasis and obesity. *Neuron* 110(21):3597–3626. <https://doi.org/10.1016/j.neuron.2022.10.017>
- Miller WL, Borlaug BA (2020) Impact of obesity on volume status in patients with ambulatory chronic heart failure. *J Card Fail* 26(2):112–117. <https://doi.org/10.1016/j.cardfail.2019.09.010>
- Nakamura A, Fukuda Y, Kuwaki T (2003) Sleep apnea and effect of chemostimulation on breathing instability in mice. *J Appl Physiol* 94(2):525–532. <https://doi.org/10.1152/jappphysiol.00226.2002>
- Powell FL, Milsom WK, Mitchell GS (1998) Time domains of the hypoxic ventilatory response. *Respir Physiol* 112(2):123–134. [https://doi.org/10.1016/S0034-5687\(98\)00026-7](https://doi.org/10.1016/S0034-5687(98)00026-7)
- Prabhakar NR, Peng Y-J, Kumar GK, Nanduri J (2015) Peripheral chemoreception and arterial pressure responses to intermittent hypoxia. In: Terjung R (ed) *Comprehensive physiology*. Wiley, New York, pp 561–577. <https://doi.org/10.1002/cphy.c140039>
- Russell G, Lightman S (2019) The human stress response. *Nat Rev Endocrinol* 15(9):525–534. <https://doi.org/10.1038/s41574-019-0228-0>
- Sahlman J, Miettinen K, Peuhkurinen K, Seppä J, Peltonen M, Herder C, Punnonen K, Vanninen E, Gylling H, Partinen M, Uusitupa M, Tuomilehto H, on behalf of the Kuopio Sleep Apnoea Group (2009) The activation of the inflammatory cytokines in overweight patients with mild obstructive sleep apnoea: mild OSA and cytokines. *J Sleep Res* 19(2):341–348. <https://doi.org/10.1111/j.1365-2869.2009.00787.x>
- Shamsuzzaman ASM, Gersh BJ, Somers VK (2003) Obstructive sleep apnea: implications for cardiac and vascular disease. *JAMA* 290(14):1906. <https://doi.org/10.1001/jama.290.14.1906>

- Sunwoo J-S, Hwangbo Y, Kim W-J, Chu MK, Yun C-H, Yang KI (2018) Prevalence, sleep characteristics, and comorbidities in a population at high risk for obstructive sleep apnea: a nationwide questionnaire study in South Korea. *PLoS ONE* 13(2):e0193549. <https://doi.org/10.1371/journal.pone.0193549>
- Toth LA, Bhargava P (2013) Animal models of sleep disorders. *Comp Med* 63(2):14
- White, Bradley TD (2013) Role of nocturnal rostral fluid shift in the pathogenesis of obstructive and central sleep apnoea: nocturnal rostral fluid shift in apnoea. *J Physiol* 591(5):1179–1193. <https://doi.org/10.1113/jphysiol.2012.245159>
- White, Younes MK (2012) Obstructive sleep apnea. *Compr Physiol* 2(4):2541–2594. <https://doi.org/10.1002/cphy.c110064>
- Young T, Peppard PE, Taheri S (2005) Excess weight and sleep-disordered breathing. *J Appl Physiol* 99(4):1592–1599. <https://doi.org/10.1152/japplphysiol.00587.2005>



Effects of Gestational Intermittent Hypoxia on Placental Morphology and Fetal Development in a Murine Model of Sleep Apnea

Esther Valverde-Pérez, Jesús Prieto-Lloret, Elvira Gonzalez-Obeso, María I. Cabero, Maria L. Nieto, Marta I. Pablos, Ana Obeso, Angela Gomez-Niño, Rosa M. Cárdbaba-García, Asunción Rocher, and Elena Olea

Abstract

Obstructive sleep apnea (OSA) during pregnancy is characterized by episodes of intermittent hypoxia (IH) during sleep, resulting in adverse health outcomes for mother and offspring. Despite a prevalence of 8–20% in pregnant women, this disorder is often underdiagnosed.

We have developed a murine model of gestational OSA to study IH effects on pregnant

mothers, placentas, fetuses, and offspring. One group of pregnant rats was exposed to IH during the last 2 weeks of gestation (GIH). One day before the delivery date, a cesarean section was performed. Other group of pregnant rats was allowed to give birth at term to study offspring's evolution.

Preliminary results showed no significant weight differences in mothers and fetuses. However, the weight of GIH male offspring

E. Valverde-Pérez · J. Prieto-Lloret · A. Obeso
A. Rocher
Departamento de Bioquímica y Biología Molecular y Fisiología, Facultad de Medicina, Universidad de Valladolid, Valladolid, Spain

Instituto de Biomedicina y Genética Molecular (IBGM), UVa-CSIC, Valladolid, Spain

E. Gonzalez-Obeso
Instituto de Biomedicina y Genética Molecular (IBGM), UVa-CSIC, Valladolid, Spain

Servicio de Anatomía Patológica, Hospital Clínico Universitario de Valladolid, Valladolid, Spain

M. I. Cabero · M. L. Nieto
Instituto de Biomedicina y Genética Molecular (IBGM), UVa-CSIC, Valladolid, Spain

M. I. Pablos
Departamento de Bioquímica y Biología Molecular y Fisiología, Facultad de Medicina, Universidad de Valladolid, Valladolid, Spain

A. Gomez-Niño
Instituto de Biomedicina y Genética Molecular (IBGM), UVa-CSIC, Valladolid, Spain

Departamento de Biología Celular, Genética, Histología y Farmacología, Universidad de Valladolid, Valladolid, Spain

R. M. Cárdbaba-García
Departamento de Enfermería, Grupo de Investigación en Cuidados Enfermeros (GICE), Facultad de Enfermería, Universidad de Valladolid, Valladolid, Spain

E. Olea (✉)
Instituto de Biomedicina y Genética Molecular (IBGM), UVa-CSIC, Valladolid, Spain

Departamento de Enfermería, Grupo de Investigación en Cuidados Enfermeros (GICE), Facultad de Enfermería, Universidad de Valladolid, Valladolid, Spain
e-mail: elena.olea@uva.es

was significantly lower than the controls at 14 days ($p < 0.01$). The morphological study of the placentas showed an increase in fetal capillary branching, expansion of maternal blood spaces, and number of cells of the external trophoblast in the tissues from GIH-exposed mothers. Additionally, the placentas from the experimental males were enlarged ($p < 0.05$). Further studies are needed to follow the long-term evolution of these changes to relate the histological findings of the placentas with functional development of the offspring in adulthood.

Keywords

Intermittent hypoxia · Pregnancy · Placenta · Obstructive sleep apnea · Morphology · Histology

8.1 Introduction

Obstructive sleep apnea (OSA), characterized by chronic intermittent hypoxia (IH), is associated with oxidative stress, inflammation, and increased risk of cardiovascular and metabolic diseases (Martins and Conde 2021). OSA is a frequently underdiagnosed sleep disorder, particularly during pregnancy, even though the prevalence of gestational OSA ranges from 8% to 20% (Zhu et al. 2020). There is increasing evidence that hypoxia-reoxygenation events, distinctive features of OSA, adversely affect maternal and fetal health. Gestational OSA has been related to an increased levels of morbidity and mortality, causing in mothers arterial hypertension, preeclampsia, and gestational diabetes while negatively affecting fetal development, causing growth disorders, premature delivery, low birth weight, and even fetal death (Louis et al. 2014; Ramírez Guirado and Morales Rodríguez 2014). It can also lead to maladaptive responses that will develop during postnatal hypoxia events, increasing the vulnerability of the newborn to fatal conditions, such as the syndrome of sudden infant death (Gozal et al. 2003). Additionally, OSA during pregnancy may also alter fetus epigenetics,

with effects persisting, or manifesting, into adulthood, such metabolic alterations already described in male offspring (Khalyfa et al. 2017; Pires et al. 2021). Cellular and molecular mechanisms triggering gestational IH (GIH) adverse effects on fetal outcomes have not been fully explored yet. In a mice model, Badran et al. (2019) found that GIH pregnant mice have higher plasma levels of oxidative stress (8-isoprostane) and inflammatory markers (tumor necrosis factor- α) than controls. GIH significantly reduced endothelium-dependent vasodilatation in uterine arteries, and immunostaining for markers of hypoxia and oxidative stress was higher in mice exposed to GIH. They conclude that GIH adversely affects uterine vascular function and may be a mechanism by which gestational OSA leads to adverse maternal and fetal outcomes (Badran et al. 2019).

Recurrent episodes of IH decrease arterial PO_2 and hemoglobin saturation. Repeated IH cycles stimulates the carotid body (CB) chemoreceptors generating respiratory reflex and cardiovascular responses to minimize the deleterious effects of hypoxia. This repeated stimulation sensitizes the CB, increasing sympathetic tone and generating maladaptation such as hypertension, cardiovascular, and metabolic disorders (Iturriaga 2018).

Episodes of hypoxia/reoxygenation during GIH also increase the production of reactive oxygen species (ROS) in the mothers, resulting in tissue damage and the influx of inflammatory cells to injured sites, as well as to the fetus through the placenta (Dahlgren et al. 2006). GIH has been associated with fetoplacental hypoxia, as manifested by fetal normoblastemia and increased placental carbonic anhydrase IX immunoreactivity, marker of tissue hypoxia (Ravishankar et al. 2015). It has also been reported that fetus exposed to GIH have altered neural control of respiration months after birth and increased tendency for overweight in adulthood when compared with offspring from normoxic pregnant rats, despite the lower birth weight (Gozal et al. 2003).

In fetus, the placenta plays a role similar to that of the lungs after birth, i.e., it is the organ in which blood gases are interchanged with the environment. Fetal blood extracts oxygen from

maternal blood, similarly to how blood extracts oxygen from alveolar gas. Therefore, it would be expected that oxygenation changes in maternal blood would be transmitted to the fetus. Interestingly, in a recent study on a sheep model of gestational sleep apnea, Almendros et al. (2019) found that placental oxygen transfer reduces hypoxia-reoxygenation oscillations in fetal blood during GIH. Fetal plasma glucose levels are also unaffected by maternal hypoxia (Cuffe et al. 2014). Together, these data reveal that despite the effects of hypoxia on the placenta, the fetus receives an adequate oxygen supply and nutrition due to compensatory mechanisms.

The placenta is the organ responsible for fetal growth and development, and it is the main factor in birthweight, which points to the placenta as an organ sensitive to IH and sympathetic activation, the main hallmarks of OSA. The study of the effect of GIH on placental morphology and histology may be key to understand the pathophysiology of this gestational breathing disorder and its implication on fetal development. In the present work, our aims were to develop an animal model of OSA in pregnancy that will allow us to evaluate the morphological (macro and microscopic) changes in the placentas of mothers exposed to GIH and determine if there is any sexual dimorphism between these changes and the weight of fetuses and newborn rats.

8.2 Methods

8.2.1 Animal Models and Anesthesia

All experiments were approved by the University of Valladolid Institutional Committee for Animal Care and Use (Project Approval Ethical Code: 9601981) and were conducted in accordance with the international laws and policies (European Community Council Directive for Protection of Vertebrates Used for Experimental and Other Scientific Ends (2010/63/EU)).

Experiments were performed on female pregnant Wistar rats (3 months old; initial weight of

control rats: 263.8 ± 9.2 g and GIH: 249.8 ± 8.4 g; there are no statistically significant differences; $p = 0.3$). Breeding rats have been used for the first time for this purpose. Male rats were removed once inspection of the female revealed the presence of a copulation plug, considering the first day of gestation. After 7 days of pregnancy, the rats were randomly divided into two groups: gestational control rats (GC group; $n = 4$) exposed to room air throughout the entire pregnancy and gestational intermittent hypoxia rats (GIH group; $n = 4$) (Fig. 8.1a). Briefly, the protocol of IH consisted of cycles of exposure for 40 s to 5% O₂, then exposure to air for 80 s, repeating this cycle for 8 h each day (from 8:00 a.m. to 16:00 p.m.), corresponding to the inactive period of the animals, during the last 14 days of gestation. A gas control delivery system regulated the flow of room air, N₂, and O₂ into the customized cages housing the rats. From 16:00 p.m. to 8:00 a.m., these animals were exposed to room air. All pregnant rats (GC and GIH) were housed in the same room in the vivarium of the University of Valladolid, with free access to food and water, under controlled conditions of temperature and humidity. After 21 days, half pregnant rats gave birth to about 50 gender identified pups which were kept in the maternal company until weaning. The other pregnant rats were weighed (Fig. 8.1b) and anesthetized with isoflurane for cesarean section 1 or 2 days before the delivery date. Placentas and fetus were weighed and snap frozen in liquid nitrogen or fixed in 4% paraformaldehyde. Fetus tails were taken for identification of fetal sex by PCR genotyping.

At the end of experiments, animals were euthanized by the administration of a lethal dose of sodium pentobarbital.

8.2.2 Macroscopic and Microscopic Study of Placentas

The gestation period of the rat is about 21 days. Each pregnant rat has an average of 12–14 offspring, and each offspring has its own placenta. The animal model used for this study is suitable for extrapolation of the results to human placenta

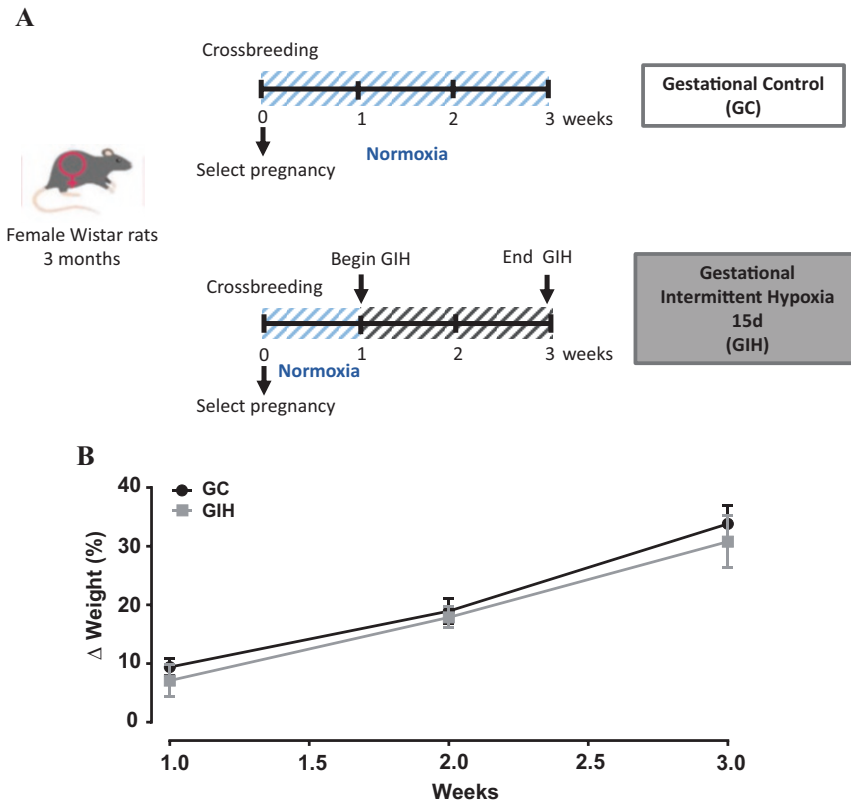


Fig. 8.1 Scheme of animal models and evolution of pregnant female body weight. (A) Two groups of study: gestational control rats (GC) exposed to normoxia the entire pregnancy and gestational intermittent hypoxia rats (GIH)

exposed to IH during the last 2 weeks of pregnancy. (B) Evolution of body weight gain in both groups at 1, 2 and 3 weeks of gestation. Data are means \pm SEM ($n = 4$). Two-way ANOVA. (Sidak's multiple comparison test)

since both, human and rat placentas, are hemochorionic type (Soares et al. 2012).

On the day of cesarean section, fetuses and placentas were removed and weighed. Placentas were fixated in 4% paraformaldehyde in 0.2 M PB for 48 h. After processing, they were embedded in paraffin; 5 μ m section were made and stained with hematoxylin and eosin (H & E). Histological photographs were taken with a digital camera (CoolSNAP Photometric Roper Scientific) attached to the microscope and analyzed using Image J software to measure: the placental area (A), placental labyrinth area (B),

central placental thickness (C), and central thickness of the labyrinth area (D) (Fig. 8.2).

8.2.3 Statistical Analysis

All results are represented as the mean \pm SEM. Statistical analysis was performed using Graphpad Prism 6. The significance of the differences between the mean values was calculated by t-test, one-way ANOVA, or two-way ANOVA according to data representation. Differences were considered significant at $p < 0.05$.

8.3 Results

8.3.1 Maternal, Placenta and Fetus Body Weight

Body weight of pregnant rats at the end of pregnancy of the two groups, GC and GIH, were compared. Placental, fetal and offspring weights at 14 days of age were also analyzed, taking into account the mean value of the sexed individuals of each litter. In Table 8.1, it is observed that the weights of GIH pregnant rats tend to be lower than those of the control group (CG), but there are no statistically significant differences (326.3 ± 13.4 g vs. 353.8 ± 20.7 g; $p = 0.3$). The weights of placentas, fetuses, and offspring at 14 days were compared by sex between the two study groups (GC and GIH). The weights of fetuses and placentas were very similar in both sexes in the two groups studied. However, the offspring at 14 days showed statistically significant differences in the males, being the weight of the GIH offspring lower than the controls (GC) (28.6 ± 0.7 g vs. 33.5 ± 1.6 g; $***p < 0.001$). No significant differences were observed between both groups in the females at 14 days of age, although the weights of GC females at this age were significantly smaller than those of GC males ($**p < 0.01$).

8.3.2 Macroscopic and Microscopic Study of Placentas

After the extraction and processing of the placentas, a macroscopic study was performed

(Fig. 8.2) to measure the placental area (A), placental labyrinth area (B), central placental thickness (C), and central thickness of the labyrinth area (D). In Fig. 8.2a, the placental area is larger in the GIH males than in the GC males ($*p < 0.05$). The labyrinth area presented the same trend, the area was larger in GIH males, but in this case with no statistically significant differences ($p = 0.0709$) (Fig. 8.2b). No differences were observed in the areas of the placenta or the labyrinth between the female groups.

Regarding the thickness of the placenta (Fig. 8.2c) and labyrinth (Fig. 8.2d), we found no differences between the control (GC) and experimental groups (GIH) or between the males and females.

In the microscopic (histological) study, the most relevant findings were located in the labyrinth zone (Fig. 8.3).

All the experimental placentas (GIH) presented expansion of the labyrinth zone due to a relative increase in the ramification of the fetal capillaries and expansion of the maternal blood spaces, accompanied by an increase in the amount of blood in them (congestion). A relative increase of the number of outer trophoblast cells was also observed, see Fig. 8.3. Other less relevant histological findings were reactive-type atypia in the spongiotrophoblasts with isolated apoptotic figures, in the basal area of experimental placentas (GIH). The yolk sac epithelium was slightly hyperplastic with a decrease in the intracytoplasmic vacuolization in the experimental cases. No gender differences were found.

Table 8.1 Weight of mothers at term, fetuses, placentas, and offspring at 14 days from gestational control and gestational intermittent hypoxia rats

Weight (g)	GC		GIH	
Mothers at term	353.8 ± 20.7 ($n = 4$)		326.3 ± 13.4 ($n = 4$)	
Weight (g)	GC-male	GIH-male	GC-female	GIH-female
Placenta	0.46 ± 0.02 ($n = 10$)	0.44 ± 0.02 ($n = 13$)	0.43 ± 0.02 ($n = 14$)	0.44 ± 0.02 ($n = 13$)
Fetus	4.4 ± 0.7 ($n = 10$)	4.6 ± 0.9 ($n = 13$)	4.7 ± 0.7 ($n = 13$)	4.3 ± 0.7 ($n = 13$)
Offspring 14 days	33.5 ± 1.6 ($n = 8$)	$28.6 \pm 0.7***$ ($n = 10$)	$27.9 \pm 0.7**$ ($n = 11$)	29.1 ± 0.8 ($n = 10$)

Data are means \pm SEM. $**p < 0.01$; $***p < 0.001$ vs. GC male. Student's unpaired t-test

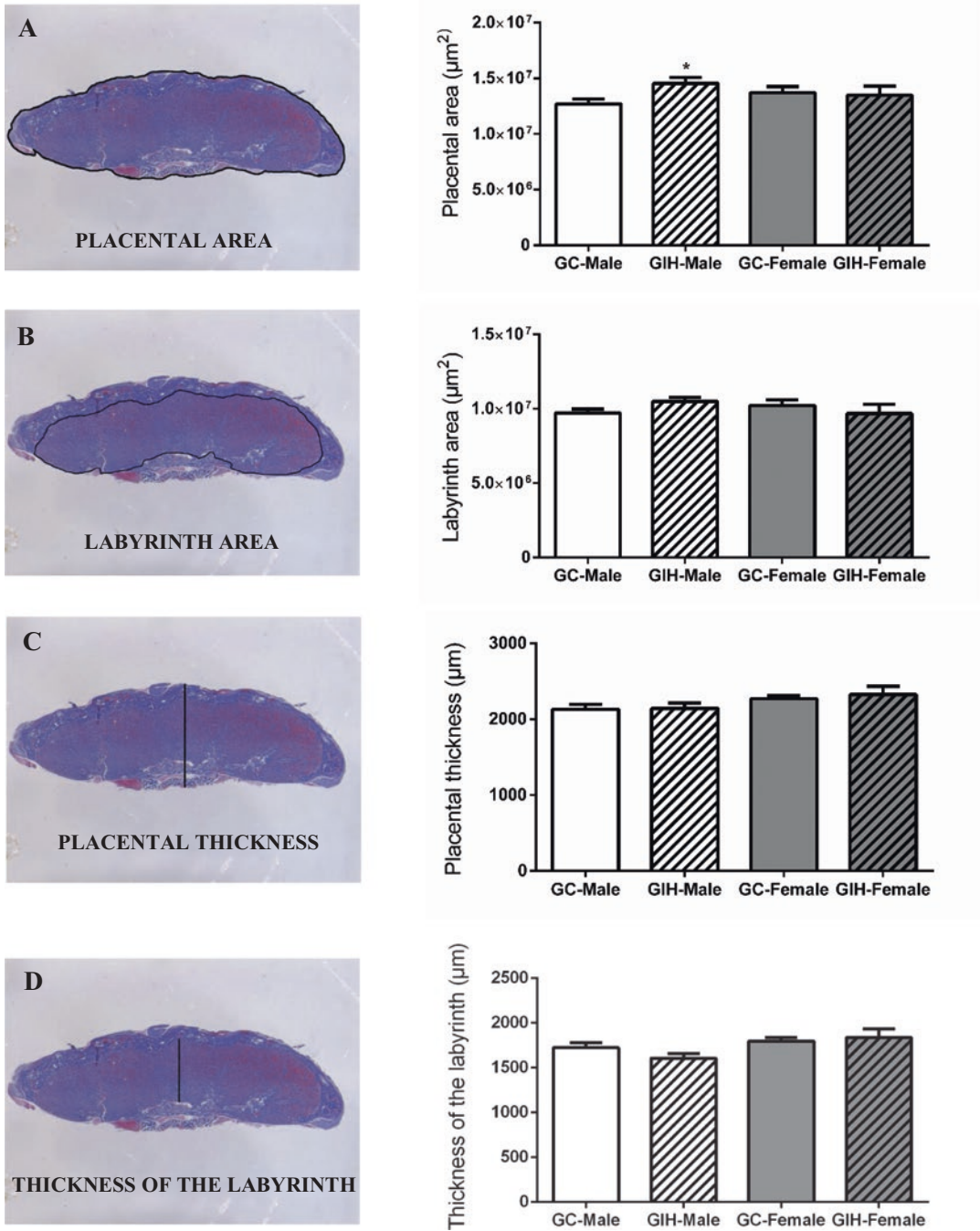
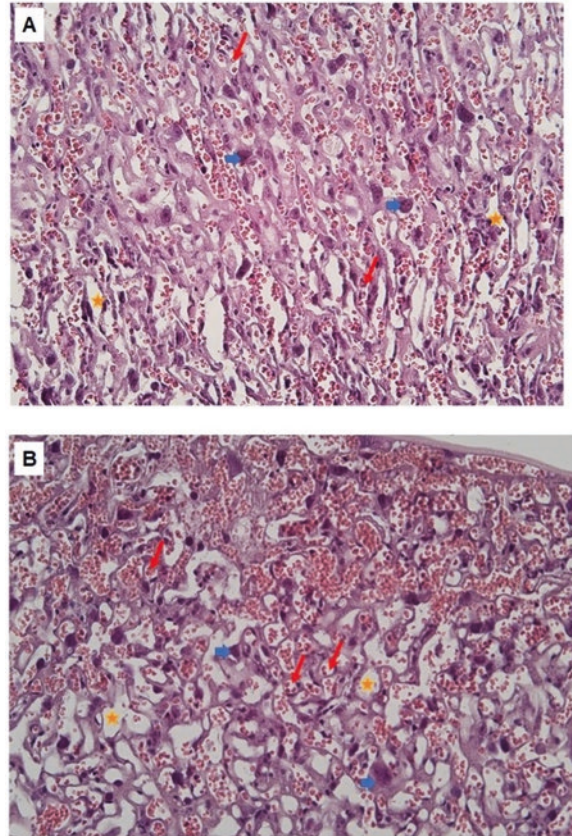


Fig. 8.2 Macroscopic study of the placenta. (A) Placental area (B) Labyrinth area (C) Placental thickness (D) Labyrinth thickness. In both groups, GC and GIH (males and females). * $p < 0.05$ vs. GIH-Male. Student's t-test

Fig. 8.3 Histological study of the placenta. Labyrinth zone of a control placenta (GC) (HE x40) (a) and experimental placenta (GIH) (HE x40) (b). There is a relative increase in the ramification of the fetal capillaries (red arrows), maternal blood spaces expansion (orange stars), and in the number of outer trophoblast cells (blue arrows) in GIH placentas



8.4 Discussion

Gestational OSA is related to an increased risk of adverse outcomes in the mother and the newborn. In pregnant women, it is related with a higher incidence of gestational diabetes and hypertensive pathologies, fundamentally. In the neonate, the most frequent alteration is intrauterine growth restriction (Louis et al. 2018; Pamidi and Kimoff 2018). In the present work, a gestational intermittent hypoxia model was implemented to study the effects of OSA on placental histomorphometry.

The time between conception and birth is a very vulnerable life stage during which the intrauterine environment may have immediate and lasting effects on health (Osmond and Barker 2000). The fetus undergoes rapid growth and organ development, and the maternal environment helps to direct these processes (Myatt 2006; Jansson and Powell 2007). Barker hypothesis (Barker 1998) postulates that intrauterine condi-

tions determine and program the whole life of the individual, with a correlation between birth weight and altered fetal growth (as indicatives of uterine environment) and adult diseases such as hypertension or diabetes. Our results show that the weight of fetuses (at day 20th) from GIH mothers is very similar to the one observed in fetuses from control mothers GC (Table 8.1), despite previous studies describing a negative effect of hypoxia on the developing fetus (Gozal et al. 2003). Interestingly, at 14 days postnatal period, GIH males show reduced weight ($\sim 15\%$; $p < 0.01$) versus control males. In contrast, no differences were found in female offspring (GC vs. GIH). These data agree with other authors' studies that also observe significantly greater adverse outcomes in the male offspring (Bourque et al. 2013). However, control female offspring of the same age weighed less than control males, a fact described in other mammals like humans (Gonzalez et al. 2018).

The placenta exerts, during pregnancy, different functions in the uterine environment to support fetal development. It has respiratory, nutritional, and endocrine functions and mediates the immunological crosstalk between mother and fetus (Burton and Fowden 2015). It has been established that maternal hypoxia, as experienced in gestational OSA, can induce morpho-functional changes of the placenta affecting blood flow, oxygen and nutrient supply, and secretion of hormones, cytokines, and growth factors. Our results on the morphometry (macroscopic study) of the placentas do not show appreciable differences between normoxic gestation and GIH, except in the placentas of male fetuses, which are enlarged. Although exact mechanisms involved in abnormal changes of placenta size are not fully understood, enlarged placentas may indicate that the maternal O₂ supply is low, suggesting the activation of a compensatory mechanism to improve oxygen supply (Eskild et al. 2016).

Our results on altered weight in GIH males at postnatal day 14 and other preliminary observations on altered redox status and lung function (data not shown) point to epigenetic changes induced by fetal hypoxia. Experimental evidence corroborates human studies, reinforcing that the long-term consequences of intrauterine and neonatal hypoxic insults are partially mediated by epigenetic mechanisms that make offspring more prone to chronic diseases in adulthood (Cerdeira and Weitzman 1997; Luo et al. 2006). Taking into account that intrauterine hypoxia may be a consequence of maternal OSA and that OSA is a growing disorder, the incidence of some diseases will markedly increase in future generations.

Therefore, the study of the placenta structure is important to better understand the development of these complications. In our investigation, hypoxia caused histological changes in the placenta, mainly in the labyrinth zone. Its expansion occurs secondary to changes in the fetal capillaries and in the maternal blood spaces, all aimed to increase the blood flow and counteract the oxygen deficiency. Similar changes have been described in human placentas (Parks 2017); except for syncytial knots that were not found in

our placentas, all of the others correlate. Thus, all these results make rat placentas, on the whole, a suitable model to study the hypoxic related pathologies during pregnancy.

Overall, we can conclude that despite the absence of visible effects on the evolution of pregnant rats during gestation in IH nor on the fetuses at day 20, late effects are observed at 14 days postnatal, as is the case of decreased weight of male offspring exposed to GIH. The microscopic study of the placentas exposed to GIH shows a greater branching of the fetal capillaries, with expansion of the maternal vascular lacunae and a certain increase in the number of cytotrophoblast cells. Furthermore, the increased thickness and surface area of the placentas of experimental males suggests a compensatory effect of defense against placental hypoxia.

In summary, we have developed a suitable murine model of gestational OSA that will allow us to further investigate the effects of OSA on pregnant mothers and their offspring and their vulnerability to different types of stress.

Acknowledgments We thank M^a de los Llanos Bravo and Oscar A. Ríos Rodríguez for their technical assistance. Funding: Ayudas para la realización de proyectos de investigación UVA 2021 (PROYEMER 57-E.O.)

References

- Almendros I, Martínez-Ros P et al (2019) Placental oxygen transfer reduces hypoxia-reoxygenation swings in fetal blood in a sheep model of gestational sleep apnea. *J Appl Physiol* (1985) 127(3):745–752
- Badran M, Abuyassin B, Ayas N, Laher I (2019) Intermittent hypoxia impairs uterine artery function in pregnant mice. *J Physiol* 597:2639–2650
- Barker DJ (1998) In utero programming of chronic disease. *Clin Sci (Lond)* 95:115–128
- Bourque SL, Gragasin FS, Quon AL, Mansour Y, Morton JS, Davidge ST (2013) Prenatal hypoxia causes long-term alterations in vascular endothelin-1 function in aged male, but not female, offspring. *Hypertension* 62(4):753–758
- Burton GJ, Fowden AL (2015) The placenta: a multifaceted, transient organ. *Philos Trans R Soc Lond Ser B Biol Sci* 370:20140066
- Cerdeira S, Weitzman SA (1997) Influence of oxygen radical injury on DNA methylation. *Mutat Res* 386:141–152

- Cuffe JS, Walton SL, Singh RR, Spiers JG, Bielefeldt-Ohmann H, Wilkinson L, Little MH, Moritz KM (2014) Mid- to late term hypoxia in the mouse alters placental morphology, glucocorticoid regulatory pathways and nutrient transporters in a sex-specific manner. *J Physiol* 592(14):3127–3141
- Dahlgren J, Samuelsson AM et al (2006) Interleukin-6 in the maternal circulation reaches the rat fetus in mid-gestation. *Pediatr Res* 60:147–151
- Eskild A, Strøm-Roum EM, Haavaldsen C (2016) Does the biological response to fetal hypoxia involve angiogenesis, placental enlargement and preeclampsia? *Paediatr Perinat Epidemiol* 30:305–309
- Gonzalez TL, Sun T, Koeppel AF, Lee B, Wang ET, Farber CR, Rich SS, Sundheimer LW, Buttle RA, Chen YI, Rotter JI, Turner SD, Williams J 3rd, Goodarzi MO, Pisarska MD (2018) Sex differences in the late first trimester human placenta transcriptome. *Biol Sex Differ* 9(1):4
- Gozal D, Reeves SR, Row BW, Neville JJ, Guo SZ, Lipton AJ (2003) Respiratory effects of gestational intermittent hypoxia in the developing rat. *Am J Respir Crit Care Med* 167:1540–1547
- Iturriaga R (2018) Translating carotid body function into clinical medicine. *J Physiol* 596(15):3067–3077
- Jansson T, Powell TL (2007) Role of the placenta in fetal programming: underlying mechanisms and potential interventional approaches. *Clin Sci (Lond)* 113:1–13
- Khalyfa A, Cortese R, Qiao Z, Ye H, Bao R, Andrade J, Gozal D (2017) Late gestational intermittent hypoxia induces metabolic and epigenetic changes in male adult offspring mice. *J Physiol* 595(8):2551–2568
- Louis JM, Mogos MF, Salemi JL, Redline S, Salihi HM (2014) Obstructive sleep apnea and severe maternal-infant morbidity/mortality in the United States, 1998–2009. *Sleep* 37(5):843–849
- Louis JM, Koch MA et al (2018) Predictors of sleep-disordered breathing in pregnancy. *Am J Obstet Gynecol* 218:521.e1–521.e12
- Luo ZC, Fraser WD, Julien P et al (2006) Tracing the origins of “fetal origins” of adult diseases: programming by oxidative stress? *Med Hypotheses* 66:38–44
- Martins FO, Conde SV (2021) Gender differences in the context of obstructive sleep apnea and metabolic diseases. *Front Physiol* 12:792633
- Myatt L (2006) Placental adaptive responses and fetal programming. *J Physiol* 572(Pt 1):25–30
- Osmond C, Barker DJ (2000) Fetal, infant, and childhood growth are predictors of coronary heart disease, diabetes, and hypertension in adult men and women. *Environ Health Perspect* 108(Suppl 3):545–553
- Pamidi S, Kimoff RJ (2018) Maternal sleep-disordered breathing. *Chest* 153:1052–1066
- Parks WT (2017) Manifestations of hypoxia in the second and third trimester placenta. *Birth Defect Res* 109(17):1345–1357
- Pires GN, Benedetto L, Cortese R, Gozal D, Gulia KK, Kumar VM, Tufik S, Andersen ML (2021) Effects of sleep modulation during pregnancy in the mother and offspring: evidences from preclinical research. *J Sleep Res* 30:e13135
- Ramírez Guirado A, Morales Rodríguez A (2014) Trastornos de la respiración asociados al sueño durante el embarazo. *Rev Cubana Obstet Ginecol* 40(4). Ciudad de la Habana
- Ravishankar S, Bourjeily G, Lambert-Messerlian G, He M, De Paepe ME, Gündoğan F (2015) Evidence of placental hypoxia in maternal sleep disordered breathing. *Pediatr Dev Pathol* 18(5):380–386
- Soares MJ, Chakraborty D, Karim Rumi MA, Konno T, Renaud SJ (2012) Rat placentation: an experimental model for investigating the hemochorial maternal-fetal interface. *Placenta* 33(4):233–243
- Zhu B, Bronas UG, Carley DW, Lee K, Steffen A, Kapella M, Izci-Balserak B (2020) Relationships between objective sleep parameters and inflammatory biomarkers in pregnancy. *Ann N Y Acad Sci* 1473(1):62–73



Ventilatory Effects of Acute Intermittent Hypoxia in Conscious Dystrophic Mice

Michael N. Maxwell, Anthony L. Marullo, Aoife D. Slyne, Eric F. Lucking, and Ken D. O'Halloran

Abstract

Exposure to acute intermittent hypoxia (AIH) elicits a form of respiratory plasticity known as long-term facilitation (LTF). Interest has grown in developing AIH interventions to treat ventilatory insufficiency, with promising results in spinal cord injury and amyotrophic lateral sclerosis. Therapeutic AIH may have application in neuromuscular disorders including muscular dystrophies. We sought to establish hypoxic ventilatory responsiveness and the expression of ventilatory LTF in X-linked muscular dystrophy (*mdx*) mice.

Experiments were performed in 15 male wild-type (BL10) and 15 male *mdx* mice at 4 months of age. Ventilation was assessed using whole-body plethysmography. Baseline measures of ventilation and metabolism were established. Mice were exposed to 10 successive bouts of hypoxia, each lasting 5 min, interspersed with 5-min bouts of normoxia. Measurements were taken for 60 min following termination of AIH.

In *mdx* mice, ventilation was significantly increased 60 min post-AIH compared to base-

line. However, metabolic CO₂ production was also increased. Therefore, ventilatory equivalent was unaffected by AIH exposure, i.e., no ventilatory LTF manifestation. In wild-type mice, ventilation and metabolism were not affected by AIH.

Eliciting ventilatory LTF is dependent on many factors and may require concomitant isocapnia or hypercapnia during AIH exposures and/or repeated daily AIH exposures, which is worthy of further pursuit.

Keywords

Acute intermittent hypoxia · Long term facilitation · Duchenne muscular dystrophy · *mdx* · Whole-body plethysmography

9.1 Introduction

Duchenne muscular dystrophy (DMD) is a severe monogenic neuromuscular disease caused by secondary consequences arising due to the absence of the structural protein dystrophin. Muscle contraction without dystrophin mechanically strains the plasma membrane, causing injury to the myofibres and subsequent skeletal muscle degeneration, which leads to a profound loss of function (Gumerson and Michele 2011; Manning and O'Malley 2015). Dysfunction

M. N. Maxwell · A. L. Marullo · A. D. Slyne
E. F. Lucking · K. D. O'Halloran (✉)
Department of Physiology, School of Medicine,
College of Medicine & Health, University College
Cork, Cork, Ireland
e-mail: k.ohalloran@ucc.ie

extends to the respiratory musculature (Sawnani et al. 2015).

In infancy, people with DMD present with symptoms such as frequent falls and a waddling gait, culminating in wheelchair dependency by about 10–12 years of age. Most DMD patients require assisted ventilation in some capacity around the age of 20 years. Advances in cardiorespiratory care have increased patients' life expectancy from early 20s to 30s with some living until the age of ~40 (Life expectancy – Muscular dystrophy news 2021). There is continued interest in the development of novel therapeutic strategies.

Progressive DMD is characterised by ventilatory insufficiency. People with DMD hypoventilate, especially during sleep (Sawnani et al. 2015). Exposure to acute intermittent hypoxia (AIH) elicits a form of respiratory plasticity known as long-term facilitation (LTF), which increases respiratory motor output. Following decades of basic fundamental research in animal models, therapeutic intermittent hypoxia is now an established modality with proven capacity to increase ventilation in various disease states characterised by ventilatory compromise including amyotrophic lateral sclerosis and incomplete spinal cord injury, restoring normal or near-normal levels of breathing (Golder and Mitchell 2005; Nichols et al. 2017; Sajjadi et al. 2022; Sutor et al. 2021).

Therapeutic intermittent hypoxia may be useful as an adjunctive therapy in the treatment of DMD. The aim of this study was to establish the capacity for the expression of ventilatory LTF in X-linked muscular dystrophy using *mdx* mice.

9.2 Materials and Methods

9.2.1 Ethical Approval

Procedures on live animals were performed under authorisation from the Health Products Regulatory Authority in accordance with Irish and European law following approval by University College Cork's ethics committee (AEEC no. 2021/019). Experiments were carried

out in accordance with guidelines laid down by University College Cork's Animal Welfare Body.

9.2.2 Experimental Animals

Male wild-type (C57BL/10; $n = 15$) and *mdx* (C57BL/10ScSn-*Dmd*^{*mdx*}/J; $n = 15$) mice were bred in our institution's animal housing facility and were studied at 4 months of age. Animals were housed in individually ventilated cages in temperature- and humidity-controlled rooms, operating under a 12:12 h light/dark cycle with food and water available ad libitum.

9.2.3 Whole-Body Plethysmography

Whole-body plethysmography was used to assess respiratory flow in unrestrained, unanaesthetised mice. Mice were introduced into plethysmograph chambers (Model PLY4211; volume 600 mL; Buxco Research Systems, Wilmington, NC, USA) and allowed to acclimate to the chamber environment for ~2 h. Following completion of exploration and grooming behaviours, mice settled and were studied during quiet rest.

Experimental Protocol Following acclimation and a settling period, a 30-min baseline recording was performed in normoxia. This was followed by 10 successive bouts of hypoxia ($FiO_2 = 0.10$), lasting 5 min, interspersed with 5-min bouts of normoxia ($FiO_2 = 0.21$). Measurements were taken for 60 min following termination of AIH. Following the experimental protocol, mice were anaesthetised using 5% isoflurane in air and killed by cervical dislocation.

9.2.4 Data and Statistical Analysis

Minute ventilation (V_I) and metabolic CO_2 production (VCO_2) were normalised for body mass (g). Data are shown as individual data points in box and whisker plots with median, interquartile

ranges and maximum and minimum values. The ventilatory equivalent (V_I/V_{CO_2}) was determined. One-way ANOVA was performed with Bonferroni post hoc comparisons. $P < 0.05$ was considered statistically significant.

9.3 Results

9.3.1 Effect of AIH on Ventilation

In wild-type mice, there was no significant difference in minute ventilation at either 30 min ($p = 0.4355$) or 60 min ($p = 0.8310$) compared with the initial baseline pre-AIH (Fig. 9.1a). In *mdx* mice, there was no significant difference between the initial baseline values and 30 min post-AIH ($p = 0.1167$); however, a significant increase was observed at 60 min post-AIH ($p = 0.0124$) (Fig. 9.1b).

9.3.2 Effect of AIH on Metabolism

In wild-type mice, there was no significant difference in metabolic CO_2 production at either 30 min ($p = 0.9766$) or 60 min ($p = 0.1964$) compared with the initial baseline pre-AIH (Fig. 9.2a). In *mdx* mice, there was a significant increase in metabolic CO_2 production at 30 min

post-AIH ($p = 0.0019$) and 60 min post-AIH ($p = 0.0122$) (Fig. 9.2b).

9.3.3 Effect of AIH on the Ventilatory Equivalent

In wild-type mice, the ventilatory equivalent (V_I/V_{CO_2}) was comparable to baseline at 30 min ($p = 0.6557$) and 60 min ($p = 0.7626$) (Fig. 9.3a). Similarly, in *mdx* mice, there was no significant difference in the ventilatory equivalent comparing the initial baseline values and values at 30 min post-AIH ($p = 0.8315$) and 60 min post-AIH ($p = 0.7447$) (Fig. 9.3b).

9.4 Discussion

We sought to establish the capacity for the expression of ventilatory LTF in X-linked muscular dystrophy using *mdx* mice. Ventilation, metabolism and the ventilatory equivalent were examined at baseline and for 60 min following AIH. We fully anticipated that the AIH protocol employed in the study would elicit LTF in wild-type mice, based upon prior literature, albeit mostly in rats (Hoffman and Mitchell 2013; Mendonça-Junior et al. 2021). Whether AIH would elicit LTF in *mdx* mice was an open ques-

Fig. 9.1 Ventilation following exposure to AIH. Minute ventilation during baseline (pre-AIH) and 30 and 60 min post-AIH for (a) wild-type and (b) *mdx* mice

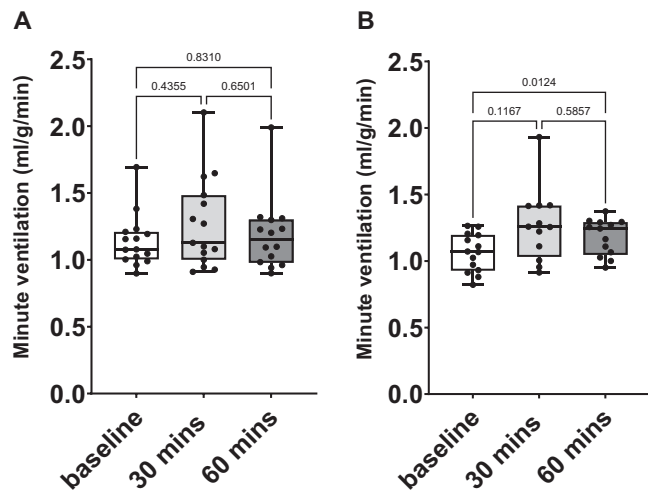


Fig. 9.2 Metabolism following exposure to AIH. Metabolic CO_2 production during baseline (pre-AIH) and 30 and 60 min post-AIH for (a) wild-type and (b) *mdx* mice

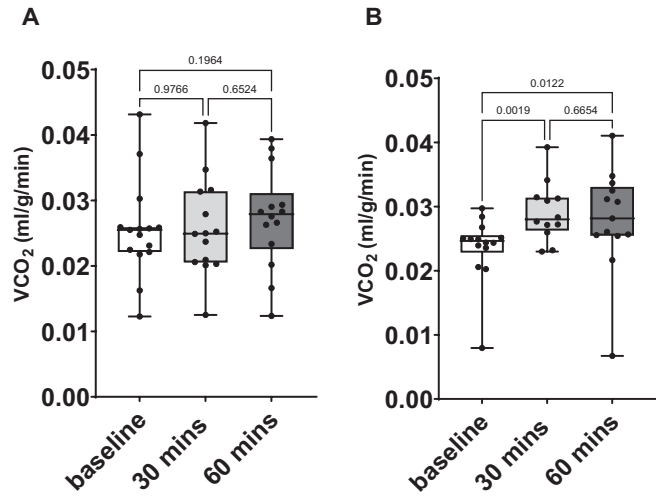
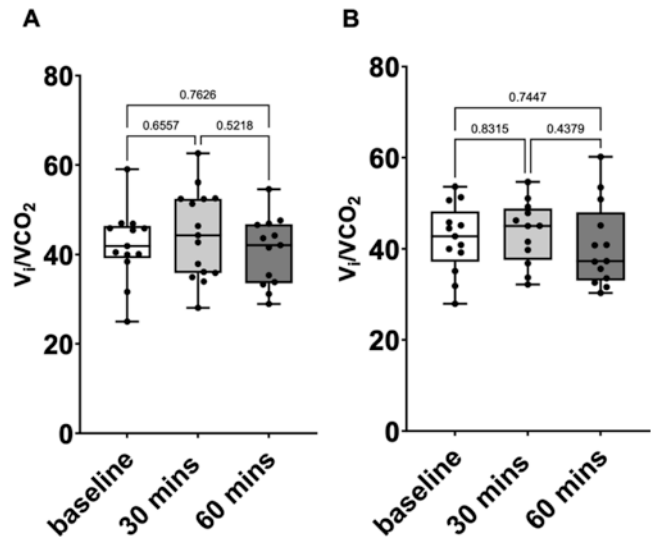


Fig. 9.3 Ventilatory equivalent following exposure to AIH. Ventilatory equivalent pre-AIH, and 30 and 60 min post-AIH for (a) wild-type and (b) *mdx* mice



tion given that there are impairments at several sites of the respiratory network in *mdx* mice (Burns et al. 2017, 2018; 2019a, b; Lovering et al. 2020; Mhandire et al. 2022), which could conceivably limit the capacity to elicit LTF.

In *mdx* mice, upon examination of the data for ventilation, it is evident that minute ventilation was significantly increased 60 min following exposure to AIH compared to the initial baseline period. On the face of it, this is suggestive of the expression of LTF of breathing. However, upon examination of the metabolic CO_2 production at the same timepoints, we determined that there were also significant increases in metabolism at

both 30 and 60 min compared with baseline values. There was no overt difference in animal activity or behaviour between the respective timepoints suggesting that the metabolic effect may have been a direct effect of exposure to AIH. However, as illustrated by the data for ventilatory equivalent ($V_i/V\text{CO}_2$), it is clear that the increase in ventilation following AIH was an appropriate adjustment for the increase in metabolism. As such, there was no expression of ventilatory LTF in dystrophic mice.

Surprisingly, LTF did not manifest in wild-type mice also. Indeed, neither ventilation nor metabolism were affected by exposure to AIH in

wild-type mice. As such, given this unexpected finding, the issue as to whether LTF can be expressed in muscular dystrophy remains inconclusive. Further studies are required to establish a model of LTF in conscious BL-10 mice that can be applied to the *mdx* mouse model of muscular dystrophy.

The capacity to elicit ventilatory LTF is dependent on many factors and future experimental studies could consider the following modifications to the current study. First, it may be necessary to employ concomitant isocapnia or hypercapnia during AIH exposure. The combined effect of hypoxia and CO₂ to enhance chemoreceptor activation of breathing may be required to elicit long-lasting robust facilitation of breathing (Wakai et al. 2015). Second, daily AIH exposure to elicit metaplasticity may be required for sustained functional gains and will be important to establish in the context of chronic rehabilitative therapy for DMD (Hickner et al. 2014). Third, pharmacological co-treatment could be applied in tandem with AIH, for example, the use of adenosine receptor blockade to avoid cross-talk inhibition of serotonergic mechanisms contributing to LTF (Hoffman et al. 2010). And finally, albeit more readily applicable to the clinical scenario, task-specific co-treatment such as exposure to AIH in tandem with ventilatory-specific exercises might amplify the plasticity priming effects of AIH to drive ventilatory LTF (Welch et al. 2020).

We acknowledge too that whereas our study was an attempt at proof of principle, to consider the manifestation of LTF in a mouse model of DMD, whether AIH can be safely and effectively applied in human DMD is an issue requiring careful consideration. Whereas DMD is characterised by ventilatory insufficiency, interventions that increase neural drive to recruit respiratory muscles could potentially exacerbate muscle dysfunction through enhanced contraction-induced injury. Interestingly, however, repeated exposure to AIH has the potential to influence many other aspects of the respiratory system including respiratory muscles. Whereas chronic intermittent hypoxia modelling human sleep apnoea results in respiratory dysfunction, including respiratory muscle weakness

(Drummond et al. 2021, 2022; O'Halloran 2016; O'Halloran et al. 2017; Skelly et al. 2012), that must clearly be avoided in therapeutic strategies for muscle weakness disorders, there is scope for modest application of AIH paradigms to evoke muscle plasticity in favour of improved functional outcomes and/or resilience to stressors associated with disease. We suggest that further study of the potential benefits of AIH for the treatment of muscular dystrophy is worthy of pursuit.

References

- Burns DP, Roy A, Lucking EF, McDonald FB, Gray S, Wilson RJ et al (2017) Sensorimotor control of breathing in the *mdx* mouse model of Duchenne muscular dystrophy. *J Physiol* 595(21):6653–6672. [Internet] [cited 2022 Nov 15]. Available from: <https://pubmed.ncbi.nlm.nih.gov/28952155/>
- Burns DP, Canavan L, Rowland J, O'Flaherty R, Brannock M, Drummond SE et al (2018) Recovery of respiratory function in *mdx* mice co-treated with neutralizing interleukin-6 receptor antibodies and urocortin-2. *J Physiol* 596(21):5175–5197. [Internet] [cited 2022 Nov 15]. Available from: <https://pubmed.ncbi.nlm.nih.gov/30160301/>
- Burns DP, Murphy KH, Lucking EF, O'Halloran KD (2019a) Inspiratory pressure-generating capacity is preserved during ventilatory and non-ventilatory behaviours in young dystrophic *mdx* mice despite profound diaphragm muscle weakness. *J Physiol* 597(3):831. [Internet] [cited 2022 Nov 15]. Available from: <https://physoc.onlinelibrary.wiley.com/doi/10.1113/JP277443>
- Burns DP, Drummond SE, Bolger D, Coiscaud A, Murphy KH, Edge D et al (2019b) N-acetylcysteine decreases fibrosis and increases force-generating capacity of *mdx* diaphragm. *Antioxidants* 8(12). [Internet] [cited 2022 Nov 15]. Available from: <https://www.mdpi.com/2076-3921/8/12/581>
- Drummond SE, Burns DP, O'Connor KM, Clarke G, O'Halloran KD (2021) The role of NADPH oxidase in chronic intermittent hypoxia-induced respiratory plasticity in adult male mice. *Respir Physiol Neurobiol* 292:103713. [Internet] [cited 2022 Nov 15]. Available from: <https://linkinghub.elsevier.com/retrieve/pii/S1569904821000987>
- Drummond SE, Burns DP, El Maghrani S, Ziegler O, Healy V, O'Halloran KD (2022) NADPH oxidase 2 is necessary for chronic intermittent hypoxia-induced sternohyoid muscle weakness in adult male mice. *Exp Physiol* 107(8):946–964. [Internet] [cited 2022 Nov 15]. Available from: <https://pubmed.ncbi.nlm.nih.gov/35728802/>

- Golder FJ, Mitchell GS (2005) Spinal synaptic enhancement with acute intermittent hypoxia improves respiratory function after chronic cervical spinal cord injury. *J Neurosci* 25(11):2925. [Internet] [cited 2022 Nov 15]. Available from: <https://www.jneurosci.org/content/25/11/2925.long>
- Gumerson JD, Michele DE (2011) The dystrophin-glycoprotein complex in the prevention of muscle damage. *J Biomed Biotechnol* 2011:210797 [Internet] [cited 2021 Sep 21]. Available from: <https://www.ncbi.nlm.nih.gov/pmc/articles/PMC22007139/?tool=EBI>
- Hickner S, Hussain N, Angoa-Perez M, Francescutti DM, Kuhn DM, Mateika JH (2014) Ventilatory long-term facilitation is evident after initial and repeated exposure to intermittent hypoxia in mice genetically depleted of brain serotonin. *J Appl Physiol* 116(3):240. [Internet] [cited 2022 Nov 14]. Available from: <https://journals.physiology.org/doi/full/10.1152/jappphysiol.01197.2013>
- Hoffman MS, Mitchell GS (2013) Spinal 5-HT7 receptors and protein kinase A constrain intermittent hypoxia-induced phrenic long-term facilitation. *Neuroscience* 250:632–643. [Internet] [cited 2022 Nov 15]. Available from: <https://www.sciencedirect.com/science/article/pii/S0306452213005745?via%3Dihub>
- Hoffman MS, Golder FJ, Mahamed S, Mitchell GS (2010) Spinal adenosine A2A receptor inhibition enhances phrenic long term facilitation following acute intermittent hypoxia. *J Physiol* 588(Pt 1):255. [Internet] [cited 2022 Nov 15]. Available from: <https://physoc.onlinelibrary.wiley.com/doi/full/10.1113/jphysiol.2009.180075>
- Life expectancy – Muscular dystrophy news [Internet] [cited 2021 Sep 21]. Available from: <https://muscular-dystrophynews.com/life-expectancy/>
- Lovering RM, Iyer SR, Edwards B, Davies KE (2020) Alterations of neuromuscular junctions in Duchenne muscular dystrophy. *Neurosci Lett* 737:135304. [Internet] [cited 2022 Nov 15]. Available from: <https://www.sciencedirect.com/science/article/pii/S03043942020305747?via%3Dihub>
- Manning J, O'Malley D (2015) What has the mdx mouse model of duchenne muscular dystrophy contributed to our understanding of this disease? *J Muscle Res Cell Motil* 36:155–167 [Internet] [cited 2021 Sep 15]. Available from: <http://link.springer.com/10.1007/s10974-015-9406-4>
- Mendonça-Junior BA, Fernandes M, Zoccal DB (2021) Acute intermittent hypoxia evokes ventilatory long-term facilitation and active expiration in unanesthetized rats. *Respir Physiol Neurobiol* 294:103768. [Internet] [cited 2022 Nov 15]. Available from: <https://linkinghub.elsevier.com/retrieve/pii/S1569904821001531>
- Mhandire DZ, Burns DP, Roger AL, O'Halloran KD, ElMallah MK (2022) Breathing in Duchenne muscular dystrophy: translation to therapy. *J Physiol* 600(15):3465–3482. [Internet] [cited 2022 Nov 15]. Available from: <https://pubmed.ncbi.nlm.nih.gov/35620971/>
- Nichols NL, Satriotomo I, Allen LL, Grebe AM, Mitchell GS (2017) Mechanisms of Enhanced Phrenic Long-Term Facilitation in SOD1G93A Rats. *J Neurosci* 37(24):5834. [Internet] [cited 2022 Nov 15]. Available from: <https://www.jneurosci.org/content/37/24/5834>
- O'Halloran KD (2016) Chronic intermittent hypoxia creates the perfect storm with calamitous consequences for respiratory control. *Respir Physiol Neurobiol* 226:63–67. [Internet] [cited 2022 Nov 15]. Available from: <https://linkinghub.elsevier.com/retrieve/pii/S1569904815300677>
- O'Halloran KD, Lewis P, McDonald F (2017) Sex, stress and sleep apnoea: decreased susceptibility to upper airway muscle dysfunction following intermittent hypoxia in females. *Respir Physiol Neurobiol* 245:76–82. [Internet] [cited 2022 Nov 15]. Available from: <https://linkinghub.elsevier.com/retrieve/pii/S1569904816302154>
- Sajjadi E, Seven YB, Ehrbar JG, Wymer JP, Mitchell GS, Smith BK (2022) Acute intermittent hypoxia and respiratory muscle recruitment in people with amyotrophic lateral sclerosis: a preliminary study. *Exp Neurol* 347. [Internet] [cited 2022 May 6]. Available from: <https://pubmed.ncbi.nlm.nih.gov/34624328/>
- Sawnani H, Thampratankul L, Szczesniak RD, Fenchel MC, Simakajornboon N (2015) Sleep disordered breathing in young boys with Duchenne muscular dystrophy. *J Pediatr* 166(3):640–645.e1. [Internet] [cited 2022 Nov 15]. Available from: <https://linkinghub.elsevier.com/retrieve/pii/S002234761401155X>
- Skelly JR, Edge D, Shortt CM, Jones JFX, Bradford A, O'Halloran KD (2012) Tempol ameliorates pharyngeal dilator muscle dysfunction in a rodent model of chronic intermittent hypoxia. *Am J Respir Cell Mol Biol* 46(2):139–48. [Internet] [cited 2022 Nov 15]. Available from: <https://pubmed.ncbi.nlm.nih.gov/21868712/>
- Sutor T, Cavka K, Vose AK, Welch JF, Davenport P, Fuller DD et al (2021) Single-session effects of acute intermittent hypoxia on breathing function after human spinal cord injury. *Exp Neurol* 342:113735. [Internet] [cited 2022 Nov 15]. Available from: <https://linkinghub.elsevier.com/retrieve/pii/S0014488621001412>
- Wakai J, Takamura D, Morinaga R, Nakamuta N, Yamamoto Y (2015) Differences in respiratory changes and Fos expression in the ventrolateral medulla of rats exposed to hypoxia, hypercapnia, and hypercapnic hypoxia. *Respir Physiol Neurobiol* 215:64–72. [Internet] [cited 2022 Nov 14]. Available from: <https://linkinghub.elsevier.com/retrieve/pii/S156990481500110X>
- Welch JF, Sutor TW, Vose AK, Perim RR, Fox EJ, Mitchell GS (2020). Synergy between acute intermittent hypoxia and task-specific training. *Exerc Sport Sci Rev* [Internet] [cited 2022 Nov 15];48(3):125. Available from: https://journals.lww.com/acsm-essr/Fulltext/2020/07000/Synergy_between_Acute_Intermittent_Hypoxia_and_4.aspx



Intermittent Hypoxia and Diet-Induced Obesity on the Intestinal Wall Morphology in a Murine Model of Sleep Apnea

Esther Valverde-Pérez, Elena Olea, Ana Obeso, Jesús Prieto-Lloret, Asunción Rocher, and Elvira Gonzalez-Obeso

Abstract

This work analyzes the impact of two conditions, intermittent hypoxia exposure and high-fat diet in rats as models of sleep apnea. We studied the autonomic activity and histological structure of the rat jejunum and whether the overlapping of both conditions, as often observed in patients, induces more deleterious effects on the intestinal barrier. We found alterations in jejunum wall histology, predominantly in HF rats, based on increased crypt depth and submucosal thickness, as well as decreased muscularis propria thickness. These

alterations were maintained with the IH and HF overlap. An increase in the number and size of goblet cells in the villi and crypts and the infiltration of eosinophils and lymphocytes in the lamina propria suggest an inflammatory status, confirmed by the increase in plasma CRP levels in all experimental groups. Regarding the CAs analysis, IH, alone or combined with HF, causes a preferential accumulation of NE in the catecholaminergic nerve fibers of the jejunum. In contrast, serotonin increases in all three experimental conditions, with the highest level in the HF group. It remains to be elucidated whether the alterations found in the present work could affect the permeability of the intestinal barrier, promoting sleep apnea-induced morbidities.

E. Valverde-Pérez · A. Obeso · J. Prieto-Lloret
A. Rocher (✉)
Departamento de Bioquímica y Biología Molecular y Fisiología, Facultad de Medicina, Universidad de Valladolid, Valladolid, Spain

Instituto de Biomedicina y Genética Molecular (IBGM), UVa-CSIC, Valladolid, Spain
e-mail: asun.rocher@uva.es

E. Olea
Instituto de Biomedicina y Genética Molecular (IBGM), UVa-CSIC, Valladolid, Spain

Departamento de Enfermería, Facultad de Enfermería, Universidad de Valladolid, Valladolid, Spain

E. Gonzalez-Obeso
Instituto de Biomedicina y Genética Molecular (IBGM), UVa-CSIC, Valladolid, Spain

Servicio de Anatomía Patológica, Hospital Clínico Universitario de Valladolid, Valladolid, Spain

Keywords

Intermittent hypoxia · High fat diet · Intestinal wall · Sympathetic activity · Inflammation · Adiposity index

10.1 Introduction

Obesity is a well-defined risk factor for cardiovascular and metabolic disorders and, especially, for obstructive sleep apnea (OSA), both emerging health issues. It is well recognized that there is a high prevalence of OSA among

obese subjects due to alterations in pulmonary function by increased airflow resistances (due to peripharyngeal fat) and an abnormal restrictive ventilatory pattern (due to intrathoracic and intra-abdominal fat) leading to a ventilatory depression (Gifford et al. 2010; Zammit et al. 2010; Piper and Grunstein 2011). OSA is also related with many comorbidities, including cardiovascular, metabolic, endocrine, and neurologic disorders, leading to an overall increase in morbidity and mortality (Nieto et al. 2000; Young et al. 2009).

It is already established a reciprocal interaction between obesity and OSA. The frequency and severity of OSA correlates with body mass index and weight loss; bariatric surgery ameliorates the sleep disorder (Gozal et al. 2001). When comparing obese people with and without OSA, Vgontzas et al. (2000) showed that the major difference between both groups was the higher amount of visceral fat depots in patients with OSA. This increase in visceral fat content was strongly correlated with the degree of respiratory disturbance or severity of nocturnal intermittent hypoxemia. Thus, OSA itself has a role in the development and reinforcement of obese status via changes to energy expenditure, neurohormonal mechanisms controlling satiety and hunger, and sleep quality and duration (Ong et al. 2013).

Both pathologies, obesity and OSA, represent a mild chronic systemic inflammatory process, with increased cytokines such as tumor necrosis factor- α (TNF- α), interleukin-1 (IL-1) and interleukin-6 (IL-6), and C-reactive protein (CRP). While in obese patients this appears to be due to excessive production of these mediators in adipose tissue, intermittent hypoxemia represents a pivotal factor in the activation of oxidative stress and inflammatory pathways in OSA (Hotamisligil 2006; Lavie 2014). Thus, recurrent blood oxygen desaturation and consequent changes in oxygen supply of circulation elicit oscillations in the oxygen partial pressure in tissues. These oscillating changes in the oxygen availability of tissues are widely considered as an important source of reactive oxygen species (ROS) which can be generated from different subcellular compartments

and organelles. Most cells respond to increased ROS by upregulating the redox-sensitive transcriptional factor NF- κ B, a key molecule in the proinflammatory response. In the nucleus, NF- κ B upregulates the transcription of several proinflammatory genes responsible for encoding inflammatory cytokines, chemokines, surface adhesion molecules, and other enzymes such as cyclooxygenase-2 (COX-2) that further damage the endothelium, decreasing vasodilator mediators and facilitating hypertension, and cardiovascular accidents (Ryan et al. 2005).

Several studies demonstrate that altered sleep and oxygenation patterns, as observed in OSA, also promote specific alterations in the gut microbiota that, in turn, can cause immunological alterations leading to OSA-induced morbidities (Moreno-Indias et al. 2015; Poroyko et al. 2016). Attention has also focused on the role of the gut microbiota in the regulation of adiposity and body weight. In genetically obese mice and obese patients, there is a significant change in the composition of the gut microbiota compared with lean controls (Ley et al. 2005), and, in mice, these modifications can be induced by ingestion of an HF diet. In addition, immune cell activation of the intestinal mucosa with fat intake could generate the secretion of inflammatory cytokines (Cani et al. 2008; Backhed et al. 2004).

On the contrary, few studies have analyzed the gut barrier status, i.e., whether inflammation caused by obesity or IH affects intestinal function or whether inflammation occurs in the gut itself due to treatments. Other mechanisms, such as altered activity in the peripheral and central nervous system or changes in the gut structure, have also not been fully explored.

This work attempts to analyze whether exposure to IH or HF diet produces changes in intestinal autonomic activity or morphological alterations in the histological structure of rat jejunum and whether the overlapping of both conditions produces a higher impact on the intestinal barrier. To address this aim, we performed a pilot study in rats subjected to a four variable design combining oxygen derangements (intermittent hypoxia or normoxia) and two dietary conditions (high-fat or standard diet).

10.2 Methods

10.2.1 Animal Protocols

In handling the animals, we followed the European Community Council Directive for Protection of Vertebrates Used for Experimental and Other Scientific Ends (2010/63/EU). All experiments were performed in accordance with protocols approved by the University of Valladolid Institutional Committee for Animal Care and Use (Project Approval Ethical Code: 4505502).

The study was carried out with 32 adults male Wistar rats. Rats were housed four per cage in the vivarium of the University of Valladolid, with free access to food and water, under controlled conditions of temperature and humidity, and in a stationary light-dark cycle (12:12). Animals were randomly assigned to four experimental groups with different combinations of diet and oxygen treatment. The control group (C) was fed standard rat solid diet providing 3.8 kcal/g with 10% kcal from fat (D12450B; Open-Source Diets) until they reached 12 weeks of age. A second group was equally standard fed and subjected to IH (chronic intermittent hypoxia group, CIH) from week 9 to 12. The third group, rats received a high-fat diet (5.2 kcal/g with 60% kcal from fat; D12492; Open-Source Diets) until they reached 12 weeks of age (HF group). The fourth group was given the same diet as the HF group, and during week 9–12 was exposed to IH (HF plus intermittent hypoxia group, HFIH) (Fig. 10.1).

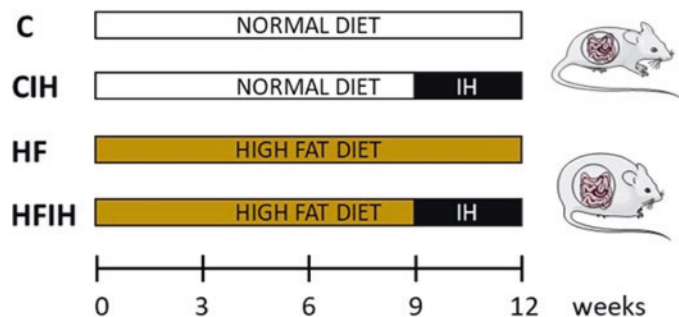
The specific protocol of IH used consisted of 30 cycles/hour of exposure for 40 s to 5% O₂ and

then exposure for 80 s to air for 8 h per day (from 08:00 to 16:00; i.e., during the animals' time of inactivity) for 3 weeks. In this condition, in previous experiments, we found that the lowest value of arterial PO₂ measured was 37.2 ± 0.9 mmHg, with the percentage of HbO₂ prior to hypoxic episodes being 96.5 ± 0.8% and lowest mean values being 73.5 ± 1.4%. The time that SaO₂ was below 90% represented 25% of the 8-h duration of the hypoxic exposure (Quintero et al. 2013).

10.2.2 Tissue Collection

At the beginning and weekly until the end of the treatment, animals were weighed. After overnight fasting, basal glucose was determined in collected tail blood (Ascensia Breeze 2 glucometer, Bayer). After anesthesia with sodium pentobarbital (ip; 60 mg/kg body weight), rats were tracheotomized and pump-ventilated with air. The chest was opened, and blood was slowly withdrawn by direct puncture to the left ventricle. Citrated blood was centrifuged at 1000 g for 5 min at RT. Supernatant was frozen at -80 °C until use. Plasma catecholamines (CAs) were analyzed by HPLC and plasma C-reactive protein (CRP) levels by a commercial rat-specific ELISA (bioNova Cientifica, Madrid, Spain). For analysis of endogenous CAs in small intestine, segments of jejunum were collected and weighed, and supernatants of glass-to-glass (0.1 N perchloric acid, 0.1 mM EDTA) homogenized tissues directly injected into an HPLC system. The chromatographic system and conditions have been described in detail elsewhere (Prieto-Lloret et al. 2021).

Fig. 10.1 Chronogram of treatments in $n = 8$ rats/group



Additional segments of jejunum were collected, fixed in 4% paraformaldehyde in 0.1 M PB, and embedded in paraffin. Transversal 5 μ m sections were stained with hematoxylin and eosin (H/E). Photographs were taken with a digital camera (CoolSNAP Photometric Roper Scientific) attached to the microscope and processed with ImageJ software.

10.2.3 Statistical Analysis

Data were evaluated using GraphPad Prism Software, version 6 (GraphPad Software Inc., USA), expressed as mean \pm SEM. The significance of the differences between the mean values was calculated by Student's t-Test and one- and two-way ANOVA with Tukey's and/or Bonferroni multiple comparison test. Differences were considered significant at $p < 0.05$. Different letters denote significant differences between groups.

10.3 Results

10.3.1 Body Weight Gain and Visceral Fat Deposits

Figure 10.2a shows the body weight gain after the 12 weeks of the experiment. As expected, weight gain was greater in the animals fed with a

high-fat diet (HF final weight 607.8 ± 15.6 g; HFIH final weight, 624.3 ± 33.9 g) than in control animals (C final weight, 502.3 ± 19.2 g). Exposure to IH alone caused a nonsignificant (10%) decrease in weight gain (CIH, 447.8 ± 8.5 g) absent when combining with high fat (HFIH). Weight of visceral fat pads was not different in CIH but were 2–2.5 times greater in animals fed with high fat (HF and HFIH group) than in those fed with a standard diet (Fig. 10.2b).

10.3.2 Basal Glycemia and Markers of Sympathetic and Inflammatory Activity

Table 10.1 shows the basal plasma glucose levels in the four groups of rats. Fasting glycemia in C animals was 107.3 ± 1.5 mg/dL, with no significant changes between experimental groups, although all of them trend toward hyperglycemia and HF almost significantly ($p = 0.063$). There was no positive interaction between HF and IH promoting a further increase in glycemia.

CRP is an acute-phase protein that is synthesized mainly in hepatocytes in response to inflammatory mediators and released into the plasma. In turn, at the cellular level, CRP can trigger the generation of ROS, creating a vicious cycle that leads to the development of chronic inflammation (Zhang et al. 2012). Table 10.1 shows that plasma

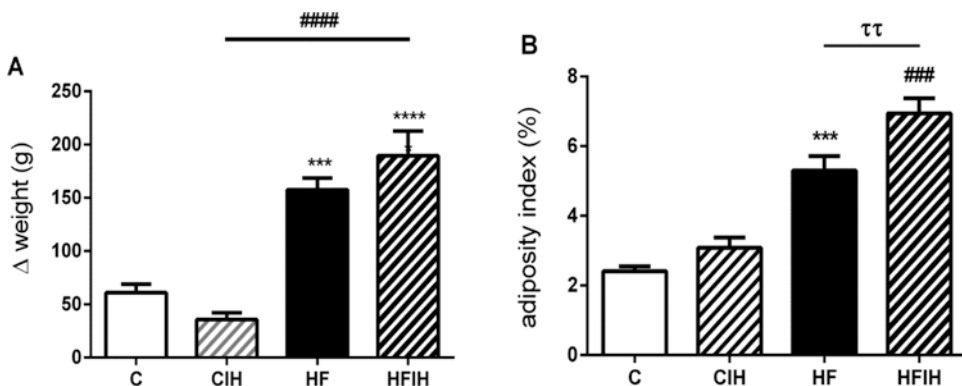


Fig. 10.2 Effects of high-fat diet and chronic intermittent hypoxia on body weight gain and visceral fat deposits. (a) Body weight gain in the four groups of animals (C control, CIH chronic intermittent hypoxia, HF high-fat diet,

HFIH high-fat diet + intermittent hypoxia). (b) Visceral adipose tissue expressed as % body weight. Data are means \pm SEM ($n = 8$). *** $P < 0.001$ vs C; #### $p < 0.001$ vs CIH and $\tau\tau p < 0.01$ vs H. One-way ANOVA

Table 10.1 Markers of sympathetic and inflammatory activity

Parameters	Control	CIH	HF	HFIH
Basal glycemia (mg/dl)	107.3 ± 1.5	121.3 ± 7.3	134.9 ± 7.7	118.3 ± 7.2
CRP (µg/ml plasma)	65 ± 6	128.1 ± 5.3***	139.8 ± 3.6***	151.2 ± 2.7***#
NE (pmol/mg intestine)	4.7 ± 0.1	5.2 ± 0.2*	4.3 ± 0.2	5.2 ± 0.2 #
DA (pmol/mg intestine)	0.16 ± 0.02	0.21 ± 0.01	0.18 ± 0.02	0.20 ± 0.01
5HT (pmol/mg intestine)	20.6 ± 1.1	23.2 ± 1.9*	26.1 ± 1.9*	24.1 ± 2.1

Data are means ± SEM ($n = 8$). * $p < 0.05$ and *** $p < 0.001$ vs C; # $p < 0.05$ vs HF. One-way ANOVA

CRP levels in the CIH and HF groups were approximately doubled relative to C group ($p < 0.001$) and further increased in the HFIH group ($p < 0.05$ vs HF). According to these data, CIH and HF diet elicit an inflammatory state that is reinforced in the HFIH group.

Gut levels of monoamine neurotransmitters contained in the jejunum wall and their changes after IH and HF treatments were measured in homogenates of jejunum segments. The NE content of the sympathetic endings of the jejunum wall increased in CIH and HFIH groups indicating an increase in sympathetic tone after the hypoxic treatment (Table 10.1). Regarding DA levels, no significant changes were observed between the four groups of animals. Serotonin (5-HT), the main amine in the intestine, increased in all experimental groups by about 20% ($p < 0.05$). If the 5-HT content accurately reflects the activity of endocrine-like cells, our findings suggest that an increased activity of the endocrine-like cells can play a role in the hypoxic and HF gut response, acting on neural elements as well as on smooth muscle cells via paracrine action.

10.3.3 Morphology of Jejunum Wall

To evaluate possible alterations of intestinal barrier properties, we analyzed jejunum morphology after treatment with IH, HF, and HFIH (Fig. 10.3a). Transversal sections from the jejunum revealed a significant decrease in jejunum villus length in HFIH group ($p < 0.05$) and a trend in CIH (Fig. 10.3b), whereas crypt depth (Fig. 10.3c) increased in HF animals ($p < 0.001$) versus control rats. In addition, the thickness of the jejunum muscularis propria in HF and HFIH groups was significantly decreased (Fig. 10.3d).

In contrast, analysis of submucosal layer revealed a significant enlarged thickness in HF ($p < 0.01$; Fig. 10.3e). Taken all together, these data show a possible correlation between an HF diet and altered intestinal morphology as well as a negative interaction when HF diet overlapped with IH. The histological analysis reveals an intraepithelial increase of eosinophils and lymphocytes in the CIH and HF groups. Likewise, an increase in the number and size of goblet cells is observed, with greater accumulation in the villi and intestinal crypts of the CIH and HF groups. In addition, we found increased mucosal neuroendocrine cells in HF rats.

10.4 Discussion

Rodent models of sleep apnea have been long used to provide new insights into the generation and predisposition to apneas as well as to characterize the impact of intermittent hypoxia on cardiovascular and metabolic health in humans. Loss of intestinal barrier function or changes in gut microbiota seems to be key ingredients involved in the pathogenesis of metabolic disorders (Serre et al. 2010). But to date, no studies have been conducted on the effect of OSA on the intestinal barrier, except for alterations in the microbiota (Farre et al. 2018). Therefore, the aim of this study was to analyze the effect of IH, obesity induced by an HF diet (as a natural model of sleep apnea), and the overlap of both pathologies, on the architecture and components of intestinal mucosa in a murine model. The latter group, HFIH, mimics the common clinical situation in which obesity often precedes the onset of OSA (Sutherland et al. 2012). Our findings confirm that HF feeding generates obesity because it

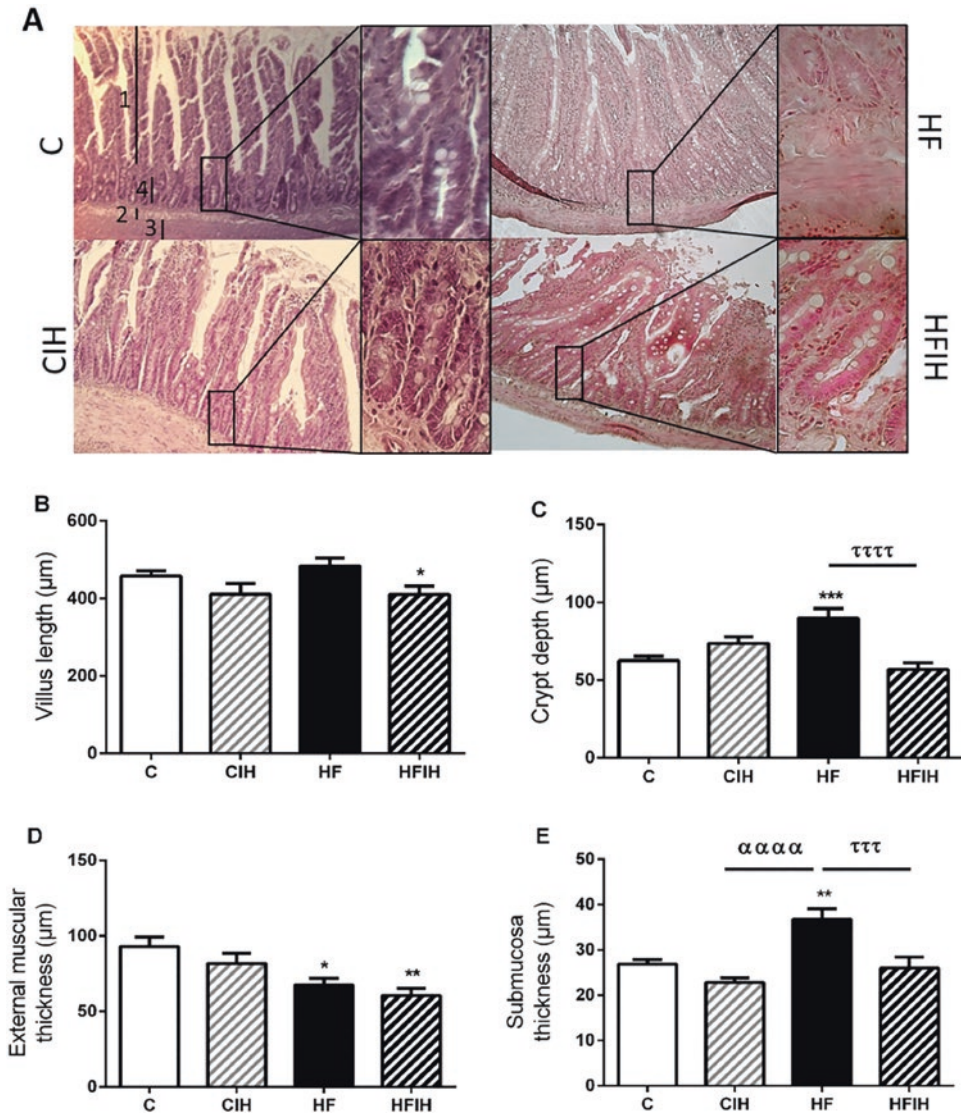


Fig. 10.3 Altered intestinal architecture in the small intestine. (a) H & E-stained sections from jejunum isolated from the four groups of rats (*C* control, *CIH* chronic intermittent hypoxia, *HF* high-fat diet, *HFIH* high-fat diet + intermittent hypoxia). Sections were examined and different measurements collected as detailed: villus length (1), crypt depth (2), muscularis thickness (3), and submu-

cosa thickness (4). (b) Villi length. (c) Crypt depth, defined as the length from crypt base to villus crypt junction. (d) External muscularis thickness. (e) Submucosal thickness. Magnification $\times 10$; insets $\times 40$. Each bar represent means \pm S.E.M of 6–8 analyzed section per animal ($n = 5$). * $p < 0.05$; ** $p < 0.01$ and *** $p < 0.001$ vs *C*. $\tau\tau\tau$ $p < 0.001$ vs *HF*. $\alpha\alpha\alpha$ $p < 0.001$ vs *CIH*. One-way ANOVA

increases total body weight and visceral fat, whereas IH does not. The combined treatment produces a synergic effect only in the adiposity index (Fig. 10.2). Basal glycemia exhibited pre-diabetic deviations in *CIH* and *HF* rats toward insulin resistance, with the deviation being more

pronounced in the *HF* group although not statistically different from the *C* group (Table 10.1).

Nevertheless, we found alterations in the intestinal morphology predominantly in *HF* rats. These alterations are manifested by an increase in crypt depth and submucosa thickness, as well

as a decrease in muscularis propria thickness which are maintained when HF is overlapped with IH (Fig. 10.3). The decrease in muscularis thickness in the HF group could be due to muscular dystrophy, while the infiltration of immune cells into the submucosa would contribute to the thickening of the submucosa layer. The mechanisms underlying the alteration of the normal villus crypt structure induced by HF are unclear but could be related to an altered proliferation of crypt stem cells, as proposed in intestinal barrier dysfunction developed in other pathologies such as multiple sclerosis (Nouri et al. 2014). An increase in the number and size of goblet cells in the villi and crypts is observed in all experimental groups. Goblet cells, as well as the enterocytes, and enteroendocrine cells of the gut mucosa, arise from multipotent stem cells at the base of the crypts of Lieberkühn (Gordon et al. 1992). During their maturation, goblet cells migrate from the base of the crypts to the villi, where are dispersed among the intestinal epithelial cells. They are chiefly responsible for the synthesis and secretion of mucins within the gut and are heavily influenced by interactions with the immune system in inflammatory processes (Grondin et al. 2021).

We also found increased infiltration of eosinophils and lymphocytes in the lamina propria indicating an inflammatory status in the small intestine. This inflammatory status is also evidenced by the fact that IH and HF increase plasma CRP levels, even more when combining the two treatments, as in the HFIH group. We have described that IH causes plasma CRP levels parallel to HI intensity (Quintero et al. 2013) with HF generating inflammatory mediators in adipose tissue and liver. The different origin of these signals would explain the summative effect in the HFIH group (Table 10.1).

Our present results correlate well with a previous study from our laboratory (Olea et al. 2014). In rats subjected to a very similar experimental design, with a combination of oxygen derangement (intermittent hypoxia/normoxia) and dietary conditions (high-fat diet/standard diet), we found that the combination of IH and HF caused a higher degree of oxidative status, inflam-

matory status (increased CRP and NF- κ B activation), and a higher increase in sympathetic tone than the individual treatments. The combination of obesity and IH produced a restrictive ventilatory pattern and hypoventilation, making rats more prone to episodes of hypoxemia. Taken all together, data suggest that CIH and obesity may cause comparable metabolic and cardiovascular pathologies through dysregulation of redox status and sympathetic hyperactivity, further revealing a more deleterious interactive effect in the combined treatment (Olea et al. 2014).

Catecholamines and other biogenic amines play many physiological roles in intestinal function. The CA analysis in the jejunum indicates that IH causes a preferential accumulation of NE on gut catecholaminergic nerve fibers which is maintained in the HFIH group but absent in the HF group. The biogenic amine 5-HT increases in all three experimental conditions (CIH, HF, and HFIH) with a maximum level in the HF group. Enterochromaffin cells are the source of 5-HT in the digestive tract, as there is minimal 5-HT content in enterocytes. According to the literature, 5-HT influences the cell differentiation and may contribute to the increased number of goblet cells mentioned above (Yakovleva and Lubovtseva 2013).

The results obtained in this study again correlate well with elevated levels of plasma CA in IH, as we found increased NE levels in the jejunum wall after IH treatment (alone or overlapped with HF). The likely source of this NE is the intermuscular plexuses of the intramural muscularis (Yakovleva and Lubovtseva 2013). Sympathetic activation in IH is mediated by the carotid body (CB; Fletcher et al. 1992), whereas in HF diet, it could be mediated, at least in part, by leptin (Rahmouni 2010). Recently, 5-HT and CA have been demonstrated to produce changes in microbiota composition as well as on the host-microbe interaction (Lyte et al. 2021). Dysbiosis in the gut has been linked to inflammatory disorders including inflammatory bowel disease, metabolic disorders such as obesity and diabetes, neurologic diseases, and atherosclerotic heart disease (Tang and Hazen 2014). Furthermore, as a result of the dynamic changes in arterial blood oxygenation in

OSA, it is expected that the intermittent hypoxemia in the blood entering the gut capillaries is transmitted to the intestinal lumen by a process of gas diffusion. Accordingly, relevant portions of the microbiota close to the epithelium are indeed subjected to oscillatory events of hypoxia, thereby inducing significant changes in the gut microbiome (Moreno-Indias et al. 2015).

Together, the effects of HF-induced inflammation and OSA-induced sympathetic activation may result in further dysbiosis, gut barrier disruption, translocation of gut bacteria, and systemic inflammation, which has been demonstrated to contribute to the development of hypertension and other OSA-linked pathologies in various models (Singh et al. 2014; Farré et al. 2018). It remains to be elucidated whether the alterations found in this work could affect the permeability of the intestinal barrier and promote sleep apnea-induced morbidities.

Acknowledgments We thank M^a de los Llanos Bravo and A. Gordillo for their technical assistance.


References

- Backhed F, Ding H, Wang T, Hooper LV, Koh GY, Nagy A, Semenkovich CF, Gordon JI (2004) The gut microbiota as an environmental factor that regulates fat storage. *Proc Natl Acad Sci U S A* 101:15718–15723
- Cani PD, Delzenne NM, Amar J, Burcelin R (2008) Role of gut microflora in the development of obesity and insulin resistance following high-fat diet feeding. *Pathol Biol* 56:305–309
- Farre N, Farré R, Gozal D (2018) Sleep apnea morbidity a consequence of microbial-immune crosstalk? *Chest* 154(4):754–759
- Fletcher EC, Lesske J, Qian W, Miller CC 3rd, Unger T (1992) Repetitive, episodic hypoxia causes diurnal elevation of blood pressure in rats. *Hypertension* 19:555–556
- Gifford AH, Leiter JC, Manning HL (2010) Respiratory function in an obese patient with sleep-disordered breathing. *Chest* 138(3):704e15
- Gordon JI, Schmidt GH, Roth KA (1992) Studies of intestinal stem cells using normal, chimeric, and transgenic mice. *FASEB J* 6:3039–3050
- Gozal D, Daniel JM, Dohanich GP (2001) Behavioral and anatomical correlates of chronic episodic hypoxia during sleep in the rat. *J Neurosci* 21:2442–2450
- Grondin JA, Kwon YH, Far PM, Haq S, Khan WI (2021) Mucins in intestinal mucosal defense and inflammation: learning from clinical and experimental studies. *Front Immunol* 11:2054
- Hotamisligil GS (2006) Inflammation and metabolic disorders. *Nature* 444:860–867
- Lavie L (2014) Oxidative stress in obstructive sleep apnea and intermittent hypoxia – the bad ugly and good: implications to the heart and brain. *Sleep Med Rev* 20C:27–45
- Ley RE, Backhed F, Turnbaugh P, Lozupone CA, Knight RD, Gordon JI (2005) Obesity alters gut microbial ecology. *Proc Natl Acad Sci U S A* 102:11070–11075
- Lyte JM, Shrestha S, Wagle BR, Liyanage R, Martinez DA, Donoghue AM, Daniels KM, Lyte M (2021) Serotonin modulates *Campylobacter jejuni* physiology and invitro interaction with the gut epithelium. *Poult Sci* 100(3):100944
- Moreno-Indias I, Torres M, Montserrat JM, Sanchez-Alcoholado L, Cardona F, Tinahones FJ, Gozal D, Poroyko VA, Navajas D, Queipo-Ortuño MI et al (2015) Intermittent hypoxia alters gut microbiota diversity in a mouse model of sleep apnoea. *Eur Respir J* 45:1055–1065
- Nieto FJ, Young TB, Lind BK et al (2000) Association of sleep-disordered breathing, sleep apnea, and hypertension in a large community-based study. Sleep heart health study. *JAMA* 283(14):1829–1836
- Nouri M, Bredberg A, Weström B, Lavasani S (2014) Intestinal barrier dysfunction develops at the onset of experimental autoimmune encephalomyelitis and can be induced by adoptive transfer of auto-reactive T cells. *PLoS One* 9(9):e106335
- Olea E, Agapito MT, Gallego-Martin T, Rocher A, Gomez-Niño A, Obeso A, Gonzalez C, Yubero S (2014) Intermittent hypoxia and diet-induced obesity: effects on oxidative status, sympathetic tone, plasma glucose and insulin levels, and arterial pressure. *J Appl Physiol* (1985) 117:706–719
- Ong CW, O'Driscoll DM, Truby H et al (2013) The reciprocal interaction between obesity and obstructive sleep apnoea. *Sleep Med Rev* 17:123–131
- Piper AJ, Grunstein RR (2011) Obesity hypoventilation syndrome: mechanisms and management. *Am J Respir Crit Care Med* 183(3):292–298
- Poroyko VA, Carreras A, Khalyfa A et al (2016) Chronic sleep disruption alters gut microbiota, induces systemic and adipose tissue inflammation and insulin resistance in mice. *Sci Rep* 6:35405
- Prieto-Lloret J, Olea E, Gordillo-Cano A, Docio I, Obeso A, Gomez-Niño A, Aaronson PI, Rocher A (2021) Maladaptive pulmonary vascular responses to chronic sustained and chronic intermittent hypoxia in rat. *Antioxidants* 11:54
- Quintero M, Gonzalez-Martin MC, Vega-Agapito V, Gonzalez C, Obeso A, Farre R, Agapito T, Yubero S (2013) The effects of intermittent hypoxia on redox status, NF-κB activation, and plasma lipid levels are dependent on the lowest oxygen saturation. *Free Radic Biol Med* 65:1143–1154
- Rahmouni K (2010) Leptin-induced sympathetic nerve activation: signaling mechanisms and cardiovascular

- lar consequences in obesity. *Curr Hypertens Rev* 6:104–209
- Ryan S, Taylor CT, McNicholas WT (2005) Selective activation of inflammatory pathways by intermittent hypoxia in obstructive sleep apnea syndrome. *Circulation* 112(17):2660–2667
- Serre de la CB, Ellis CL, Lee J, Hartman AL, Rutledge JC, Raybould HE (2010) Propensity to high-fat diet-induced obesity in rats is associated with changes in the gut microbiota and gut inflammation. *Am J Physiol Gastrointest Liver Physiol* 299:G440–G448
- Singh MV, Chapleau MW, Harwani SC, Abboud FM (2014) The immune system and hypertension. *Immunol Res* 59:243–253
- Sutherland K, Lee RW, Cistulli PA (2012) Obesity and craniofacial structure as risk factors for obstructive sleep apnoea: impact of ethnicity. *Respirology* 17:213–222
- Tang WH, Hazen SL (2014) The contributory role of gut microbiota in cardiovascular disease. *J Clin Invest* 124:4204–4211
- Vgontzas AN, Papanicolaou DA, Bixler EO, Hopper K, Lotsikas A, Lin HM, Kales A, Chrousos GP (2000) Sleep apnea and daytime sleepiness and fatigue: relation to visceral obesity, insulin resistance, and hypercytokinemia. *J Clin Endocrinol Metab* 85:1151–1158
- Yakovleva LM, Lubovtseva LA (2013) Dynamics of neurotransmitters in the structures of the rat jejunum during chronic alcohol intoxication. *Bull Exp Biol Med* 155(1):30–33
- Young T, Palta M, Dempsey J, Peppard, Nieto FJ, Hla KM (2009) Burden of sleep apnea: rationale, design, and major findings of the Wisconsin Sleep Cohort study. *WMJ* 108(5):246–249
- Zammit C, Liddicoat H, Moonsie I, Makker H (2010) Obesity and respiratory diseases. *Int J Gen Med* 3:335–343
- Zhang Z, Yang Y, Hill MA, Wu J (2012) Does C-reactive protein contribute to atherothrombosis via oxidant-mediated release of pro-thrombotic factors and activation of platelets? *Front Physiol* 3:433



Enhanced Peripheral Chemoreflex Drive Is Associated with Cardiorespiratory Disorders in Mice with Coronary Heart Disease

Liena Bravo, Katherin V. Pereyra, Hugo S. Diaz, Mariajosé Flores, Karla G. Schwarz, Camilo Toledo, Esteban Díaz-Jara, Leticia González, Marcelo E. Andia, and Rodrigo Del Rio 

Abstract

Coronary heart disease (CHD) is a prevalent cardiovascular disease characterized by coronary artery blood flow reductions caused by lipid deposition and oxidation within the coronary arteries. Dyslipidemia is associated with local tissue damage by oxidative stress/inflammation and carotid bodies (CB) peripheral chemoreceptors are heavily modulated by both reactive oxygen species and pro-inflammatory molecules (i.e., cytokines). Despite this, it is not known whether CB-mediated chemoreflex drive may be affected in CHD. In the present study,

we evaluated peripheral CB-mediated chemoreflex drive, cardiac autonomic function, and the incidence of breathing disorders in a murine model of CHD. Compared to age-matched control mice, CHD mice showed enhanced CB-chemoreflex drive (twofold increase in the hypoxic ventilatory response), cardiac sympathoexcitation, and irregular breathing disorders. Remarkably, all these were closely linked to the enhanced CB-mediated chemoreflex drive. Our results showed that mice with CHD displayed an enhanced CB chemoreflex, sympathoexcitation, and disordered breathing and suggest that CBs may be involved in chronic cardiorespiratory alterations in the setting of CHD.

L. Bravo · K. V. Pereyra · H. S. Díaz · M. Flores
K. G. Schwarz · C. Toledo · E. Díaz-Jara
Laboratory of Cardiorespiratory Control, Pontificia
Universidad Católica de Chile, Santiago, Chile

L. González · M. E. Andia
Radiology Department & ANID – Millennium
Institute for Intelligent Healthcare Engineering –
iHEALTH, Pontificia Universidad Católica de Chile,
Santiago, Chile

R. Del Rio (✉)
Laboratory of Cardiorespiratory Control, Pontificia
Universidad Católica de Chile, Santiago, Chile

Centro de Excelencia en Biomedicina de Magallanes
(CEBIMA), Universidad de Magallanes, Punta
Arenas, Chile
e-mail: rdelrio@bio.puc.cl

Keywords

Coronary heart disease · Atherosclerosis ·
Carotid body · Hypomorphic · Scavenger
receptor class B type 1 · Apolipoprotein E

11.1 Introduction

Cardiovascular diseases affect more than 285 million people worldwide (Mensah et al. 2019). Of this deaths, 7.3 million were due to coronary heart

disease (CHD). It is worth noting that CHD is a leading cause of disability and death in people aged <59 years old (Vilahur et al. 2014). CHD is caused by atherosclerotic plaque buildup on the walls of the coronary arteries that block/interrupt heart blood supply (Benjamin et al. 2019). There are several pathophysiological factors that contribute to atherosclerotic plaque formation including but not limited to impaired lipid metabolism, inflammation, oxidative stress, endothelial dysfunction, and sympathetic overactivity (Nabel 2003; Hansson and Libby 2006; Chen et al. 2020). Interestingly, enhanced activity of the sympathetic nervous system (SNS) is closely related to coronary artery disease. Particularly, SNS can promote atherosclerosis through increases in sympathetic vasomotor activity to the coronary circulation leading to coronary vasoconstriction and, as myocardial oxygen demand increases, myocardial ischemia. The subsequent result demonstrates the activation of several neurohormonal systems, including the renin-angiotensin system (Remme 1998), which further activates SNS being the outcome the formation of a vicious cycle that hastens cardiac dysfunction (Díaz et al. 2020; Esler and Kaye 2000). Despite, it is likely that the precise mechanism that may trigger the early activation of SNS and its relationship with molecular footprints associated with dyslipidemia, if any, have not been fully studied.

In addition to the cardiovascular consequences of CHD, several observational studies and meta-analyses support the existence of a link between dyslipidemia and alterations in breathing function (Barros and García-Río 2019). Despite, no comprehensive studies have addressed the presence of SNS and breathing disorders (BD) in the setting of CHD. Notably, both sympathoexcitation and disordered breathing have been linked to altered chemoreflex function in cardiovascular disease (Toledo et al. 2017). Indeed, higher peripheral chemoreflex drive is tightly related with poor prognosis in patients with heart failure (Giannoni et al. 2009; Giannoni et al. 2008). Carotid bodies (CB) are the main peripheral chemoreceptors, and their activation elicits both a reflex SNS activation and increases in breathing rhythm and/or amplitude (Iturriaga et al. 2021). Whether alterations in CB-mediated chemoreflex

function take place in CHD and its potential association with cardiorespiratory disorders during the progression of the disease has not been previously determined. Accordingly, in the present study, we evaluated chemoreflex drive, cardiac autonomic control, and breathing function in a double transgenic murine model of CHD that display deficient LDL clearance and then develop increased plasma lipid markers and low atherosclerosis (Zhang et al. 2005).

11.2 Methodology

11.2.1 Animal Model

Adult male knockout mice for the scavenging receptor class B type 1 and hypomorphic for apolipoprotein E (SR-B1^{-/-}/hypoApoE) (n = 6), obtained from Dr. Monty Krieger (Massachusetts Institute of Technology, Cambridge, MA, United States), and C57BL6 (n = 6) were used. Mice were maintained in a temperature-controlled room under a 12-h light/dark cycle with ad libitum access to food and water. Experimental protocols were approved by the Ethics Committee for Animal Experiments of the Pontificia Universidad Católica de Chile.

11.2.2 Resting Breathing and Chemoreflex Function

Whole-body plethysmography (Emka Technologies, France) in unrestrained mice was used to record resting breathing (RB) and chemoreflex function. Peripheral chemoreflex function was evaluated during a brief hypoxic challenge (10% FiO₂/balance with N₂). Tidal volume (V_T), respiratory frequency (Rf, breath/min), and minute volume (V_E, ml/min/10 g) were obtained using ecgAUTO software (Emka Technologies, France). The hypoxic ventilatory responses (HVR) were obtained by magnitude of hypoxic response (ΔV_E). Resting breathing was monitored for 2 h while the mice rest at normoxic conditions. Irregularity score (IS) was calculated as a proxy of disordered breathing according to the following equation: $100 * (T_{TOTn} - T_{TOTn-1}) / T_{TOTn-1}$ for the

nth respiratory cycle (30), with T_{TOTn} corresponding to the total respiratory time of the nth cycle.

11.2.3 Electrocardiogram and Autonomic Balance

Electrocardiogram (EKG) were recorded in anesthetized mice using the DII lead (mixture with α -chloralose and urethane, 800 mg/Kg and 40 mg/Kg, respectively). Cardiac sympathetic-vagal control was directly assessed by intraperitoneal injection of propranolol (1 mg/kg i.p.; 1,576,005 Sigma-Aldrich, USA) or atropine (1 mg/kg i.p.; A0132 Sigma-Aldrich, USA) as previously described (Toledo et al. 2017). Delta heart rate (Δ HR), calculated from R-R wave distance from EKG signal, was used to study the difference between baseline HR and the peak response for each stimulus.

11.2.4 Data Analysis

All data is expressed as mean \pm standard error of the mean (S.E.M.). Statistical comparisons were performed with unpaired t-test, and $p < 0.05$ was considered statistically significant. Analysis was performed with GraphPad Prism version 8.0 (La Jolla, CA, USA).

11.3 Results

11.3.1 SR-B1^{-/-}/HypoApoE Mice Display Increased Peripheral Chemoreflex Drive

Breathing parameters are shown in Table 11.1. Compared to age-matched control wild-type

(WT) mice, SR-B1^{-/-}/hypoApoE mice displayed an increase minute ventilation in normoxic condition (Table 11.1). In addition, SR-B1^{-/-}/hypoApoE mice showed enhanced peripheral ventilatory chemoreflex drive compared to WT mice as evidenced by a larger HVR (Fig. 11.1). Indeed, HVR was almost enhanced by twofold in the SR-B1^{-/-}/hypoApoE mice compared to WT (0.2 ± 0.03 vs. 0.5 ± 0.07 Δ VE/% FiO₂, WT vs. SR-B1^{-/-}/hypoApoE, respectively).

11.3.2 SR-B1^{-/-}/HypoApoE Mice Show Breathing Pattern Irregularity

SR-B1^{-/-}/hypoApoE mice displayed overt signs of disordered breathing compared to WT mice (Fig. 11.2). Indeed, resting breathing regularity was compromised in the SR-B1^{-/-}/hypoApoE mice at both tidal volume magnitude and breath-to-breath interval. The latter results in a significant increase in the irregularity score values obtained in SR-B1^{-/-}/hypoApoE mice compared to the ones obtained in age-matched control WT mice (IS: 7.8 ± 0.6 vs. $10.8 \pm 1.0\%$, WT vs. SR-B1^{-/-}/hypoApoE, respectively. Figure 11.2). Additionally, we found that increased peripheral chemoreflex drive is related to higher irregularity score of the respiratory pattern in SR-B1^{-/-}/hypoApoE ($R^2: 0.5638$, $P: 0.0854$) compared to WT animals ($R^2: 0.5141$, $P: 0.2830$).

11.3.3 Cardiac Sympathetic Tone Is Enhanced in SR-B1^{-/-}/HypoApoE Mice

To determine sympathetic and parasympathetic contribution, Δ HR was measured under the

Table 11.1 Ventilatory parameters

	WT		SR-B1 ^{-/-} /hypoApoE	
	Normoxia	Hypoxia	Normoxia	Hypoxia
V_T (ml/10 g)	0.02 ± 0.0	0.02 ± 0.0	$0.04 \pm 0.0^*$	$0.04 \pm 0.0^*$
R_F (bpm)	155.6 ± 13.4	277.7 ± 22.7	134.1 ± 5.6	273.7 ± 17.4
V_E (ml/min/10 g)	3.2 ± 0.4	4.6 ± 0.8	$5.8 \pm 1.1^*$	$11.5 \pm 1.1^*$

Data is presented as mean \pm SEM. WT wild type, V_T tidal volume, R_F respiratory frequency, V_E minute volume; unpaired T-test; * $P < 0.05$

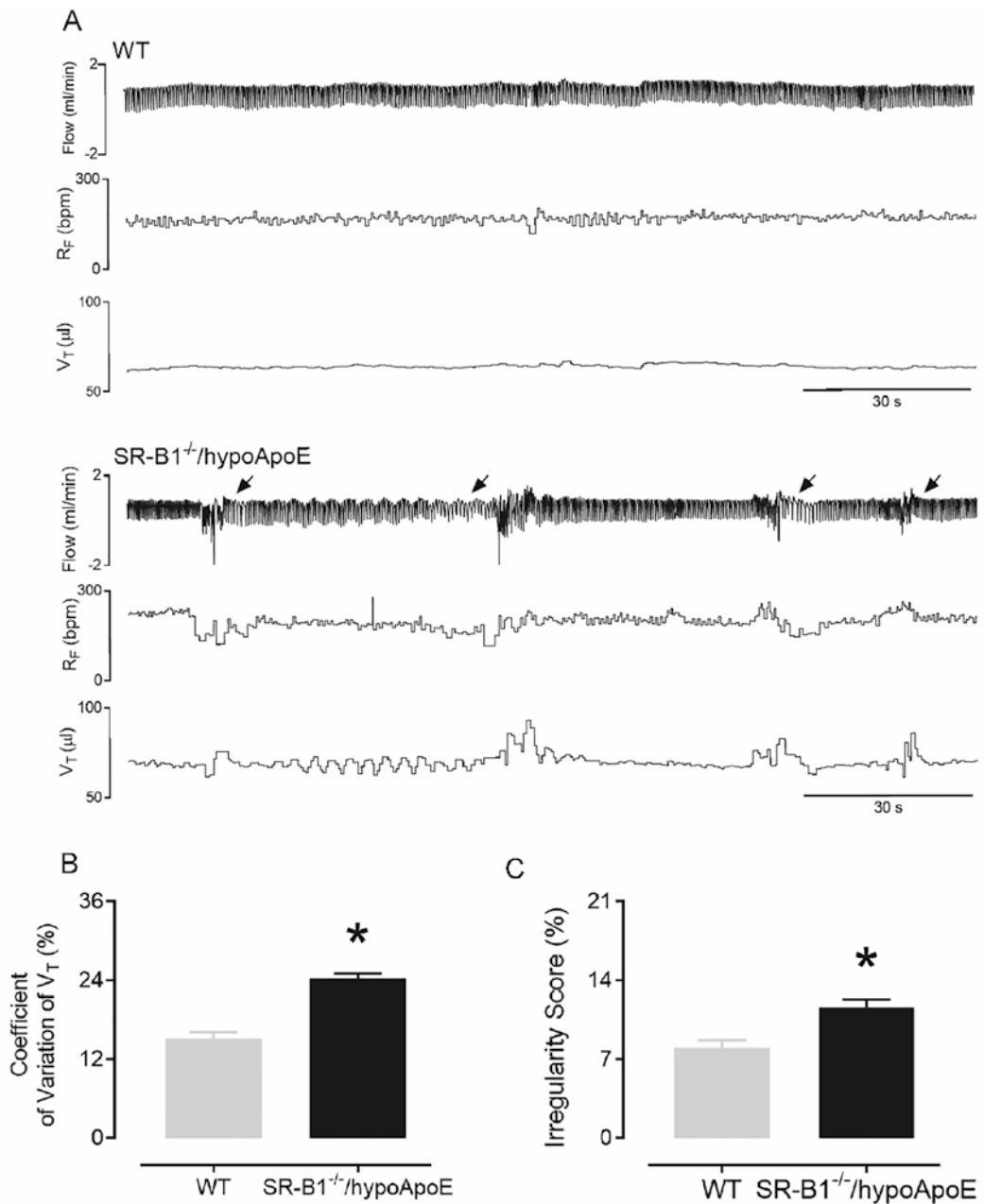


Fig. 11.2 SR-B1^{-/-}/hypoApoE mice show breathing pattern irregularity. (a) Representative recording of one WT and SR-B1^{-/-}/hypoApoE mice at rest in normoxic conditions. Arrows indicate alterations in respiratory frequency

(RF) and/or tidal volume (V_T). (b) Summary data showing irregularity score (IS) in age-matched control WT mice SR-B1^{-/-}/hypoApoE mice. Unpaired t-test. *P < 0.05. WT, n = 6. SR-B1^{-/-}/hypoApoE, n = 6

and ventilatory drive (Paton et al. 2013). Importantly, sympathoexcitation is a hallmark of several cardiovascular diseases, and ablation of

the CBs restored normal sympathetic activity and ventilatory drive suggesting that CBs may play a pivotal role in the development/maintenance of

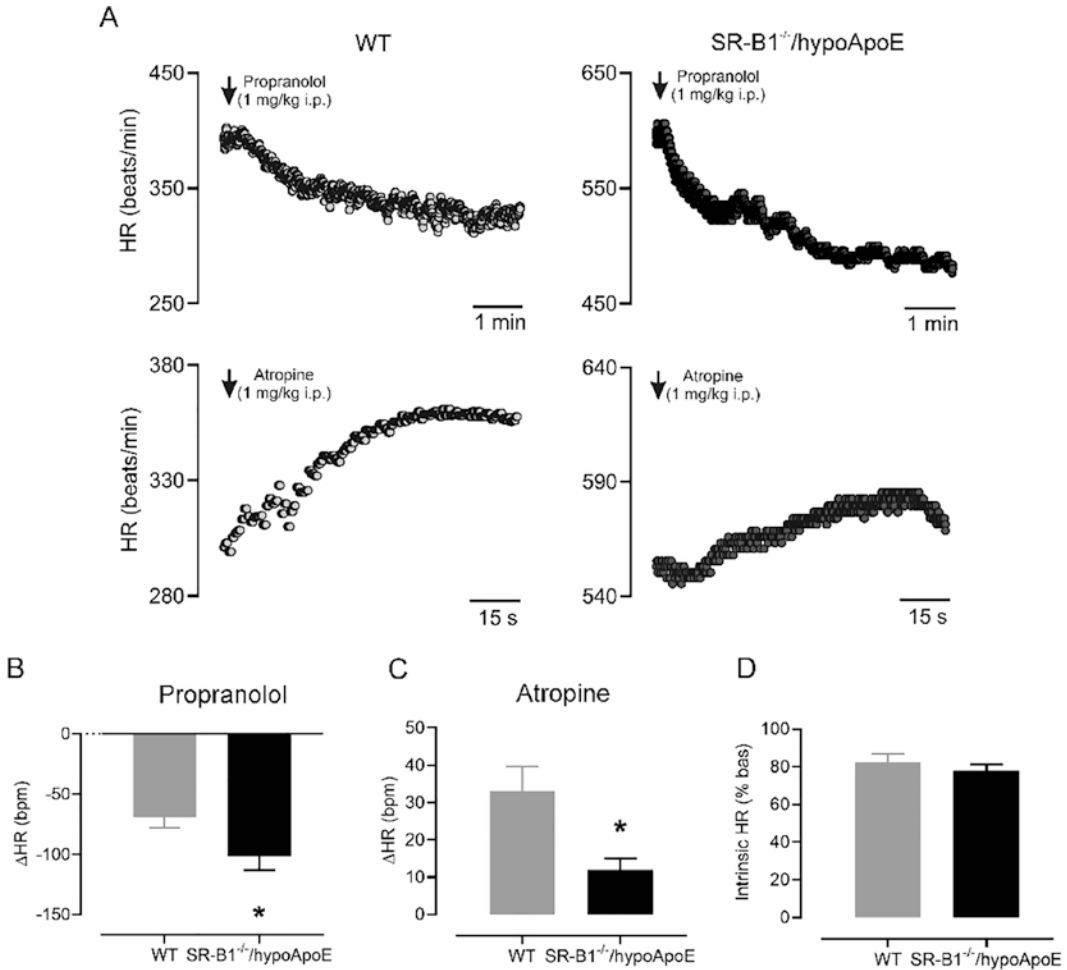


Fig. 11.3 Cardiac autonomic imbalance in SR-B1^{-/-}/hypoApoE mice. **(a)** Representative recordings exhibiting changes in heart rate (HR) after acute propranolol or atropine stimulation in one WT and SR-B1^{-/-}/hypoApoE mice. Arrows indicate intraperitoneal (i.p.) injection. **(b)**

(c) Summary data showing delta HR (Δ HR) responses to propranolol or atropine stimulation, respectively. **(d)** Summary data showing intrinsic HR. Unpaired t-test. * $P < 0.05$. WT, $n = 6$. SR-B1^{-/-}/hypoApoE, $n = 6$

cardiorespiratory disorders in cardiovascular disease (Marcus et al. 2014; Del Rio et al. 2013). Here, we showed that SR-B1^{-/-}/hypoApoE mice exhibited an enhanced CB-mediated chemoreflex drive and that this was associated with both cardiac sympathoexcitation and disordered breathing. These results support that those alterations in CB function (i.e., chemosensory potentiation) in the setting of CHD may contribute to hemodynamic and respiratory dysfunction during the onset/maintenance/progression of the disease.

The precise molecular mechanism underpinning CB potentiation in the setting of CHD remain to be determined. However, due to the nature of the model, we can speculate that enhanced CB activity in the SR-B1^{-/-}/hypoApoE mice may result, at least in part, from oxidative stress/inflammation conditions linked to dyslipidemia. Indeed, in the present study, we use the SR-B1^{-/-}/hypoApoE mice model for CHD. Deletion of the scavenger receptor B type 1 (SR-B1) impacts directly the selective cellular

uptake of cholesteryl esters, cholesterol, and other lipids from high density lipoprotein (HDL) and promotes efflux of nonesterified cholesterol from cells producing dyslipidemia (Toth 2003; Kosmas et al. 2018). In addition, reductions in the expression of apoE (hypomorphic apolipoprotein E, hypoApoE) result in inefficient clearance of remnants of triglyceride-rich lipoprotein (Hermann et al. 2016; Luk et al. 2016). Furthermore, atherosclerosis plaques in the vicinity of the CB, which may result from the lipid accumulation on vascular walls, normally contain blood-borne inflammatory and immune cells (mainly macrophages and T cells) that secretes several pro-inflammatory signaling molecules promoting the establishment of an inflammatory niche (Hansson and Libby 2006; Bobryshev and Lord 1995; Tabas and Bornfeldt 2016). Interestingly, pro-inflammatory cytokines (i.e., interleukin-1 β , interleukin-6, tumor necrosis factor- α) modulate CB chemoreception (Porzionto et al. 2013; Iturriaga et al. 2021). Finally, we cannot rule out that atherosclerotic plaques located in the carotid artery may modify blood flow to the CB tissue having additional effects on CB function (besides the ones linked to inflammation). Future studies should focus on the mechanism linking SR-B1^{-/-}/hypoApoE deficiency on CB dysfunction.

In summary, our results showed that experimental CHD is characterized by enhanced CB chemoreflex drive, cardiac sympathoexcitation, and breathing disorders. Together our results support a potential role for the CBs on the regulation of cardiorespiratory function in mice with CHD.

Acknowledgments This work was supported by Fondo de Desarrollo Científico y Tecnológico FONDECYT 12209505, 1180525, 11220962 and 3210564; ANID – Millennium Science Initiative Program – ICN2021_004.

References

Barros D, García-Río F (2019) Obstructive sleep apnea and dyslipidemia: from animal models to clinical evidence. *Sleep* 42(3):zsy236

Benjamin EJ, Muntner P, Alonso A, Bittencourt MS, Callaway CW, Carson AP, Virani SS (2019) Heart

disease and stroke statistics-2019 update: a report from the American Heart Association. *Circulation* 139(10):e56–e528

Bobryshev YV, Lord RSA (1995) S-100 positive cells in human arterial intima and in atherosclerotic lesions. *Cardiovascular* 29(5):689–696

Chen H, Wang R, Xu F, Zang T, Ji M, Yin J, Chen J, Shen L, Ge J (2020) Renal denervation mitigates atherosclerosis in ApoE^{-/-} mice via the suppression of inflammation. *Am J Transl Res* 12(9):5362–5380

Del Rio R, Marcus NJ, Schultz HD (2013) Carotid chemoreceptor ablation improves survival in heart failure: rescuing autonomic control of cardiorespiratory function. *J Am Coll Cardiol* 62(25):2422–2430

Díaz HS, Toledo C, Andrade DC, Marcus NJ, Del Rio R (2020) Neuroinflammation in heart failure: new insights for an old disease. *J Physiol* 598(1):33–59

Esler M, Kaye D (2000) Sympathetic nervous system activation in essential hypertension, cardiac failure and psychosomatic heart disease. *J Cardiovasc Pharmacol* 35(7 Suppl 4):S1–S7

Giannoni A, Emdin M, Poletti R, Bramanti F, Prontera C, Piepoli M, Passino C (2008) Clinical significance of chemosensitivity in chronic heart failure: influence on neurohormonal derangement, Cheyne-stokes respiration and arrhythmias. *Clin Sci* 114(7):489–497

Giannoni A, Emdin M, Bramanti F, Iudice G, Francis DP, Barsotti A, Piepoli MF, Passino C (2009) Combined increased chemosensitivity to hypoxia and hypercapnia as a prognosticator in heart failure. *J Am Coll Cardiol* 53(21):1975–1980

Hansson GK, Libby P (2006) The immune response in atherosclerosis: a double-edged sword. *Nat Rev Immunol* 6(7):508–519

Hermann S, Kuhlmann M, Staršičová A, Eligehausen S, Schäfers KP, Stypmann J, Tiemann K, Levkau B, Schäfers M (2016) Imaging reveals the connection between spontaneous coronary plaque ruptures, atherothrombosis, and myocardial infarctions in HypoE/SRBI^{-/-} mice. *J Nucl Med* 57(9):1420–1427

Iturriaga R, Del Rio R, Alcayaga J (2021) Carotid body inflammation: role in hypoxia and in the anti-inflammatory reflex. *Physiology* 37(3):128–140

Kosmas CE, Martinez I, Sourlas A, Bouza KV, Campos F, Torres V, Montan PD, Guzman E (2018) High-density lipoprotein (HDL) functionality and its relevance to atherosclerotic cardiovascular disease. *Drug Context* 28(7):212525

Luk FS, Kim RY, Li K, Ching D, Wong DK, Joshi SK, Imhof I, Honbo N, Hoover HE, Zhu B, Lovett DH, Karliner JS, Raffai RL (2016) Immunosuppression with FTY720 reverses cardiac dysfunction in hypomorphic apoE mice deficient in SR-BI expression that survive Myocardial Infarction caused by coronary atherosclerosis. *J Cardiovasc Pharmacol* 67(1):47–56


Marcus NJ, Río RD, Schultz E, Xia X, Schultz HD (2014) Carotid body denervation improves autonomic and cardiac function and attenuates disordered breathing in congestive heart failure. *J Physiol* 592(2):391–408

- Mensah GA, Roth GA, Fuster V (2019) The global burden of cardiovascular diseases and risk factors: 2020 and beyond. *J Am Coll Cardiol* 74(20):2529–2532
- Nabel EG (2003) Cardiovascular disease. *N Engl J Med* 349(1):60–72
- Paton JF, Sobotka PA, Fudim M, Engelman ZJ, Hart EC, McBryde FD, Abdala AP, Marina N, Gourine AV, Lobo M, Patel N, Burchell A, Ratcliffe L, Nightingale A (2013) The carotid body as a therapeutic target for the treatment of sympathetically mediated diseases. *Hypertension* 61(1):5–13
- Porzionto A, Macchi V, De Caro R, Di Giulio C (2013) Inflammatory and immunomodulatory mechanisms in the carotid body. *Respir Physiol Neurobiol* 187(1):31–40
- Remme WJ (1998) The sympathetic nervous system and ischaemic heart disease. *Eur Heart J* 19(Suppl F):F62–F71
- Tabas I, Bornfeldt KE (2016) Macrophage phenotype and function in different stages of atherosclerosis. *Circ Res* 118(4):653–667
- Toledo C, Andrade DC, Lucero C et al (2017) Contribution of peripheral and central chemoreceptors to sympatho-excitation in heart failure. *J Physiol* 595(1):43–51
- Toth PP (2003) Reverse cholesterol transport: high-density lipoprotein's magnificent mile. *Curr Atheroscler* 5(5):386–393
- Vilahur G, Badimón JJ, Bugiardini R, Badimón L (2014) Perspectives: the burden of cardiovascular risk factors and coronary heart disease in Europe and worldwide. *Eur Heart J* 16:7–11
- Zhang S, Picard MH, Vasile E, Zhu Y, Raffai RL, Weisgraber KH, Krieger M (2005) Diet-induced occlusive coronary atherosclerosis, myocardial infarction, cardiac dysfunction, and premature death in scavenger receptor class B type I-deficient, hypomorphic apolipoprotein ER61 mice. *Circulation* 111:3457–3464



Role of Peripheral Chemoreceptors on Enhanced Central Chemoreflex Drive in Nonischemic Heart Failure

12

Katherin Pereyra, Esteban Díaz-Jara, Paulina Arias, Liena Bravo, Camilo Toledo, Karla Schwarz, and Rodrigo Del Rio 

Abstract

Heart failure (HF) is a prevalent disease in elderly population. Potentiation of the ventilatory chemoreflex drive plays a pivotal role in disease progression, at least in part, through their contribution to the generation/maintenance of breathing disorders. Peripheral and central chemoreflexes are mainly regulated by carotid body (CB) and the retrotrapezoid nuclei (RTN), respectively. Recent evidence showed an enhanced central chemoreflex drive in rats with nonischemic HF along with breathing disorders. Importantly, increase activity from RTN chemoreceptors contribute to the potentiation of central chemoreflex response to hypercapnia. The precise mechanism driving RTN potentiation in HF is still elusive. Since interdependency of RTN and

CB chemoreceptors has been described, we hypothesized that CB afferent activity is required to increase RTN chemosensitivity in the setting of HF. Accordingly, we studied central/peripheral chemoreflex drive and breathing disorders in HF rats with and without functional CBs (CB denervation). We found that CB afferent activity was required to increase central chemoreflex drive in HF. Indeed, CB denervation restored normal central chemoreflex drive and reduced the incidence of apneas by twofold. Our results support the notion that CB afferent activity plays an important role in central chemoreflex potentiation in rats with HF.

Keyword

Carotid body denervation · Heart failure · RTN · Central chemoreflex potentiation

K. Pereyra · E. Díaz-Jara · P. Arias · L. Bravo
C. Toledo · K. Schwarz
Laboratory of Cardiorespiratory Control, Pontificia Universidad Católica de Chile, Santiago, Chile

R. Del Rio (✉)
Laboratory of Cardiorespiratory Control, Pontificia Universidad Católica de Chile, Santiago, Chile

Centro de Excelencia en Biomedicina de Magallanes (CEBIMA), Universidad de Magallanes, Punta Arenas, Chile
e-mail: rdelrio@bio.puc.cl

12.1 Introduction

Chronic heart failure (CHF) is a pathophysiological condition characterized by a progressive loss of cardiac function, autonomic imbalance, and presence of ventilatory disorders among other symptoms (Toledo et al. 2017). Approximately 64.3 million people suffer this disease worldwide (Groenewegen et al. 2020), which makes it a potential epidemiological problem with no clear

treatment (Ilieşiu and Hodoroega 2018). To support a dysfunctional heart, compensatory neurohumoral mechanisms activate, but in the long term, they become detrimental. One of these mechanisms is the potentiation of the chemoreflex drive, which contribute to CHF mortality (Giannoni et al. 2009). While both cardiac autonomic imbalance and disordered breathing patterns in ischemic CHF (ejection fraction, EF <40%) have been linked to chronically potentiated peripheral chemoreflex activity (Del Río et al. 2017; Marcus et al. 2014), there is limited information regarding pathophysiological mechanism associated to nonischemic CHF (EF > 50%). However, central chemoreflex sensitivity is augmented in animal models of nonischemic CHF and is tightly associated with enhanced cardiac sympathetic tone and irregular breathing patterns (Toledo et al. 2017).

The carotid body (CB) and the retrotrapezoid nucleus (RTN) command peripheral and central chemoreflex, respectively. CBs are chemoreceptors located in the carotid bifurcation that sense changes in arterial pressure of O₂ (PaO₂) and CO₂ (PaCO₂) and respond rapidly to hypoxia contributing to 95% of the ventilatory response to hypoxia (HVR) (Iturriaga et al. 2021). The RTN, main chemoreceptor for hypercapnia, is a neuronal group that resides in the parafacial region under the facial motor nucleus and detect changes in PaCO₂, contributing to 90% of the ventilatory response to hypercapnia (HCVR) (Kumar et al. 2015; Guyenet et al. 2018, 2019; Wang et al. 2013; Stornetta et al. 2006). Interestingly, CBs communicate with RTN neurons through a glutamatergic anatomical-functional connection mediated by the nucleus of the tractus solitarius (NTS) (Takakura et al. 2006). In addition, previous studies have reported that acute and long-term removal of CB in dogs and humans generate a depressive effect on the central chemoreflex response (Blain et al. 2010; Lugliani et al. 1971). This strongly suggests that both chemoreceptors work cooperatively to modulate the ventilatory response through interdependent feedback and provides evidence that central chemosensory activity could be modulated by the functional inputs coming from CB (Guyenet et al. 2018).

The cellular/molecular mechanisms by which CB could modulate the central chemoreflex response are completely unknown. However, previous studies involving pharmacological inhibition of NMDA (N-methyl-D-aspartic acid) and non-NMDA ionotropic glutamate receptors in the RTN attenuate cardiorespiratory effects triggered by CB activation (Takakura and Moreira 2011; Nattie et al. 1993). Although these receptors are not recognized as the chemosensor units in the RTN their inhibition produce reduced the ventilatory response to hypercapnic stimuli (Nattie and Li 1995), suggesting that glutamatergic signaling could play a role in ventilatory response at the RTN level.

Interestingly, the increase in the central chemoreflex response in CHF patients or in the rodent model is closely associated with the presence of ventilatory disorders, autonomic imbalance, and cardiac dysfunction (Toledo et al. 2017), all of which is associated with poor prognostic events and mortality. Notably, the selective ablation of the chemosensitive neurons of the RTN in experimental nonischemic CHF rats not only normalizes the central chemoreflex drive but also the presence of ventilatory disorders and the regularity of the breathing pattern (Díaz et al. 2019).

Nowadays, there is a lack of interventions aimed to normalize the chemoreflex ventilatory drive in nonischemic CHF. Notably, unilateral CB denervation either surgically or by radiofrequency has proof to be a safe and feasible approach to reduce chemoreflex function in humans (Iturriaga 2018). Taking this into account, it is plausible to hypothesize that CB afferent chemosensory activity may contribute to the potentiation of the RTN-mediated central chemoreflex drive in the setting of nonischemic CHF.

12.2 Methodology

12.2.1 Animals

All animal experiments were approved by the Ethical Committee of the Facultad de Ciencias Biológicas, Pontificia Universidad Católica de

Chile in accordance with the National Institutes of Health (NIH) Guide for the Care and Use of Laboratory. Sprague–Dawley rats ($n = 12$) were kept in a controlled temperature room ($25\text{ }^{\circ}\text{C}$) with 12:12 light/dark cycle and ad libitum access to water and food. Animals were randomly assigned into three groups: (i) Sham ($n = 4$), (ii) nonischemic chronic heart failure (CHF, $n = 4$), and (iii) CHF with bilateral carotid body denervation (CBD) (CHF_{CBD}, $n = 4$). At the end of protocol, animals were humanely euthanized with sodium pentobarbital (100 mg/kg i.p.).

12.2.2 Heart Failure Model

Nonischemic CHF (called as CHF in this paper) was induced by volume overload through arteriovenous fistula as previously described (Toledo et al. 2017; Díaz et al. 2019). Briefly, under isoflurane anesthesia (5% for induction, 2% for maintenance, balanced with oxygen), a laparotomy was performed, and the inferior cava vein and the abdominal aorta were cleaned and isolated. Using a needle (19G), the artery and the vein were punctured, and then the arterial wall was closed with tissue glue (Hystoacryl™). Anastomosis was corroborated by seeing the color change in of the blood in the vein. Finally, laparotomy was sutured. Sham surgery consider the same procedure, but fistula was not made.

12.2.3 Echocardiography

Transthoracic M-mode echocardiography (Mindray Z6 Vet) was performed in anesthetized rats (isoflurane 2% in O₂). At 8 weeks after CHF induction, left ventricle (LV) chamber diameters were measure at the end of diastole (EDD) and end of systole (ESD) from three consecutive cycles, as well as the heart rate (HR). End diastolic and systolic volumes were calculated according to the Teicholz method: $LVEDV = 7 * EDD^3 / (2.4 + EDD)$ and $LVESV = 7 * ESD^3 / (2.4 + ESD)$. Animals with ≥ 2.5 -fold increase in ESV, EDV and cardiac out-

put (CO) were in nonischemic CHF (Toledo et al. 2017; Díaz et al. 2019).

12.2.4 Plethysmography

Resting breathing (RB) recordings (120 min) were performed in unrestrained conscious freely moving animals using whole-body plethysmography (Emka Technology) at 8 weeks. Only the last hour of each RB recording was used to quantify the incidence of breathing disorders. Spontaneous apneas (cessation of breathing) and post-sigh apneas (apnea immediately after a sigh) were visually identified and counted by a non-biased operator. Peripheral and central ventilatory chemoreflex responses were evaluated by using hypoxic (F_IO₂ 10%) and hypercapnic (F_ICO₂ 7%) stimuli, respectively. Then, the magnitude (ΔV_E : F_IO₂ 10%) and the gain of the hypoxic ($\Delta V_E / \% F_{I}O_2$) and hypercapnic ($\Delta V_E / \% F_{I}CO_2$) ventilatory response (HVR and HCVR, respectively) were calculated (Toledo et al. 2017; Díaz et al. 2019).

12.2.5 Carotid Body Denervation

Carotid body denervation (CBD) was performed before to nonischemic CHF induction as previously described (Gary et al. 2012). Briefly, under isoflurane anesthesia (2% in O₂), an incision was made in the ventral region of the neck to expose the carotid artery bifurcation. Then, carotid sinus nerve (CSN) was identified and cut close to the junction of the CSN to the IX. Postsurgery care included subcutaneous injection of enrofloxacin (5 mg/kg), meloxicam (2 mg/kg), and tramadol (5 mg/kg). Carotid body ablation was corroborated through plethysmography, 2 days after bilateral carotid body denervation (CBD), by analyzing HVR (F_IO₂ 10%) before and after CBD.

12.2.6 Statistical Analysis

Data is presented as mean \pm standard error mean (SEM). One-way ANOVA followed by Holm-

Sidak post hoc was performed to compare the experimental groups. P value < 0.05 is considered as significant.

12.3 Results

12.3.1 Cardiac Morphology and Carotid Body Denervation in Heart Failure

First, we evaluate if CBD in CHF rats influences cardiac hypertrophy at 8 weeks post CHF induction. LV chamber diameters increase in rats with CHF compared to Sham rats (Fig. 12.1a). Importantly, no differences in LV chamber dilatation either at end systolic (ESV; CHF: 109.5 ± 13.9 vs. CHF_{CBD}: 123.9 ± 16.2 μ L) or diastolic volume (EDV; CHF: 377.3 ± 17.7 vs. CHF_{CBD}: 419.4 ± 19.5 μ L) (Fig. 12.1a–c) were found between CHF groups. Furthermore, no differences in heart rate were found (HR; CHF:

348.3 ± 13.21 vs. CHF_{CBD}: 337.0 ± 6.7 bpm) (Fig. 12.1d).

12.3.2 Carotid Body Resection Restores Normal Hypercapnic Ventilatory Responses and Breathing Disorders in CHF Rats

At 8 weeks post CHF induction, we evaluate both peripheral and central ventilatory chemoreflex response in all conditions. No significant changes were detected in hypoxic ventilatory response (Sham: 1.9 ± 0.1 , CHF: 1.9 ± 0.7 , CHF_{CBD}: 2.2 ± 0.1 $\Delta V_E/F_{I O_2}$ 10%) among groups (Fig. 12.2a, b). Importantly, the enhanced hypercapnic ventilatory response, observed in CHF rats compared to Sham rats, was completely abolished by CB denervation in CHF animals (Sham: 2.7 ± 0.4 , CHF: 5.5 ± 0.4 , CHF_{CBD}: 3.6 ± 0.3 $\Delta V_E/F_{I CO_2}$ 7%).

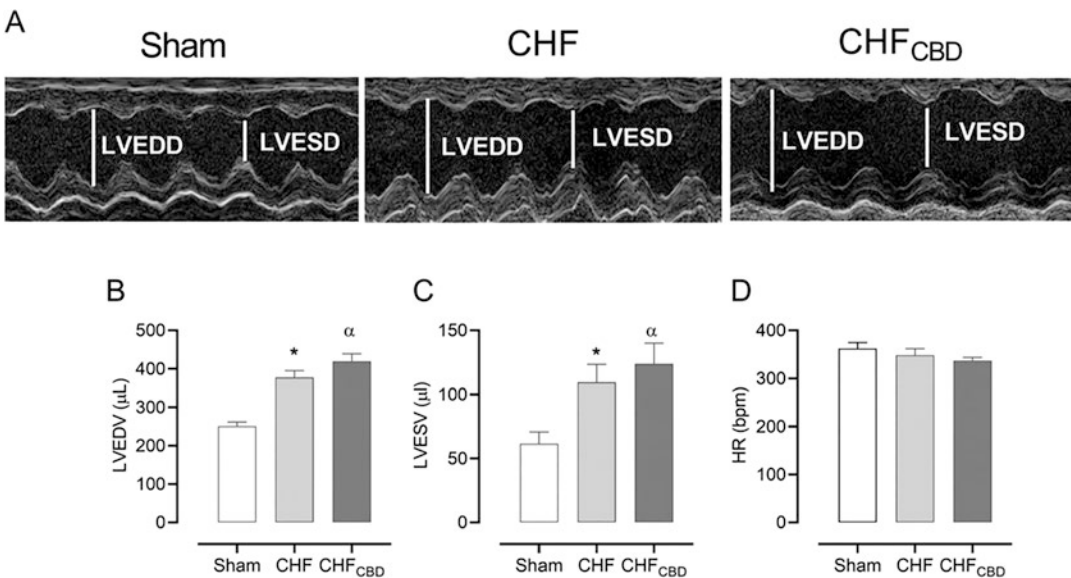


Fig. 12.1 Echocardiographic parameters following carotid body denervation in CHF rats. (a) Representative echocardiography recording obtained in one Sham, non-ischemic chronic heart failure (CHF) and CHF with bilateral carotid body denervation (CHF_{CBD}) rat, (b) Summary

data showing changes in left ventricle end diastolic volume (LVEDV) and (c) systolic volume (LVESV) and (d) heart rate (HR). One-way ANOVA followed by Holm-Sidak post hoc test. *P < 0.05 Sham vs. CHF and ^αP < 0.05, Sham vs. CHF_{CBD}. N = 4 per group

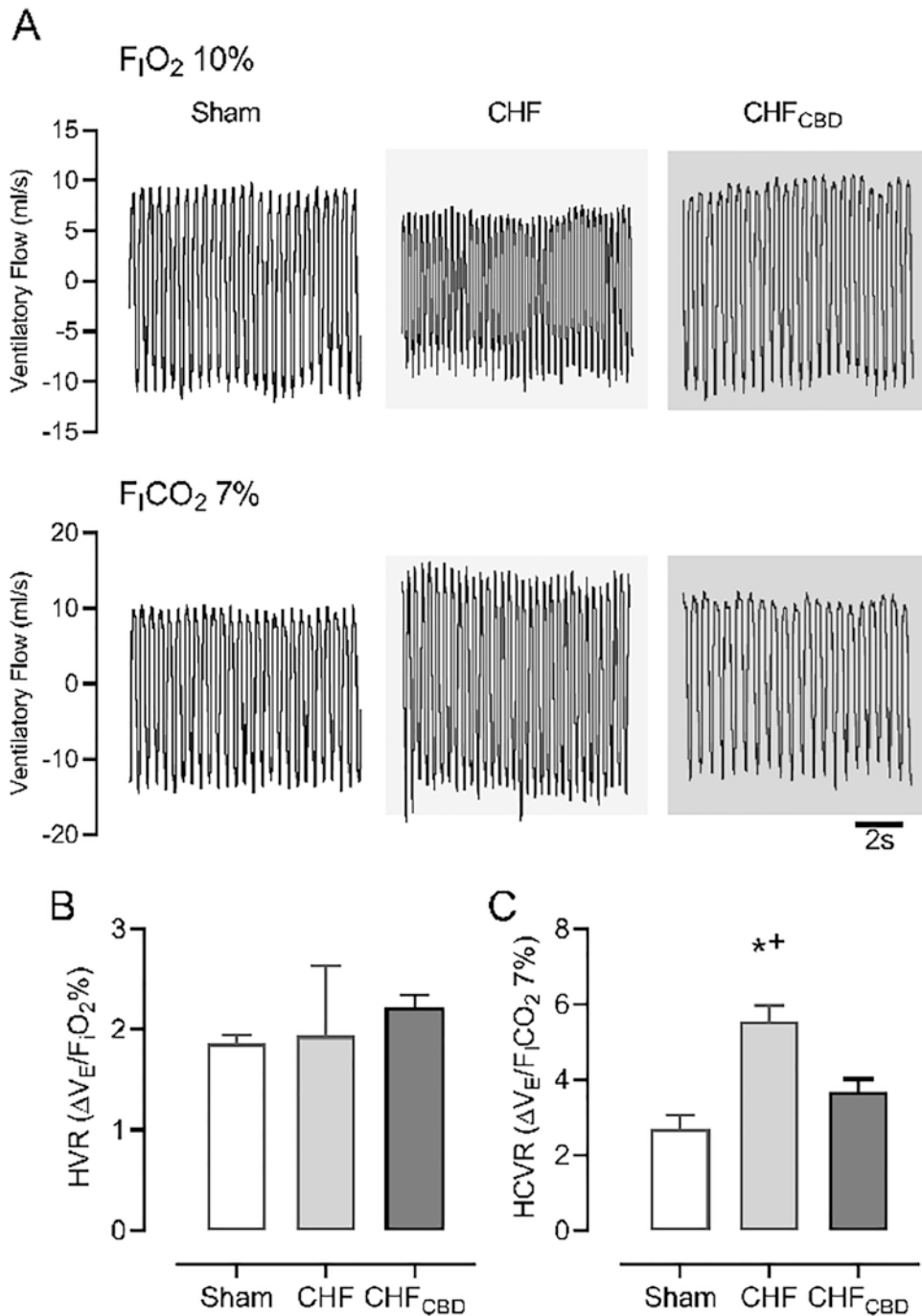


Fig. 12.2 Carotid body denervation in CHF restored central chemoreflex drive. (a) Representative recording of ventilatory flow during hypoxia ($F_{I}O_2$ 10%) and hypercapnia ($F_{I}CO_2$ 7%) in one Sham, nonischemic chronic heart failure (CHF) and CHF with bilateral carotid body denervation (CHF_{CBD}) rat. (b) Summary data showing the

changes in the hypoxic ventilatory response (HVR, $F_{I}O_2$ 10%) and (c) hypercapnic ventilatory response (HCVR, $F_{I}CO_2$ 7%). One-way ANOVA followed by Holm-Sidak post hoc test. * $P < 0.05$ Sham vs. CHF and $\alpha P < 0.05$, Sham vs. CHF_{CBD}. $N = 4$ per group

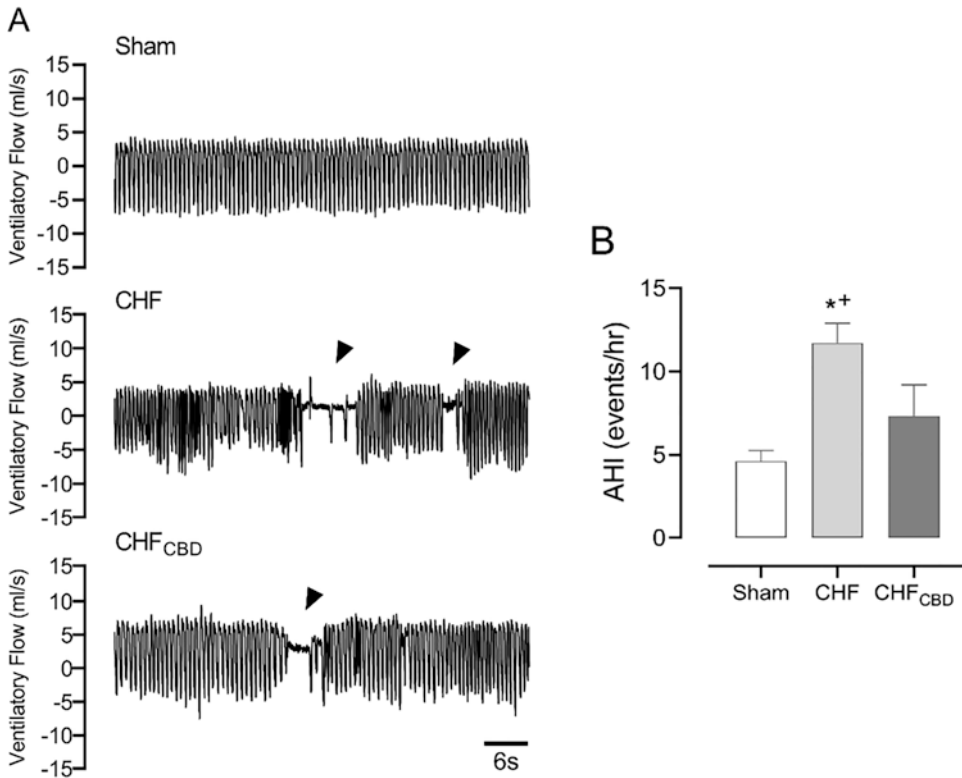


Fig. 12.3 Carotid body denervation in CHF decreases apnea incidence. **(a)** Representative ventilatory recordings obtained at rest from one Sham, nonischemic chronic heart failure (CHF) and CHF with bilateral carotid body denervation (CHF_{CBD}) per group. Black arrowheads show

apnea/hypopnea events. **(b)** Summary data showing the apnea-hypopnea index (AHI) in all groups. One-way ANOVA followed by Holm-Sidak post hoc test. * $P < 0.05$ Sham vs. CHF and $\alpha P < 0.05$, Sham vs. CHF_{CBD}. $N = 4$ per group

Concomitant with decreases in central chemoreflex response to hypercapnia, CB-denervated-CHF animals showed marked decreases in the incidence of breathing disorders. Indeed, the values for apnea incidence in CHF_{CBD} animals were comparable to the ones obtained in Sham animals (Sham: 4.6 ± 0.7 , CHF: 11.7 ± 1.2 and CHF_{CBD}: 7.3 ± 1.9 events/h) (Fig. 12.3a, b).

12.4 Discussion

In this paper, we showed for the first time that intact CB is necessary for the development of enhanced central chemoreflex in nonischemic chronic heart failure. We performed CBD before heart failure induction and found that (i) enhanced central chemoreflex in CHF was completely

restored in animals that underwent CBD and (ii) disordered breathing was significantly improved by CBD in CHF animals. Together our results suggest that CBs are necessary for the development of respiratory disturbances in nonischemic CHF.

In CHF, central chemoreflex potentiation is associated with major incidence of breathing disorders (i.e., apnea-hypopnea events), irregularity, impairment of cardiac function, and sympathetic hyperactivity (Toledo et al. 2017; Díaz et al. 2019). Recently our group showed that selective ablation of RTN neurons using substance P-conjugated saporin toxin in CHF rats completely normalizes the central chemoreflex response and improves breathing regularity and disorders (Díaz et al. 2019). Furthermore, episodic hypercapnic stimulation in CHF triggers

ventilatory plasticity and elicits cardiorespiratory abnormalities that are largely dependent on RTN chemoreceptor neurons (Díaz et al. 2019). Despite this evidence, there are still no studies providing evidence of an intervention that may target RTN neurons in the setting of CHF.

The CB is a peripheral chemosensor with indirect projections to RTN (Stornetta et al. 2006; Takakura et al. 2006; Mulkey et al. 2004). Primary afferences from CB connect the periphery with the commissural part of the NTS predominantly through a glutamatergic projection (Takakura et al. 2006). Then, commissural NTS excitatory projections reach RTN chemoreceptor neurons (Stornetta et al. 2006; Takakura et al. 2006; Mulkey et al. 2004). Thus, CB and RTN, the most important chemoreceptors, are spatially and indirectly connected through second-order synapses (Guyenet et al. 2018; Takakura et al. 2006). Previous studies showed that RTN neurons, positive for the vesicular glutamate transporter 2 (VGLUT2), became activated by systemic hypoxia (Takakura et al. 2006; Smith et al. 2015). Furthermore, single unit recording of RTN neurons in rats showed that CB activation trigger increased firing rate of RTN neurons (Guyenet et al. 2018; Nattie et al. 1993). In addition, evidence obtained in awake dogs showing that stimulation of extracorporeal perfused CB with hypercapnia results in increases in central chemoreflex responses support the notion that CBs enhance central chemoreflex drive (Žera et al. 2019). Together, current evidence supports the presence of a functional connection between CB and RTN neurons that contribute to regulate the central hypercapnic ventilatory response. Importantly, CHF patients displaying an enhanced peripheral/central chemoreflex drive showed higher mortality rates (Giannoni et al. 2009). Accordingly, a positive correlation between CO₂ chemosensitivity and the incidence of breathing disorders in CHF patients has been shown (Solin et al. 2000). The precise pathophysiological mechanism underlying chemoreflex potentiation in the setting on nonischemic CHF remains to be determined. However, in the present study, we found that CBs are needed for the development of enhanced HCVR in experimental

nonischemic CHF. More important, restoration of normal chemoreflex in CHF rats by CB denervation markedly reduced the incidence of breathing disorders.

A plausible explanation about how CB regulates central chemoreflex responses in CHF may be associated with CB-RTN interdependency. Indeed, CB displays tonic afferent activity (Iturriaga et al. 2021) which is integrated at the NTS level and then relies to the RTN. The latter has been shown to be glutamatergic in nature. Interestingly, pharmacological inhibition of NMDA and non-NMDA glutamate receptors at the RTN level decreases cardiorespiratory effects triggered by CB activation (Takakura and Moreira 2011; Nattie et al. 1993). Therefore, glutamatergic signaling between CB and RTN (through the NTS neural circuitry) could play a pivotal role on cardiorespiratory alterations in nonischemic CHF. Whether this pathway remain functional in CHF and/or became hyperactivated in CHF remains to be determined.

Together, our results provide preliminary evidence showing that intact CBs are necessary for the development of enhanced central chemoreflex drive in experimental nonischemic CHF and support the salutary potential of CB denervation on the restoration of normal chemoreflex function and breathing regulation in nonischemic CHF.

Acknowledgments This work was supported by Fondo de Desarrollo Científico y Tecnológico (FONDECYT 1220950 and 3190659). We thank Mr. Fidel Flores and Paulina Arias for their help in managing the animal facility.


References

- Blain GM, Smith CA, Henderson KS, Dempsey JA (2010) Peripheral chemoreceptors determine the respiratory sensitivity of central chemoreceptors to CO₂. *J Physiol* 588(Pt 13):2455–2471
- Del Río R, Andrade DC, Toledo C, Díaz HS, Lucero CM, Arce-Álvarez A, Marcus NJ, Schultz HD (2017) Carotid body-mediated chemoreflex drive in the setting of low and high output heart failure. *Sci Rep* 7(1):8035
- Díaz HS, Andrade DC, Toledo C, Pereyra KV, Schwarz KG, Díaz-Jara E, Lucero CM, Arce-Álvarez A,

- Schultz HD, Silva JD, Takakura AC, Moreira TS, Marcus NJ, Del Río R (2019) Episodic stimulation of central chemoreceptor neurons elicits disordered breathing and autonomic dysfunction in volume overload heart failure. *Am J Physiol Lung Cell Mol Physiol* 318:L27–L40
- Giannoni A, Emdin M, Bramanti F, Iudice G, Francis D, Barsotti A, Piepoli M, Passino C (2009) Combined increased chemosensitivity to hypoxia and hypercapnia as a prognosticator in heart failure. *J Am Coll Cardiol* 53(21):1975–1980
- Groenewegen A, Rutten F, Mosterd A, Hoes A (2020) Epidemiology of heart failure. *Eur J Heart Fail* 22:1342–1356
- Guyenet PG, Bayliss DA, Stornetta RL, Kanbar R, Shi Y, Holloway BB, Souza GM, Basting T, Abbott SB, Wenker IC (2018) Interdependent feedback regulation of breathing by the carotid bodies and the retrotrapezoid nucleus. *J Physiol* 596:3029
- Guyenet PG, Stornetta RL, Souza GM, Abbott SB, Shi Y, Bayliss DA (2019) The retrotrapezoid nucleus: central chemoreceptor and regulator of breathing automaticity. *Trends Neurosci* 42:807–824
- Ilieşiu AM, Hodoroaga AS (2018) Treatment of heart failure with preserved ejection fraction. *Adv Exp Med Biol* 1067:67–87
- Iturriaga R (2018) Carotid body ablation: a new target to address central autonomic dysfunction. *Curr Hypertens Rep* 20:53
- Iturriaga R, Alcayaga J, Chappleau MW, Somers VK (2021) Carotid body chemoreceptors: physiology, pathology, and implications for health and disease. *Physiol Rev* 101:1177
- Kumar NN, Velic A, Soliz J, Shi Y, Li K, Wang S, Weaver JL, Sen J, Abbott SB, Laz-arenko RM, Ludwig M, Perez-Reyes E, Mohebbi N, Bettoni C, Gassmann M, Suply T, Seuwen K, Guyenet PG, Wagner CA, Bayliss DA (2015) Regulation of breathing by CO₂ requires the proton-activated receptor GPR4 in retrotrapezoid nucleus neurons. *Science* 348:1255–1260
- Lugliani R, Whipp BJ, Seard C, Wasserman K (1971) Effect of bilateral carotid-body resection on ventilatory control at rest and during exercise in man. *N Engl J Med* 285(20):1105–1111
- Marcus NJ, Río RD, Schultz E, Xia X, Schultz HD (2014) Carotid body denervation improves autonomic and cardiac function and attenuates disordered breathing in congestive heart failure. *J Physiol* 592:391
- Mouradian Jr GC, Forster HV, Hodges MR (2012) Acute and chronic effects of carotid body denervation on ventilation and chemoreflexes in three rat strains. *J Physiol* 590(14):3335–3347
- Mulkey DK, Stornetta RL, Weston MC, Simmons JR, Parker A, Bayliss DA, Guyenet PG (2004) Respiratory control by ventral surface chemoreceptor neurons in rats. *Nat Neurosci* 7:1360–1369
- Nattie EE, Li A (1995) Rat retrotrapezoid nucleus iono- and metabotropic glutamate receptors and the control of breathing. *J Appl Physiol* 78(1):153–163
- Nattie EE, Gdovin M, Li A (1993) Retrotrapezoid nucleus glutamate receptors: control of CO₂-sensitive phrenic and sympathetic output. *J Appl Physiol* 74(6):2958–2968
- Smith CA, Blain GM, Henderson KS, Dempsey JA (2015) Peripheral chemoreceptors determine the respiratory sensitivity of central chemoreceptors to CO₂: role of carotid body CO₂. *J Physiol* 593:4225
- Solin PA, Roebuck T, Johns DP, Walters EH, Naughton MT (2000) Peripheral and central ventilatory responses in central sleep apnea with and without congestive heart failure. *Am J Respir Crit Care Med* 162(6):2194–2200
- Stornetta RL, Moreira TS, Takakura AC, Kang BJ, Chang DA, West GH, Brunet J, Mulkey DK, Bayliss DA, Guyenet PG (2006) Expression of Phox2b by brainstem neurons involved in chemosensory integration in the adult rat. *J Neurosci* 26:10305–10314
- Takakura AC, Moreira TS (2011) Contribution of excitatory amino acid receptors of the retrotrapezoid nucleus to the sympathetic chemoreflex in rats. *Exp Physiol* 96(10):989–999
- Takakura AC, Moreira TS, Colombari E, West GH, Stornetta RL, Guyenet PG (2006) Peripheral chemoreceptor inputs to retrotrapezoid nucleus (RTN) CO₂-sensitive neurons in rats. *J Physiol* 572(Pt 2):503–523
- Toledo C, Andrade DC, Lucero C, Arce-Alvarez A, Díaz HS, Aliaga V, Schultz HD, Marcus NJ, Manríquez M, Faúndez M, Del Río R (2017) Cardiac diastolic and autonomic dysfunction are aggravated by central chemoreflex activation in heart failure with preserved ejection fraction rats. *J Physiol* 595(8):2479–2495
- Wang S, Benamer N, Zanella S, Kumar NN, Shi Y, Bévéngut M, Pentón D, Guyenet PG, Lesage F, Gestreau C, Barhanin J, Bayliss DA (2013) TASK-2 channels contribute to pH sensitivity of retrotrapezoid nucleus chemoreceptor neurons. *J Neurosci* 33:16033–16044
- Žera T, Moraes DJ, da Silva MP, Fisher JP, Paton JF (2019) The logic of carotid body connectivity to the brain. *Physiology* 34(4):264–282



Effect of Carotid Body Denervation on Systemic Endothelial Function in a Diabetic Animal Model

Marlene D. Cabral, Fátima O. Martins, Inês B. Martins, Bernardete F. Melo, Joana F. Sacramento, Silvia V. Conde , and Jesus Prieto-Lloret

Abstract

Endothelial dysfunction is an essential intermediary for development of cardiovascular diseases associated with diabetes and hypertension (HT). The carotid body (CB) dysfunction contributes to dysmetabolic states, and the resection of carotid sinus nerve (CSN) prevents and reverts dysmetabolism and HT. Herein, we investigated if CSN denervation ameliorates systemic endothelial dysfunction in an animal model of type 2 diabetes mellitus (T2DM).

We used Wistar male rats submitted to HFHSu diet during 25 weeks and the correspondent age-matched controls fed with a standard diet. CSN resection was performed

in half of the groups after 14 weeks of diet. In vivo insulin sensitivity, glucose tolerance and blood pressure, ex vivo aortic artery contraction and relaxation and nitric oxide (NO) levels in plasma and aorta, aorta nitric oxide synthase (NOS) isoforms, and PGF2 α R levels were evaluated.

We demonstrated that, alongside to dysmetabolism and HT reversion, CSN resection restores endothelial function in the aorta and decreases the NO levels in plasma and aorta at the same time that restores normal levels of iNOS in aorta without changing eNOS or PGF2 α R levels.

These results suggest that the modulation of CB activity can be important for the treatment of HT and endothelial dysfunction related with T2DM.

M. D. Cabral · F. O. Martins · I. B. Martins
B. F. Melo · J. F. Sacramento · S. V. Conde (✉)
iNOVA4Health, NOVA Medical School, Faculdade de Ciências Médicas, Universidade NOVA de Lisboa, Lisbon, Portugal
e-mail: silvia.conde@mms.unl.pt

J. Prieto-Lloret
NOVA Medical School, Faculdade de Ciências Médicas, Universidade NOVA de Lisboa, Lisbon, Portugal

Instituto de Biología y Genética Molecular (IBGM), Consejo Superior de Investigaciones Científicas, Universidad de Valladolid, Valladolid, Spain

Departamento de Bioquímica, Biología Molecular y Fisiología, Universidad de Valladolid, Valladolid, Spain

Keywords

Carotid body · Endothelial dysfunction · CSN denervation · Type 2 diabetes mellitus · Hypertension

13.1 Introduction

Endothelial dysfunction is described as an imbalance between vasodilation and vasoconstricting substances, produced by endothelial cells (Deanfield et al. 2005). It is recognized as an

essential intermediary for development of cardiovascular diseases covering vascular diseases associated with diabetes and hypertension (HT) (Kövamees et al. 2016).

Current evidences showed that endothelial dysfunction is linked with type 2 diabetes mellitus (T2DM) and HT-associated impaired vasorelaxation (Kang 2014; Lopez-Lopez et al. 2008), with this significantly enhancing the risk of endothelial dysfunction (Radenković et al. 2013). Moreover, T2DM is associated with the decrease in vasculature elasticity, resulting in the reduction of the vascular lumen and in HT (Mahmoudian et al. 1996) with consequent excessive vasoconstriction (Humbert et al. 2004).

Physiologically, the endothelium produces and releases numerous endothelium-derived relaxation factors (EDRF) that regulate vascular tone (Roberts and Porter 2013) including NO, endothelium-derived hyperpolarizing factor, prostacyclin, angiotensin II, adhesion molecules, and cytokines (Dhananjayan et al. 2016). Several of these factors are altered in pathological conditions, such as T2DM and HT (De Vriese et al. 2000).

One hallmark commonly used to investigate endothelial function is the vasodilator responses to acetylcholine (ACh) (Humbert et al. 2004; McGuire et al. 2002). It is consensual that there is an impairment of endothelium-dependent vasorelaxation in response to ACh in animal models of HT and T2DM (Melo et al. 2021) and in hypertensive and diabetic patients (Kang 2014). Prostanoids, particularly $\text{PGF2}\alpha$, are also involved in endothelium function (Ozen et al. 2013; Uski et al. 1984) with alterations on its receptor being associated with diabetes and its cardiovascular complications (Kang et al. 1996).

The carotid body (CB), classically defined as a blood O_2 , CO_2 , and pH sensor, is also a metabolic sensor involved in the genesis of metabolic diseases. This organ is overactivated in metabolic syndrome and prediabetes animals and patients (Cunha-Guimaraes et al. 2020), and the denervation of its sensitive nerve, the carotid sinus nerve (CSN), prevents and reverts dysmetabolism and HT in hypercaloric animal models (Ribeiro et al. 2013; Sacramento et al. 2017). Moreover, the

link CBs-HT was corroborated by others by showing that HT is dependent on CB input that drives increased sympathetic tone in spontaneously hypertensive rats (McBryde et al. 2013; Pijacka et al. 2016), this being ameliorated by CB ablation (McBryde et al. 2013; Abdala et al. 2012). As well, CSN denervation ameliorates glucose metabolism and HT in chronic intermittent hypoxia animals (Shin et al. 2014; Fletcher et al. 1992) that mimic obstructive sleep apnea.

Knowing that endothelial dysfunction can result from and/or contribute to several diseases associated with HT and T2DM and that CB overactivation drives these diseases, we investigated if CSN denervation can ameliorate systemic endothelial dysfunction in an animal model of T2DM.

13.2 Methods

13.2.1 Animals

Experiments were performed in 8-week-old male Wistar rats (200–300 g), obtained from the vivarium of NOVA Medical School, Faculdade de Ciências Médicas. Animals were housed in a controlled environment (21 ± 1 °C; $55 \pm 10\%$ humidity) with a 12-h light/dark cycle and free access to food and water. An early-phase type 2 diabetes model (combined IR, hyperinsulinemia, and increased total fat mass (Kinzig et al. 2010)) with HT was obtained by submitting animals to a high-fat and high-sucrose (HFHSu) diet (lipid-rich diet with 60% of energy from fat and 35% sucrose in drinking water) for 25 weeks and compared with an age-matched control group (CTL), fed with a standard diet. After 14 weeks of diet, both groups were randomly divided, and half of each was submitted to bilateral CSN resection or to a sham surgery. Surgeries were performed under a mixture of ketamine (30 mg/kg)/medetomidine (4 mg/kg) and carprofen (5 mg/kg). After surgery, animals were kept under the respective diet. Insulin sensitivity was evaluated by an insulin tolerance test (ITT) and glucose tolerance through oral glucose tolerance test (OGTT) (Monzillo and Hamdy 2003) along the diet proto-

col. Twenty-five weeks after beginning the diet, rats were submitted to a terminal experiment in which they were anesthetized with pentobarbital (60 mg/kg) and femoral artery was catheterized for mean blood pressure (MBP) recording using a pressure transducer (Emka, Paris, France) and a pressure amplifier (Emka, Paris, France). MBP was analyzed using the software IOX 2.9.5.73 (Emka, Paris, France). Blood was collected through cardiac puncture to measure NO levels. The aorta artery was collected for vascular function studies or stored at -80°C for later analyses.

All experiments and animal care were performed in accordance with the European Union Directive for Protection of Vertebrates Used for Experimental and Other Scientific Ends (2010/63/EU), and all the experimental protocols were approved by the ethics committee of the NOVA Medical School/Faculdade de Ciências Médicas.

13.2.2 Evaluation of Endothelial Function

The physiological function of the aorta artery was studied using a small vessel wire myograph (DMT, Denmark). The bath chambers for isolated organs were gassed with normoxia (21% O_2 + 5% CO_2) and the temperature was maintained at 37°C . The aorta was dissected in cold Krebs-Henseleit buffer. Rings of aorta (inner diameter: 0.5–1.0 mm) were dissected and withdrawn of all adventitia and parenchyma. The arteries were connected to isometric force transducers to measure changes in isometric tension and then stretched to give a basal tension of 5–6 mN. After stabilization, to check the viability of the vessels, three responses of physiological salt solution (KPSS) were performed. To constrict the vessels, increasing doses of $\text{PGF2}\alpha$ (0.03–10 μM) were added to the chamber solution. Twenty minutes after washing and on a stable $\text{PGF2}\alpha$ contraction, a cumulative concentration response curve to ACh (0.03 μM –30 μM) was performed to determine endothelial integrity.

13.2.3 Nitric Oxide Quantification in Plasma and Aorta

Aorta arteries were dissected and homogenized in a glass tissue homogenizer with buffer (25 mM Tris HCL, 1 mM EDTA, 1 mM EGTA). Afterward, the homogenates were centrifuged, and the supernatant was collected. Aorta supernatants and plasma samples were deproteinized by diluting the samples with absolute ethanol at 4°C . NO levels were quantified using the Sievers Nitric Oxide Analyzer (NOA 280i; Sievers Research Inc., Boulder Colorado, USA) by chemiluminescence (Wu and Yen 1999). NO concentrations were calculated by comparison with an interpolation of a calibration curve made from increasing concentrations of sodium nitrate.

13.2.4 Western Blot Analyses of eNOS, Inos, and $\text{PGF2}\alpha\text{R}$ Protein Levels in Aorta Artery

For Western blot analysis, aorta arteries were homogenized in liquid nitrogen and placed in Zurich medium with protease inhibitors as previously described (Sacramento et al. 2017). Samples were denatured, centrifuged, and separated by electrophoresis (SDS-PAGE). Proteins were transferred to a nitrocellulose membrane (Bio-Rad, Germany) and blocked in I-Block solution (0.5%) (Applied Biosystems, Foster City, USA). A three-step Western blot protocol was used to enhance detection sensitivity (Johnson et al. 2009). After blocking, membranes were incubated overnight at 4°C with primary polyclonal rabbit anti-eNOS antibody (bands in the 140 kDa region, 1:500; Santa Cruz Biotechnology, Madrid, Spain), primary polyclonal rabbit anti-iNOS antibody (bands in the 130 kDa region, 1:200; Santa Cruz Biotechnology, Madrid, Spain), or primary polyclonal rabbit anti- $\text{PGF2}\alpha\text{R}$ antibody (bands in the 45 kDa region, 1:200; Santa Cruz Biotechnology, Madrid, Spain). Afterwards, the membranes were incubated with biotin-conjugated goat anti-rabbit IgG (1:5000) for 2 h and with horseradish peroxidase-conjugated streptavidin (1:10000) for

30 min at room temperature. Chemiluminescence signals were developed with enhanced chemiluminescence reagent (Clarity Western ECL, Bio-Rad, USA); the signals were detected in a ChemiDoc Molecular Imager (ChemiDoc; Bio-Rad, Madrid, Spain) and quantified using the Quantity-One software (Bio-Rad). The membranes were reprobed with polyclonal goat anti-calnexin (bands in the 90 kDa region, 1:1000; SicGen, Portugal) to compare and normalize the levels of proteins with the amount of protein loaded.

13.2.5 Statistical Analysis

Data was evaluated using GraphPad Prism Software, version 6 (GraphPad Software Inc., San Diego, CA, USA) and was expressed as mean \pm SEM. The significance of the differences between the means was calculated by one-way or two-way analysis of variance (ANOVA) with Bonferroni multiple comparison tests. Differences were considered significant at $p \leq 0.05$.

13.3 Results

13.3.1 Effect of HFHSu Diet and CSN Resection on In Vivo Metabolic Parameters

In table 13.1 is represented the effect of HFHSu diet and CSN resection on insulin sensitivity, determined by the ITT, before diet and after 25 weeks of diet.

As expected, and previously described, HFHSu diet decreased insulin sensitivity, an effect reverted by CSN resection (Table 13.1) (Sacramento et al. 2018; Melo et al. 2022). In addition, HFHSu diet promoted the development of glucose intolerance, an effect also reversed by CSN resection (Table 13.1). At 25 weeks, HFHSu diet increases the MBP by 52% in relation to CTL diet (CTL = 80.9 ± 9.6 mmHg; HFHSu = 123.4 ± 4.4 mmHg). CSN resection did not alter MBP in CTL animals, but in HFHSu rats, it significantly decreased by 23% (CTL

DEN = 79.0 ± 6.7 mmHg; HFHSu DEN = 95.3 ± 7.5 mmHg).

13.3.2 Effect of HFHSu Diet and of CSN Resection on Vasoconstrictor Responses and Endothelial Function in Aorta Artery

The effect of HFHSu diet and of CSN resection on the contractile responses induced by KPSS (80 mM) in the aorta artery is represented in Fig. 13.1a. HFHSu diet did not modify the contractile responses to the unspecific stimulus KPSS in aorta artery (Fig. 13.1a). CSN resection decreased the contractile responses in CTL and HFHSu animals (Fig. 13.1a) by 35% and by 26%, respectively (contractile responses to KPSS: CTL = 8.76 ± 0.73 mN; CTL DEN = 5.69 ± 0.54 mN; HFHSu = 9.25 ± 0.82 mN; HFHSu DEN = 6.83 ± 0.6 mN). Figure 13.1b shows the contractile responses to increasing doses of PGF2 α (0.03–10 μ M) in the aorta artery. HFHSu presented a higher contractile response to PGF2 α , and for the higher concentration tested, 10 μ M, HFHSu diet significantly increased the contractile response by 79% (contractile response to PGF2 α : CTL = $70.6 \pm 10.4\%$; HFHSu = $126.9 \pm 13.3\%$). CSN resection increased the contractile dose-response curve for PGF2 α , for the highest concentration tested (10 μ M), by 32% and 10% in CTL and HFHSu, respectively (contractile response to PGF2 α : CTL DEN = $93 \pm 10\%$; HFHSu DEN = $139 \pm 6.1\%$). Figure 13.1c displays the evaluation of endothelial integrity, evaluated by concentration-response curve (CRC) for relaxation to ACh, previously contracted with PGF2 α in aorta artery. The HFHSu diet significantly decreased the relaxation curve. For the highest concentration tested, 30 μ M, the HFHSu diet decreased by 262% (relaxation response to ACh at 30 μ M: CTL = $10.1 \pm 3.19\%$; HFHSu = $36.7 \pm 4.41\%$). CSN resection did not significantly modify the CRC for relaxation in the CTL animals (relaxation response to ACh at 30 μ M: CTL DEN = $10.64 \pm 3.16\%$). However,

Table 13.1 Effect of HFHSu diet and of CSN resection on in vivo metabolic function before diet and at 25 weeks of diet

Metabolic parameters	Animal group		Before diet	25 weeks of diet
kITT (% glucose/min)	CTL	SHAM	4.36 ± 0.56	4.21 ± 0.52
		DEN	5.17 ± 0.75	4.34 ± 0.53
	HFHSu	SHAM	4.36 ± 0.25	1.35 ± 0.79****
		DEN	4.25 ± 0.33	4.51 ± 0.35####
AUC OGTT (mg/dl*min)	CTL	SHAM	21,459 ± 1643	21,897 ± 1600
		DEN	21,240 ± 1027	20,447 ± 2567
	HFHSu	SHAM	21,446 ± 1163	24,334 ± 1769***
		DEN	20,703 ± 938	22,140 ± 2275
MBP (mmHg)	CTL	SHAM	–	80.9 ± 9.6
		DEN	–	79.0 ± 6.7
	HFHSu	SHAM	–	123.4 ± 4.4****
		DEN	–	95.3 ± 7.5####

Two-way ANOVA with Bonferroni multiple comparison tests; *** $p < 0.001$, **** $p < 0.0001$ vs CTL; #### $p < 0.0001$ comparing values with HFHSu sham animals. CTL control animals

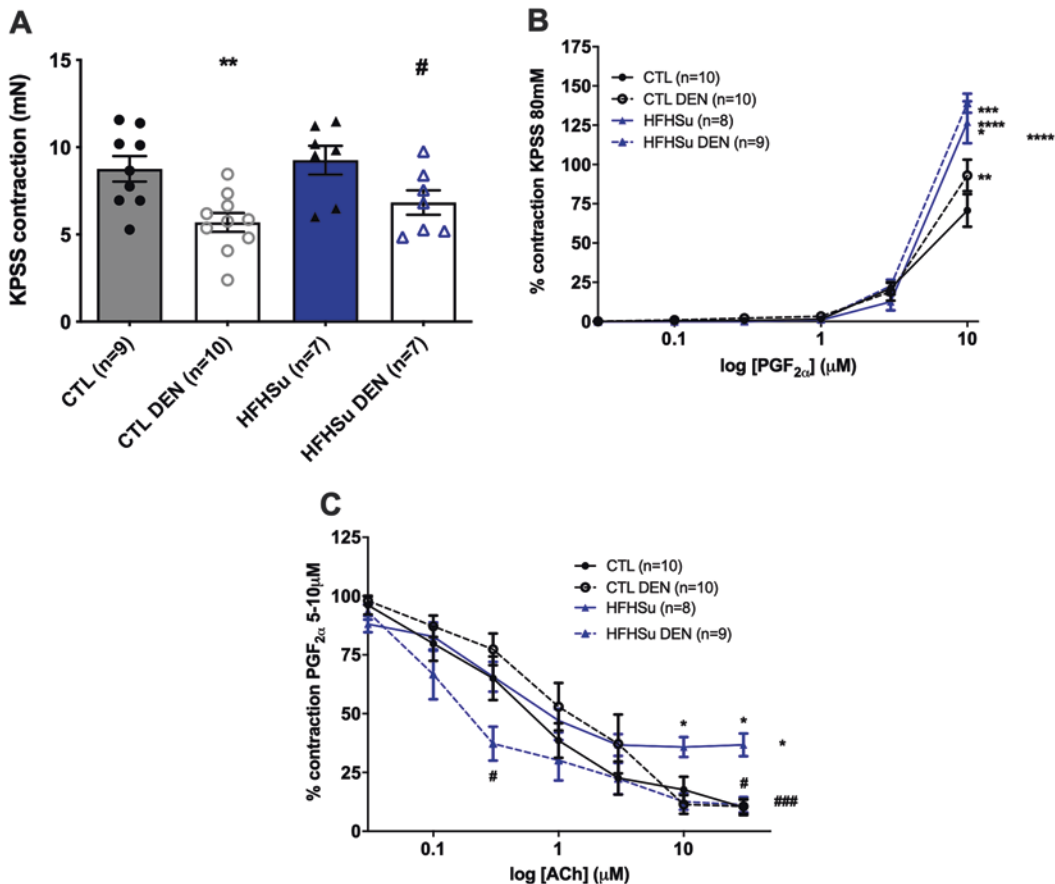


Fig. 13.1 Effect of HFHSu diet and of carotid sinus nerve (CSN) resection on aorta artery vasoconstrictor responses to 80 mM of K⁺ (KPSS) (a), contractile responses to PGF_{2α} given by the concentration response curves for contraction to PGF_{2α} (b), and relaxation responses to ACh given by the concentration response curves for relaxation to ACh (c). In (a) bars represent

mean ± SEM and in (b) and (c) CTL (black line), CTL DEN (black dashed line), HFHSu (blue line), and HFHSu DEN (blue dashed line) groups. Two-way ANOVA with Bonferroni multiple comparison tests; * $p < 0.05$, ** $p < 0.01$ vs CTL; # $p < 0.05$, ### $p < 0.001$, #### $p < 0.0001$ vs HFHSu sham animals. CTL control

for the highest concentration, 30 μM , the CSN resection of the HFHSu animals increased by 69% (relaxation response to ACh at 30 μM : HFHSu DEN = $11.2 \pm 1.84\%$).

13.3.3 Effect of HFHSu Diet and of CSN Resection on NO Levels in Plasma and Aorta Artery

The effect of HFHSu diet and CSN resection in the NO levels in plasma is represented in Fig. 13.2a. HFHSu diet significantly increased the NO levels in plasma by 74% (NO levels: CTL = $15.34 \pm 0.4 \mu\text{M}$; HFHSu = $26.67 \pm 1.64 \mu\text{M}$). CSN resection decreased them by 16% and 24% in CTL and HFHSu animals, respectively (NO levels: CTL DEN = $12.85 \pm 0.5 \mu\text{M}$; HFHSu DEN = $20.34 \pm 0.5 \mu\text{M}$). Figure 13.2b displays the effect of HFHSu diet and CSN resection on NO levels in the aorta artery. HFHSu diet significantly increased NO levels by 40% (NO levels: CTL = $334 \pm 17.1 \mu\text{moles/g}$; HFHSu = $469 \pm 20.23 \mu\text{moles/g}$). CSN resection increased by 29% NO levels in aorta artery (NO levels: CTL DEN = $430 \pm 12.67 \mu\text{moles/g}$)

when compared with the CTL. Moreover, CSN resection significantly decreased NO levels of HFHSu rats (NO levels: HFHSu DEN = $132 \pm 3.4 \mu\text{moles/g}$) (Fig. 13.2b).

13.3.4 Effect of HFHSu Diet and of CSN Resection on eNOS, iNOS, and PGF2 α R Levels in Aorta Artery

Figure 13.3 presents the effect of HFHSu diet and of CSN resection on eNOS (Fig. 13.3a), iNOS (Fig. 13.3b), and PGF2 α R (Fig. 13.3c) levels in the aorta artery. Fig. 13.3d displays the representative Western blots comparing the levels of each protein with calnexin. HFHSu diet or CSN resection did not significantly alter the levels of eNOS (Fig. 13.3a). HFHSu diet significantly increased the iNOS levels in the aorta by 44% (iNOS levels: CTL = $100 \pm 3.84\%$; HFHSu = $144.49 \pm 14.45\%$). CSN resection in CTL animals did not modify the iNOS levels but significantly decreased by 53% the iNOS levels in HFHSu animals (HFHSu = $144.49 \pm 14.45\%$; HFHSu DEN = $68 \pm 9.89\%$) to levels even below the control levels (Fig. 13.3b).

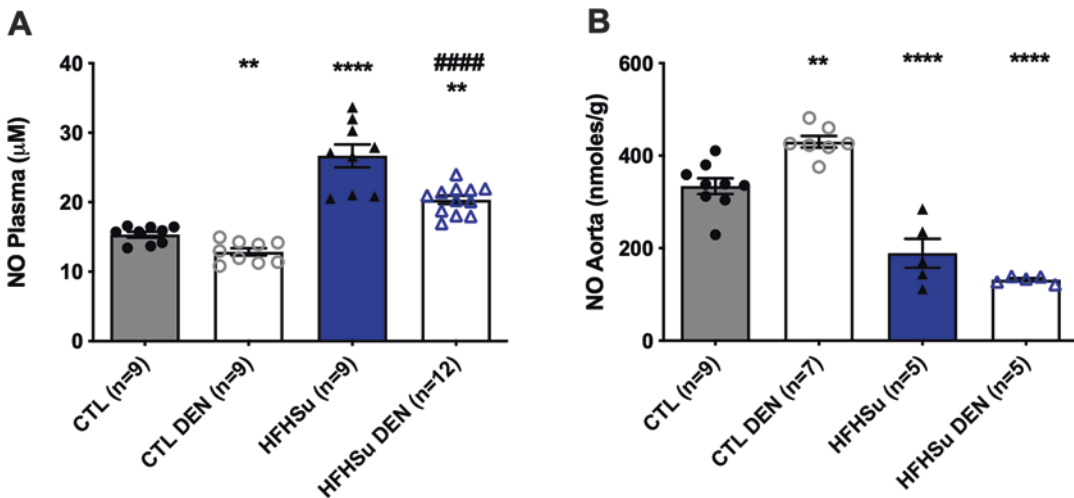


Fig. 13.2 Effect of HFHSu diet and of CSN resection on NO levels in plasma (a) and in aorta artery (b). Bars represent mean \pm SEM. One-way ANOVA with Bonferroni

multiple comparison tests; ** $p < 0.01$, **** $p < 0.0001$ vs CTL; ##### $p < 0.0001$ comparing values with HFHSu sham animals. CTL control animals

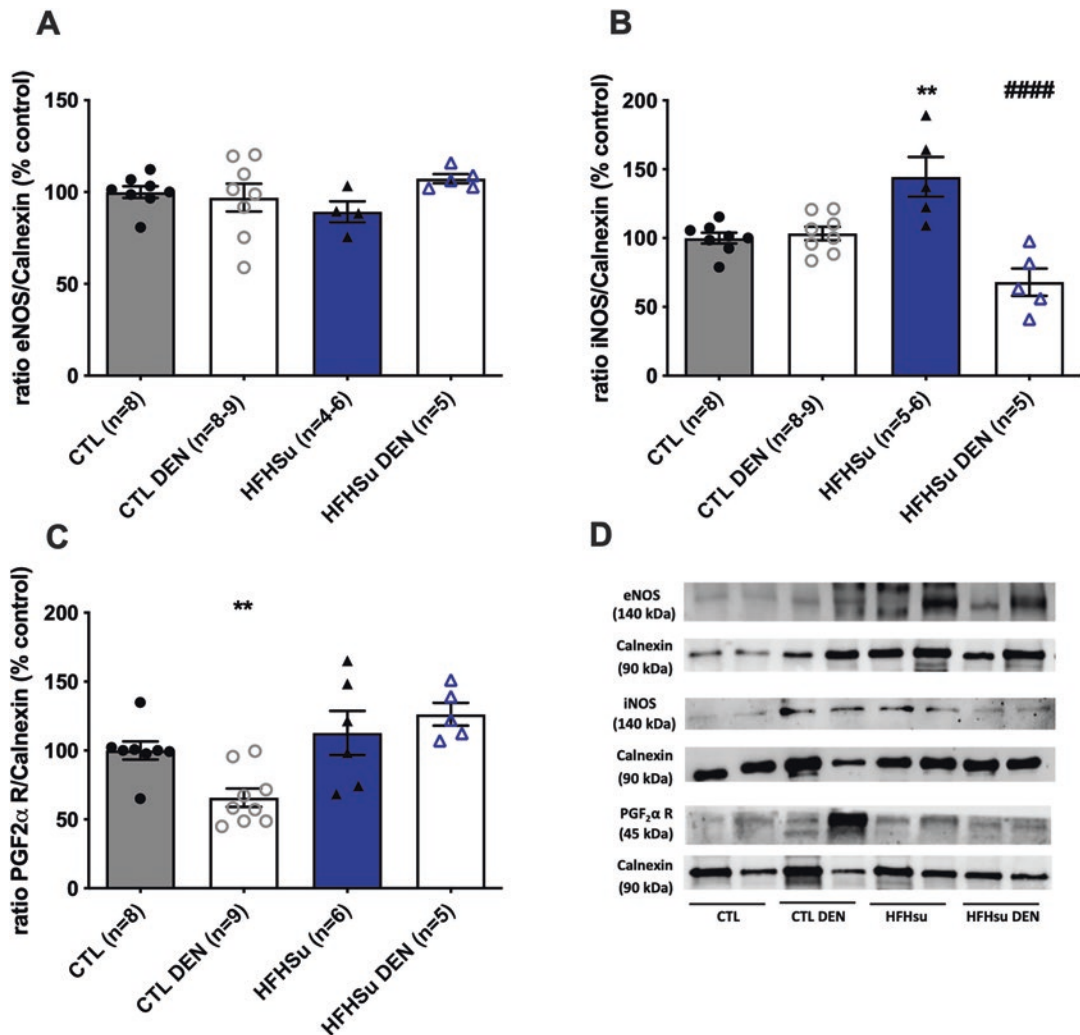


Fig. 13.3 Effect of HFHSu diet and of CSN resection on eNOS (a), iNOS (b), and PGF2 α R protein levels in the aorta artery (c). Bars represent mean \pm SEM. Panel (D) displays representative images of Western blot for the protein levels of eNOS (140 kDa), iNOS (140 kDa), and PGF2 α R (45 kDa), respectively, and calnexin (90 kDa),

the loading protein. Graphs on (a), (b), and (c) represent the mean values for the protein levels of eNOS, iNOS, and PGF2 α R, respectively, expressed in relation to calnexin. One-way ANOVA with Bonferroni multiple comparison tests; ** $p < 0.01$ vs CTL; ##### $p < 0.0001$ comparing values with HFHSu sham animals

HFHSu diet did not alter the PGF2 α R levels in the aorta (CTL = $100 \pm 6.62\%$, HFHSu = $112.74 \pm 16.07\%$). CSN resection significantly decreased the PGF2 α R levels in control animals by 34% (CTL = $100 \pm 6.62\%$, CTL DEN = $65.78 \pm 6.68\%$) but did not change significantly in HFHSu animals (HFHSu = $112.74 \pm 16.07\%$; HFHSu DEN = $126.32 \pm 8.25\%$) (Fig. 13.3c).

13.4 Discussion

We demonstrated that CSN resection restores endothelial function in the aorta in conditions of T2DM. Furthermore, we also show that CSN resection decreases the NO levels in plasma and restores normal levels of iNOS in aorta in hypercaloric diet animal model.

T2DM is one of the main health problems worldwide, and it is well known that it is related

with an augmented risk of microvascular and macrovascular problems, which include HT and atherosclerosis (Lopez-Lopez et al. 2008). Insulin resistance when associated with TD2M is indispensable for endothelial dysfunction (Yki-Järvinen 2003), which is an important pathophysiological hallmark related with HT, obesity, and dyslipidemia (Huang 2009).

In the current study, we showed that CSN resection in HFHSu rats completely restored insulin resistance and brought back glucose tolerance to control values. These results agree with our previous findings using this HFHSu animal model (Sacramento et al. 2018; Melo et al. 2022) and using other diet models, the 6-week 45% lipid-rich diet rat or the 7-week 35% sucrose diet rat in which bilateral CSN resection led to complete restoration of the insulin sensitivity and improved glucose intolerance (Sacramento et al. 2017).

Herein, we also describe that HFHSu animals exhibit a significant increase in MBP in comparison with controls (Table 13.1), agreeing with our previous results in animals submitted to high-fat or high sucrose diets (Ribeiro et al. 2013) and with the data from (Bourgoin et al. 2008), where 6-week-old male Sprague Dawley rats were fed with a HFHSu diet. As previously described as well (Ribeiro et al. 2013), herein CSN resection in HFHSu model decreased MBP. This consolidates the role of the CB in the setting and maintenance of high blood pressure not only in essential HT (Abdala et al. 2012) or obstructive sleep apnea-associated HT (Fletcher et al. 1992) but also in hypertensive states associated with dysmetabolism.

In the present study, we also showed, as previously described by our group (Melo et al. 2021), that HFHSu diet did not change the contractile response to high K^+ , effects that are in agreement with the absence of high K^+ -induced contractile responses in streptozotocin-induced diabetic rats (Silan 2008). Altogether, these results suggest that diabetes did not alter the contractile responses to unspecific stimuli. Moreover, we tested $PGF2\alpha$, another powerful vasoconstrictor in the aorta (Snetkov et al. 2006), and showed, as previously demonstrated (Melo et al. 2021), that

HFHSu diet promotes an increase in the contractile responses to $PGF2\alpha$. Similar results were obtained by Miike et al. (2008) in 11-week-old male db/db mice (Miike et al. 2008). Interestingly, CSN resection decreased aorta contractility in response to unspecific stimuli, but not to $PGF2\alpha$, which may indicate that CSN resection could be useful in disease conditions associated with increased arterial contractility that is not mediated by $PGF2\alpha$.

Diabetes and insulin resistance are associated with impaired endothelium-dependent relaxation (Moral-Sanz et al. 2011), and as previously described by our group (Melo et al. 2021), we found herein that HFHSu diet animals displayed an impairment in the relaxation curve to ACh. Several factors have been pointed out as possible contributors to this impaired endothelium-dependent relaxation in diabetes, such as hyperglycemia, a decrease influx of Ca^{2+} into endothelium or diminished release of Ca^{2+} from its intracellular stores, a reduced diffusion of NO into the vascular smooth muscle cells (Ozyazgan et al. 2000), or endothelial damage resulting from increased ROS induced by diabetes (Silan 2008). In HFHSu animals we showed previously that this impaired-aorta relaxation is associated with increased advanced glycation end products (AGEs) and alterations on its receptors, inflammation, and oxidative stress (Melo et al. 2021). One of the most remarkable results of our work is that herein we describe for the first time that the CSN resection in the HFHSu animals has the capacity to improve the relaxation in aorta artery, restoring almost completely the endothelial function, without alterations in the relaxation in control animals.

Multiple mechanisms can function simultaneously to induce endothelial dysfunction. Therefore, we investigated two of the possible mechanisms essential to explain the reduced endothelium-dependent vasodilation induced by the HFHSu diet and its recovery by CSN resection. The consensual feature in endothelial dysfunction is a decrease in the bioavailability of NO in the vasculature (Huang 2009), so herein, we quantified the NO levels in plasma and aorta (Fig. 13.2a, b, respectively). As expected, and

previously described in HFHSu animals (Melo et al. 2021) and in other hypercaloric diet models (Sacramento et al. 2017; Conde et al. 2012), we observed that NO levels in plasma were significantly higher in HFHSu groups. In humans, Maejima et al. (2001) also described in TD2M subjects an increase in NO levels in plasma compared with the nondiabetic subjects (Maejima et al. 2001). In addition, and as we previously showed in hypercaloric models of metabolic syndrome, CSN resection decreased the NO levels in the plasma of animals fed with the standard and HFHSu diet. In the aorta, the HFHSu diet significantly increased the NO levels compared to CTL values. This result is in accordance to our previous results in the same animal model (Melo et al. 2021). This increase in NO levels can be explained by an augmented expression of iNOS (Fig. 13.3b), reflecting an inflammatory-induced NO production that we and others also previously showed and known to be associated with dysmetabolic diseases (Melo et al. 2021; Aktan 2004). Additionally, the common feature of endothelial dysfunction is a diminished eNOS expression, as described by Yang et al. (2007) that displayed lower level of eNOS in aorta in male Sprague Dawley rats fed with a high-fat diet (Yang et al. 2007). However, our results show that there are no significant changes in the eNOS levels in the aorta artery with any experimental condition (Fig. 13.3a). Similar results were described in aorta of 6-month-old Goto-Kakizaki rats by Carvalho (Carvalho 2011). CSN resection in HFHSu animals decreased the levels of iNOS in aorta artery to values like the controls, suggesting an amelioration of inflammatory conditions promoted by the CSN denervation and consequent normalization of NO levels in the tissue.

As previously reported by our group (Melo et al. 2021), we showed that aorta PGF2 α receptor levels did not change under HFHSu diet (Fig. 13.3c), which contrasts with the increase in PGF2 α receptor levels in aorta described in male Sprague Dawley rats fed with a high-fat diet and injected with streptozotocin (Li et al. 2015). These discrepancies may rely on the animal model and on the method used for inducing diabetes. CSN resection decreased PGF2 α receptor

levels in control animals but not in HFHSu animals, an effect that was not surprising as the contraction in response to PGF2 α was not modified by CSN resection in the aorta of HFHSu animals.

To conclude, this study demonstrates for the first time, that CSN resection can restore the systemic endothelial dysfunction in a model of an early phase of T2DM, reversing the impaired relaxation to ACh and re-establishing the normal levels of NO in plasma and the expression levels of iNOS in aorta artery. Altogether these results suggest that the modulation of CB activity may be important therapeutically for the treatment of HT and endothelial dysfunction related with T2DM.

Acknowledgments This study was supported by Fundação para a Ciência e Tecnologia (FCT): FOM and JFS – CEECIND/04266/2017 and CEECIND/02428/2018, respectively.

References


- Abdala AP, McBryde FD, Marina N, Hendy EB, Engelman ZJ, Fudim M et al (2012 Sep) Hypertension is critically dependent on the carotid body input in the spontaneously hypertensive rat. *J Physiol* 590(17):4269–4277
- Aktan F (2004 Jun) iNOS-mediated nitric oxide production and its regulation. *Life Sci* 75(6):639–653
- Bourgoin F, Bachelard H, Badeau M, Mélançon S, Pitre M, Larivière R et al (2008 Sep) Endothelial and vascular dysfunctions and insulin resistance in rats fed a high-fat, high-sucrose diet. *Am J Physiol Heart Circ Physiol* 295(3):H1044–H1055
- Carvalho DAF (2011) Potencial efeito terapêutico da piridoxamina na disfunção endotelial macrovascular na diabetes tipo 2 [Internet]. University of Coimbra. Available from: <http://hdl.handle.net/10316/25809>
- Conde SV, Nunes Da Silva T, Gonzalez C, Mota Carmo M, Monteiro EC, Guarino MP (2012) Chronic caffeine intake decreases circulating catecholamines and prevents diet-induced insulin resistance and hypertension in rats. *Br J Nutr* 107(1):86–95.
- Cunha-Guimaraes JP, Guarino MP, Timóteo AT, Caires I, Sacramento JF, Ribeiro MJ et al (2020) Carotid body chemosensitivity: early biomarker of dysmetabolism in humans. *Eur J Endocrinol* 182(6):549–557
- De Vriese AS, Verbeuren TJ, Van de Voorde J, Lameire NH, Vanhoute PM (2000 Jul) Endothelial dysfunction in diabetes. *Br J Pharmacol* 130(5):963–974

- Deanfield J, Donald A, Ferri C, Giannattasio C, Halcox J, Halligan S et al (2005 Jan) Endothelial function and dysfunction. Part I: methodological issues for assessment in the different vascular beds: a statement by the working group on endothelin and endothelial factors of the European Society of Hypertension. *J Hypertens* 23(1):7–17
- Dhananjayan R, Koundinya KSS, Malati T, Kutala VK (2016 Oct) Endothelial dysfunction in type 2 diabetes mellitus. *Indian J Clin Biochem* 31(4):372–379
- Fletcher EC, Lesske J, Behm R, Miller CC, Stauss H, Unger T (1992) Carotid chemoreceptors, systemic blood pressure, and chronic episodic hypoxia mimicking sleep apnea. *J Appl Physiol* 72(5):1978–1984
- Huang PL (2009 Aug) eNOS, metabolic syndrome and cardiovascular disease. *Trends Endocrinol Metab* 20(6):295–302
- Humbert M, Morrell NW, Archer SL, Stenmark KR, MacLean MR, Lang IM et al (2004 Jun) Cellular and molecular pathobiology of pulmonary arterial hypertension. *J Am Coll Cardiol* 43(12 Suppl S):13S–24S
- Johnson RP, El-Yazbi AF, Takeya K, Walsh EJ, Walsh MP, Cole WC (2009 Jun) Ca²⁺ sensitization via phosphorylation of myosin phosphatase targeting subunit at threonine-855 by rho kinase contributes to the arterial myogenic response. *J Physiol* 587(Pt 11):2537–2553
- Kang KT (2014 Sep) Endothelium-derived relaxing factors of small resistance arteries in hypertension. *Toxicol Res* 30(3):141–148
- Kang KH, Shim JJ, Banerjee M, Newman JH (1996 Jan) PGF₂ alpha causes bronchoconstriction and pulmonary vasoconstriction via thromboxane receptors in rat lung. *Korean J Intern Med* 11(1):74–81
- Kinzig KP, Honors MA, Hargrave SL (2010 Jul) Insulin sensitivity and glucose tolerance are altered by maintenance on a ketogenic diet. *Endocrinology* 151(7):3105–3114
- Kövamees O, Shemyakin A, Pernow J (2016 Sep) Amino acid metabolism reflecting arginase activity is increased in patients with type 2 diabetes and associated with endothelial dysfunction. *Diab Vasc Dis Res* 13(5):354–360
- Li Y, Han L, Ding WY, Ti Y, Li YH, Tang MX et al (2015 Dec) Prostaglandin F₂α receptor silencing attenuates vascular remodeling in rats with type 2 diabetes. *Exp Mol Pathol* 99(3):517–523
- Lopez-Lopez JG, Moral-Sanz J, Frazziano G, Gomez-Villalobos MJ, Flores-Hernandez J, Monjaraz E et al (2008 Nov) Diabetes induces pulmonary artery endothelial dysfunction by NADPH oxidase induction. *Am J Physiol Lung Cell Mol Physiol* 295(5):L727–L732
- Maejima K, Nakano S, Himeno M, Tsuda S, Makiishi H, Ito T et al (2001) Increased basal levels of plasma nitric oxide in Type 2 diabetic subjects. Relationship to microvascular complications. *J Diabetes Complicat* 15(3):135–143
- Mahmoudian M, Behnaz F, Rezaei E (1996 Jul) Diabetes-induced changes in the contractility of the aorta and pA2 of nifedipine in the rat. *Acta Diabetol* 33(2):114–117
- McBryde FD, Abdala AP, Hendy EB, Pijacka W, Marvar P, Moraes DJA et al (2013) The carotid body as a putative therapeutic target for the treatment of neurogenic hypertension. *Nat Commun* 4:2395
- McGuire JJ, Hollenberg MD, Andrade-Gordon P, Triggle CR (2002 Jan) Multiple mechanisms of vascular smooth muscle relaxation by the activation of proteinase-activated receptor 2 in mouse mesenteric arterioles. *Br J Pharmacol* 135(1):155–169
- Melo BF, Prieto-Lloret J, Cabral MD, Martins FO, Martins IB, Sacramento JF et al (2021 Mar) Type 2 diabetes progression differently affects endothelial function and vascular contractility in the aorta and the pulmonary artery. *Sci Rep* 11(1):6052
- Melo BF, Sacramento JF, Capucho AM, Sampaio-Pires D, Prego CS, Conde SV (2022) Long-term Hypercaloric diet consumption exacerbates age-induced Dysmetabolism and carotid body dysfunction: beneficial effects of CSN denervation. *Front Physiol* 13:889660
- Miike T, Kunishiro K, Kanda M, Azukizawa S, Kurahashi K, Shirahase H (2008 Jun) Impairment of endothelium-dependent ACh-induced relaxation in aorta of diabetic db/db mice—possible dysfunction of receptor and/or receptor-G protein coupling. *Naunyn Schmiedeberg's Arch Pharmacol* 377(4–6):401–410
- Monzillo LU, Hamdy O (2003 Dec) Evaluation of insulin sensitivity in clinical practice and in research settings. *Nutr Rev* 61(12):397–412
- Moral-Sanz J, Menendez C, Moreno L, Moreno E, Cogolludo A, Perez-Vizcaino F (2011 Apr) Pulmonary arterial dysfunction in insulin resistant obese Zucker rats. *Respir Res* 12(1):51
- Ozen G, Topal G, Gomez I, Ghorreshi A, Boukais K, Benyahia C et al (2013 Dec) Control of human vascular tone by prostanoids derived from perivascular adipose tissue. *Prostaglandins Other Lipid Mediat* 107:13–17
- Ozyazgan S, Unlucerci Y, Bekpınar S, Akkan AG (2000) Impaired relaxation in aorta from streptozotocin-diabetic rats: effect of aminoguanidine (AMNG) treatment. *Int J Exp Diabetes Res* 1(2):145–153
- Pijacka W, Moraes DJA, Ratcliffe LEK, Nightingale AK, Hart EC, da Silva MP et al (2016 Oct) Purinergic receptors in the carotid body as a new drug target for controlling hypertension. *Nat Med* 22(10):1151–1159
- Radenković M, Stojanović M, Potpara T, Prostran M (2013) Therapeutic approach in the improvement of endothelial dysfunction: the current state of the art. *Biomed Res Int* 2013:252158
- Ribeiro MJ, Sacramento JF, Gonzalez C, Guarino MP, Monteiro EC, Conde SV (2013) Carotid body denervation prevents the development of insulin resistance and hypertension induced by hypercaloric diets. *Diabetes* 62(8):2905–2916
- Roberts AC, Porter KE (2013 Nov) Cellular and molecular mechanisms of endothelial dysfunction in diabetes. *Diab Vasc Dis Res* 10(6):472–482
- Sacramento JF, Ribeiro MJ, Rodrigues T, Olea E, Melo BF, Guarino MP et al (2017) Functional abolition of

- carotid body activity restores insulin action and glucose homeostasis in rats: key roles for visceral adipose tissue and the liver. *Diabetologia* [Internet] 60(1):158–168. <https://doi.org/10.1007/s00125-016-4133-y>
- Sacramento JF, Chew DJ, Melo BF, Donegá M, Dopson W, Guarino MP et al (2018) Bioelectronic modulation of carotid sinus nerve activity in the rat: a potential therapeutic approach for type 2 diabetes. *Diabetologia* 61(3):700–710
- Shin MK, Yao Q, Jun JC, Bevans-Fonti S, Yoo DY, Han W et al (2014) Carotid body denervation prevents fasting hyperglycemia during chronic intermittent hypoxia. *J Appl Physiol* 117(7):765–776
- Silan C (2008 May) The effects of chronic resveratrol treatment on vascular responsiveness of streptozotocin-induced diabetic rats. *Biol Pharm Bull* 31(5):897–902
- Snetkov VA, Knock GA, Baxter L, Thomas GD, Ward JPT, Aaronson PI (2006 Feb) Mechanisms of the prostaglandin F₂α-induced rise in [Ca²⁺]_i in rat intrapulmonary arteries. *J Physiol* 571(Pt 1):147–163
- Uski TK, Andersson KE, Brandt L, Ljunggren B (1984 Aug) Characterization of the prostanoid receptors and of the contractile effects of prostaglandin F₂α in human pial arteries. *Acta Physiol Scand* 121(4):369–378
- Wu CC, Yen MH (1999 May) Higher level of plasma nitric oxide in spontaneously hypertensive rats. *Am J Hypertens* 12(5):476–482
- Yang N, Ying C, Xu M, Zuo X, Ye X, Liu L et al (2007 Oct) High-fat diet up-regulates caveolin-1 expression in aorta of diet-induced obese but not in diet-resistant rats. *Cardiovasc Res* 76(1):167–174
- Yki-Järvinen H (2003 Sep) Insulin resistance and endothelial dysfunction. *Best Pract Res Clin Endocrinol Metab* 17(3):411–430



Contribution of Carotid Bodies on Pulmonary Function During Normoxia and Acute Hypoxia

Karla G. Schwarz, Maríajose Flores,
Nicolas Voituron, and Rodrigo Del Rio 

Abstract

Carotid bodies (CBs) are main peripheral chemoreceptors involved in breathing regulation. Despite the well-known role played by CBs on breathing control, the precise contribution of CBs on the regulation of lung mechanics remains controversial. Accordingly, we study changes in lung mechanics in normoxia (FiO₂ 21%) and hypoxia (FiO₂ 8%) in mice with or without functional CBs. For this, we used adult male mice that underwent sham or CB denervation (CBD) surgery. Compared to sham-operated mice, we found that CBD induced an increase in lung resistance (R_L)

while breathing normoxic air (sham vs. CBD, $p < 0.05$). Importantly, changes in R_L were accompanied by an approximately threefold reduction in dynamic compliance (C_{dyn}). Additionally, end-expiratory work (EEW) was increased in normoxia in the CBD group. Contrarily, we found that CBD has no effect on lung mechanics during hypoxic stimulation. Indeed, R_L, C_{dyn}, and EEW values in CBD mice were undistinguishable from the ones obtained in sham mice. Finally, we found that CBD induces lung parenchyma morphological alterations characterized by reduced alveoli space. Together our results showed that CBD progressively increases lung resistance at normoxic conditions and suggest that CB tonic afferent discharges are needed for the proper regulation of lung mechanics at rest.

K. G. Schwarz · M. Flores
Laboratory of Cardiorespiratory Control, Department of Physiology, Pontificia Universidad Católica de Chile, Santiago, Chile
e-mail: karlaschwarz@uc.cl

N. Voituron
Laboratoire Hypoxie & Poumon UMR INSERM U1272, Université Sorbonne Paris Nord, Paris, France
e-mail: nicolas.voituron@univ-paris13.fr

R. Del Rio (✉)
Laboratory of Cardiorespiratory Control, Department of Physiology, Pontificia Universidad Católica de Chile, Santiago, Chile
Centro de Excelencia en Biomedicina de Magallanes (CEBIMA), Universidad de Magallanes, Punta Arenas, Chile
e-mail: rdelrio@bio.puc.cl

Keywords

Carotid body · Normoxia · Hypoxia · Dynamic compliance · Lung resistance · Carotid body denervation

14.1 Introduction

The carotid body (CB) located in the bifurcation of the common carotid artery plays a pivotal role in the maintenance of respiratory gas homeostasis (Ortega-Sáenz and López-Barneo 2019;

Iturriaga et al. 2021). Upon an acute hypoxemic challenge, the CB became activated, increasing the neural discharge toward brainstem cardiorespiratory nuclei to elicit reflex hyperventilation to cope with reductions in arterial PO_2 (Iturriaga et al. 2021). Besides their role in the regulation of the hypoxic ventilatory response, CBs also contribute to the maintenance of eupneic ventilation at rest since inhibition of the CB drive in normoxia results in hypoventilation (Dejours 1962). In addition, it has been proposed that CB can also play a role in the regulation of lower airway dilation/constriction since activation of the CB is able to induce reflex bronchoconstriction (Denjean et al. 1991). The latter suggests that CBs may contribute to hasten pulmonary alterations in hypoxia-associated respiratory diseases (Winter 1973; Vermeire et al. 1987). Indeed, Winter and Whipp showed that bilateral CB resection induces a fast reduction in total airway pressure in patients with chronic obstructive pulmonary disease (Winter and Whipp 2004). While this evidence supports the notion that targeting the CB may offer salutary potential to relieve elevated pulmonary pressures in the short term, the long-lasting effects of this intervention on pulmonary function in pathological settings have been questioned (Anderson et al. 1986).

Previous reports suggested that breathing hypoxic gas increases lower airway resistance through activation of cholinergic receptors within the airway tissue following a reflex increase in vagal efferent activity (Nadel and Widdicombe 1962; Haxhiu et al. 2005). However, experiments performed in rats showed that hypoxia results in a moderate increase in pulmonary dynamic compliance (C_{dyn}) and in reductions in lung resistance (R_L). Moreover, parasympathetic blockade (i.e., atropine) did not change R_L (Bonora and Vizek 1999). Therefore, there are still conflicting results concerning the effect, if any, of CB chemosensory activity under both normoxia and hypoxia on lung mechanics. Accordingly, we aimed to determine the contribution of CB activity on the regulation of lung mechanics during normoxia and acute hypoxia in adult mice with and without functional CBs.

14.2 Methods

14.2.1 Ethical Considerations and Animals

Male C57BL/6, 12–14 weeks of age ($n = 8$), were kept in the rodent animal facility of the Physiology Department of Université Sorbonne Paris Nord, France, on a 12 h light/dark schedule. Mice were provided with food and water ad libitum. All experiments were approved by the Institutional Ethical Committee of the Université Sorbonne Paris Nord and were conducted in accordance with the guide for the care and use of laboratory animals and the European communities council directive 2010/63/EU.

14.2.2 Carotid Body Denervation

Carotid body denervation (CBD) was performed under ketamine/xylazine cocktail anesthesia (100/10 mg/kg i.p., respectively). Briefly, an incision was made in the anterior neck and the carotid bifurcation was exposed. The carotid sinus nerve was visualized and resected close to the CB tissue. This procedure was performed bilaterally at both sides of the neck. Finally, the neck skin was sutured with absorbable multifilament sutures (Vicryl 4-0) and the animal transferred to a recovery cage. Postsurgical care included buprenorphine 0.1 mg/kg s.c. and sterile saline (1 ml i.p.). Sham-operated mice underwent the same anesthesia and surgical isolation of carotid bifurcation but without denervation of the CBs. Mice were allowed to recover from surgery for 5 days before performing any physiological experiment.

14.2.3 Noninvasive Measurement of Pulmonary Function

Noninvasive respiratory function was assessed by whole-body plethysmography (Emka Technologies, France). After a 3-h acclimation period, ventilation under normoxic (F_iO_2 21%) condition was recorded in freely moving animals.

Then, peripheral chemoreflex function was evaluated via a 2-min exposure to F_iO_2 8%. Tidal volume (V_T , ml/10 g), respiratory frequency (Rf, breath/min), and minute volume (V_E , ml/min/10 g) were obtained using ecgAUTO software (Emka Technologies, France). The hypoxic ventilatory response (HVR) was obtained by calculating the slope of the ΔV_E between F_iO_2 21% and F_iO_2 8%.

14.2.4 Invasive Measurement of Pulmonary Function

Lung mechanics were assessed by invasive measurement of pulmonary function (Emka Technologies, France) in tracheal intubated mice. Briefly, sham and CBD mice were anesthetized with ketamine/xylazine cocktail anesthesia (100/10 mg/kg i.p., respectively), the trachea was cannulated and mice were subsequently located in the plethysmographic chamber in a prone position and attached to a rodent mechanical ventilator (150 breath/min; 0.27 ml; Insp/exp. ratio = 0.40). After 5 min of baseline recordings, 1-min hypoxic challenges (F_iO_2 8%) spaced by 5-min recovery periods were performed to study the effect of hypoxia in lung mechanics. V_T , airway pressure, pulmonary dynamic compliance (C_{dyn}), lung resistance (R_L), and end-expiratory work (EEW) were obtained using ecgAUTO software (Emka Technologies, France).

14.2.5 Lung Histology

At the end of the physiological experiments, animals were deeply anesthetized with an intraperitoneal injection of 100 mg/kg sodium pentobarbital and perfused through the ascending aorta with saline solution (NaCl 0.9%) followed by 4% phosphate-buffered paraformaldehyde. Fixed lungs were dehydrated with an ethanol battery of increasing concentration, embedded in paraffin, and subsequently sectioned in a microtome at 5- μ m-thick sections. Then, sections were de-paraffinized with xylol and rehydrated with a battery of decreasing concentration ethanol for

hematoxylin and eosin staining as described elsewhere (Fischer et al. 2008a, b). Alveolar area was analyzed using the image processing software ImageJ. Briefly, the area of ten different alveoli from eight different lung captions per animal was measured. Histological analysis was performed by an independent investigator who was not aware about group allocation and/or involved in the physiological experiments.

14.2.6 Statistical Analysis

Data is expressed as mean \pm standard error mean (SEM). Unpaired Student's t-test was employed to evaluate differences between sham and CBD. $P < 0.05$ was considered as statistically significant. All the statistical analyses were performed using GraphPad Prism 8.0 software (GraphPad Software Inc., La Jolla, USA).

14.3 Results

14.3.1 Carotid Body Ablation and Resting Ventilatory Parameters

After 5 days of CBD, mice displayed a 20% decrease in Rf at rest compared to sham (Table 14.1). Conversely, V_T was significantly increased by 20% in CBD mice compared to sham (Table 14.1). Nevertheless, baseline V_E were unaltered between sham and CBD animals (Table 14.1).

14.3.2 Carotid Body Ablation Blunted the Hypoxic Ventilatory Response in Mice

Elimination of CB-mediated chemoreflex drive was confirmed by allowing the animal to breathe a hypoxic gas mixture (F_iO_2 8%) for 120 s. Sham-operated mice showed a robust HVR (Table 14.1). Contrarily, HVR was almost completely abolished by CBD in mice (Table 14.1). Indeed, the V_E response to hypoxia in CBD animals was neg-

Table 14.1 Ventilatory responses to normoxia and hypoxia (F_{iO_2} 8%) in sham and CBD mice

	Sham		CBD	
	Normoxia	Hypoxia	Normoxia	Hypoxia
V_E , ml/min/10 g	6.2 ± 0.1	8.7 ± 0.7	5.9 ± 0.3	6.3 ± 0.3 ⁺
V_T , μ l/10 g	29.4 ± 0.9	39.1 ± 3.3	35.3 ± 1.0*	33.4 ± 1.2
Rf, breath/min	210.3 ± 7.5	228.4 ± 24.8	167.1 ± 6.5*	187 ± 4.7
HVR	–	0.20 ± 0.06	–	0.02 ± 0.01 ⁺

Values are expressed as mean ± S.E.M. V_E minute ventilation, V_T tidal volume, Rf respiratory frequency, HVR hypoxic ventilatory response. Unpaired t-test, * $p < 0.05$ vs. sham normoxia, ⁺ $p < 0.05$ vs. sham hypoxia. $n = 4$ mice per group

ligible compared to the one obtained in sham animals.

CBD group (C_{dyn} : 0.008 ± 0.001 vs. 0.008 ± 0.001 ml/cmH₂O, normoxia vs. hypoxia, respectively, $p > 0.05$).

14.3.3 Lung Mechanics in Normoxia and the Effect of Carotid Body Denervation

We found that CBD in mice results in marked changes in lung mechanics while animals breathe normoxic gas. Indeed, compared to sham-operated mice, CBD mice showed a significant increase in airway pressure (Fig. 14.1a), reduced dynamic compliance (C_{dyn} : 0.018 ± 0.002 vs. 0.007 ± 0.001 ml/cmH₂O, sham vs. CBD, respectively, $p < 0.05$) (Fig. 14.1b), increased lung resistance (R_L : 0.224 ± 0.089 vs. 0.737 ± 0.184 ml/s/cmH₂O, sham vs. CBD, respectively, $p < 0.05$) (Fig. 14.1c), and increased end-expiratory work (EEW: 283.4 ± 31.7 vs. 644.5 ± 117.9 cmH₂O *ml/s, sham vs. CBD, respectively, $p < 0.05$) (Fig. 14.1d).

14.3.4 Hypoxia and Lung Mechanics Following Carotid Body Denervation in Mice

As shown in Fig. 14.2, no effects of acute hypoxia on lung mechanics were found in sham nor in CBD groups. Indeed, values of lung compliance obtained in normoxia were undistinguishable from the ones obtained during hypoxic stimulation in sham mice (C_{dyn} : 0.018 ± 0.002 vs. 0.018 ± 0.002 ml/cmH₂O, normoxia vs. hypoxia, respectively, $p > 0.05$). Similarly, no effect of hypoxia on lung compliance was found in the

14.3.5 Alveolar Morphology and Carotid Body Denervation

Alterations in lung parenchymal architecture were quantified after 5 days of CBD. Accordingly, we measured alveolar size and alveolar wall thickness in lungs obtained from sham and CBD mice. Quantitative analysis revealed that mean alveolar size of CBD mice was decreased compared to ones obtained in sham mice (3281 ± 126 vs. 2621 ± 134 μ m², sham vs. CBD, respectively, $p < 0.05$) (Fig. 14.3b). Furthermore, CBD mice displayed thickened alveolar walls compared to sham mice (9.286 ± 0.662 vs. 14.160 ± 1.660 μ m, sham vs. CBD, respectively, $p < 0.05$) (Fig. 14.3c).

14.4 Discussion

The importance of the CBs in respiratory and cardiovascular regulation and its role as a multimodal chemoreceptor have led to a growing interest on its potential contribution on the progression of several diseases. In this proof-of-concept study, we evaluated the contribution of the CB in lung mechanics during both normoxia and hypoxia. The main findings of the present study show that (i) CB denervation did not change baseline minute ventilation but modifies the contribution of the Rf and the V_T , (ii) CB denervation results in a significant decrease in dynamic compliance and increases in lung resistance in nor-

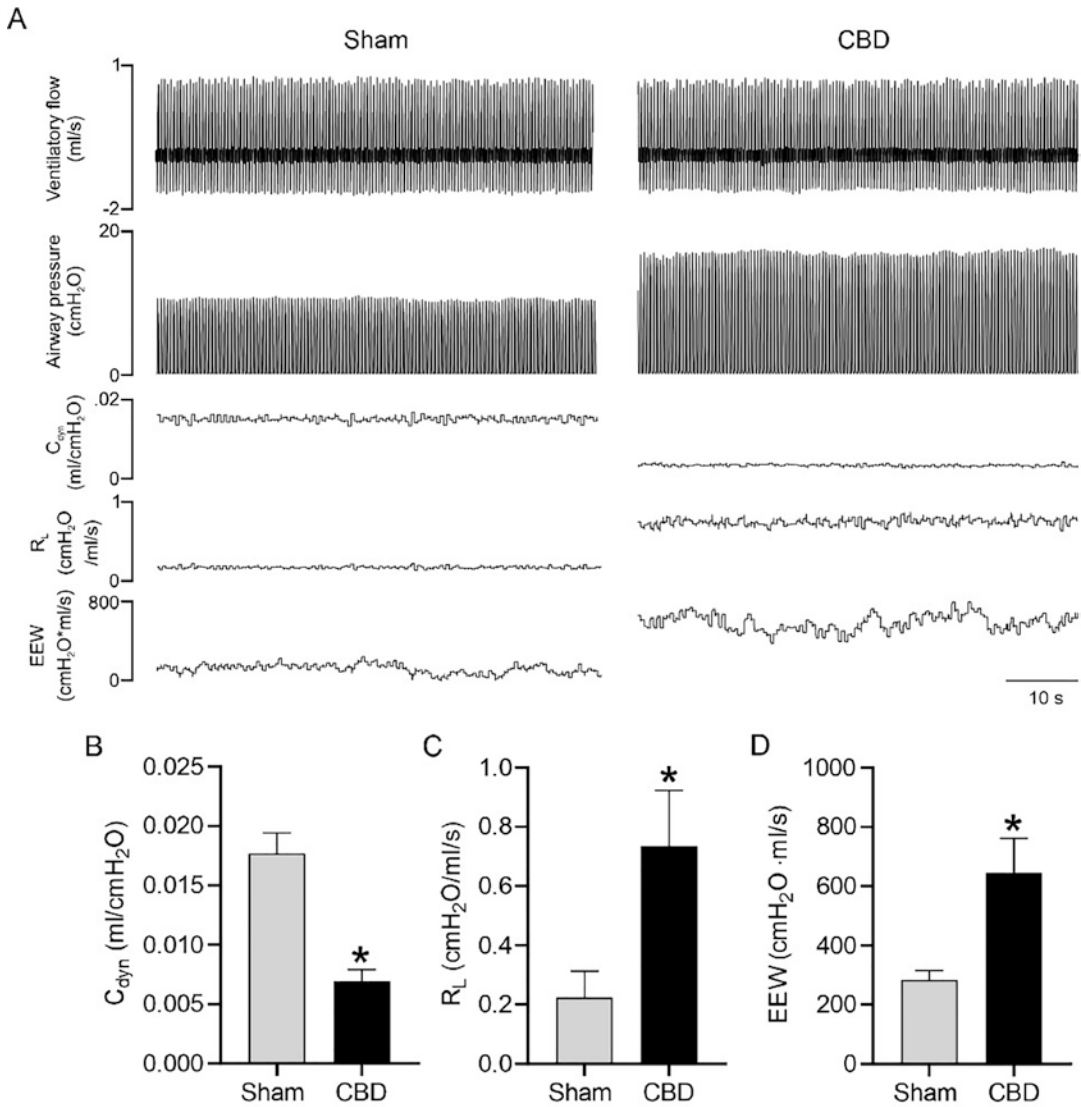


Fig. 14.1 Lung mechanics are affected by carotid body denervation (CBD) during normoxia. (a) Representative traces of artificial ventilation, airway pressure, dynamic compliance (C_{dyn}), lung resistance (R_L), and end-

expiratory work (EEW) during normoxia in unconscious sham and CBD mice. (b–d) Summary data showing C_{dyn} , R_L , and EEW. Unpaired t-test, * $p < 0.05$, $n = 4$ mice per group

moxic conditions, (iii) CB denervation did not change lung mechanics during hypoxic stimulation, and (iv) CB denervation triggers lung parenchyma remodeling.

Enhanced CB activity has been identified as one main pathophysiological mechanism underpinning altered cardiorespiratory function in highly prevalent diseases such as chronic obstructive pulmonary disease and sleep apnea

(Iturriaga et al. 2021). Although the precise mechanism(s) for CB malfunction in disease remain to be determined, several groups have shown that bilateral CB denervation improves cardiorespiratory function in disease conditions (Paton et al. 2013; Del R o et al. 2013, 2016). Besides the contribution of CBs on the neural control of both cardiovascular and breathing function, less is known about CB reflex regula-

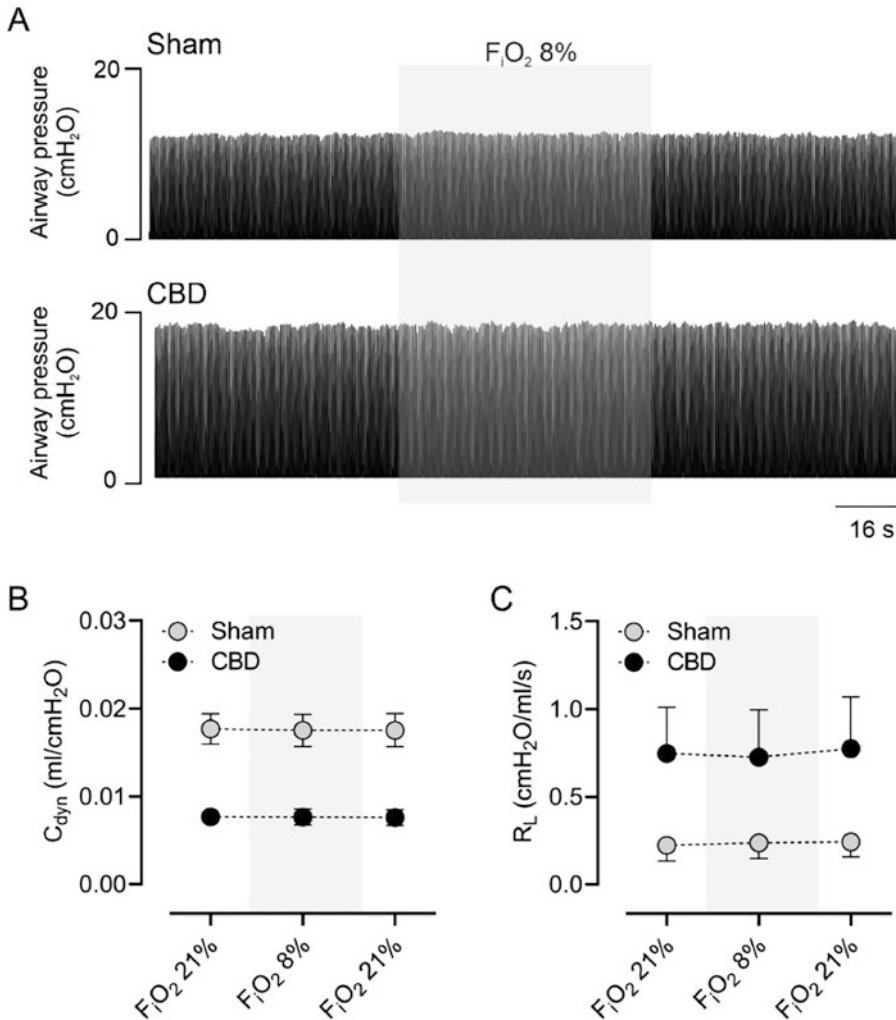


Fig. 14.2 Hypoxic challenge did not change lung mechanics in sham and CBD mice. **(a)** Representative traces showing airway pressure during 1-min hypoxic challenge (F_IO₂ 8%) between normoxia periods in uncon-

scious sham and CBD mice. **(b, c)** Summary data showing C_{dyn} and R_L. Unpaired t-test, **p* < 0.05, *n* = 4 mice per group

tion of pulmonary function. It has been hypothesized that activation of CB may control bronchoconstriction/dilation by a mechanism encompassing the vagal reflex (Denjean et al. 1991; Nadel and Widdicombe 1962; Widdicombe 1992; Iscoe and Fisher 1995; Haxhiu et al. 2005; Ahmed and Marchette 1985; Bencini and Pulerà 1991). However, considerable variability among different species and different experimental preparations has preclude the potential benefit of CB modulation in lung disease. Indeed, conflicting results on the role of CB on lung mechanics

have been reported in the literature. While airway constriction during hypoxia has been reported in dogs (Nadel and Widdicombe 1962; Strieder et al. 1974), airway dilation during hypoxia has been reported in minipigs and rats (Wetzel et al. 1992; Bonora and Vízek 1999). In addition, some studies showed null effects of hypoxia on lung mechanics (Simon et al. 1997; Yu et al. 1984). Similar conflicting results have been described in humans, with hypoxia causing bronchoconstriction (Sterling 1968), bronchodilation (Juliá-Serdá et al. 1993), or no effects

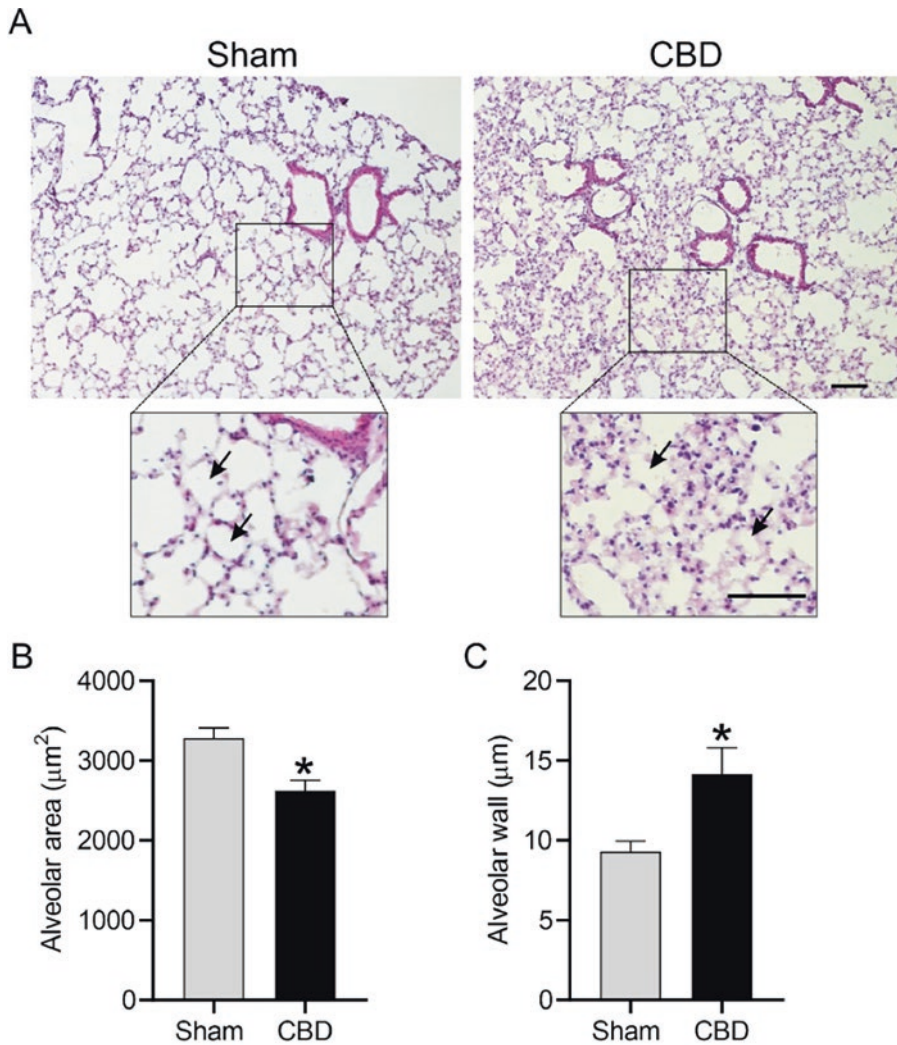


Fig. 14.3 CBD-induced changes in lung parenchymal architecture. (a) Representative hematoxylin-eosin staining lung section of one sham and one CBD mice. Insets are enlargements of the delineated area. Arrows indicate

representative alveoli. (b, c) Summary data of alveolar area and alveolar wall thickness, respectively. Unpaired t-test, * $p < 0.05$, $n = 4$ mice per group

(Saunders et al. 1977; Goldstein et al. 1979). In our study we intended to provide definite evidence in the mice about the contribution of CBs in the regulation of lung mechanics at both normoxic and hypoxic conditions. We found no changes in lung mechanics during acute CB stimulation with hypoxia in healthy mice. Contrarily, we found that CBs play an important role in setting lung mechanics at resting eupneic normoxic conditions in mice. Indeed, we found that denervation of CBs eliminates afferent tonic chemosensory activity, reduced lung compliance

and increases lung resistance at rest in normoxic conditions. Furthermore, 5 days after denervation of the CBs, lung parenchyma showed signs of adverse remodeling toward a less compliant territory. Indeed, we found that CBD decreases alveolar area and enlarged alveolar walls. The later suggest that CBD may have long-term profound effects on proper ventilation associated with lung parenchyma remodeling. Further and more chronic studies will be needed to understand the long-term consequences of CBD on pulmonary function.

In summary, our findings support the notion that CB tonic afferent activity contributes to the regulation of pulmonary function at rest during eupneic normoxic conditions in healthy mice.


Acknowledgments This work was supported by FONDECYT 1220950 grants from the National Fund for Scientific and Technological Development of Chile and ECOS-CONICYT CS1603 and by the “Bonus Qualité Recherche” and “Institut Fédératif de Recherche Biomédicale” programs of the University Sorbonne Paris Nord and by a Legs Poix grant (NV-2018).

References

- Ahmed T, Marchette B (1985) Hypoxia enhances non-specific bronchial reactivity. *Am Rev Respir Dis* 132(4):839–844
- Anderson JA, Chai H, Claman HN, Ellis EF, Fink JN, Kaplan AP, Lieberman PL, Pierson WE, Salvaggio JE, Sheffer AL, Slavin RG (1986) Carotid body resection. Executive Committee of the American Academy of Allergy and Immunology. *J Allergy Clin Immunol* 78(2):273–275
- Bencini C, Pulerà N (1991) The carotid bodies in bronchial asthma. *Histopathology* 18(3):195–200
- Bonora M, Vízek M (1999) Lung mechanics and end-expiratory lung volume during hypoxia in rats. *J Appl Physiol* 87(1):15–21
- Dejours P (1962) Chemoreflexes in breathing. *Physiol Rev* 42:335–358
- Del Río R, Marcus NJ, Schultz HD (2013) Carotid chemoreceptor ablation improves survival in heart failure: rescuing autonomic control of cardiorespiratory function. *J Am Coll Cardiol* 62(25):2422–2430
- Del Río R, Andrade DC, Lucero CM, Arias P, Iturriaga R (2016) Carotid body ablation abrogates hypertension and autonomic alterations induced by intermittent hypoxia in rats. *Hypertension* 68:436–445
- Denjean A, Canet E, Praud J, Gaultier C, Bureau MA (1991) Hypoxia-induced bronchial responsiveness in awake sheep: role of carotid chemoreceptors. *Respir Physiol* 83(2):201–210
- Fischer AH, Jacobson KA, Rose J, Zeller R (2008a) Hematoxylin and eosin staining of tissue and cell sections. *CSH protocols*, 2008, pdb.prot4986
- Fischer AH, Jacobson KA, Rose J, Zeller R (2008b) Paraffin embedding tissue samples for sectioning. *CSH protocols*, 2008, pdb.prot4989
- Goldstein RS, Zamel N, Rebuck AS (1979) Absence of effects of hypoxia on small airway function in humans. *J Appl Physiol Respir Environ Exerc Physiol* 47(2):251–256
- Haxhiu MA, Kc P, Moore CT, Acquah SS, Wilson CG, Zaidi SI, Massari VJ, Ferguson DG (2005) Brain stem excitatory and inhibitory signaling pathways regulating bronchoconstrictive responses. *J Appl Physiol* 98(6):1961–1982
- Iscoe S, Fisher JT (1995) Bronchomotor responses to hypoxia and hypercapnia in decerebrate cats. *J Appl Physiol* 78(1):117–123
- Iturriaga R, Alcayaga J, Chappleau MW, Somers VK (2021) Carotid body chemoreceptors: physiology, pathology, and implications for health and disease. *Physiol Rev* 101(3):1177–1235
- Juliá-Serdá G, Molfino NA, Furlott H, Mcclean PA, Rebuck AS, Hoffstein V, Slutsky AS, Zamel N, Chapman KR (1993) Tracheobronchial dilation during isocapnic hypoxia in conscious humans. *J Appl Physiol* 75(4):1728–1733
- Nadel JA, Widdicombe JG (1962) Effect of changes in blood gas tensions and carotid sinus pressure on tracheal volume and total lung resistance to airflow. *J Physiol* 163(1):13–33
- Ortega-Sáenz P, López-Barneo J (2019) Physiology of the carotid body: from molecules to disease. *Annu Rev Physiol* 82:127–149
- Paton JF, Sobotka PA, Fudim M, Engleman Z, Hart EC, McBryde FD, Abdala AP, Marina N, Gourine AV, Lobo MD, Patel N, Burchell AE, Ratcliffe LE, Nightingale AK (2013) The carotid body as a therapeutic target for the treatment of sympathetically mediated diseases. *Hypertension* 61:5–13
- Saunders NA, Betts MF, Pengelly LD, Rebuck AS (1977) Changes in lung mechanics induced by acute isocapnic hypoxia. *J Appl Physiol Respir Environ Exerc Physiol* 42(3):413–419
- Simon B, Zanaboni PB, Nyhan D (1997) Effect of hypoxia on respiratory system impedance in dogs. *J Appl Physiol* 83(2):451–458
- Sterling GM (1968) The mechanism of bronchoconstriction due to hypoxia in man. *Clin Sci* 35(1):105–114
- Strieder DJ, Laguarda R, Stigol LC, Wohl ME (1974) Increased lung recoil during acute hypoxia in dogs. *Respir Physiol* 21(2):193–201
- Vermeire PA, De Backer W, van Maele R, Bal JS, Van Kerckhoven W (1987) Carotid body resection in patients with severe chronic airflow limitation. *Bulletin europeen de physiopathologie respiratoire* 23(Suppl 11):165s–166s
- Wetzel RC, Herold C, Zerhouni EA, Robotham JL (1992) Hypoxic bronchodilation. *J Appl Physiol* 73(3):1202–1206
- Widdicombe JG (1992) Chemoreceptor control of the airways. *Respir Physiol* 87(3):373–381
- Winter B (1973) Carotid body resection. Controversy–confusion–conflict. *Ann Thorac Surg* 16(6):648–659
- Winter B, Whipp B (2004) Immediate effects of bilateral carotid body resection on total respiratory resistance and compliance in humans. *Adv Exp Med Biol* 551:15–21
- Yu LK, Lee LY, Frazier DT (1984) Effects of bronchoconstriction on breathing during normoxia and hypoxia in anesthetized cats. *Respir Physiol* 57(1):31–45



Increased Abdominal Perimeter Differently Affects Respiratory Function in Men and Women

Joana F. Sacramento, Iolanda Caires,
Maria P. Guarino, Maria J. Ribeiro,
João C. P. Santiago, Ana T. Timóteo, Mafalda Selas,
Miguel Mota-Carmo, and Silvia V. Conde 

Abstract

Obesity is a worldwide epidemic being the main cause of cardiovascular, metabolic disturbances and chronic pulmonary diseases. The increase in body weight may affect the respiratory system due to fat deposition and systemic inflammation. Herein, we evaluated the sex differences in the impact of obesity and high abdominal circumference on basal ventilation. Thirty-five subjects, 23 women and 12 men with a median age of 61 and 67, respectively, were studied and classified as overweight and obese according to body mass

index (BMI) and were also divided by the abdominal circumference. Basal ventilation, namely, respiratory frequency, tidal volume, and minute ventilation, was evaluated. In normal and overweight women, basal ventilation did not change, but obese women exhibited a decrease in tidal volume. In men, overweight and obese subjects did not exhibit altered basal ventilation. In contrast, when subjects were subdivided based on the abdominal perimeter, a higher circumference did not change the respiratory frequency but induced a decrease in tidal volume and minute ventilation in women, while in men these two parameters increased. In conclusion, higher abdominal circumference rather than BMI is associated with alterations in basal ventilation in women and men.

J. F. Sacramento · I. Caires · M. J. Ribeiro
J. C. P. Santiago · S. V. Conde (✉)
iNOVA4Health, NOVA Medical School/Faculdade de Ciências Médicas, NMSIFCM, Universidade Nova de Lisboa, Lisbon, Portugal
e-mail: silvia.conde@nms.unl.pt

M. P. Guarino
ciTechCare, Escola Superior de Saúde de Leiria,
Instituto Politécnico de Leiria, Leiria, Portugal

A. T. Timóteo · M. Mota-Carmo
NOVA Medical School/Faculdade de Ciências Médicas, NMSIFCM, Universidade Nova de Lisboa, Lisbon, Portugal

Serviço de Cardiologia, Hospital Santa Marta, Centro Hospital Lisboa Central, EPE, Lisbon, Portugal

M. Selas
Serviço de Cardiologia, Hospital Santa Marta, Centro Hospital Lisboa Central, EPE, Lisbon, Portugal

Keywords

Abdominal circumference · Basal ventilation · Obesity · Overweight

15.1 Introduction

Obesity has reached epidemic proportions and it is considered one of the major diseases of the last decades, contributing to significant morbidity and mortality worldwide (WHO Consultation on Obesity 1998). Overweight and obesity have

been associated with risks of developing type 2 diabetes, cardiovascular diseases, chronic kidney diseases, non-alcoholic fatty liver disease, and cancer (Malnick and Knobler 2006). The excess of adiposity is also associated with chronic pulmonary diseases such as obstructive sleep apnea, obesity hypoventilation syndrome, and asthma (Zammit et al. 2010).

The respiratory system may be affected by obesity due to a direct effect of fat deposition in the chest wall, abdomen, and upper airway promoting a decrease in lung volumes with a reduction in the functional residual capacity and expiratory reserve volume, being this observed even at a moderate augment in weight (Jones and Nzekwu 2006; Peralta et al. 2020). Moreover, in obese subjects it was also described an increase in the airway resistance, due to a decrease in lung volume (Zerah et al. 1993). Additionally, obesity may also change muscle respiratory strength (Sanchez et al. 2016). In obese patients with morbid obesity, which exhibited a body mass index (BMI) higher than 40 kg/m², the respiratory rates were increased due to a reduction in the expiratory time per breath (Sampson and Grassino 1983; Pankow et al. 1998; Chlif et al. 2009). Morbidly obese patients have been also shown to exhibit a decrease in tidal volume (Sampson and Grassino 1983; Pankow et al. 1998; Chlif et al. 2009). All these alterations promoted by obesity are fundamental to maintain an appropriate ventilation in obese states, and in fact, it has been observed that weight loss is associated with an improvement in pulmonary function (Alsumali et al. 2018; Nguyen et al. 2009).

Adipose tissue is an endocrine organ that secretes adipokines (e.g., adiponectin, leptin) and inflammatory cytokines (e.g., interleukin 6, tumor necrosis factor alpha, monocyte chemoattractant protein-1), having a key role in the metabolic dysfunction and inflammation observed in obesity (Chait and den Hartigh 2020). Adipokines have been also associated with respiratory disorders (Palma et al. 2022). In obese patients with obstructive sleep apnea and obesity hypoventilation syndrome, it was observed that an increase in interleukin 6 (Roytblat et al. 2000) and continuous positive airway pressure therapy diminished

inflammatory cytokines in patients with obstructive sleep apnea (Jin et al. 2017). Additionally, there are two main areas of fat accumulation in the body: a peripheral region that is characterized by fat deposition in the subcutaneous tissue and a central region that is characterized by fat deposition in the thorax, abdomen, and visceral organs (Sari et al. 2019). Abdominal adiposity appears to have a higher effect on pulmonary mechanics (Collins et al. 1995). A large-scale study showed that abdominal obesity, rather than weight and body mass index (BMI), was associated with lung function impairment, being this association consistent in men and women (Leone et al. 2009).

In the present study, we evaluated the sex differences in the effects of obesity and high abdominal perimeter on basal ventilation. We found that higher abdominal circumference, rather than BMI, impacts basal ventilation in old men and women, with the increased abdominal perimeter correlating negatively with tidal volume in women and positively in men.

15.2 Methods

15.2.1 Ethical Approval

The study was approved by Hospital Santa Marta, Centro Hospitalar Lisboa Central EPE (CHLC-EPE, n°63/2010), and NOVA Medical School Ethics Committee and performed in accordance with the Helsinki Declaration. Written informed consent was obtained from all individuals.

15.2.2 Subjects and Study Design

Subjects were recruited at the Cardiology Service, Hospital Santa Marta, CHLC-EPE. Individuals eligible for the study were adults over 18 years of age. Exclusion criteria were cardiovascular disorders, except hypertension, renal diseases, obesity hypoventilation syndrome, chronic respiratory failure, and psychiatric diseases.

The study was conducted in two visits. The first visit occurred in the CHLC-EPE. Sociodemographic and anthropometric

data, comorbidities, and ongoing medication profile were documented. Weight, height, and abdominal circumference were assessed. The BMI (kg/m^2) was calculated as weight (kilograms) divided by square of the height (meters). Subjects were categorized into normal weight, overweight, and obese according to their BMI and following the recommendations of the World Health Organization (WHO) (WHO Consultation on Obesity 1998): normal weight, 18.5–24.9 kg/m^2 ; overweight, 25–29.9 kg/m^2 ; and obese, $\geq 30 \text{ kg}/\text{m}^2$. Subjects were also divided based on the abdominal circumference, according to WHO (WHO Consultation on Obesity 1998): $\geq 80 \text{ cm}$ in women and $\geq 94 \text{ cm}$ in men, which indicate an increased risk of metabolic complications. The second visit was at NOVA Medical School, Faculdade de Ciências Médicas. Basal ventilation, namely, respiratory frequency, tidal volume, and minute ventilation, was measured via a mouthpiece connected to a three-way valve in a whole-body plethysmography system (MasterScreen Body, Jaeger, Germany). The measure of the basal ventilation was repeated three times.

15.2.3 Statistical Analysis

Data was evaluated using Prism version 9 (GraphPad Software Inc., La Jolla, CA, USA) and was presented as mean \pm SEM. The normal distribution of the variables was confirmed with

the Shapiro-Wilk test. The significance of the differences between the mean values was calculated by Student's t test and one-way ANOVA with Dunnett's multiple comparison test. Differences were considered significant at $p < 0.05$.

15.3 Results

15.3.1 Demographic and Clinical Information of the Participants

Table 15.1 illustrates the demographic and clinical characteristics of the study participants. A total of 35 subjects were included in the study, 23 women and 12 men, with a median age of 61 and 67 years, respectively. When patients were divided based on the BMI, in women, five exhibit normal weight, eight were overweight, and ten were obese. Men subjects included four with normal weight, four overweight, and four obese. In both groups, a high percentage of the participants had hypertension and dyslipidemia.

15.3.2 Effect of Overweight and Obesity on Basal Ventilation

Figure 15.1 shows the impact of overweight and obesity on basal ventilation in women and men. In women, the increase in body weight did not

Table 15.1 Demographic and clinical characteristics

Characteristics	Women <i>n</i> = 23	Men <i>n</i> = 12
Age (years)	61.36 \pm 2.68	67.31 \pm 2.40
Abdominal circumference (cm)	<i>Normal</i>	72.80 \pm 2.06
	<i>High</i>	98.25 \pm 2.88 ^{###}
Body mass index (kg/cm^2)	<i>Normal weight: 18.5–24.9</i>	22.28 \pm 1.15
	<i>Overweight: 25–29.9</i>	27.26 \pm 0.52 [#]
	<i>Obese: ≥ 30</i>	35.97 \pm 3.73 ^{###}
Type 2 diabetes (%)	17.39	41.67
Hypertension (%)	69.57	83.33
Dyslipidemia (%)	73.91	83.33

Normal abdominal circumference: women $< 80 \text{ cm}$ and men $< 94 \text{ cm}$. High abdominal circumference: women $\geq 80 \text{ cm}$ and men $\geq 94 \text{ cm}$. Values are presented as mean \pm SEM. One-way ANOVA with Dunnett's multicomparison test or Student's t -test: [#] $p < 0.05$, ^{##} $p < 0.01$ and ^{###} $p < 0.001$, comparing with normal abdominal circumference or normal weight

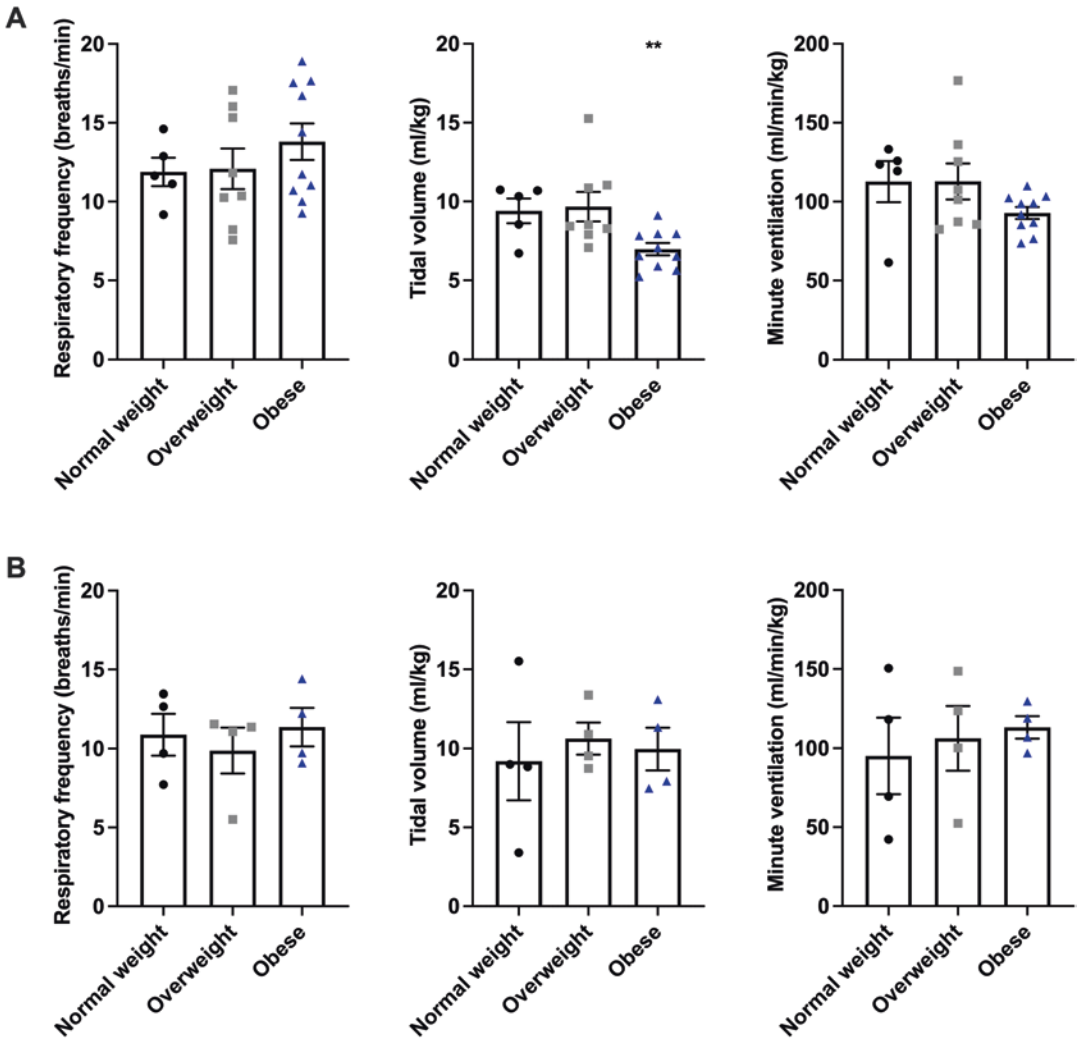


Fig. 15.1 Effect of overweight and obesity on basal ventilation in women and men subjects. Basal ventilatory parameters, respiratory frequency, tidal volume, and minute ventilation in women (**a**) and men (**b**) with normal weight (BMI = 18.5–24.9 kg/m²), overweight

(BMI = 25–29.9 kg/m²), and obesity (BMI ≥ 30 kg/m²). Data represent the mean ± SEM of 25 women and 13 men subjects. One-way ANOVA with Dunnett's multicomparison test: $p < 0.01$ comparing with normal weight subjects

modify the respiratory frequency but decreased tidal volume in the obese stage by 26% (Fig. 15.1a). The decrease in tidal volume in obese women was not sufficient to promote alterations in minute volume. In contrast, increased BMI in men did not impact the respiratory frequency, tidal volume, and minute ventilation (Fig. 15.1b).

15.3.3 Effect of Increased Abdominal Circumference on Basal Ventilation

Despite BMI is currently used to diagnose and classify obesity, recent studies proposed that BMI underestimates the prevalence of overweight and obesity, since it only contemplates

subjects' weight and height and not total body fat (Gómez-Ambrosi et al. 2011). Therefore, herein we also classified study subjects considering the abdominal circumference, as an indicator of increased visceral fat. Figure 15.2 depicts the impact of increased abdominal perimeter on basal ventilation in women and men. In women, the increase in abdominal circumference (≥ 80 cm) did not modify respiratory frequency and the minute ventilation; however, tidal volume decreased significantly by 22% (Fig. 15.2a). In men, the respiratory frequency did not change with the increase in the abdominal circumference (≥ 94 cm) (Fig. 15.2b). However, tidal volume and minute ventilation increased significantly by 51% and 59%, respectively, when men exhibited a higher abdominal circumference (Fig. 15.2b).

15.4 Discussion

The present study demonstrates that an increase in abdominal circumference, rather than BMI, has a higher impact on basal ventilation both in women and men. Moreover, the increase in abdominal circumference correlates differently in both sexes: in women it correlates negatively with tidal volume where in men it correlates positively.

It was previously described that morbid obesity, classified according with BMI, is associated with an increase in the respiratory rate and a decrease in the tidal volume (Sampson and Grassino 1983; Pankow et al. 1998; Chlif et al. 2009). Herein, this effect was only observed in women, since in men, basal ventilation did not change with the increased body weight. The absence of effects of obesity on basal ventilation in men herein observed could be related with the degree of obesity of the subjects. In the present study, obese men had a BMI of 33.94 kg/m^2 , corresponding to a class I obesity and therefore to moderate obesity. This agrees with previous findings showing that patients with moderate obesity ($\text{BMI} \geq 30 \text{ kg/m}^2$) did not exhibit alterations in tidal volume (Boulet et al. 2005; Torchio et al.

2009). In contrast, in morbidly obese patients ($\text{BMI} \geq 40 \text{ kg/m}^2$), it was described as an increase in the respiratory rate and a decrease in the tidal volume (Sampson and Grassino 1983; Pankow et al. 1998; Chlif et al. 2009). Altogether, these findings suggested that in men, when obesity is defined by the BMI, the tidal volume is only affected in higher degrees of obesity, as morbid obesity ($\text{BMI} \geq 40 \text{ kg/m}^2$).

The BMI is often used to define obesity and to classify its severity; however, it did not consider the total body fat, since it only takes into consideration the weight and the height of the individuals (Gómez-Ambrosi et al. 2011). Besides, fat distribution and accumulation in the central/abdominal area appear to have a higher effect on pulmonary mechanics (Collins et al. 1995). In fact, when we divided the subjects by the abdominal circumference, we observed significant effects on tidal volume and minute ventilation, rather than with BMI, being the effects opposite in women and men. This difference may be related with a higher abdominal circumference that is observed in women, 98.25 cm, a perimeter that characterized women with substantial increased risk of developing metabolic disturbances (WHO reference value is ≥ 88 cm). This high abdominal perimeter also showed that the women included in the present study have a higher accumulation of fat in the abdominal area. Women and men exhibit different patterns of body fat distribution, since women have more subcutaneous fat and men are characterized by an accumulation of fat in the abdominal area (Karastergiou et al. 2012). However, menopause transition is associated with augmented of total and abdominal adiposity (Svendson et al. 1995; Panotopoulos et al. 1996), an effect that could be due to the decrease in estrogen levels (Lovejoy et al. 2008). In the present study, the mean age of women was 61 years old, which indicates that most of the women are in menopause or in the post-menopause. Moreover, menopause in non-obese women promoted a decline in tidal volume (Preston et al. 2009) and lung function (Triebner et al. 2017). Therefore, we can suggest that in the

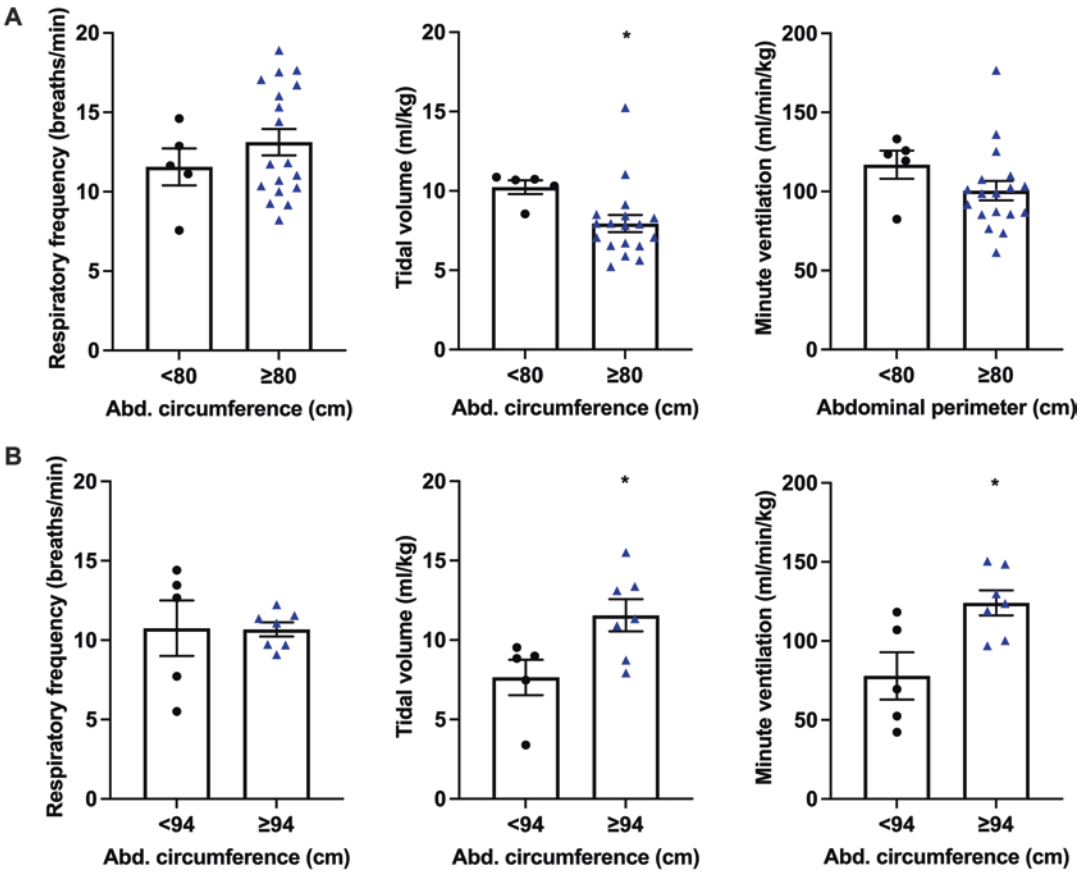


Fig. 15.2 Effect of abdominal circumference on basal ventilation in women and men subjects. Basal ventilatory parameters, respiratory frequency, tidal volume, and minute ventilation in women (a) and men (b) with normal (women <80 cm and men <94 cm) and high abdominal

circumference (women ≥80 cm and men ≥94 cm). Data represent the mean ± SEM of 25 women and 12 men subjects. Student's *t* test: *p* < 0.01 comparing with normal abdominal circumference

present study, the decrease in the tidal volume and the increase in minute ventilation observed in women are due to the elevated abdominal circumference and to the decrease in estrogens due to menopause.

We can conclude that the degree of obesity impacts differently basal ventilation in men and women, particularly in tidal volume. Moreover, our results also highlight the importance of classify obesity taking into consideration not only the BMI but also the abdominal perimeter.

Acknowledgments This work was funded with a grant from the Portuguese Foundation for Science and Technology (FCT) with the reference PTDC/SAU-

ORG/111417/2009. JFS is supported by a contract from FCT with the reference CEEC IND/02428/2018.

We deeply thank Prof. Miguel Mota Carmo for his enormous support to the Neuronal Control of Metabolic Disturbances Research Group (NeuroMetab.Lab). He passed away during the development of this project which would never have happened without his dedication.

References


Alsumali A, Al-Hawag A, Bairdain S, Eguale T (2018) The impact of bariatric surgery on pulmonary function: a meta-analysis. *Surg Obes Relat Dis* 14:225–236

Boulet L-P, Turcotte H, Boulet Dec G et al (2005) Deep inspiration avoidance and airway response to methacholine: influence of body mass index. *Can Respir J* 12:371–376

- Chait A, den Hartigh LJ (2020) Adipose tissue distribution, inflammation and its metabolic consequences, including diabetes and cardiovascular disease. *Front Cardiovasc Med* 7:22
- Chlif M, Keochkerian D, Choquet D et al (2009) Effects of obesity on breathing pattern, ventilatory neural drive and mechanics. *Respir Physiol Neurobiol* 168:198–202
- Collins LC, Hoberty PD, Walker JF et al (1995) The effect of body fat distribution on pulmonary function tests. *Chest* 107:1298–1302
- Gómez-Ambrosi J, Silva C, Galofré JC et al (2011) Body mass index classification misses subjects with increased cardiometabolic risk factors related to elevated adiposity. *Int J Obes* 36:286–294
- Jin F, Liu J, Zhang X et al (2017) Effect of continuous positive airway pressure therapy on inflammatory cytokines and atherosclerosis in patients with obstructive sleep apnea syndrome. *Mol Med Rep* 16:6334–6339
- Jones RL, Nzekwu MMU (2006) The effects of body mass index on lung volumes. *Chest* 130:827–833
- Karastergiou K, Smith SR, Greenberg AS, Fried SK (2012) Sex differences in human adipose tissues – the biology of pear shape. *Biol Sex Differ* 3:13
- Leone N, Courbon D, Thomas F et al (2009) Lung function impairment and metabolic syndrome the critical role of abdominal obesity. *Am J Respir Crit Care Med* 179:509–516
- Lovejoy JC, Champagne CM, de Jonge L et al (2008) Increased visceral fat and decreased energy expenditure during the menopausal transition. *Int J Obes* 32(6):949–958
- Malnick SDH, Knobler H (2006) The medical complications of obesity. *QJM* 99:565–579
- Nguyen NT, Hinojosa MW, Smith BR et al (2009) Improvement of restrictive and obstructive pulmonary mechanics following laparoscopic bariatric surgery. *Surg Endosc* 23:808–812
- Palma G, Sorice GP, Genchi VA et al (2022) Adipose tissue inflammation and pulmonary dysfunction in obesity. *Int J Mol Sci* 23:7349
- Pankow W, Podszus T, Gutheil T et al (1998) Expiratory flow limitation and intrinsic positive end-expiratory pressure in obesity. *J Appl Physiol* (1985) 85:1236–1243
- Panotopoulos G, Ruiz JC, Raison J et al (1996) Menopause, fat and lean distribution in obese women. *Maturitas* 25:11–19
- Peralta GP, Marcon A, Carsin AE et al (2020) Body mass index and weight change are associated with adult lung function trajectories: the prospective ECRHS study. *Thorax* 75:313–320
- Preston ME, Jensen D, Janssen I, Fisher JT (2009) Effect of menopause on the chemical control of breathing and its relationship with acid-base status. *Am J Physiol Regul Integr Comp Physiol* 296:722–727
- Roytblat L, Rachinsky M, Fisher A et al (2000) Raised interleukin-6 levels in obese patients. *Obes Res* 8:673–675
- Sampson MG, Grassino AE (1983) Load compensation in obese patients during quiet tidal breathing. *J Appl Physiol Respir Environ Exerc Physiol* 55:1269–1276
- Sanchez FF, Silva CDA, Maciel MCP de S et al (2016) Overweight and obesity influence on respiratory muscle strength. *Eur Respir J* 48:PA1361
- Sari CI, Eikelis N, Head GA et al (2019) Android fat deposition and its association with cardiovascular risk factors in overweight young males. *Front Physiol* 10:1162
- Svensden OL, Hassager C, Christiansen C (1995) Age- and menopause-associated variations in body composition and fat distribution in healthy women as measured by dual-energy X-ray absorptiometry. *Metabolism* 44:369–373
- Torchio R, Gobbi A, Gulotta C et al (2009) Mechanical effects of obesity on airway responsiveness in otherwise healthy humans. *J Appl Physiol* (1985) 107:408–416
- Triebner K, Matulonga B, Johannessen A et al (2017) Menopause is associated with accelerated lung function decline. *Am J Respir Crit Care Med* 195:1058–1065
- WHO Consultation on Obesity (1998) Obesity: preventing and managing the global epidemic: report of a World Health Organization consultation on obesity, Geneva, 3–5 June 1997. <https://apps.who.int/iris/handle/10665/63854>. Accessed 10 Nov 2022
- Zammit C, Liddicoat H, Moonsie I, Makker H (2010) Obesity and respiratory diseases. *Int J Gen Med* 3:335–343
- Zerah F, Harf A, Perlemuter L et al (1993) Effects of obesity on respiratory resistance. *Chest* 103:1470–1476



Carotid Body Resection Prevents Short-Term Spatial Memory Decline in Prediabetic Rats Without Changing Insulin Signaling in the Hippocampus and Prefrontal Cortex

Adriana M. Capucho, Ana Chegão, Fátima O. Martins, Bernardete F. Melo, Natália Madeira, Joana F. Sacramento, Rosalina Fonseca, Hugo Vicente Miranda, and Sílvia V. Conde 

Abstract

Individuals who develop type 2 diabetes (T2D) at an early age are at higher risk of developing neurodegenerative disorders such as Alzheimer's and Parkinson's disease. A shared dysfunctional characteristic between T2D and these neurodegenerative disorders is insulin resistance. Recently, it was shown that prediabetes animals and patients exhibited increased carotid body (CB) activity. Moreover, these organs are deeply involved in the development of metabolic diseases, since upon abolishment of their activity via carotid sinus nerve (CSN) resection, several dysmetabolic features of T2D were reverted. Herein, we investigated if CSN resection may also

prevent cognitive impairment associated with brain insulin resistance. We explored a diet-induced prediabetes animal model where Wistar rats are kept in a high fat–high sucrose (HFHSu) diet for 20 weeks. We evaluated CSN resection effects on behavioral parameters and on insulin signaling-related proteins levels, in the prefrontal cortex and the hippocampus. HFHSu animals exhibited impaired short-term memory evaluated by the y-maze test. Remarkably, CSN resection prevented the development of this phenotype. HFHSu diet or CSN resection did not promote significant alterations in insulin signaling-associated proteins levels. Our findings suggest that CBs modulation might have a role in preventing short-term spatial memory deficits associated with peripheral dysmetabolic states.

A. M. Capucho · A. Chegão · F. O. Martins
B. F. Melo · N. Madeira · J. F. Sacramento
R. Fonseca · H. Vicente Miranda (✉) · S. V. Conde (✉)
iNOVA4Health, NOVA Medical School, Faculdade
de Ciências Médicas, Universidade NOVA de Lisboa,
Lisbon, Portugal
e-mail: hvmiranda@nms.unl.pt;
silvia.conde@nms.unl.pt

Keyword

Carotid body · Insulin resistance · Metabolic diseases · Neurodegenerative disorders

16.1 Introduction

Metabolic disorders are mainly associated with a modern lifestyle, characterized by physical inactivity, sedentarism, and increased intake of hypercaloric diets (Golay and Ybarra 2005; Egger and Dixon 2014). Type 2 diabetes (T2D) is one of the most common metabolic disorders worldwide, accounting for 90% of all cases of diabetes (Rhys et al. 2019). This pathology is characterized by a state of insulin resistance (DeFronzo 2004; Kahn and Flier 2000). Several comorbidities are associated with T2D such as hypertension, and more recently, several epidemiological studies suggest that T2D patients are at higher risk of developing neurodegenerative disorders such as Alzheimer's disease (AD) and Parkinson's disease (PD) (Capucho et al. 2022; Chatterjee and Mudher 2018; Crane et al. 2013; Pagano et al. 2018; Yang et al. 2017). Importantly, insulin resistance is a shared feature between these pathologies. Insulin acts in insulin-sensitive peripheral tissues such as the liver, the skeletal muscle, the pancreas, and the adipose tissue to regulate glucose homeostasis. In addition, insulin has been described to play a key role in the brain, where it regulates processes such as energy expenditure, glucose homeostasis, feeding behavior and satiety, reward pathways, and reproduction (Capucho et al. 2022). Insulin also has neuroprotective and neuromodulatory properties, playing a crucial role in neuronal transmission and survival, neurogenesis, plasticity, and memory and cognition (Nadkarni et al. 2014; Dingezweni 2020; Banks 2004). Therefore, understanding how neurodegenerative and metabolic diseases interconnect will allow to identify novel therapeutic targets that may overcome the absence of effective treatments for patients exhibiting both pathologies. In the last decade, we have been focused on understanding the role of the carotid bodies (CBs) in the development of metabolic disorders. CBs are peripheral chemoreceptors located near the bifurcation of the common carotid artery. While CBs are classically defined as O₂ sensors, it is now becoming consensual that they are also metabolic sensors with an important role in energy homeostasis (Gonzalez et al. 1994; Conde et al. 2014;

Koyama et al. 2000, 2001). During the last decade, it was described that while both animal models of dysmetabolism and prediabetes patients exhibit increased CB chemosensitivity, the ablation of CBs activity via carotid sinus nerve (CSN) denervation or CSN neuromodulation prevents and reverts several pathological features associated with metabolic diseases (Ribeiro et al. 2013; Sacramento et al. 2017, 2018; Conde et al. 2018; Cunha-Guimaraes et al. 2020). In this work we aimed to investigate if CB activity ablation has an impact on the development of brain insulin resistance and in the development of neurodegenerative-associated processes such as short-term spatial memory cognitive impairment.

16.2 Methods

16.2.1 Animals

Experiments were performed in 12-week male Wistar rats (200–320 g), obtained from Charles River Laboratories (Barcelona, Spain) and maintained at the NOVA Medical School animal facility. Animals were kept under temperature and humidity control (21 ± 1 °C; $55 \pm 10\%$ humidity) and a regular light (08.00–20.00 h) and dark (20.00–08.00 h) cycle, with food and water ad libitum. After randomization, animals were divided into a normal chow diet group (NC) or a high fat–high sucrose (HFHSu) diet group. The NC group fed a standard diet (7.4% fat + 75% carbohydrates (4% sugar) + 17% protein, SDS diets RM1, Probiológica, Portugal), and the HFHSu diet group fed a 60% lipid-rich diet (61.6% fat + 20.3% carbohydrate + 19.1% protein, TestDiet, Missouri, USA) and 35% wt./vol. sucrose (Enzymatic, SA, Portugal) in drinking water (Melo et al. 2019). Insulin sensitivity was assessed via an insulin tolerance test (ITT), glucose tolerance through an oral glucose tolerance test (OGTT), ventilatory responses to hypoxia and hypercapnia by plethysmographic recordings, and the short-term spatial memory by the y-maze test, after 14 weeks of diet. At week 15 of diet, the animals from each group were divided

into two groups that were submitted either to a sham surgery or to a surgery for the bilateral resection of the CSN. Surgery was performed in animals under ketamine (30 mg/kg)/medetomidine (4 mg/kg) anesthesia and buprenorphine (10 µg/kg) analgesia (Sacramento et al. 2018). Animals were maintained in their corresponding diet for 5 more weeks (20 weeks post-diet, 5 weeks postsurgery) and were tested as before. At week 22 of diet, the animals were anaesthetized and sacrificed with pentobarbital (60 mg/kg i.p.) and the brains were dissected and frozen at -80°C , for protein analysis.

16.2.2 Insulin Tolerance Test (ITT) and Glucose Tolerance Test (OGTT)

Insulin sensitivity and glucose tolerance were assessed using the ITT and OGTT in conscious animals as previously described in (Ribeiro et al. 2013; Sacramento et al. 2018).

For the ITTs, animals were fasted overnight. In the morning, an intravenous insulin bolus of 0.1 U/kg body weight was administered in the tail vein in conscious animals followed by the measure of the decline in plasma glucose concentration over 15 min at 1 min intervals. Glucose was measured from blood collected from the tip of the tail with a glucometer (Precision Xtra Meter, Abbott Diabetes Care, Portugal) and test strips (Abbott Diabetes Care, Portugal). The constant rate of glucose disappearance (KITT) was calculated using the formula $0.693/t_{1/2}$, and glucose half-time ($t_{1/2}$) was calculated from the slope of the least-square analysis of plasma glucose concentrations during the linear decay phase.

For the OGTTs, overnight fasted animals were administrated with a glucose solution (2 g/kg in a 10 ul/g body weight volume) by gavage after the measurement of basal glycemia. Glucose levels were measured at 15, 30, 60, and 120 min after glucose administration, by tail tipping using a glucometer (Precision Xtra Meter, Abbott Diabetes Care, Portugal) and test strips (Abbott Diabetes Care, Portugal).

16.2.3 Whole-Body Plethysmography Recordings of Ventilation

Ventilation was measured in conscious animals by whole-body plethysmography. Animals were acclimatized in plethysmographic chambers during 30 min in normoxia (20% O₂) and afterwards submitted to the following protocol: normoxia (10 min), hypoxia (10%O₂, 10 min), normoxia (10 min), hypercapnia (20%O₂ + 5%CO₂, 10 min), normoxia (10 min). Tidal volume (VT; ml), respiratory frequency (breaths/min [bpm]), and minute ventilation (VE; ml min⁻¹ kg⁻¹) were monitored as previously described in (Melo et al. 2022).

16.2.4 Y- Maze Test

For assessing short-term spatial memory, animals were challenged to a Y-shaped maze with 120° between each arm with 10 cm wide and 30 cm high. Animals were initially submitted to a training session in which the rat was placed in the start point (A arm) of the Y-maze with a closed arm and allowed to freely explore it for 5 min. The experimental session occurred 1 h after training where the “novel” arm was open. The animal was allowed to freely explore the maze for 5 min. The exploratory capacity of the animal was evaluated as well as the time spent both in the novel arm and in the arm that is always open. The first arm choice when both arms are open was also evaluated, as well as the number of triads (i.e., ABC, CAB, or BCA) and entries. The spontaneous alternative behavior score (%) for each rat was calculated as the ratio of the number of alternations to the possible number (total number of arm entries minus two) multiplied by 100.

16.2.5 Protein Analysis (Western Blot)

After brain collection, the prefrontal cortex and the hippocampus were separated, protein extraction was performed, and the levels of several pro-

teins involved in insulin signaling pathways evaluated as previously (Chegão et al. 2022). Briefly, proteins were separated by SDS-PAGE and transferred to nitrocellulose/PVDF membranes which were probed with the following antibodies: total insulin receptor (IR-T) (anti-IR mouse 1:1000, Santa Cruz Biotechnology; 1:5000 anti-mouse Santa Cruz Biotechnology); protein kinase B (AKT) (anti-AKT rabbit 1:1000 Cell Signaling; 1:5000 anti-rabbit 1:5000 GE Healthcare); phosphorylated mitogen activated protein kinase (AMPK) (anti-pAMPK 1:500 rabbit cell signaling; 1:1000 anti-rabbit GE Healthcare) and total AMPK (anti-AMPK rabbit 1:1000 Cell Signaling; 1:5000 rabbit GE Healthcare). After stripping, as in (Chegão et al. 2022), membranes were re-probed for beta-actin (anti-beta-actin mouse 1:5000 GE Healthcare; anti-mouse 1:10000 anti-mouse, Santa Cruz Biotechnology) and analyzed as described in (Ribeiro et al. 2013).

16.2.6 Statistical Analysis

Data was evaluated using GraphPad Prism Software, version 7 and is presented as the mean \pm SEM. The significance of the differences between the means was calculated by unpaired t test and one-way analysis of variance (ANOVA) with Bonferroni's multiple comparison tests. Differences were considered significant at $p < 0.05$.

16.3 Results

16.3.1 Impact of HFHSu Diet and CSN Resection on Glycaemia, Insulin Sensitivity, and Glucose Tolerance

We depict in Table 16.1 the impact of HFHSu diet consumption and CSN resection on metabolic parameters. As previously described

(Sacramento et al. 2018; Melo et al. 2019) HFHSu diet promoted an increase in basal glycaemia that aggravates with increased diet duration (NC = 69.86 ± 3.84 mg/dL; HFHSu 15 weeks = 84.43 ± 1.77 mg/dL; HFHSu 20 weeks = 117.7 ± 3.79 mg/dL). The increase of basal glycemia in rats under HFHSu diet was abolished in CSN denervated animals (HFHSu 20 weeks-CSN den = 91.17 ± 1.51 mg/dL). HFHSu diet also decreased insulin sensitivity by 54.27% or 64.5% in 15 or 20 weeks under HFHSu diet, respectively (NC = 4.38 ± 0.2165 glucose/min; HFHSu 15 weeks = 2.00 ± 0.3822 glucose/min; NC 20 weeks = 5.28 ± 0.27 glucose/min; HFHSu 20 weeks = 1.89 ± 0.2816 glucose/min). This impairment was absent in CSN resected animals (HFHSu 20 weeks-CSN den = 6.06 ± 0.4174 glucose/min).

HFHSu animals exhibit glucose intolerance (Sacramento et al. 2018), an effect that also aggravates with increased diet duration in comparison with NC animals (NC = 15212.4 ± 1060 mg/dL/min; HFHSu 15 weeks = 17309.3 ± 1291 mg/dL/min; HFHSu 20 weeks = 22028.9 ± 333.2 mg/dL/min). HFHSu animals with CSN resection present a decrease in the area under the curve (AUC) of the glucose excursion curves when compared to the HFHSu sham animals (HFHSu 20 weeks-CSN den = 17854.2 ± 797.1 mg/dL/min).

16.3.2 Effect of HFHSu Diet and CSN Resection on the Responses to Hypoxia and Hypercapnia

To confirm CSN resection procedure, hypoxic ventilatory responses were assessed. As expected, and previously described (Melo et al. 2022), animals submitted to 15 weeks of HFHSu diet exhibited increased hypoxic ventilatory responses (NC = $39.14\% \pm 7.78\%$; HFHSu 15 weeks = $90.15 \pm 15.68\%$), with no changes in hypercapnic ventilatory responses (Table 16.2). CSN resection decreased by 526.4% and 329.6%

Table 16.1 Effect of HFHSu diet and CSN resection on fasting plasma glucose levels; insulin sensitivity expressed as the constant rate of glucose disappearance (KITT); and glucose tolerance expressed as the area under the curve (AUC) of the glucose excursion curves of the OGTTs from NC and HFHSu animals before CSN resection and 5 weeks after surgery

Basal glycemia (mg/dL)		Before surgery (15 weeks of diet)	After surgery (20 weeks of diet)
NC	Sham	69.86 ± 3.84	94.86 ± 3.06
	Den	72.57 ± 4.29	89.19 ± 6.36
HFHSu	Sham	84.43 ± 1.77**	117.7 ± 3.79***.5555
	Den	93.33 ± 5.62	91.17 ± 1.51 [#]
Insulin sensitivity (glucose/min)		Before surgery (15 weeks of diet)	After surgery (20 weeks of diet)
NC	Sham	4.38 ± 0.22	5.28 ± 0.27
	Den	4.66 ± 0.55	4.69 ± 0.55
HFHSu	Sham	2.00 ± 0.38***	1.89 ± 0.28***
	Den	1.76 ± 0.39	6.06 ± 0.42####
Glucose tolerance (mg/dL/min)		Before surgery (15 weeks of diet)	After surgery (20 weeks of diet)
NC	Sham	15,212 ± 1060	15,477 ± 679
	Den	14,743 ± 1322	15,086 ± 575
HFHSu	Sham	17,309 ± 1291*	22,029 ± 332***.55
	Den	19,685 ± 1685	17,854 ± 797###

Data are means ± SEM of 6–7 animals. One-way ANOVA with Bonferroni multicomparison tests: * $p < 0.05$, ** $p < 0.01$, *** $p < 0.001$ vs. NC group; # $p < 0.001$ comparison within the group; \$ $p < 0.001$ HFHSu before vs. HFHSu after surgery

Table 16.2 Effect of HFHSu diet and CSN resection on hypoxic and hypercapnic ventilatory responses

% Hypoxic response over basal		Before surgery (15 weeks of diet)	After surgery (20 weeks of diet)
NC	Sham	39.14 ± 7.78	76.42 ± 3.68
	Den	58.89 ± 6.13	12.20 ± 5.06####
HFHSu	Sham	90.15 ± 15.68*	104.9 ± 8.70*
	Den	97.21 ± 18.95	24.42 ± 5.25####
% Hypercapnic response over basal		Before surgery (15 weeks of diet)	After surgery (20 weeks of diet)
NC	Sham	46.05 ± 4.37	35.60 ± 3.62
	Den	43.74 ± 4.83	28.13 ± 2.46
HFHSu	Sham	36.4 ± 3.44	46.18 ± 4.24
	Den	37.26 ± 5.26	48.54 ± 7.92

Ventilatory responses were expressed as % of the baseline ventilation. Data are means ± SEM of 6–7 animals. One-way ANOVA with Bonferroni multicomparison tests: * $p < 0.05$, ** $p < 0.01$, *** $p < 0.001$ vs. NC group; #### $p < 0.001$ within each group

the hypoxic ventilatory responses in NC and HFHSu animals, respectively (Table 16.2). CSN resection did not alter hypercapnic responses both in NC and HFHSu animals, confirming that

the response to this stimulus is mainly mediated by the central nervous system.

16.3.3 Effect of HFHSu Diet Consumption and CSN Resection on Short-Term Spatial Memory

We evaluated short-term spatial memory by performing the y-maze. Animals under HFHSu diet for 15 weeks did not change the time spent in the novel arm (Fig. 16.1a). In contrast, after 20 weeks of HFHSu diet, animals spent 62.1% less time in the novel arm in comparison to the NC animals of the same age (NC = 109.24 ± 5.62 s; HFHSu = 41.41 ± 10.30 s). Interestingly, this decrease is not observed in CSN denervated animals under HFHSu diet (HFHSu 20 weeks = 41.4 ± 10.30%; HFHSu 20 weeks -CSN den = 94.78 ± 19.97%) (Fig. 16.1a). All groups of animals show similar alternative behavior pattern (Fig. 16.1b).

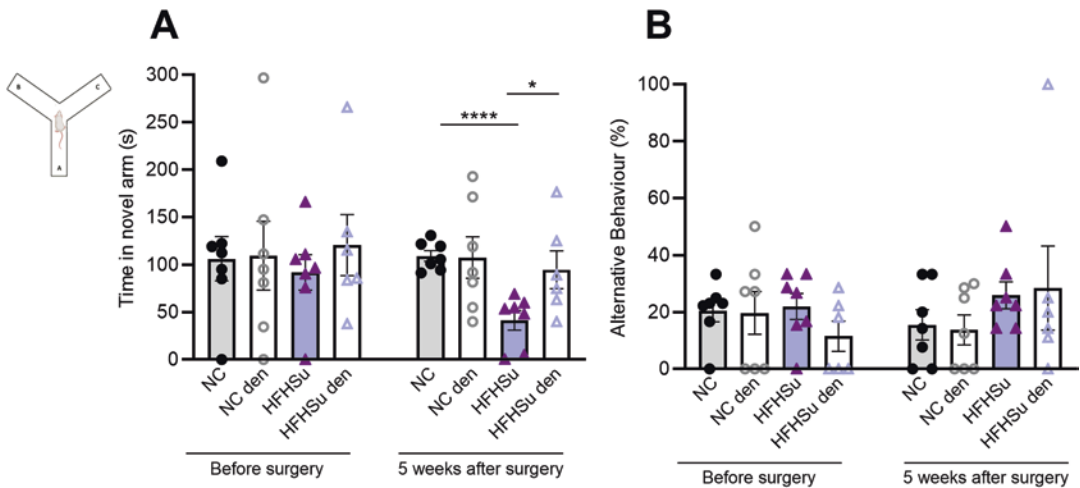


Fig. 16.1 Effect of HFHSu diet and CSN resection on short-term spatial memory evaluated by the y-maze test in NC and HFHSu animals before (15 weeks of diet) and 5-week postsurgery (20 weeks of diet). (a) shows the time that the animals spent in the novel arm (s); (b) shows the alternative behavior score calculated by the ratio of the number of alternations to the possible total number (total

number of arm entries minus two). Black circles represent NC animals; open gray circles represent NC denervated animals; purple triangles represent HFHSu animals; open lilac triangles represent HFHSu denervated animals. Data are means \pm SEM of 6–7 animals. One-way ANOVA with Bonferroni multicomparison tests: * $p < 0.05$, ** $p < 0.01$, *** $p < 0.001$

16.3.4 Impact of HFHSu Diet and CSN Resection on Insulin Signaling-Related Proteins in the Hippocampus and Prefrontal Cortex

HFHSu diet or CSN resection did not change the levels of important proteins on insulin signaling pathways such as IR, AKT, and pAMPK/t-AMPK in the prefrontal cortex (Fig. 16.2a). However, we may observe a non-significant decrease of the levels of IR-T and pAMPK/t-AMPK in this brain region in animals under HFHSu diet. For the case of the hippocampus, both HFHSu diet and CSN resection did not impact the levels of IR or AKT (Fig. 16.2b left and mid panel). However, HFHSu diet promoted an almost significant $\sim 47\%$ decrease of the ratio p-AMPK/t-AMPK ($p = 0.0503$) (Fig. 16.2b right panel), an effect attenuated by CSN resection in $\sim 41\%$ (HFHSu = $53.35 \pm 5.71\%$; HFHSu den = $75.16 \pm 12.37\%$) (Fig. 16.2b, right panel).

16.4 Discussion

In this study, we show for the first time that the abolishment of CBs activity, via the resection of CSN, prevents short-term spatial memory decline in prediabetic rats without significantly altering insulin sensitivity in the prefrontal cortex and in the hippocampus. As expected, and previously reported by our group (Sacramento et al. 2018; Melo et al. 2019), HFHSu diet intake promotes a significant increase in basal glycaemia, insulin resistance, and glucose intolerance, effects that were aggravated with the duration of HFHSu diet and reverted/attenuated upon CSN denervation. We further demonstrate that hypercaloric diets, as described by several authors (Fiory et al. 2019; Ninomiya 2014; Porte et al. 2005), have a negative impact in cognition-associated brain functions. In our experimental approach, we show that 20 weeks of HFHSu diet are sufficient to impair short-term spatial memory, as measured in the modified y-maze test. These results are in line

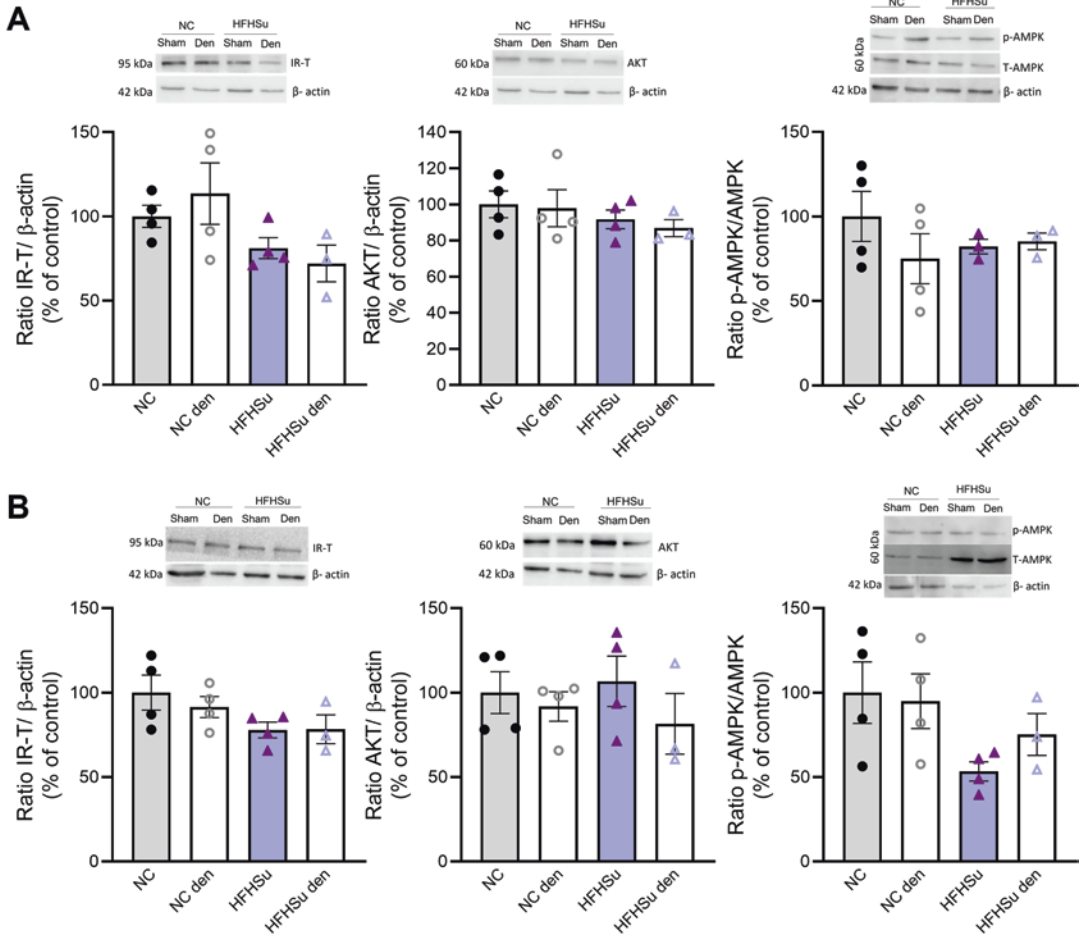


Fig. 16.2 Effect of HFHSu diet and CSN resection on the levels of proteins involved in insulin signaling in the prefrontal cortex (a) and hippocampus (b), evaluated by Western blot. Left panels in a and b represent the levels of insulin receptor (IR- 95 kDa), in the prefrontal cortex and hippocampus, respectively. Middle panels in a and b depict the levels of protein kinase B (AKT- 60 kDa) in the prefrontal cortex and hippocampus, respectively; right panels in a and b depict the ratio between phosphorylated

AMPK/total AMPK (AMPK- 60 kDa) in the prefrontal cortex and hippocampus, respectively. Proteins were normalized to the loading control β -actin (42 kDa). Representative Western blots are presented on top of the plots for each protein studied. Black circles represent NC animals; open gray circles represent NC denervated animals; purple triangles represent HFHSu animals; open lilac triangles represent HFHSu denervated animals. Data are means \pm SEM of 3–4 animals

with previous reports. For instance, Abbott and coworkers (2019) conducted a meta-analysis of the impact of different diets (high fat (HF), high sucrose (Hsu), or HFHSu and reported that each type of diet adversely affects cognitive performance, with the largest effect produced by exposure to a combined HFHSu diet for 8 weeks

(Abbott et al. 2019). Fu and colleagues (2017) also demonstrated that long-term HF diet induces hippocampal microvascular insulin resistance and cognitive dysfunction. In particular, the intake of a HF diet for 6 months significantly decreased the cognitive function of 8-month animals assessed by the two-trial spontaneous alter-

nation behavior and the novel object recognition tests (Fu et al. 2017). Thériault and colleagues (2016) showed that a HF diet exacerbated AD-related pathology in APPswe/PS1 mice. In this study, 3- and 12-month-old APPswe/PS1 mice were fed for 4 months with a HF diet and demonstrated that this diet accelerated age-associated cognitive decline without affecting parenchymal A β (Thériault et al. 2016). A major outcome, our work suggests that the resection of the CSN has a beneficial effect on cognitive process herein assessed in the modified y-maze test. Knowing the important role of insulin in brain functions such as cognition, we evaluated the levels of several insulin signaling associated proteins such as IR and AKT and also determined the ratio between p-AMPK and t-AMPK in both the prefrontal cortex and hippocampus, two major areas related with brain cognitive processes. In our experimental setup, we did not observe alterations in the levels of these proteins upon HFHSu diet consumption or CSN resection. This is in contrast with what is described in the literature, since several authors described that the consumption of hypercaloric diets promote brain insulin resistance (Capucho et al. 2022; De La Monte and Wands 2008; Spinelli et al. 2019; Kamal et al. 2013). For instance, HSu diet triggers insulin resistance in the brain by decreasing the levels of tyrosine phosphorylation of insulin receptor, by increasing serine phosphorylation of IRS-1, and by increasing the levels of pAKT/AKT, accessed by Western blot technique (Kothari et al. 2017). While we did not observe statistically significant alterations, the levels of IR seem to be decreased in both regions of HFHSu animal. These findings suggest that in our experimental setup, hypercaloric diets may also trigger the development of central IR. One of the possible explanations for the differences observed between our data and the literature can be because we only have assessed the levels of the total isoforms of the proteins IR and AKT, without assessing the levels of phosphorylated forms, and it is well known that hypercaloric diets promote the downregulation of IRS-1 and promote the phosphorylation of AKT (Bhat and Thirumangalakudi 2013). Therefore, the assess-

ment of the phosphorylated forms of the proteins involved in insulin signaling cascade and/or the assessment of the levels of proteins activated by the binding of insulin to its receptor will be key to take further conclusions. Another possible explanation can be the time of exposure of the animals to the hypercaloric diet. It is consensual that metabolic and neurodegenerative disorders progress with time. Therefore, the absence of significant effects of HFHSu diet on insulin signaling cascades might be due to the short period of the time that animals were kept under diet, although they already caused short-term memory alterations. It would be important to explore the effects of a longer period of diet in insulin signaling, to better correlate with the positive outcome of CB modulation. Altogether, we can conclude that the improvement in peripheral metabolic function promoted by the abolishment of CB activity is associated with the prevention of short term memory decline in prediabetic rats.

Acknowledgments This study was supported by Fundação para a Ciência e Tecnologia (FCT) EXPL/MED-NEU/0733/2021, by iNOVA4Health UID/Multi/04462/2013 – UIDB/04462/2020 and UIDP/04462/2020, a program financially supported by FCT/Ministério da Ciência, Tecnologia e Ensino Superior, through national funds. JFS and FOM were supported by CEEC contracts, CEEC IND/02428/2018 and CEEC IND/04266/2017, respectively, from FCT; AC by a PhD grant from FCT with reference PD/BD/136863/2018.

References

- Abbott KN, Arnott CK, Westbrook RF, Tran DMD (2019) The effect of high fat, high sugar, and combined high fat-high sugar diets on spatial learning and memory in rodents: a meta-analysis. *Neurosci Biobehav Rev* [Internet];107(August):399–421. Available from: <https://doi.org/10.1016/j.neubiorev.2019.08.010>
- Banks WA (2004) The source of cerebral insulin. *Eur J Pharmacol* 490(1–3):5–12
- Bhat NR, Thirumangalakudi L (2013) Increased tau phosphorylation and impaired brain insulin/Igf signaling in mice fed a high fat/high cholesterol diet. *J Alzheimers Dis* 36(4):781–789. <https://doi.org/10.3233/JAD-2012-121030>. <https://www.ncbi.nlm.nih.gov/pmc/articles/PMC4445975/>
- Capucho A, Chegão A, Martins F, Vicente Miranda H, Conde S (2022) Dysmetabolism and neurodegeneration: trick or treat? *Nutrients* 14(7):1425

- Chatterjee S, Mudher A (2018) Alzheimer's disease and type 2 diabetes: a critical assessment of the shared pathological traits. *Front Neurosci* 12:383
- Chegão A, Guarda M, Alexandre BM, Shvachiy L, Temido-Ferreira M, Marques-Morgado I et al (2022) Glycation modulates glutamatergic signaling and exacerbates Parkinson's disease-like phenotypes. *npj Park Dis* 8(1):51
- Conde SV, Sacramento JF, Guarino MP, Gonzalez C, Obeso A, Diogo LN et al (2014) Carotid body, insulin and metabolic diseases: unravelling the links. *Front Physiol* 5(OCT):1–15
- Conde SV, Sacramento JF, Guarino MP (2018) Carotid body: a metabolic sensor implicated in insulin resistance. *Physiol Genomics* 50(3):208–214
- Crane PK, Walker R, Hubbard RA, Li G, Nathan DM, Zheng H et al (2013) Glucose levels and risk of dementia. *N Engl J Med* [Internet]. [cited 2022 Jan 23];369(6):386–387. Available from: <https://pubmed.ncbi.nlm.nih.gov/23924004/>
- Cunha-Guimaraes JP et al (2020) Carotid body chemosensitivity: early biomarker of dysmetabolism in humans. *Eur J Endocrinol*;182 549–555(6):549–557
- De La Monte SM, Wands JR (2008) Alzheimer's disease is type 3 diabetes—evidence reviewed. *J Diabetes Sci Technol* [Internet] 2(6):1101–1113. Available from: <https://doi.org/10.1177/193229680800200619>
- DeFronzo RA (2004) Pathogenesis of type 2 diabetes mellitus. *Med Clin North Am* 88(4):787–835
- Dingezweni S (2020) The blood–brain barrier. *S Afr J Anaesth Analg* 26(6):S32–S34
- Egger G, Dixon J (2014) Beyond obesity and lifestyle: a review of 21st century chronic disease determinants. *Biomed Res Int* 2014:731685
- Fiory F, Perruolo G, Cimmino I, Cabaro S, Pignalosa FC, Miele C et al (2019) The relevance of insulin action in the dopaminergic system. *Front Neurosci* 13(August):1–16
- Fu Z, Wu J, Nesil T, Li MD, Aylor KW, Liu Z (2017) Long-term high-fat diet induces hippocampal microvascular insulin resistance and cognitive dysfunction. *Am J Physiol Endocrinol Metab* [Internet]. [cited 2022 Jan 23];312(2): E89–E97. Available from: <https://pubmed.ncbi.nlm.nih.gov/27899343/>
- Golay A, Ybarra J (2005) Link between obesity and type 2 diabetes. *Best Pract Res Clin Endocrinol Metab* 19(4):649–663
- Gonzalez C, Almaraz L, Obeso A, Rigual R (1994) Carotid body chemoreceptors: from natural stimuli to sensory discharges. *Physiol Rev* 74:829–898 p
- Kahn BB, Flier JS (2000) Obesity and insulin resistance. *J Clin Invest* [Internet]. [cited 2022 Jan 22];106(4):473–481. Available from: <https://pubmed.ncbi.nlm.nih.gov/10953022/>
- Kamal A, Ramakers GMJ, Gispen WH, Biessels GJ, Al Ansari A (2013) Hyperinsulinemia in rats causes impairment of spatial memory and learning with defects in hippocampal synaptic plasticity by involvement of postsynaptic mechanisms. *Exp Brain Res* 226(1):45–51
- Kothari V, Luo Y, Tornabene T, O'Neill AM, Greene MW, Geetha T et al (2017) High fat diet induces brain insulin resistance and cognitive impairment in mice. *Biochim Biophys Acta Mol Basis Dis* [Internet]. [cited 2022 Jan 23];1863(2):499–508. Available from: <https://pubmed.ncbi.nlm.nih.gov/27771511/>
- Koyama Y, Coker RH, Stone EE, Lacy DB, Jabbour K, Williams PE et al (2000) Evidence that carotid bodies play an important role in glucoregulation in vivo. *Diabetes* 49(9):1434–1442
- Koyama Y, Coker RH, Denny JC, Lacy DB, Jabbour K, Williams PE et al (2001) Role of carotid bodies in control of the neuroendocrine response to exercise. *Am J Phys Endocrinol Metab* 281(4 44–4):742–748
- Melo BF, Sacramento JF, Ribeiro MJ, Prego CS, Correia MC, Coelho JC et al (2019) Evaluating the impact of different hypercaloric diets on weight gain, insulin resistance, glucose intolerance, and its comorbidities in rats. *Nutrients* 11:1197
- Melo BF, Sacramento JF, Capucho AM, Sampaio-Pires D, Prego CS, Conde SV (2022) Long-term hypercaloric diet consumption exacerbates age-induced dysmetabolism and carotid body dysfunction: beneficial effects of CSN denervation. *Front Physiol* 13(May):1–14
- Nadkarni P, Chepurny OG, Holz GG (2014) Regulation of glucose homeostasis by GLP-1. *Prog Mol Biol Transl Sci* 121:23–65 p
- Ninomiya T (2014) Diabetes mellitus and dementia. *Curr Diab Rep* [Internet]. [cited 2022 Jan 23];14(5). Available from: <https://pubmed.ncbi.nlm.nih.gov/24623199/>
- Pagano G, Polychronis S, Wilson H, Giordano B, Ferrara N, Niccolini F et al (2018) Diabetes mellitus and Parkinson disease. *Neurology* 90(19):E1654–E1662
- Porte D, Baskin DG, Schwartz MW (2005) Insulin signaling in the central nervous system: a critical role in metabolic homeostasis and disease from *C. elegans* to humans. *Diabetes* [Internet]. May [cited 2022 Jan 23];54(5):1264–1276. Available from: <https://pubmed.ncbi.nlm.nih.gov/15855309/>
- Rhys W et al (2019) IDF: diabetes Atlas [Internet]. 9th ed. [place unknown: publisher unknown]; [cited 2022 Oct 10]. 176 p. 9 vol. ISBN: 978-2-930229-87-4. Available from: <https://diabetesatlas.org/atlas/ninth-edition/>
- Ribeiro MJ, Sacramento JF, Gonzalez C, Guarino MP, Monteiro EC, Conde SV (2013) Carotid body denervation prevents the development of insulin resistance and hypertension induced by hypercaloric diets. *Diabetes* 62(8):2905–2916
- Sacramento JF, Ribeiro MJ, Rodrigues T, Olea E, Melo BF, Guarino MP et al (2017) Functional abolition of carotid body activity restores insulin action and glucose homeostasis in rats: key roles for visceral adipose tissue and the liver. *Diabetologia* [Internet];158–168. Available from: <https://doi.org/10.1007/s00125-016-4133-y>
- Sacramento JF, Chew DJ, Melo BF, Donegá M, Dopson W, Guarino MP et al (2018) Bioelectronic modulation

- of carotid sinus nerve activity in the rat: a potential therapeutic approach for type 2 diabetes. *Diabetologia* 4:700–710
- Spinelli M, Fusco S, Grassi C (2019) Brain insulin resistance and hippocampal plasticity: mechanisms and biomarkers of cognitive decline. *Front Neurosci* 10(JUL):1–13
- Thériault P, ElAli A, Rivest S (2016) High fat diet exacerbates Alzheimer's disease-related pathology in APPswe/PS1 mice. *Oncotarget* [Internet]. [cited 2022 Jan 23];7(42):67808–67827. Available from: <https://pubmed.ncbi.nlm.nih.gov/27661129/>
- Yang YW, Hsieh TF, Li CI, Liu CS, Lin WY, Chiang JH et al (2017) Increased risk of Parkinson disease with diabetes mellitus in a population-based study. *Medicine (Baltimore)* [Internet]. [cited 2022 Jan 23];96(3). Available from: <https://pubmed.ncbi.nlm.nih.gov/28099356/>



Constitutive Expression of Hif2 α Confers Acute O₂ Sensitivity to Carotid Body Glomus Cells

Olalla Colinas, Alejandro Moreno-Domínguez, Patricia Ortega-Sáenz, and José López-Barneo

Abstract

Acute oxygen (O₂) sensing and adaptation to hypoxia are essential for physiological homeostasis. The prototypical acute O₂ sensing organ is the carotid body, which contains chemosensory glomus cells expressing O₂-sensitive K⁺ channels. Inhibition of these channels during hypoxia leads to cell depolarization, transmitter release, and activation of afferent sensory fibers terminating in the brain stem respiratory and autonomic centers. Focusing on recent data, here we discuss the special sensitivity of glomus cell mitochondria to changes in O₂ tension due to Hif2 α -dependent expression of several atypical mitochondrial electron transport chain subunits and enzymes. These are

responsible for an accelerated oxidative metabolism and the strict dependence of mitochondrial complex IV activity on O₂ availability. We report that ablation of *Epas1* (the gene coding Hif2 α) causes a selective downregulation of the atypical mitochondrial genes and a strong inhibition of glomus cell acute responsiveness to hypoxia. Our observations indicate that Hif2 α expression is required for the characteristic metabolic profile of glomus cells and provide a mechanistic explanation for the acute O₂ regulation of breathing.

Keywords

Carotid body · Glomus cells · Acute oxygen sensing · Hypoxia · Mitochondrial subunit isoforms · Cell physiology

Authors Olalla Colinas and Alejandro Moreno-Domínguez have equally contributed to this chapter.

O. Colinas · A. Moreno-Domínguez · P. Ortega-Sáenz
J. López-Barneo (✉)
Instituto de Biomedicina de Sevilla (IBiS), Hospital
Universitario Virgen del Rocío/CSIC/Universidad de
Sevilla, Seville, Spain

Departamento de Fisiología Médica y Biofísica,
Facultad de Medicina, Universidad de Sevilla,
Seville, Spain

Centro de Investigación Biomédica en Red sobre
Enfermedades Neurodegenerativas (CIBERNED),
Madrid, Spain
e-mail: lbarneo@us.es

17.1 Introduction

Oxygen (O₂) is essential for life, with mammals being particularly susceptible to low O₂ environments, even for brief periods. Decreases in blood O₂ tension (PO₂) induce acute adaptive responses, such as hyperventilation or increased cardiac output that within a few seconds augments O₂ uptake by the lungs and its distribution to the most vulnerable organs such as the brain or heart (Weir et al. 2005; Teppema and Dahan 2010). These systemic acute responses to O₂ deficiency (hypoxia) are pri-

marily mediated by the carotid body (CB), an arterial chemoreceptor and prototypical acute O₂-sensing organ located in the carotid bifurcation. The CB contains neurosensory glomus cells (also called type I cells) with O₂-sensitive K⁺ channels that are inhibited by hypoxia, thus leading to cell depolarization, Ca²⁺ influx, and the release of transmitters that activate afferent nerve fibers impinging upon the brainstem respiratory and autonomic centers (López-Barneo et al. 2001; Perez-Garcia et al. 2004; Buckler 2015). The molecular mechanisms by which glomus cells acutely detect hypoxia have remained elusive (Prabhakar and Peers 2014; Ortega-Sáenz and López-Barneo 2020; Iturriaga et al. 2021). Although several O₂-sensing mechanisms have been postulated (Lopez-Barneo et al. 2016; Rakoczy and Wyatt 2018), none have proven to be essential for CB function, because mice with ablation of genes coding for the relevant enzymes or receptors exhibit normal CB responses to hypoxia (Roy et al. 2000; He et al. 2002; Ortega-Saenz et al. 2006; Mahmoud et al. 2016; Wang et al. 2017; Torres-Torrel et al. 2018).

Mitochondria have been classically considered to be involved in CB O₂ sensing due to the exquisite sensitivity of CB cells to mitochondrial inhibitors (Mills and Jobsis 1972; Mulligan and Lahiri 1982). Experiments performed on CB slices showed that similar to the response to hypoxia, the secretory response of single glomus cells to inhibitors of the mitochondrial electron transport chain (ETC), such as rotenone or cyanide, was dependent on extracellular Ca²⁺ influx. In addition, it was also shown that rotenone, a lipophilic membrane-permeant agent that inhibits mitochondrial complex (MC) I NADH (reduced form of nicotinamide adenine dinucleotide) dehydrogenase activity, is highly effective in occluding glomus cell responsiveness to hypoxia. These observations suggested that the mitochondria signal the plasma membrane to regulate glomus cell excitability and that MCI could be involved in glomus cell O₂ sensing (Ortega-Saenz et al. 2003). For the last few years, a series of experiments performed on genetically modified mice have shown that CB glomus cells can repurpose their metabo-

lism to survive after disruption of MCI. However, these cells are insensitive to hypoxia although they exhibit normal responses to hypercapnia, lactate, and hypoglycemia (Fernandez-Aguera et al. 2015; Arias-Mayenco et al. 2018; Torres-Torrel et al. 2021). These experimental findings have suggested a model of acute O₂ sensing in which the mitochondria, possibly located near the plasma membrane of glomus cells (Rakoczy et al. 2022), act as O₂ sensors and effectors (Ortega-Sáenz and López-Barneo 2020). In this model, acute hypoxia slows down the mitochondrial ETC, consequently producing an accumulation of NADH and reactive oxygen species (ROS), which after equilibration with the cytosol modulate ion channels to elicit membrane depolarization (Fernandez-Aguera et al. 2015; Arias-Mayenco et al. 2018; Moreno-Dominguez et al. 2020). In parallel with the functional experiments, gene expression analyses have provided relevant clues for advancing in the understanding of the molecular bases of glomus cell acute O₂ sensing (Zhou et al. 2016; Gao et al. 2017). These studies have described a gene expression “signature profile,” conferring acute O₂ sensitivity upon glomus cells, which includes Hif2 α , atypical mitochondrial ETC subunits, enzymes and receptors, as well as several types of ion channels. In this paper we focus on Hif2 α and its role as the main responsible for the specialized acute O₂ sensing properties of CB glomus cells.

17.2 HIF2 α -Dependent Gene Expression Profile in Carotid Body Cells

Hif2 α is a hypoxia-inducible transcription factor that, similar to Hif1 α , regulates the expression of numerous genes. However, the actions of Hif1 α and Hif2 α are not redundant, but rather complementary, as Hif2 α expression is restricted to specific tissues to serve specialized adaptive functions (Ema et al. 1997). During development, Hif2 α is constitutively expressed at high levels in catecholaminergic tissues (Tian et al. 1998); however, in adults, high levels of Hif2 α expres-

sion in normoxic conditions are restricted to the CB (Fig. 17.1a) and to a lesser extent to adrenal medulla (AM) cells (Gao et al. 2017).

Overexpression of nondegradable Hif2 α in embryonic catecholaminergic (TH positive) tissues produces an ~2.5-fold enlargement of the CB with increase in the number of TH positive cells (Macias et al. 2014). In contrast, embryonic deletion of the gene coding Hif2 α (*Epas1*) in catecholaminergic cells results in viable animals although with a marked CB atrophy and abnormal cardiorespiratory and metabolic responses to hypoxia (Macias et al. 2018). Conditional generalized Hif2 α ablation in adult mice causes anemia and cardiac hypertrophy (Gruber et al. 2007; Moreno-Dominguez et al. 2020), as well as inhibition of the hypoxic ventilatory response (HVR) (Hodson et al. 2016; Moreno-Dominguez et al. 2020) and of CB cellular proliferation in chronic hypoxia (Hodson et al. 2016).

Knowledge of the impact of Hif2 α on the molecular properties of CB chemoreceptor cells has come from studies performed in mice with ubiquitous conditional ablation of *Epas1* in adulthood (Moreno-Dominguez et al. 2020). These mice were studied 2–3 months after initiation of tamoxifen treatment to allow for complete disappearance of Hif2 α - and Hif2 α -dependent genes. The strict compliance with this experimental protocol was critical given the slow turnover of some proteins, in particular those expressed in mitochondria (Fornasiero et al. 2018). CBs of *Epas1*-null mice appeared normal without clear structural modifications and were removed to study the level of expression of specific genes by qPCR. In addition to *Epas1* mRNA downregulation, which was clearly seen in comparison with *Hif1 α* mRNA (Fig. 17.1b), we studied 19 selected genes with potential relevance in CB chemoreception (Zhou et al. 2016; Gao et al. 2017) (Fig. 17.1c–e). Ablation of *Epas1* produced downregulation of four ETC subunits (Fig. 17.1c) and altered the expression of three enzymes/receptors (Fig. 17.1d). mRNA encoding some ion channels believed to participate in modulation of glomus cell excitability in response to hypoxia, such as Task1 (Kcnk3), Task 3 (Kcnk9), T-type Ca²⁺ channels (Cacna1h),

or cationic Trp5 channels, was not significantly altered in Hif2 α -deficient CB cells (Fig. 17.1e) (Moreno-Dominguez et al. 2020).

The four mitochondrial ETC subunits (Ndufa4l2, Cox4i2, Cox8b, and Higd1C) downregulated in *Epas1*-null (*Epas1*^{fl/fl}, *Cre*) CB in comparison with wild-type (*Epas1*^{+/+}) CB encode tissue-specific mitochondrial ETC subunit isoforms highly expressed in the CB (Zhou et al. 2016; Gao et al. 2017; Timón-Gómez et al. 2022). CB expression of Ndufa4l2, Cox4i2, and Cox8b was known to be regulated by Hif2 α (Moreno-Dominguez et al. 2020). We now extend the action of Hif2 α to Higd1C mRNA, whose level in *Epas1* null cells decreased below 30% the values observed in wild-type CBs (Fig. 17.1c). Cox4 and Cox8 are part of the 13 subunits forming the catalytic core of MCIV (Tsukihara et al. 1996; Kadenbach and Huttemann 2015). These subunits have adjacent single transmembrane segments which run in parallel in the periphery of MCIV. Cox4i2 is an atypical isoform of the more broadly distributed Cox4i1 subunit. Besides the CB, Cox4i2 is expressed in organs (e.g., lungs, brain, and fish gills) involved in oxygen delivery or that are oxygen sensitive (Huttemann et al. 2001; Zhou et al. 2016). Cox4i2 induction by hypoxia has been observed in several cell types (Fukuda et al. 2007; Aras et al. 2013). Cox8b is a tissue-specific isoform of the ubiquitously expressed Cox8a subunit. Interestingly, Cox8b promoter also contains Hif binding sites (Gao et al. 2017), although induction of Cox8b by hypoxia has not been reported. The functional roles of Cox4i2 and Cox8b are unknown. Cox4i2 lacks ATP regulatory sites present in Cox4i1, and its expression could accelerate the catalytic rate of cytochrome c oxidase (Napiwotzki et al. 1997; Napiwotzki and Kadenbach 1998; Pajuelo-Reguera et al. 2020). On the other hand, structural studies have suggested that the Cox8 subunit contributes to the formation of mitochondrial supercomplexes (Wu et al. 2016; Rieger et al. 2017). Although Cox4i2 and Cox8b are located relatively far from the catalytic site (heme a₃/CuB), they could induce subtle structural changes in MCIV and decrease the affinity for O₂, thus

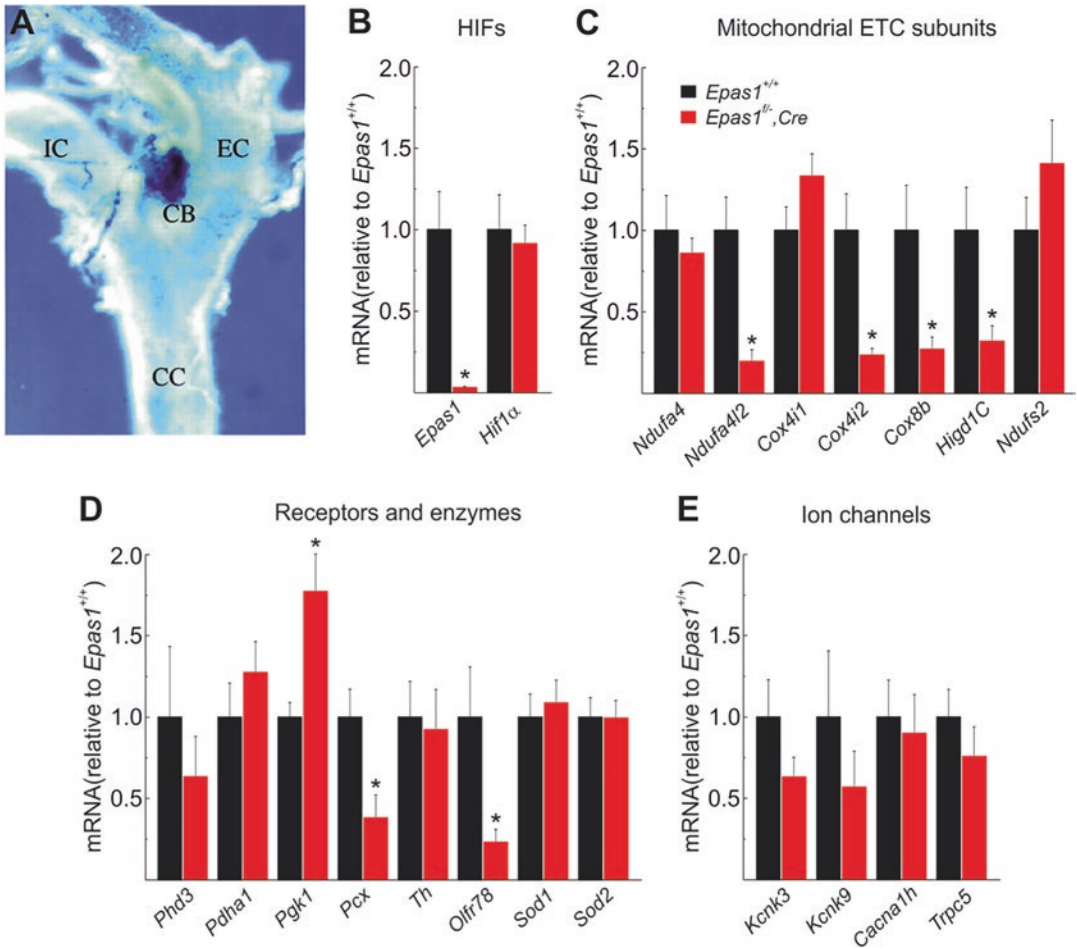


Fig. 17.1 Changes in the expression of selected genes in CB cells from *Epas1*-null mice. (a) *Epas1* expression determined by β -galactosidase staining in adult mice carotid body (CB), which is located at the bifurcation of the common carotid artery (CC) into the internal carotid (IC) and external carotid (EC) arteries (modified from

Tian et al. 1998). (b–d) mRNA levels of CB signature metabolic profile genes from *Epas1*^{+/+} and *Epas1*^{-/-}; Cre mice ($n = 6$ replicates per group, with each replicate consisting of five mice for each genotype). Data are presented as mean \pm SEM. * $P < 0.05$ (modified from Moreno-Dominguez et al. 2020)

explaining the modulation of MCIV activity in glomus cells within physiological levels of PO_2 . It could be also that *Cox4i2* and *Cox8b* decrease the accessibility of O_2 to the catalytic site and therefore make cytochrome c oxidase activity highly sensitive to changes in O_2 tension (Moreno-Dominguez et al. 2020). *Ndufa4l2*, one of the most abundant mRNA species in CB glomus cells (Zhou et al. 2016; Gao et al. 2017), encodes an isoform of the most widely expressed *Ndufa4* subunit, which appears to be associated with MCIV rather than with MCI (Carroll et al.

2006; Balsa et al. 2012). *Ndufa4l2* is highly expressed in lung and brain pericytes and some tumor cells (Lucarelli et al. 2018), but its function is poorly known. Expression of *Ndufa4l2*, which is induced by hypoxia in a HIF-dependent manner, attenuates oxygen consumption and decreases ROS production in mitochondria (Tello et al. 2011). *Higd1C* is a member of the hypoxia-inducible gene domain (*HIGD*) family that is highly expressed in the CB. *Higd1C* is a MCIV-associated protein that may interact with *Cox4i2* and contribute to the O_2 sensitivity of mitochon-

dria in CB cells (Timón-Gómez et al. 2022). However, the location and function of this protein is not yet well known.

In addition to the changes in the expression of mitochondrial ETC subunits, CBs from *Epas1*-null mice also show alterations in the mRNA expression of two enzymes, phosphoglycerate kinase 1 (*Pgk1*) and pyruvate carboxylase (*Pcx*), and one olfactory receptor (Olf1r78) (Moreno-Dominguez et al. 2020) (Fig. 17.1d). *Pgk1* is a typical Hif1 α -dependent gene encoding a glycolytic enzyme, whose expression also increases in the liver (Rankin et al. 2007) and lung (Elorza et al. 2012) after *Epas1* ablation. Hif2 α probably exerts a dominant negative action on *Pgk1* expression, which is relieved in *Epas1*-deficient cells. Pyruvate carboxylase (*Pcx*) is an enzyme highly expressed in CB cells in comparison with other peripheral catecholaminergic tissues (Gao et al. 2017). *Pcx* expression is compatible with the long-standing view that CB glomus cells contain highly active mitochondria with an elevated O₂ consumption. *Pcx* accelerates oxidative phosphorylation by the generation of oxaloacetate from pyruvate, thereby replenishing the pool of TCA cycle intermediates. In this anaplerotic reaction (Owen et al. 2002), *Pcx* utilizes biotin, a cofactor which is stored in high quantities in CB glomus cells and in lesser amounts in AM chromaffin cells (Ortega-Saenz et al. 2016). Olf1r78 is an atypical olfactory receptor that is expressed outside the nasal mucosa and particularly in CB glomus cells. CB Olf1r78 expression is strongly dependent on Hif2 α (Fig. 17.1d); however, its relevance in glomus cell function is unknown (see below).

17.3 Selective Inhibition of Acute Responsiveness to Hypoxia in Hif2 α -Deficient Glomus Cells

The alteration in gene expression profile induced by *Epas1* deficiency does not have obvious consequences on the normal structure and function of resting glomus cells. Glomus cell capacitance (proportional to cell membrane surface) and input resistance (determined by the density of

background ion channels in the plasma membrane) measured with the whole cell configuration of the patch clamp technique are unchanged in *Epas1* null cells in comparison with controls (Moreno-Dominguez et al. 2020). In addition, the time course and density of voltage-gated K⁺ and Ca²⁺ currents, which influence cell excitability, are also remarkably similar in control and *Epas1*-null glomus cells (Fig. 17.2a–d).

However, *Epas1*-deficient glomus cells loaded with Fura-2 exhibit a clear inhibition of the hypoxia-induced increase in cytosolic [Ca²⁺] without changes in the responses to CO₂ or high K⁺ (Fig. 17.3a–e). In *Epas1*-null CBs, there is a drastic decrease in the number of cells that respond to hypoxia (Fig. 17.3c) and in the amplitude of the Ca²⁺ signals (Fig. 17.3d). In agreement with these results, the responsiveness of glomus cells to hypoxia, as determined by amperometric measurement of exocytotic dopamine release with a carbon fiber electrode (Fernandez-Aguera et al. 2015; Moreno-Dominguez et al. 2020), is markedly inhibited in *Epas1*^{−/−}, *Cre* mice in comparison with wild-type mice (Fig. 17.4a, b). The percentage of cells that respond to hypoxia is decreased in *Epas1*-null mice, whereas responsiveness to hypercapnia and high K⁺ is unchanged (Fig. 17.4c, d). In addition, *Epas1*-deficient cells that exhibit some secretory activity in hypoxia also have a decreased secretion rate in comparison with controls (Fig. 17.4d). These data indicate that although *Epas1*-deficient glomus cells have normal electrical parameters and excitability, as well as some chemosensory functions, they are practically unresponsive to hypoxia.

The absolute requirement for Hif2 α to maintain acute sensitivity to hypoxia in glomus cells depends on the gene expression profile described above. Conditional deletion of *Cox4i2* in catecholaminergic tissues result in a phenotype similar to the one described in *Epas1*-deficient glomus cells (Moreno-Dominguez et al. 2020). In addition, deletion of *Higd1C* also inhibits the sensitivity to hypoxia in glomus cells (Timón-Gómez et al. 2022). The role of other Hif2 α -dependent transcripts in acute O₂ sensing is as yet unknown. Deletion of *Ndufa4l2* does not seem to elicit any clear alteration in systemic HVR or glomus cell

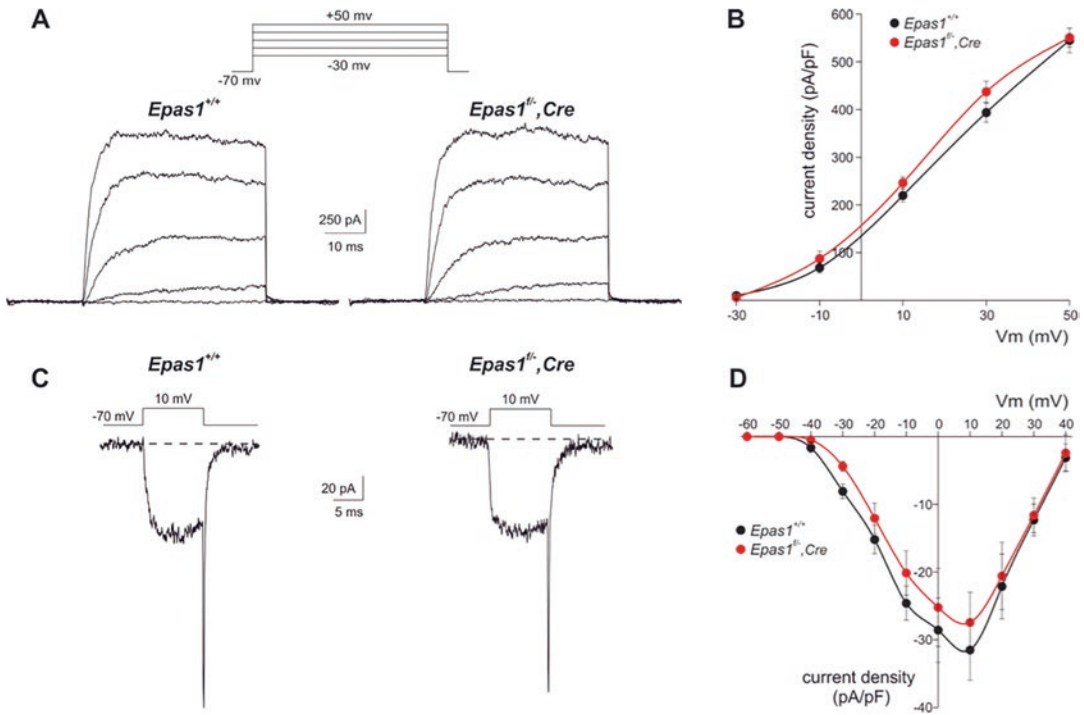


Fig. 17.2 Electrophysiological properties of CB glomus cells from *Epas1*^{+/+} and *Epas1*-null mice. (a) Representative recordings of outward K⁺ currents in whole-cell patch clamped glomus cells from *Epas1*^{+/+} and *Epas1*^{fl/Cre} mice. Depolarizing (50 ms) voltage steps between -30 and $+50$ mV were applied from a holding potential of -70 mV. (b) Average peak K⁺ current density versus membrane potential relationship obtained from *Epas1*^{+/+} (black) and *Epas1*^{fl/Cre} (red) glomus cells. (c)

Representative macroscopic Ca²⁺ currents recorded in glomus cells from *Epas1*^{+/+} and *Epas1*^{fl/Cre} mice. Depolarizing (10 ms) voltage steps (to 10 mV) were applied from a holding potential of -70 mV. (d) Average peak Ca²⁺ current density versus membrane potential relationship measured in glomus cells obtained from *Epas1*^{+/+} (black) and *Epas1*^{fl/Cre} (red) mice (modified from Moreno-Dominguez et al. 2020)

response to hypoxia (Moreno-Dominguez et al. 2020). Therefore, the precise role of Ndufa4l2 in the context of acute O₂ sensing remains to be determined. On the other hand, Olfr78, which is a G protein-coupled receptor highly expressed in glomus cells (Zhou et al. 2016; Gao et al. 2017), was proposed to be a lactate receptor essential for the hypoxic ventilatory response (Chang et al. 2015). However, subsequent studies have shown that CB responsiveness to hypoxia and the HVR are maintained in Olfr78-null mice (Torres-Torrelo et al. 2018). Moreover, glomus cell activation by lactate is independent on Olfr78 expression (Torres-Torrelo et al. 2018, 2021). Although Olfr78 is dispensable for lactate or acute O₂ sensing, it may have a relevant role in glomus cell homeostasis. Decreased sensitivity to

mild hypoxia of Olfr78-null mice has been reported in some studies (Peng et al. 2020); however, the mechanisms of action of Olfr78 in glomus cells remain unknown.

In addition to its role in acute O₂ sensing, Hif2 α might be also necessary for the homeostasis of dopaminergic granules in glomus cells (Brown et al. 2009). *Epas1*-null cells have a decrease in the size of secretory quantal events (Fig. 17.4e), which in many aspects resemble those described in biotin-deficient glomus cells due to inhibition of VMAT2-dependent vesicular dopamine transport (Ortega-Saenz et al. 2016). Although the biochemical details are unknown, the alteration of dopamine vesicles homeostasis in Hif2 α -deficient glomus cells could be related to downregulation of Pcx and/or to deficits in the

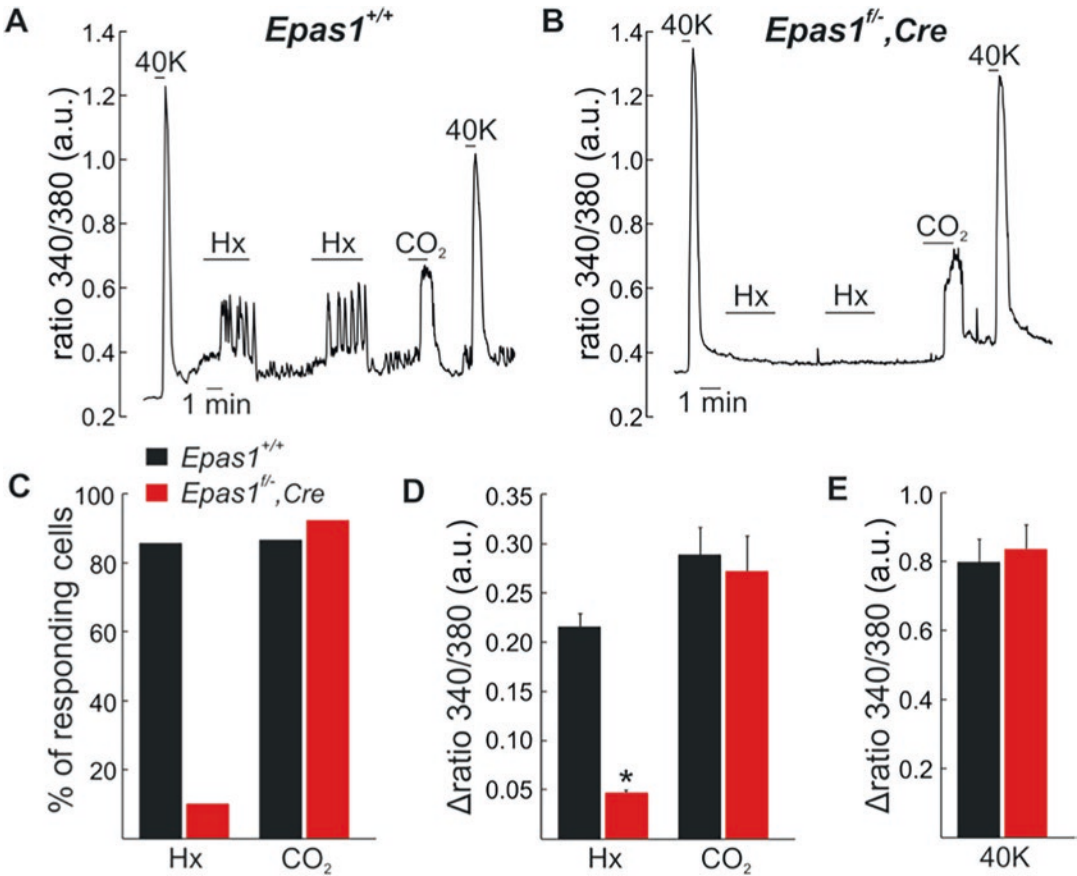


Fig. 17.3 Cytosolic [Ca²⁺] signals elicited by hypoxia, hypercapnia, and high K⁺ in dispersed glomus cells from *Epas1*^{+/+} and *Epas1*-null mice. (a and b) Representative recordings of the increases in cytosolic [Ca²⁺] elicited by hypoxia (Hx; ~10–15 mmHg), hypercapnia (CO₂; 20% CO₂), and high K⁺ (40 K; 40 mM KCl) in Fura2-loaded glomus cells from *Epas1*^{+/+} and *Epas1*-null mice. (c) Percentage of responding cells (exhibiting an increase in

cytosolic [Ca²⁺] in response to hypoxia or hypercapnia) relative to high K⁺ responding cells from *Epas1*^{+/+} and *Epas1*^{fl/Cre} mice. (d and e) Quantification of the increase in cytosolic [Ca²⁺] elicited by hypoxia or hypercapnia (d) and high K⁺ (e) in dispersed cells from *Epas1*^{+/+} and *Epas1*-null mice. Data are presented as mean ± SEM. **P* < 0.05 (from Moreno-Dominguez et al. 2020)

expression of enzymes involved in dopamine synthesis (Brown et al. 2009).

17.4 Conclusions and Perspectives

The experimental data discussed in this article highlight the importance of Hif2 α in determining the chemoreceptor properties of carotid body glomus cells. The constitutive high levels of Hif2 α induce the expression of genes that confer characteristics to glomus cell mitochondria that

render them able to be the sensor and effector of the hypoxic responses within physiological ranges of O₂ tension. In glomus cells cytochrome c oxidase behaves as an enzyme with low O₂ affinity due to the expression of specific subunit isoforms (Cox4i2 and Higd1C, among others). The way in which these subunits modulate the kinetics of the enzyme is unknown and should be addressed in future experimental work. Moreover, the role of Cox8b, Olf1r78, and Ndufa4i2 should also be clarified. The latter, one of the most highly expressed molecules in glomus cells, interacts with MCIV but seems to be dispensable

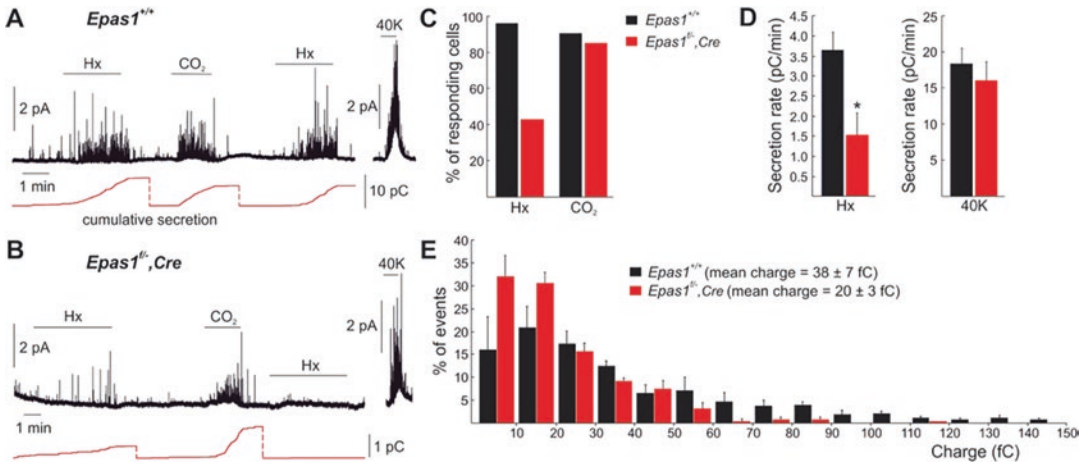


Fig. 17.4 Glomus cell catecholamine secretion elicited by hypoxia, hypercapnia, and high K^+ in CB slices from *Epas1^{+/+}* and *Epas1*-null mice. (a and b) Representative amperometric recordings of dopamine secretion induced by hypoxia (Hx), hypercapnia (CO_2) and high K^+ (40 K) in CB slices from *Epas1^{+/+}* and *Epas1^{fl/Cre}* mice. Cumulative secretion signals are in red. The vertical discontinuous lines indicate resetting of the integrator. (c) Percentage of cells with a secretory response to hypoxia and hypercapnia in *Epas1^{+/+}* and *Epas1^{fl/Cre}* mice. (d)

Average secretion rate (picocoulombs per minute) measured during exposure to hypoxia and 40 mM KCl in control *Epas1^{+/+}* and *Epas1*-null mice. (e) Frequency-charge distribution of individual exocytotic events elicited in response to hypercapnia in glomus cells from *Epas1^{+/+}* and *Epas1^{fl/Cre}* mice. Mean vesicle charge (in femtocoulombs, fC) obtained from both groups of mice is indicated in the inset. Data are presented as mean \pm SEM. * $P < 0.05$ (modified from Moreno-Dominguez et al. 2020)

for acute O_2 -sensing. Together with the molecules that regulate the sensitivity of MCIV to O_2 , others, such as Pcx, may be essential to accelerate the glomus cell mitochondrial ETC. In this manner, the slowing of electron transport in hypoxia leads to the production of mitochondrial signals (NADH and H_2O_2) that regulate membrane ion channels (López-Barneo and Ortega-Sáenz 2022). Finally, it will be important to study whether the mitochondria-to-membrane signaling model of acute O_2 sensing defined in CB chemoreceptor cells is applicable to other hypoxia-sensitive cell classes and whether in these cells *Hif2 α* -dependent genes play the same fundamental physiological role.

References

Aras S, Pak O, Sommer N, Finley R Jr, Huttemann M, Weissmann N, Grossman LI (2013) Oxygen-dependent expression of cytochrome c oxidase subunit 4-2 gene expression is mediated by transcription factors RBPJ, CXXC5 and CHCHD2. *Nucleic Acids Res* 41(4):2255–2266

Arias-Mayenco I, Gonzalez-Rodriguez P, Torres-Torrel H, Gao L, Fernandez-Aguera MC, Bonilla-Henao V, Ortega-Saenz P, Lopez-Barneo J (2018) Acute O_2 sensing: role of coenzyme QH2/Q ratio and mitochondrial ROS compartmentalization. *Cell Metab* 28(1):145–158 e144

Balsa E, Marco R, Perales-Clemente E, Szklarczyk R, Calvo E, Landazuri MO et al (2012) NDUFA4 is a subunit of complex IV of the mammalian electron transport chain. *Cell Metab* 16:378–386

Brown ST, Kelly KF, Daniel JM, Nurse CA (2009) Hypoxia inducible factor (HIF)-2 alpha is required for the development of the catecholaminergic phenotype of sympathoadrenal cells. *J Neurochem* 110(2):622–630

Buckler KJ (2015) TASK channels in arterial chemoreceptors and their role in oxygen and acid sensing. *Pflugers Arch* 467(5):1013–1025

Carroll J, Fearnley IM, Skehel JM, Shannon RJ, Hirst J, Walker JE (2006) Bovine complex I is a complex of 45 different subunits. *J Biol Chem* 281:32724–32727

Chang AJ, Ortega FE, Riegler J, Madison DV, Krasnow MA (2015) Oxygen regulation of breathing through an olfactory receptor activated by lactate. *Nature* 527(7577):240–244

Elorza A, Soro-Arnáiz I, Meléndez-Rodríguez F, Rodríguez-Vaello V, Marsboom G, Cárcer G, Acosta-Iborra B, Albacete-Albacete L, Ordóñez A, Serrano-Oviedo L, Giménez-Bachs JM, Vara-Vega A, Salinas A, Sánchez-Prieto R, Martín del Río R, Sánchez-

- Madrid F, Malumbres M, Landázuri MO, Aragonés J (2012) HIF2 α acts as an mTORC1 activator through the amino acid carrier SLC7A5. *Mol Cell* 48:681–691
- Ena M, Taya S, Yokotani N, Sogawa K, Matsuda Y, Fujii-Kuriyama Y (1997) A novel bHLH-PAS factor with close sequence similarity to hypoxia-inducible factor 1 α regulates the VEGF expression and is potentially involved in lung and vascular development. *Proc Natl Acad Sci U S A* 94(9):4273–4278
- Fernandez-Aguera MC, Gao L, Gonzalez-Rodriguez P, Pintado CO, Arias-Mayenco I, Garcia-Flores P, Garcia-Pergañeda A, Pascual A, Ortega-Saenz P, Lopez-Barneo J (2015) Oxygen sensing by arterial chemoreceptors depends on mitochondrial complex I signaling. *Cell Metab* 22(5):825–837
- Fornasiero EF, Mandat S, Wildhagen H, Alevra M, Rammner B, Keihani S, Opazo F, Urban I, Schebeck T, Sakib MS et al (2018) Precisely measured protein lifetimes in the mouse brain reveal differences across tissues and subcellular fractions. *Nat Commun* 9(1):4230
- Fukuda R, Zhang H, Kim JW, Shimoda L, Dang CV, Semenza GL (2007) HIF-1 regulates cytochrome oxidase subunits to optimize efficiency of respiration in hypoxic cells. *Cell* 129(1):111–122
- Gao L, Bonilla-Henao V, Garcia-Flores P, Arias-Mayenco I, Ortega-Saenz P, Lopez-Barneo J (2017) Gene expression analyses reveal metabolic specifications in acute O₂-sensing chemoreceptor cells. *J Physiol* 595(18):6091–6120
- Gruber M, Hu CJ, Johnson RS, Brown EJ, Keith B, Simon MC (2007) Acute postnatal ablation of Hif-2 α results in anemia. *Proc Natl Acad Sci U S A* 104(7):2301–2306
- He L, Chen J, Dinger B, Sanders K, Sundar K, Hoidal J, Fidone S (2002) Characteristics of carotid body chemosensitivity in NADPH oxidase-deficient mice. *Am J Physiol Cell Physiol* 282(1):C27–C33
- Hodson EJ, Nicholls LG, Turner PJ, Llyr R, Fielding JW, Douglas G, Ratnayaka I, Robbings PA, Pugh CW, Buckler KJ et al (2016) Regulation of ventilatory sensitivity and carotid body proliferation in hypoxia by the PHD2/HIF-2 pathway. *J Physiol* 594(5):1179–1195
- Huttemann M, Kadenbach B, Grossman LI (2001) Mammalian subunit IV isoforms of cytochrome c oxidase. *Gene* 267(1):111–123
- Iturriaga R, Alcayaga J, Chappelle MW, Somers VK (2021) Carotid body chemoreceptors: physiology, pathology, and implications for health and disease. *Physiol Rev* 101(3):1177–1235
- Kadenbach B, Huttemann M (2015) The subunit composition and function of mammalian cytochrome c oxidase. *Mitochondrion* 24:64–76
- López-Barneo J, Ortega-Sáenz P (2022) Mitochondrial acute oxygen sensing and signaling. *Crit Rev Biochem Mol Biol* 57(2):205–225
- López-Barneo J, Pardal R, Ortega-Sáenz P (2001) Cellular mechanism of oxygen sensing. *Annu Rev Physiol* 63:259–287
- Lopez-Barneo J, Gonzalez-Rodriguez P, Gao L, Fernandez-Aguera MC, Pardal R, Ortega-Saenz P (2016) Oxygen sensing by the carotid body: mechanisms and role in adaptation to hypoxia. *Am J Physiol Cell Physiol* 310(8):C629–C642
- Lucarelli G, Rutigliano M, Sallustio F, Ribatti D, Giglio A, Lepore Signorile M et al (2018) Integrated multi-omics characterization reveals a distinctive metabolic signature and the role of NDUFA4L2 in promoting angiogenesis, chemoresistance, and mitochondrial dysfunction in clear cell renal cell carcinoma. *Aging* 10:3957–3985
- Macias D, Fernandez-Aguera MC, Bonilla-Henao V, Lopez-Barneo J (2014) Deletion of the von Hippel-Lindau gene causes sympathoadrenal cell death and impairs chemoreceptor-mediated adaptation to hypoxia. *EMBO Mol Med* 6(12):1577–1592
- Macias D, Cowburn AS, Torres-Torrel H, Ortega-Saenz P, Lopez-Barneo J, Johnson RS (2018) HIF-2 α is essential for carotid body development and function. *elife* 7:e34681
- Mahmoud AD, Lewis S, Juricic L, Udoh UA, Hartmann S, Jansen MA, Ogunbayo OA, Puggioni P, Holmes AP, Kumar P et al (2016) AMP-activated protein kinase deficiency blocks the hypoxic ventilatory response and thus precipitates hypoventilation and apnea. *Am J Respir Crit Care Med* 193(9):1032–1043
- Mills E, Jobsis FF (1972) Mitochondrial respiratory chain of carotid body and chemoreceptor response to changes in oxygen tension. *J Neurophysiol* 35:405–428
- Moreno-Dominguez A, Ortega-Saenz P, Gao L, Colinas O, Garcia-Flores P, Bonilla-Henao V, Aragonés J, Huttemann M, Grossman LI, Weissmann N et al (2020) Acute O₂ sensing through HIF2 α -dependent expression of atypical cytochrome oxidase subunits in arterial chemoreceptors. *Sci Signal* 13(615):eaay9452
- Mulligan E, Lahiri S (1982) Separation of carotid body chemoreceptor responses to O₂ and CO₂ by oligomycin and by antimycin A. *Am J Physiol Cell Physiol* 242:C200–C206
- Napiwotzki J, Kadenbach B (1998) Extramitochondrial ATP/ADP-ratios regulate cytochrome c oxidase activity via binding to the cytosolic domain of subunit IV. *Biol Chem* 379(3):335–339
- Napiwotzki J, Shinzawa-Itoh K, Yoshikawa S, Kadenbach B (1997) ATP and ADP bind to cytochrome c oxidase and regulate its activity. *Biol Chem* 378(9):1013–1021
- Ortega-Sáenz P, López-Barneo J (2020) Physiology of the carotid body: from molecules to disease. *Annu Rev Physiol* 82:127–149
- Ortega-Saenz P, Pardal R, Garcia-Fernandez M, Lopez-Barneo J (2003) Rotenone selectively occludes sensitivity to hypoxia in rat carotid body glomus cells. *J Physiol* 548(Pt 3):789–800
- Ortega-Saenz P, Pascual A, Gomez-Diaz R, Lopez-Barneo J (2006) Acute oxygen sensing in heme oxygenase-2 null mice. *J Gen Physiol* 128(4):405–411
- Ortega-Saenz P, Macias D, Levitsky KL, Rodriguez-Gomez JA, Gonzalez-Rodriguez P, Bonilla-Henao V, Arias-Mayenco I, Lopez-Barneo J (2016) Selective

- accumulation of biotin in arterial chemoreceptors: requirement for carotid body exocytotic dopamine secretion. *J Physiol* 594(24):7229–7248
- Owen OE, Kalhan SC, Hanson RW (2002) The key role of anaplerosis and cataplerosis for citric acid cycle function. *J Biol Chem* 277(34):30409–30412
- Pajuelo-Reguera D, Cunatova K, Vrbacky M, Pecinova A, Houstek J, Mracek T, Pecina P (2020) Cytochrome c oxidase subunit 4 isoform exchange results in modulation of oxygen affinity. *Cell* 9(2):443
- Peng YJ, Gridina A, Wang B, Nanduri J, Fox AP, Prabhakar NR (2020) Olfactory receptor 78 participates in carotid body response to a wide range of low O₂ levels but not severe hypoxia. *J Neurophysiol* 123(5):1886–1895
- Perez-Garcia MT, Colinas O, Miguel-Velado E, Moreno-Dominguez A, Lopez-Lopez JR (2004) Characterization of the Kv channels of mouse carotid body chemoreceptor cells and their role in oxygen sensing. *J Physiol* 557(Pt 2):457–471
- Prabhakar NR, Peers C (2014) Gasotransmitter regulation of ion channels: a key step in O₂ sensing by the carotid body. *Physiology (Bethesda)* 29(1):49–57
- Rakoczy RJ, Wyatt CN (2018) Acute oxygen sensing by the carotid body: a rattlebag of molecular mechanisms. *J Physiol* 596(15):2969–2976
- Rakoczy RJ, Schiebrel CM, Wyatt CN (2022) Acute oxygen-sensing via mitochondria-generated temperature transients in rat carotid body type I cells. *Front Physiol* 13:874039
- Rankin EB, Biju MP, Liu Q, Unger TL, Rha J, Johnson RS, Simon MC, Keith B, Haase VH (2007) Hypoxia-inducible factor-2 (HIF-2) regulates hepatic erythropoietin in vivo. *J Clin Invest* 117:1068–1077
- Rieger B, Shalaeva DN, Sohnel AC, Kohl W, Duwe P, Mulkidjanian AY, Busch KB (2017) Lifetime imaging of GFP at CoxVIIIa reports respiratory supercomplex assembly in live cells. *Sci Rep* 7:46055
- Roy A, Rozanov C, Mokashi A, Daudu P, Al-Mehdi AB, Shams H, Lahiri S (2000) Mice lacking in gp91 phox subunit of NAD(P)H oxidase showed glomus cell [Ca²⁺]_i and respiratory responses to hypoxia. *Brain Res* 872(1–2):188–193
- Tello D, Balsa E, Acosta-Iborra B, Fuertes-Yebra E, Elorza A, Ordóñez A et al (2011) Induction of the mitochondrial NDUFA4L2 protein by HIF-1 α decreases oxygen consumption by inhibiting complex I activity. *Cell Metab* 14:768–779
- Teppema LJ, Dahan A (2010) The ventilatory response to hypoxia in mammals: mechanisms, measurement, and analysis. *Physiol Rev* 90(2):675–754
- Tian H, Hammer RE, Matsumoto AM, Russell DW, McKnight SL (1998) The hypoxia-responsive transcription factor EPAS1 is essential for catecholamine homeostasis and protection against heart failure during embryonic development. *Genes Dev* 12(21):3320–3324
- Timón-Gómez A, Scharr AL, Wong NY, Ni E, Roy A, Liu M, Chau J, Lampert JL, Hireed H, Kim NS, Jan M, Gupta AR, Day RW, Gardner JM, Wilson RJA, Barrientos A, Chang AJ (2022) Tissue-specific mitochondrial HIGD1C promotes oxygen sensitivity in carotid body chemoreceptors. *Elife* 11:e78915
- Torres-Torrel H, Ortega-Saenz P, Macias D, Omura M, Zhou T, Matsunami H, Johnson RS, Mombaerts P, Lopez-Barneo J (2018) The role of Olfr78 in the breathing circuit of mice. *Nature* 561(7724):E33–E40
- Torres-Torrel H, Ortega-Saenz P, Gao L, Lopez-Barneo J (2021) Lactate sensing mechanisms in arterial chemoreceptor cells. *Nat Commun* 12(1):4166
- Tsukihara T, Aoyama H, Yamashita E, Tomizaki T, Yamaguchi H, Shinzawa-Itoh K, Nakashima R, Yaono R, Yoshikawa S (1996) The whole structure of the 13-subunit oxidized cytochrome c oxidase at 2.8 Å. *Science* 272(5265):1136–1144
- Wang J, Hogan JO, Wang R, White C, Kim D (2017) Role of cystathionine-c-lyase in hypoxia-induced changes in TASK activity, intracellular [Ca²⁺] and ventilation in mice. *Respir Physiol Neurobiol* 246:98–106
- Weir EK, Lopez-Barneo J, Buckler KJ, Archer SL (2005) Acute oxygen-sensing mechanisms. *N Engl J Med* 353:2042–2055
- Wu M, Gu J, Guo R, Huang Y, Yang M (2016) Structure of mammalian respiratory supercomplex I1III2IV1. *Cell* 167(6):1598–1609
- Zhou T, Chien MS, Kaleem S, Matsunami H (2016) Single cell transcriptome analysis of mouse carotid body glomus cells. *J Physiol* 594(15):4225–4251



Of Mice and Men and Plethysmography Systems: Does LKB1 Determine the Set Point of Carotid Body Chemosensitivity and the Hypoxic Ventilatory Response?

A. Mark Evans

Abstract

Our recent studies suggest that the level of liver kinase B1 (LKB1) expression in some way determines carotid body afferent discharge during hypoxia and to a lesser extent during hypercapnia. In short, phosphorylation by LKB1 of an as yet unidentified target(s) determines a set point for carotid body chemosensitivity. LKB1 is the principal kinase that activates the AMP-activated protein kinase (AMPK) during metabolic stresses, but conditional deletion of AMPK in catecholaminergic cells, including therein carotid body type I cells, has little or no effect on carotid body responses to hypoxia or hypercapnia. With AMPK excluded, the most likely target of LKB1 is one or other of the 12 AMPK-related kinases, which are constitutively phosphorylated by LKB1 and, in general, regulate gene expression. By contrast, the hypoxic ventilatory response is attenuated by either LKB1 or AMPK deletion in catecholaminergic cells, precipitating hypoventilation and apnea during hypoxia rather than hyperventilation. Moreover, LKB1, but not AMPK, deficiency

causes Cheyne-Stokes-like breathing. This chapter will explore further the possible mechanisms that determine these outcomes.

Keywords

LKB1 · AMPK · Mitochondria · Hypoxia · Carotid body · Brainstem · Hypoxic ventilatory response · AMPK related kinases

18.1 Introduction

We initially set out to test the hypothesis that the AMP-activated protein kinase (AMPK) regulated breathing and thus oxygen and energy (ATP) supply to the whole body (Evans 2004, 2006). At the outset of our studies, it was generally accepted that the hypoxic ventilatory response (HVR) is initiated by increases in afferent fiber discharge from the carotid bodies and that the principal sensors of arterial PO_2 and indeed arterial PCO_2 are the carotid body type I cells. In response to either stimulus, type I cells depolarize to elicit voltage-gated calcium influx, exocytotic release of ATP, and thus consequent increases in chemoafferent discharge. This ultimately modulates, via the nucleus tractus solitarius, efferent outputs from respiratory central pattern generators located in the rostral ventrolateral medulla that increase

A. M. Evans (✉)
Centre for Discovery Brain Sciences, Hugh Robson
Building, University of Edinburgh, Edinburgh, UK
e-mail: mark.evans@ed.ac.uk

ventilation (Teppema and Dahan 2010; Kumar and Prabhakar 2012; Iturriaga et al. 2021). Therefore, we set about examining the role in regulating carotid body function and thus the HVR of AMPK and liver kinase B1 (LKB1), the principal pathway by which AMPK is activated in response to metabolic stresses such as hypoxia (Gonzalez et al. 2020).

LKB1 exists in a complex with regulatory proteins Ste20-related ADAPTER (STRAD; a pseudo-kinase) and Mouse protein 25 (MO25) which have a reciprocal protein stabilization relationship with LKB1 (Boudeau et al. 2003, 2004; Hawley et al. 2003). LKB1 is coupled to AMPK through changes in the cellular AMP:ATP and ADP:ATP ratios (Gowans et al. 2013) that may be triggered in carotid body type I cells by inhibition of mitochondrial oxidative phosphorylation during hypoxia (Buckler and Turner 2013; Moreno-Dominguez et al. 2020). AMPK exists as heterotrimers comprising one each of the two α -catalytic and two β - and three γ -regulatory subunits. Binding of AMP to the AMPK- γ subunit increases activity ten-fold by allosteric activation alone, while binding of AMP or ADP triggers increases in phosphorylation of Thr172 on the AMPK- α subunit by LKB1 (conferring up to 100-fold further activation) and at the same time reduces Thr172 dephosphorylation (Gonzalez et al. 2020).

It is important to note, however, that LKB1 also regulates by direct phosphorylation of 11 of the 12 AMPK-related kinases (Lizcano et al. 2004), but in each case, this is insensitive to metabolic stresses (Bright et al. 2009).

Moreover, there are alternative AMP-independent mechanisms of AMPK activation: (i) calcium dependent Thr172 phosphorylation by the calmodulin-dependent protein kinase CaMKK2 (Woods et al. 2005), (ii) long chain fatty acyl CoA binding to the allosteric drug and metabolite (ADaM) site on the α -subunit (Pinkosky et al. 2020), and (iii) glucose deprivation (Zhang et al. 2017).

The most likely path to AMPK activation during hypoxia would be through increases in the AM(D)P:ATP ratio and thus LKB1-dependent phosphorylation. However, in neurons, evidence suggests a role for the alternative CaMKK2 path-

way, which has been proposed to contribute to energy balance regulation by hypothalamic networks (Anderson et al. 2008).

To examine the role of LKB1 and AMPK in regulating carotid body chemo-sensitivity and the HVR, we therefore employed transgenic mice with global deletion of the gene encoding CaMKK2 (*Camkk2*) and, due to embryonic lethality, conditional deletion of the genes encoding LKB1 (*Stk11*) and the AMPK- α 1 (*Prkaa1*) and/or AMPK- α 2 (*Prkaa2*) catalytic subunits in catecholaminergic cells, including therein carotid body type I cells, by directing Cre expression via the tyrosine hydroxylase (TH) promoter (Mahmoud et al. 2016).

Our investigations strongly suggest that LKB1 expression serves an essential role in establishing carotid body function and chemosensitivity and that LKB1, but not CaMKK2, is required for the HVR. By contrast, however, AMPK appears to facilitate the HVR within regions of the brainstem that receive carotid body afferent input responses (Mahmoud et al. 2016), rather than at the level of the carotid bodies (Teppema and Dahan 2010; Kumar and Prabhakar 2012; Iturriaga et al. 2021). There is, therefore, a clear divergence in dependency on LKB1 and AMPK between the carotid body on the one hand and the HVR on the other. Moreover, LKB1, but not AMPK, deficiency precipitates Cheyne-Stokes-like breathing patterns during hypoxia, which are associated with heart failure but of unknown etiology (Terziyski and Draganova 2018).

The aim of the present manuscript is to consider these studies in the context of other relevant findings, from the carotid body to brainstem.

18.2 Results and Discussion

18.2.1 LKB1 Determines a Set Point for Carotid Body Chemosensitivity

Conditional deletion of the gene encoding LKB1 (*Stk11*) in type I cells abolished hypoxia-evoked cytoplasmic calcium transients in acutely isolated carotid body type I cells. Moreover, LKB1

deletion not only attenuated carotid body afferent input responses during hypoxia but also reduced carotid body CO₂ sensitivity and thus afferent input responses during hypercapnia. Added to this, there was a significant reduction in basal carotid body afferent discharge during normoxia. In short, LKB1 deletion led to a marked and wholesale reduction in carotid body chemosensitivity. This was a surprise because there is general agreement that type I cell activation during hypoxia is determined by changes in mitochondrial metabolism (Tatsumi et al. 1994; Dasso et al. 2000; Turner and Buckler 2013; Fernandez-Aguera et al. 2015) while type I cell responses to hypercapnia are driven by carbonic anhydrase-dependent acidosis rather than mitochondrial metabolism (Lahiri et al. 1982; Mulligan and Lahiri 1982; Rigual et al. 1985; Buckler et al. 1991; Iturriaga et al. 1993; Yamamoto et al. 2003; Nunes et al. 2013).

The LKB1 knockout mice used by us offered additional insights, however, because they were generated from a floxed mouse line (homozygous LKB1 floxed) in which exons 5–7 of this gene had been replaced by a cDNA cassette encoding equivalent exon sequences where exon 4 and the cDNA cassette were flanked by loxP sequences, that in its own right delivered mice that were ~90% hypomorphic for LKB1 expression in all cells (Sakamoto et al. 2005). Contrary to our findings with homozygous LKB1 knockouts, hypoxia-evoked calcium transients in carotid body type I cells from LKB1 floxed mice were not only retained but augmented relative to controls. Paradoxically, although basal afferent discharge from carotid bodies of these LKB1 floxed mice was similar to controls during normoxia, peak carotid body afferent discharge during hypoxia was attenuated by ~50%. Moreover, although it did not reach significance CO₂ sensitivity was lower relative to controls.

By contrast, dual deletion of the genes encoding the AMPK- α 1 (*Prkaa1*) and AMPK- α 2 (*Prkaa2*) catalytic subunits had little or no effect on increases in carotid body afferent discharge during either hypoxia or hypercapnia and no discernable effect on CO₂ sensitivity.

When taken together, these findings suggest that the set point about which type I cells are activated by hypoxia and hypercapnia is somehow determined in an AMPK-independent manner by the level of LKB1 expression and that membrane depolarization and exocytotic transmitter release are differentially sensitive to this.

It has been argued that falls in cytoplasmic ATP within type I cells may trigger membrane depolarization, exocytotic ATP release, and afferent discharge during hypoxia (Varas et al. 2007; Murali and Nurse 2016; Sacramento et al. 2019). Intriguingly, previous studies on the effects of LKB1 deletion have identified consequent changes in mitochondrial activities and concomitant reductions in ATP levels and for that matter increases in AMP:ATP and ADP:ATP ratios. This has been observed in a variety of cells, such as skeletal muscle (Sakamoto et al. 2005), cardiac muscle (Sakamoto et al. 2006; Jessen et al. 2010), pancreatic β -cells (Fu et al. 2015; Swisa et al. 2015), regulatory T cells (He et al. 2017), and MIN6 cells (Fu et al. 2015).

LKB1 deletion in skeletal muscle was also shown to lower total NAD/NADH levels (Jeppesen et al. 2013) which on the one hand appears consistent with the proposal that increases in mitochondrial NADH may mediate type I cell activation but on the other hand runs counter to the view that concomitant increases in mitochondrial reactive oxygen species are critical (Ortega-Saenz and Lopez-Barneo 2020), if one accepts the view that NADH contributes to antioxidant mechanisms.

Moreover, further support for the ATP hypothesis on type I cell chemotransduction may be taken from the finding that, when compared to wild-type, ATP levels are reduced in cardiac muscle from hypomorphic LKB1 floxed mice under normoxia and reduced still further in hearts from mice with cardiac-specific LKB1 deletion. Moreover, ATP levels in cardiac muscle of LKB1 floxed and LKB1 knockouts decline even further during ischemia (Sakamoto et al. 2006).

In short, the weight of evidence suggests that LKB1 may maintain in an expression-dependent manner, by both AMPK-independent and AMPK-dependent mechanisms, the capacity for ATP

synthesis within most cells that are required to maintain activity during metabolic stress, including therein carotid body type I cells where ATP deficiency might ultimately impact on the capacity for uptake of ATP by synaptic vesicles and/or exocytotic release of ATP. Further support for this view is provided by the finding that LKB1 deletion, but not hypomorphic expression of LKB1, reduced basal afferent discharge during normoxia, when, by contrast, peak afferent discharge was mildly attenuated by hypomorphic expression of LKB1 (~50%) and virtually abolished by LKB1 deletion. This is entirely in accordance with a previous study on rat carotid bodies, which showed that exocytotic release of adenosine represents the principal transmitter contributing to carotid body afferent discharge during mild hypoxia, while ATP acts as the principal transmitter driving afferent discharge during severe hypoxia (Conde et al. 2012).

Reductions in ATP levels could also explain why hypomorphic expression of LKB1 augmented hypoxia-evoked calcium transients in carotid body type I cells, while type I cell activation was abolished by homozygous LKB1 deletion. Briefly, midrange reductions in basal ATP levels could conceivably confer increased sensitivity of TASK1/3 channels to inhibition by hypoxia (Varas et al. 2007), without greatly altering the capacity for exocytotic ATP release. By contrast, more extreme ATP deficiency in type I cells from homozygous LKB1 knockouts might render the ATP sensitive TASK1/3 channels inactive, consequently block hypoxia-evoked activation of voltage-gated calcium influx (Varas et al. 2007; Kim et al. 2009; Buckler and Turner 2013), and at the same time greatly reduce vesicular uptake and exocytotic release of ATP (Murali and Nurse 2016; Sacramento et al. 2019).

Reductions in TASK1/3 channel activity and/or vesicular ATP would also impact type I cell activation by hypercapnia, due to the fact that hypercapnic acidosis inhibits TASK1/3 channels and triggers consequent increases in exocytotic release of ATP, albeit in a manner independent of mitochondrial oxidative phosphorylation (Mulligan

and Lahiri 1982; Zhang and Nurse 2004). In this respect, it is notable that inhibition of mitochondrial oxidative phosphorylation in cat carotid bodies in-situ by using either inhibitors that increase ROS levels (antimycin A) or those that do not (oligomycin) blocked responses to hypoxia and enhanced responses to hypercapnia in vivo (Mulligan and Lahiri 1982). If LKB1 deficiency did not reduce ATP availability and/or its exocytotic release, then one might therefore expect increases in afferent discharge in response to hypercapnia rather than the decreases observed in LKB1 knockouts.

In this respect, it is interesting to note that Lkb1 deletion in pancreatic β -cells is associated with lower glucose-induced ATP accumulation, enhanced membrane excitability, and increased glucose-stimulated insulin release (Fu et al. 2015; Swisa et al. 2015). This shows that an ion channel mechanism such as that proposed above for carotid body type I cells is feasible.

However, we must also consider the possibility that LKB1 deficiency may also increase or reduce other metabolic intermediates that might impact type I cell responses to hypoxia and hypercapnia and could conceivably contribute to the $O_2:CO_2$ stimulus interaction at the level of type I cells (Pepper et al. 1995; Dasso et al. 2000). For example, it has been suggested that LKB1 deletion in pancreatic β -cells can trigger a switch from glucose to glutamine metabolism leading to consequent increases in citric acid synthesis, which can inhibit TASK channels (Richter et al. 2004). Moreover, and in turn, increased citrate synthesis and export from mitochondria can occur consequent to increased TCA cycle activity (Westergaard et al. 1994; Sonnewald 2014), which may increase levels of cytoplasmic acetyl-CoA and thus fatty acids, the latter of which have also been shown to inhibit TASK channels (Kim et al. 2000). Either way, the precise AMPK-independent mechanism(s) by which LKB1 may “rewire type I cell metabolism” remains to be determined and is worthy of further investigation (Fig. 18.1).

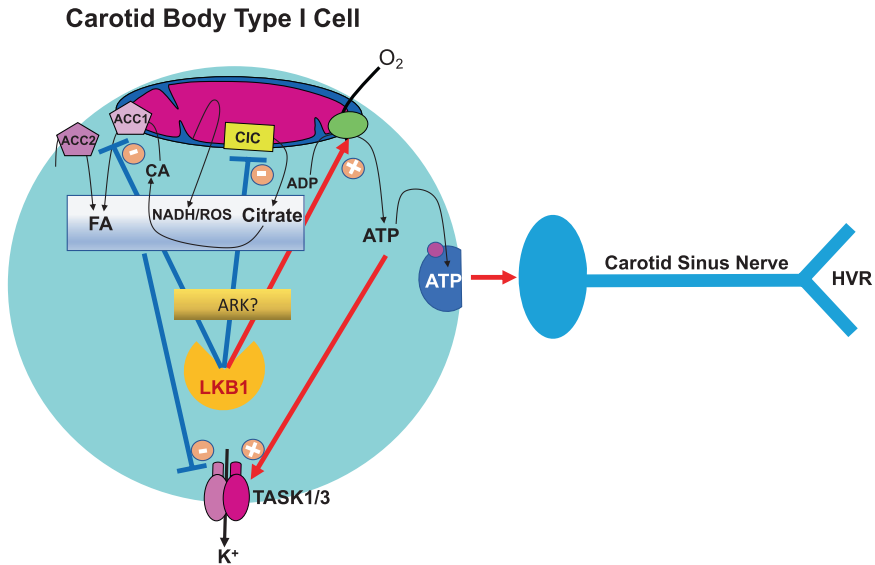


Fig. 18.1 Schematic showing hypothesis proposed as a mechanism of LKB1 expression-dependent regulation of carotid body type I cell excitability and exocytosis. *LKB1* liver kinase B1, *AMPK* AMP-activated protein kinase, *ARK* AMPK-related kinase, *FA* fatty acids, *CA* citric acid, *ROS* reactive oxygen species, *NADH* reduced nicotinamide adenine dinucleotide, *ACC* acetyl CoA carboxylase, *CIC* citrate/isocitrate transporter, *ATP* adenosine triphosphate, *ADP* adenosine diphosphate

ric acid, *ROS* reactive oxygen species, *NADH* reduced nicotinamide adenine dinucleotide, *ACC* acetyl CoA carboxylase, *CIC* citrate/isocitrate transporter, *ATP* adenosine triphosphate, *ADP* adenosine diphosphate

18.2.2 LKB1 and the AMPK-Related Kinases: From Synaptic Transmission to Gene Expression Regulation

While LKB1 may adjust glucose homeostasis (Shaw et al. 2005; Koh et al. 2006; Fu et al. 2015) and mitochondrial function through direct actions (Gan et al. 2010; Gurumurthy et al. 2010; Fu et al. 2015), it most likely impacts cell function by regulating one from 11 of the 12 AMPK-related kinases (Lizcano et al. 2004; Bright et al. 2009; Patel et al. 2014; Choi et al. 2015), which comprise the salt-inducible kinase (SIK1, SIK2, SIK3), the brain-specific kinases (BRSK1, BRSK2 (also known as synapses of the amphotericin B-sensitive kinase (SAD)-A and SAD-B)), the SNF1 (yeast homolog of AMPK)-like kinases NUAK1 and NUAK2 (also known as SNF1/AMP kinase-related kinase (SNARK)), and the microtubule affinity-regulating kinases (MARK1, MARK2, MARK3, MARK4, and MELK) (Manning et al.

2002). By contrast to its regulation of AMPK, LKB1 constitutively phosphorylates AMPK-related kinases in a manner dependent on their level of expression but entirely independent of cell autonomous metabolic status.

Of the AMPK-related kinases, the salt-inducible kinases are perhaps the most thoroughly studied. Importantly, SIK1, SIK2, and SIK3 have been implicated in the indirect regulation of cell metabolism through gene expression regulation. SIKs have been shown to regulate cyclic AMP-response-element binding protein (CREB)-regulated transcriptional coactivators (CRTC1, CRTC2, and CRTC3) and the Class 2a histone deacetylases (HDAC4, HDAC5, HDAC7, and HDAC9). Briefly, when phosphorylated by LKB1, SIKs in turn phosphorylate these transcriptional regulators and thus facilitate their association with and inhibition by 14-3-3 binding proteins. This action is opposed by, for example, phosphorylation of the same substrates by protein kinase A, leading to consequent translocation

of these transcriptional regulators to the nucleus. SIKs repress the gluconeogenic state in hepatocytes by inhibiting the transcription of genes required for gluconeogenesis, such as those encoding glucose-6-phosphatase and phosphoenolpyruvate carboxykinase. In doing so, SIKs support transcriptional regulation by insulin, which represses the transcription of genes encoding gluconeogenic enzymes by inducing the phosphorylation and inhibition of the FOXO family of transcription factors via Protein Kinase B/AKT. Moreover, SIKs have been proposed to regulate the insulin response in adipocytes by controlling glucose uptake and the transcription of lipogenic genes. That SIKs might have yet more diverse effects and cell-specific actions that could impact cell function and contribute to disorders of the nervous system is highlighted, for example, by the fact that loss of SIK function has been implicated in disturbances of circadian rhythms and sleep/wake cycles, epilepsy, and depression (Patel et al. 2014; Darling and Cohen 2021).

With respect to carotid body chemosensitivity, and also downstream neural activity, it is also evident that BRSK1-2 (by direct substrate regulation), MARK1-4 (which directly regulate their substrates and confer substrate inhibition indirectly by facilitating 14-3-3 binding) and NUA1 (direct substrate regulation) may impact neuronal cell polarity, outgrowth, axon specification, synaptic plasticity, and synaptic transmission (for review see Huang and Li 2022).

In short, there may be further twists in this tale because LKB1 holds the capacity to impact not only metabolism and exocytotic release of ATP through phosphorylation of SIKs but also cell polarity, development, and synaptic function through phosphorylation of BRSKs, MARKs, and NUA1.

18.2.3 LKB1, AMPK, and the Hypoxic Ventilatory Response

In accordance with the effect of LKB1 deletion on carotid body function, the HVR was attenuated in hypomorphic LKB1 floxed and

homozygous LKB1 knockout mice in a manner related to the degree of LKB1 deficiency. By contrast, in mice with global *Camkk2* deletion, the HVR was similar to controls.

Contrary to our findings for the carotid body, however, the HVR was markedly attenuated by deletion of AMPK- α 1, but not AMPK- α 2, in catecholaminergic cells (Mahmoud et al. 2016) even though there was no discernable effect of dual AMPK- α 1 and AMPK- α 2 deletion on carotid body afferent input responses during hypoxia. It is therefore evident that AMPK- α 1 most likely acts downstream of the carotid bodies within central respiratory networks. Here, AMPK facilitates the HVR by non-adrenergic mechanisms, although adrenergic pathways may deliver weaker AMPK-dependent negative inputs (MacMillan and Evans 2022). That is, if one accepts the view that increases in carotid body afferent discharge drive the augmenting phase of the HVR (Smith et al. 1993; Day and Wilson 2007) while direct modulation by hypoxia of brainstem respiratory networks aids maintenance of the HVR in the longer term (Smith et al. 1993, 2010; Curran et al. 2000; Teppema and Dahan 2010; Mahmoud et al. 2016; Wilson and Teppema 2016). Thus, LKB1 and AMPK are perfectly placed to exert independent influences on peripheral (Pepper et al. 1995; Dasso et al. 2000) and central (Smith et al. 1993, 2010; Day and Wilson 2007; Blain et al. 2010) stimulus interactions. This view gains further support from the finding that LKB1 deletion attenuated the rising phase of the hypercapnic and hypoxic-hypercapnic ventilatory responses but was without effect on the maximal ventilatory response, despite marked attenuation of afferent input responses to hypercapnia. LKB1 and AMPK- α 1 signaling pathways are therefore critical to the maintenance of breathing and oxygen supply during hypoxia but are not necessary for central ventilatory responses to hypercapnia.

Importantly, deletion of LKB1 and AMPK in catecholaminergic neurons precipitated hypoventilation and central apnea during hypoxia, rather than hyperventilation. In short, LKB1-AMPK signaling pathways act within central respiratory networks to oppose hypoventilation and apnea

(Mahmoud et al. 2016; MacMillan and Evans 2018, 2022; MacMillan et al. 2022).

Importantly, homozygous LKB1 deletion, but not AMPK deletion, in catecholaminergic cells not only led to marked reductions in breathing frequency (excluding apneas) but was also associated with erratic “augmentation” of tidal volume responses during severe hypoxia, consequent to induction of periodic Cheyne-Stokes-like breathing patterns (MacMillan et al. 2022). Here, the distinguishing factor is clearly the block by LKB1 deletion of not only carotid body afferent input responses to hypoxia and hypercapnia but also concomitant attenuation of downstream hypoxia-responsive circuit mechanisms. That said, we must take one further point into account here: the cardiac muscle of these knockouts is ~90% hypomorphic for LKB1 expression and exhibits clear evidence of cardiomyopathy and metabolic stress (ATP deficiency) during normoxia and ischemia, which one could argue goes some way to mimicking heart failure (Sakamoto et al. 2006). Therefore, during heart failure Cheyne-Stokes breathing may occur consequent to energy crises in peripheral and central catecholaminergic respiratory control networks. However, this runs contrary to the proposal of others, that Cheyne-Stokes breathing is triggered by hyperactivity of carotid bodies and thus augmented afferent input responses when associated with heart failure (Ponikowski et al. 2001). Such contradictory observations could be explained if enhanced carotid body afferent input responses after heart failure occur consequent to central metabolic crisis and failure of both central integration of afferent inputs and efferent ventilatory output, when allied to activation of central CO₂ sensing neurons during hypercapnia consequent to hypoventilation and apnea during hypoxia (Hall et al. 1996; Day and Wilson 2007; Topor et al. 2007).

18.3 Conclusion

In conclusion, the level of LKB1 expression is essential for establishing carotid body function and for initiating the HVR. In this respect, LKB1

and AMPK must provide for hierarchical control of the hypoxia-responsive respiratory network (Fig. 18.2). Firstly, the level of LKB1 expression determines, independent of AMPK, a set point about which carotid body afferent input responses are evoked during hypoxia and hypercapnia, rather than contributing to oxygen sensing per se. Thereafter, LKB1-AMPK signaling pathways likely govern coincidence detection and signal integration within a hypoxia-responsive circuit downstream of the carotid bodies that encompasses, at the very least, the brainstem nucleus of the solitary tract (Mahmoud et al. 2016). Afferent input responses and brainstem hypoxia could thereby determine, each in part, the set point about which AMPK and thus brainstem respiratory networks are activated during hypoxia. Subsequently, AMPK-dependent modulation of cellular metabolism (Ross et al. 2016), ion channels (Ikematsu et al. 2011; Ross et al. 2011), and thereby neuronal activities (Ikematsu et al. 2011; Lipton et al. 2001; Murphy et al. 2009) may facilitate afferent inputs and thus efferent outputs leading to increases in ventilatory drive during hypoxia. Consequently, LKB1 and/or AMPK deficiency may contribute to central sleep apnea associated with metabolic syndrome related disorders (Chau et al. 2012), ascent to altitude (Ainslie et al. 2013) and apnea of prematurity (Eichenwald et al. 2016). By contrast, Cheyne-Stokes breathing and central sleep apnea (Hall et al. 1996) associated with heart failure (Ponikowski et al. 2001) may be conferred by LKB1 deficiency and/or metabolic crises across peripheral and central hypoxia-responsive respiratory networks. Further studies are therefore warranted to elucidate the downstream targets by which LKB1 establishes carotid body function.

Acknowledgments This work was funded by Programme Grants awarded to AME by the Wellcome Trust (WT081195MA) and the British Heart Foundation (RG/12/14/29885). AME would like to take this opportunity to thank Drs. Sandy Macmillan and Andy Holmes for their continued and generous support over many more years than expected, without which publication our work on LKB1 may not have been possible. AME also thanks Professor Nanduri Prabhakar for an important prompt during ISAC XXI in Lisbon.

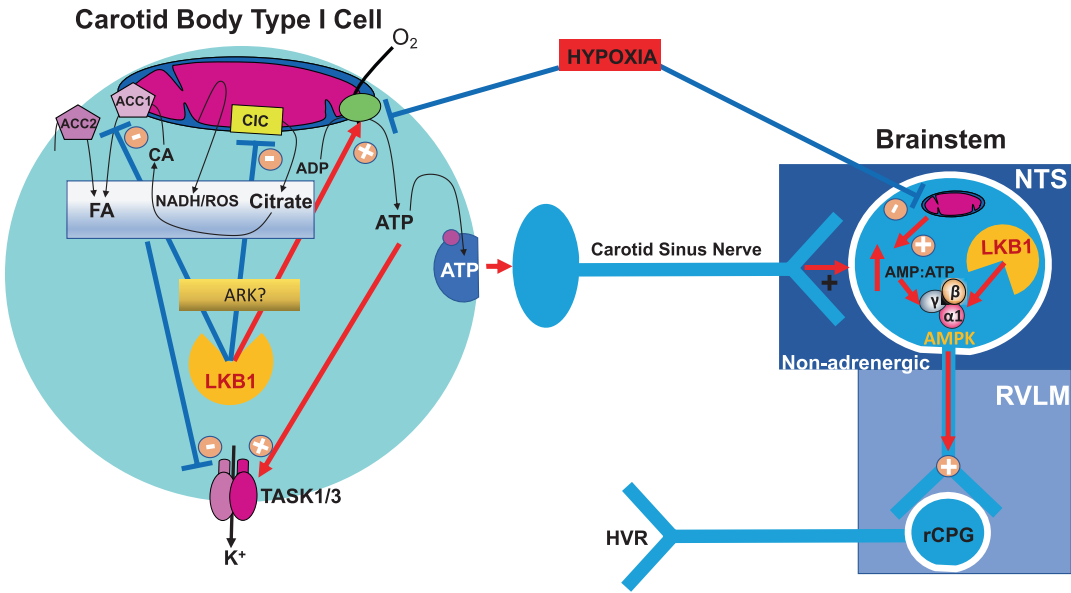


Fig. 18.2 Schematic showing the divergent pathways by which LKB1 and AMPK may coordinate the hypoxic ventilatory response. *LKB1* liver kinase B1, *AMPK*

AMP-activated protein kinase, *ARK* AMPK-related kinase, *NTS* nucleus tractus solitarius, *RVLM* rostral ventrolateral medulla

References¹

- Ainslie PN, Lucas SJ, Burgess KR (2013) Breathing and sleep at high altitude. *Respir Physiol Neurobiol* 188:233–256
- Anderson KA, Ribar TJ, Lin F, Noeldner PK, Green MF, Muehlbauer MJ, Witters LA, Kemp BE, Means AR (2008) Hypothalamic CaMKK2 contributes to the regulation of energy balance. *Cell Metab* 7:377–388
- Blain GM, Smith CA, Henderson KS, Dempsey JA (2010) Peripheral chemoreceptors determine the respiratory sensitivity of central chemoreceptors to CO₂. *J Physiol* 588:2455–2471
- Boudeau J, Baas AF, Deak M, Morrice NA, Kieloch A, Schutkowski M, Prescott AR, Clevers HC, Alessi DR (2003) MO25 α /beta interact with STRAD α /beta enhancing their ability to bind, activate and localize LKB1 in the cytoplasm. *EMBO J* 22:5102–5114
- Boudeau J, Scott JW, Resta N, Deak M, Kieloch A, Komander D, Hardie DG, Prescott AR, van Aalten DM, Alessi DR (2004) Analysis of the LKB1-STRAD-MO25 complex. *J Cell Sci* 117:6365–6375
- Bright NJ, Thornton C, Carling D (2009) The regulation and function of mammalian AMPK-related kinases. *Acta Physiol (Oxf)* 196:15–26
- Buckler KJ, Turner PJ (2013) Oxygen sensitivity of mitochondrial function in rat arterial chemoreceptor cells. *J Physiol* 591:3549–3563
- Buckler KJ, Vaughan-Jones RD, Peers C, Nye PC (1991) Intracellular pH and its regulation in isolated type I carotid body cells of the neonatal rat. *J Physiol* 436:107–129
- Chau EH, Lam D, Wong J, Mokhlesi B, Chung F (2012) Obesity hypoventilation syndrome: a review of epidemiology, pathophysiology, and perioperative considerations. *Anesthesiology* 117:188–205
- Choi S, Lim DS, Chung J (2015) Feeding and fasting signals converge on the LKB1-SIK3 pathway to regulate lipid metabolism in drosophila. *PLoS Genet* 11:e1005263
- Conde SV, Monteiro EC, Rigual R, Obeso A, Gonzalez C (2012) Hypoxic intensity: a determinant for the contribution of ATP and adenosine to the genesis of carotid body chemosensory activity. *J Appl Physiol* (1985) 112:2002–2010
- Curran AK, Rodman JR, Eastwood PR, Henderson KS, Dempsey JA, Smith CA (2000) Ventilatory responses to specific CNS hypoxia in sleeping dogs. *J Appl Physiol* (1985) 88:1840–1852
- Darling NJ, Cohen P (2021) Nuts and bolts of the salt-inducible kinases (SIKs). *Biochem J* 478:1377–1397
- Dasso LL, Buckler KJ, Vaughan-Jones RD (2000) Interactions between hypoxia and hypercapnic acidosis on calcium signaling in carotid body type I cells. *Am J Physiol Lung Cell Mol Physiol* 279:L36–L42

¹Reference citations are given in running text either with author name (s) and year of publication in parentheses or with numbers in brackets.

- Day TA, Wilson RJ (2007) Brainstem PCO₂ modulates phrenic responses to specific carotid body hypoxia in an in situ dual perfused rat preparation. *J Physiol* 578:843–857
- Eichenwald EC, Committee on F, Newborn AAoP (2016) Apnea of prematurity. *Pediatrics* 137. <https://doi.org/10.1542/peds.2015-3757>
- Evans AM (2004) Hypoxia, cell metabolism, and cadpr accumulation. Springer, Boston
- Evans AM (2006) AMP-activated protein kinase and the regulation of Ca²⁺ signalling in O₂-sensing cells. *J Physiol* 574:113–123
- Fernandez-Aguera MC, Gao L, Gonzalez-Rodriguez P, Pintado CO, Arias-Mayenco I, Garcia-Flores P, Garcia-Perganeda A, Pascual A, Ortega-Saenz P, Lopez-Barneo J (2015) Oxygen sensing by arterial chemoreceptors depends on mitochondrial complex I signaling. *Cell Metab* 22:825–837
- Fu A, Robitaille K, Faubert B, Reeks C, Dai XQ, Hardy AB, Sankar KS, Ogrel S, Al-Dirbashi OY, Rocheleau JV, Wheeler MB, MacDonald PE, Jones R, Screaton RA (2015) LKB1 couples glucose metabolism to insulin secretion in mice. *Diabetologia* 58:1513–1522
- Gan B, Hu J, Jiang S, Liu Y, Sahin E, Zhuang L, Fletcher-Sananikone E, Colla S, Wang YA, Chin L, Depinho RA (2010) Lkb1 regulates quiescence and metabolic homeostasis of haematopoietic stem cells. *Nature* 468:701–704
- Gonzalez A, Hall MN, Lin SC, Hardie DG (2020) AMPK and TOR: the Yin and Yang of cellular nutrient sensing and growth control. *Cell Metab* 31:472–492
- Gowans GJ, Hawley SA, Ross FA, Hardie DG (2013) AMP is a true physiological regulator of AMP-activated protein kinase by both allosteric activation and enhancing net phosphorylation. *Cell Metab* 18:556–566
- Gurumurthy S, Xie SZ, Alagesan B, Kim J, Yusuf RZ, Saez B, Tzatsos A, Oszolak F, Milos P, Ferrari F, Park PJ, Shirihai OS, Scadden DT, Bardeesy N (2010) The Lkb1 metabolic sensor maintains haematopoietic stem cell survival. *Nature* 468:659–663
- Hall MJ, Xie A, Rutherford R, Ando S, Floras JS, Bradley TD (1996) Cycle length of periodic breathing in patients with and without heart failure. *Am J Respir Crit Care Med* 154:376–381
- Hawley SA, Boudeau J, Reid JL, Mustard KJ, Udd L, Makela TP, Alessi DR, Hardie DG (2003) Complexes between the LKB1 tumor suppressor, STRAD alpha/beta and MO25 alpha/beta are upstream kinases in the AMP-activated protein kinase cascade. *J Biol* 2:28
- He N, Fan W, Henriquez B, Yu RT, Atkins AR, Liddle C, Zheng Y, Downes M, Evans RM (2017) Metabolic control of regulatory T cell (Treg) survival and function by Lkb1. *Proc Natl Acad Sci U S A* 114:12542–12547
- Huang E, Li S (2022) Liver kinase B1 functions as a regulator for neural development and a therapeutic target for neural repair. *Cell* 111:2861. <https://doi.org/10.3390/cells11182861>
- Ikematsu N, Dallas ML, Ross FA, Lewis RW, Rafferty JN, David JA, Suman R, Peers C, Hardie DG, Evans AM (2011) Phosphorylation of the voltage-gated potassium channel Kv2.1 by AMP-activated protein kinase regulates membrane excitability. *Proc Natl Acad Sci U S A* 108:18132–18137
- Iturriaga R, Mokashi A, Lahiri S (1993) Dynamics of carotid body responses in vitro in the presence of CO₂-HCO₃⁻: role of carbonic anhydrase. *J Appl Physiol* (1985) 75:1587–1594
- Iturriaga R, Alcayaga J, Chapleau MW, Somers VK (2021) Carotid body chemoreceptors: physiology, pathology, and implications for health and disease. *Physiol Rev* 101:1177–1235
- Jeppesen J, Maarbjerg SJ, Jordy AB, Fritzen AM, Pehmoller C, Sylow L, Serup AK, Jessen N, Thorsen K, Prats C, Qvortrup K, Dyck JR, Hunter RW, Sakamoto K, Thomson DM, Schjerling P, Wojtaszewski JF, Richter EA, Kiens B (2013) LKB1 regulates lipid oxidation during exercise independently of AMPK. *Diabetes* 62:1490–1499
- Jessen N, Koh HJ, Folmes CD, Wagg C, Fujii N, Lofgren B, Wolf CM, Berul CI, Hirshman MF, Lopaschuk GD, Goodyear LJ (2010) Ablation of LKB1 in the heart leads to energy deprivation and impaired cardiac function. *Biochim Biophys Acta* 1802:593–600
- Kim Y, Bang H, Kim D (2000) TASK-3, a new member of the tandem pore K(+) channel family. *J Biol Chem* 275:9340–9347
- Kim D, Cavanaugh EJ, Kim I, Carroll JL (2009) Heteromeric TASK-1/TASK-3 is the major oxygen-sensitive background K⁺ channel in rat carotid body glomus cells. *J Physiol* 587:2963–2975
- Koh HJ, Arnolds DE, Fujii N, Tran TT, Rogers MJ, Jessen N, Li Y, Liew CW, Ho RC, Hirshman MF, Kulkarni RN, Kahn CR, Goodyear LJ (2006) Skeletal muscle-selective knockout of LKB1 increases insulin sensitivity, improves glucose homeostasis, and decreases TRB3. *Mol Cell Biol* 26:8217–8227
- Kumar P, Prabhakar NR (2012) Peripheral chemoreceptors: function and plasticity of the carotid body. *Compr Physiol* 2:141–219
- Lahiri S, Mulligan E, Mokashi A (1982) Adaptive response of carotid body chemoreceptors to CO₂. *Brain Res* 234:137–147
- Lipton AJ, Johnson MA, Macdonald T, Lieberman MW, Gozal D, Gaston B (2001) S-nitrosothiols signal the ventilatory response to hypoxia. *Nature* 413:171–174
- Lizcano JM, Goransson O, Toth R, Deak M, Morrice NA, Boudeau J, Hawley SA, Udd L, Makela TP, Hardie DG, Alessi DR (2004) LKB1 is a master kinase that activates 13 kinases of the AMPK subfamily, including MARK/PAR-1. *EMBO J* 23:833–843
- MacMillan S, Evans AM (2018) AMPK-alpha1 or AMPK-alpha2 deletion in smooth muscles does not affect the hypoxic ventilatory response or systemic arterial blood pressure regulation during hypoxia. *Front Physiol* 9:655
- MacMillan S, Evans AM (2022) AMPK facilitates the hypoxic ventilatory response through non-adrenergic mechanisms at the brainstem. *Pflugers Archiv - Euro J Physiol* 475:89

- MacMillan S, Holmes AP, Dallas ML, Mahmoud AD, Shipston MJ, Peers C, Hardie DG, Kumar P, Evans AM (2022) LKB1 is the gatekeeper of carotid body chemosensing and the hypoxic ventilatory response. *Commun Biol* 5:642
- Mahmoud AD, Lewis S, Juricic L, Udoh UA, Hartmann S, Jansen MA, Ogunbayo OA, Puggioni P, Holmes AP, Kumar P, Navarro-Dorado J, Foretz M, Viollet B, Dutia MB, Marshall I, Evans AM (2016) AMP-activated protein kinase deficiency blocks the hypoxic ventilatory response and thus precipitates hypoventilation and apnea. *Am J Respir Crit Care Med* 193:1032–1043
- Manning G, Whyte DB, Martinez R, Hunter T, Sudarsanam S (2002) The protein kinase complement of the human genome. *Science* 298:1912–1934
- Moreno-Dominguez A, Ortega-Saenz P, Gao L, Colinas O, Garcia-Flores P, Bonilla-Henao V, Aragonés J, Huttemann M, Grossman LI, Weissmann N, Sommer N, Lopez-Barneo J (2020) Acute O₂ sensing through HIF2 α -dependent expression of atypical cytochrome oxidase subunits in arterial chemoreceptors. *Sci Signal* 13:eaay9452
- Mulligan E, Lahiri S (1982) Separation of carotid body chemoreceptor responses to O₂ and CO₂ by oligomycin and by antimycin A. *Am J Phys* 242:C200–C206
- Murali S, Nurse CA (2016) Purinergic signalling mediates bidirectional crosstalk between chemoreceptor type I and glial-like type II cells of the rat carotid body. *J Physiol* 594:391–406
- Murphy BA, Fakira KA, Song Z, Beuve A, Routh VH (2009) AMP-activated protein kinase and nitric oxide regulate the glucose sensitivity of ventromedial hypothalamic glucose-inhibited neurons. *Am J Physiol Cell Physiol* 297:C750–C758
- Nunes AR, Holmes AP, Sample V, Kumar P, Cann MJ, Monteiro EC, Zhang J, Gauda EB (2013) Bicarbonate-sensitive soluble and transmembrane adenylyl cyclases in peripheral chemoreceptors. *Respir Physiol Neurobiol* 188:83–93
- Ortega-Saenz P, Lopez-Barneo J (2020) Physiology of the carotid body: from molecules to disease. *Annu Rev Physiol* 82:127–149
- Patel K, Foretz M, Marion A, Campbell DG, Gurlay R, Boudaba N, Tournier E, Titchenell P, Peggie M, Deak M, Wan M, Kaestner KH, Goransson O, Viollet B, Gray NS, Birnbaum MJ, Sutherland C, Sakamoto K (2014) The LKB1-salt-inducible kinase pathway functions as a key gluconeogenic suppressor in the liver. *Nat Commun* 5:4535
- Pepper DR, Landauer RC, Kumar P (1995) Postnatal development of CO₂-O₂ interaction in the rat carotid body in vitro. *J Physiol* 485(Pt 2):531–541
- Pinkosky SL, Scott JW, Desjardins EM, Smith BK, Day EA, Ford RJ, Langendorf CG, Ling NXY, Nero TL, Loh K, Galic S, Hoque A, Smiles WJ, Ngoei KRW, Parker MW, Yan Y, Melcher K, Kemp BE, Oakhill JS, Steinberg GR (2020) Long-chain fatty acyl-CoA esters regulate metabolism via allosteric control of AMPK beta1 isoforms. *Nat Metab* 2:873–881
- Ponikowski P, Chua TP, Anker SD, Francis DP, Doehner W, Banasiak W, Poole-Wilson PA, Piepoli MF, Coats AJ (2001) Peripheral chemoreceptor hypersensitivity: an ominous sign in patients with chronic heart failure. *Circulation* 104:544–549
- Richter TA, Dvoryanchikov GA, Chaudhari N, Roper SD (2004) Acid-sensitive two-pore domain potassium (K₂P) channels in mouse taste buds. *J Neurophysiol* 92:1928–1936
- Rigual R, Iniguez C, Carreres J, Gonzalez C (1985) Carbonic anhydrase in the carotid body and the carotid sinus nerve. *Histochemistry* 82:577–580
- Ross FA, Rafferty JN, Dallas ML, Ogunbayo O, Ikematsu N, McClafferty H, Tian L, Widmer H, Rowe IC, Wyatt CN, Shipston MJ, Peers C, Hardie DG, Evans AM (2011) Selective expression in carotid body type I cells of a single splice variant of the large conductance calcium- and voltage-activated potassium channel confers regulation by AMP-activated protein kinase. *J Biol Chem* 286:11929–11936
- Ross FA, MacKintosh C, Hardie DG (2016) AMP-activated protein kinase: a cellular energy sensor that comes in 12 flavours. *FEBS J* 283:2987–3001
- Sacramento JF, Olea E, Ribeiro MJ, Prieto-Lloret J, Melo BF, Gonzalez C, Martins FO, Monteiro EC, Conde SV (2019) Contribution of adenosine and ATP to the carotid body chemosensory activity in ageing. *J Physiol* 597:4991–5008
- Sakamoto K, McCarthy A, Smith D, Green KA, Grahame Hardie D, Ashworth A, Alessi DR (2005) Deficiency of LKB1 in skeletal muscle prevents AMPK activation and glucose uptake during contraction. *EMBO J* 24:1810–1820
- Sakamoto K, Zarrinpashneh E, Budas GR, Pouleur AC, Dutta A, Prescott AR, Vanoverschelde JL, Ashworth A, Jovanovic A, Alessi DR, Bertrand L (2006) Deficiency of LKB1 in heart prevents ischemia-mediated activation of AMPK α 2 but not AMPK α 1. *Am J Physiol Endocrinol Metab* 290:E780–E788
- Shaw RJ, Lamia KA, Vasquez D, Koo SH, Bardeesy N, Depinho RA, Montminy M, Cantley LC (2005) The kinase LKB1 mediates glucose homeostasis in liver and therapeutic effects of metformin. *Science* 310:1642–1646
- Smith CA, Engwall MJ, Dempsey JA, Bisgard GE (1993) Effects of specific carotid body and brain hypoxia on respiratory muscle control in the awake goat. *J Physiol* 460:623–640
- Smith CA, Forster HV, Blain GM, Dempsey JA (2010) An interdependent model of central/peripheral chemoreception: evidence and implications for ventilatory control. *Respir Physiol Neurobiol* 173:288–297
- Sonnenwald U (2014) Glutamate synthesis has to be matched by its degradation – where do all the carbons go? *J Neurochem* 131:399–406
- Swisa A, Granot Z, Tamarina N, Sayers S, Bardeesy N, Philipson L, Hodson DJ, Wikstrom JD, Rutter GA, Leibowitz G, Glaser B, Dor Y (2015) Loss of Liver Kinase B1 (LKB1) in beta cells enhances glucose-

- stimulated insulin secretion despite profound mitochondrial defects. *J Biol Chem* 290:20934–20946
- Tatsumi K, Hannhart B, Pickett CK, Weil JV, Moore LG (1994) Effects of testosterone on hypoxic ventilatory and carotid body neural responsiveness. *Am J Respir Crit Care Med* 149:1248–1253
- Teppema LJ, Dahan A (2010) The ventilatory response to hypoxia in mammals: mechanisms, measurement, and analysis. *Physiol Rev* 90:675–754
- Terziyski K, Draganova A (2018) Central sleep apnea with cheyne-stokes breathing in heart failure – from research to clinical practice and beyond. *Adv Exp Med Biol* 1067:327–351
- Topor ZL, Vasilakos K, Younes M, Remmers JE (2007) Model based analysis of sleep disordered breathing in congestive heart failure. *Respir Physiol Neurobiol* 155:82–92
- Turner PJ, Buckler KJ (2013) Oxygen and mitochondrial inhibitors modulate both monomeric and heteromeric TASK-1 and TASK-3 channels in mouse carotid body type-I cells. *J Physiol* 591:5977
- Varas R, Wyatt CN, Buckler KJ (2007) Modulation of TASK-like background potassium channels in rat arterial chemoreceptor cells by intracellular ATP and other nucleotides. *J Physiol* 583:521–536
- Westergaard N, Sonnewald U, Unsgard G, Peng L, Hertz L, Schousboe A (1994) Uptake, release, and metabolism of citrate in neurons and astrocytes in primary cultures. *J Neurochem* 62:1727–1733
- Wilson RJ, Teppema LJ (2016) Integration of central and peripheral respiratory chemoreflexes. *Compr Physiol* 6:1005–1041
- Woods A, Dickerson K, Heath R, Hong SP, Momcilovic M, Johnstone SR, Carlson M, Carling D (2005) Ca²⁺/calmodulin-dependent protein kinase kinase-beta acts upstream of AMP-activated protein kinase in mammalian cells. *Cell Metab* 2:21–33
- Yamamoto Y, Fujimura M, Nishita T, Nishijima K, Atoji Y, Suzuki Y (2003) Immunohistochemical localization of carbonic anhydrase isozymes in the rat carotid body. *J Anat* 202:573–577
- Zhang M, Nurse CA (2004) CO₂/pH chemosensory signaling in CO-cultures of rat carotid body receptors and petrosal neurons: role of ATP and ACh. *J Neurophysiol* 92:3433–3445
- Zhang CS, Hawley SA, Zong Y, Li M, Wang Z, Gray A, Ma T, Cui J, Feng JW, Zhu M, Wu YQ, Li TY, Ye Z, Lin SY, Yin H, Piao HL, Hardie DG, Lin SC (2017) Fructose-1,6-bisphosphate and aldolase mediate glucose sensing by AMPK. *Nature* 548:112–116



Analyzing Angiotensin II Receptor Type 1 Clustering in PC12 Cells in Response to Hypoxia Using Direct Stochastic Optical Reconstruction Microscopy (dSTORM)

Hayyaf S. Aldossary, Daniel J. Nieves, Deirdre M. Kavanagh, Dylan Owen, Clare J. Ray, Prem Kumar, Andrew M. Coney, and Andrew P. Holmes

Abstract

Angiotensin II (Ang II) is a hormone that plays a major role in maintaining homeostasis. The Ang II receptor type 1 (AT₁R) is expressed in acute O₂ sensitive cells, including carotid body (CB) type I cells and pheochromocytoma 12 (PC12) cells, and Ang II increases cell activity. While a functional role for Ang II and AT₁R in increasing the activity of O₂ sensitive cells has been established, the nanoscale distribution of AT₁R has not. Furthermore, it is not known how exposure to hypoxia may alter the single-molecule arrangement and

clustering of AT₁R. In this study, the AT₁R nanoscale distribution under control normoxic conditions in PC12 cells was determined using direct stochastic optical reconstruction microscopy (dSTORM). AT₁R were arranged in distinct clusters with measurable parameters. Across the entire cell surface there averaged approximately 3 AT₁R clusters/μm² of cell membrane. Cluster area varied in size ranging from 1.1×10^{-4} to 3.9×10^{-2} μm². Twenty-four hours of exposure to hypoxia (1% O₂) altered clustering of AT₁R, with notable increases in the maximum cluster area, suggestive of an increase in supercluster formation. These observations could aid in

H. S. Aldossary (✉)

School of Biomedical Sciences, Institute of Clinical Sciences, University of Birmingham, Birmingham, UK

College of Medicine, Basic Medical Sciences, King Saud bin Abdulaziz University for Health Sciences, Riyadh, Saudi Arabia

e-mail: hxa807@student.bham.ac.uk

D. J. Nieves

Institute of Immunology and Immunotherapy and Centre of Membrane Proteins and Receptors (COMPARE), University of Birmingham, Birmingham, UK

D. M. Kavanagh

Micron Bioimaging Facility, University of Oxford, Oxford, UK

D. Owen

School of Mathematics, University of Birmingham, Birmingham, UK

C. J. Ray · P. Kumar · A. M. Coney

A. P. Holmes (✉)

School of Biomedical Sciences, Institute of Clinical Sciences, University of Birmingham, Birmingham, UK

e-mail: a.p.holmes@bham.ac.uk

understanding mechanisms underlying augmented Ang II sensitivity in O₂ sensitive cells in response to sustained hypoxia.

Keywords

Angiotensin II · Angiotensin II receptor type 1 · PC12 cells · Chronic hypoxia · Single-molecule localization · Direct stochastic optical reconstruction microscopy (dSTORM)

19.1 Introduction

Angiotensin II (Ang II) is a critical peptide hormone that impacts on the function of many organs and is increased in numerous cardiorespiratory diseases including heart failure, hypertension, and chronic obstructive pulmonary disease (COPD) (Andreas et al. 2006; Opie and Sack 2001; van de Wal et al. 2006). Ang II stimulates the carotid body (CB) type I cell, which in turn increases CB chemoafferent frequency (Allen 1998; Fung et al. 2001; Peng et al. 2011). RT-PCR analysis has revealed that the mRNA for both AT_{1a} and AT_{1b} subtypes is expressed in type I cells and immunohistochemistry has confirmed the presence of angiotensin II receptor type 1 (AT₁R) protein (Atanasova et al. 2018; Fung et al. 2001).

AT₁Rs are members of the G-protein-coupled receptor (GPCR) family, key players in mediating CB activity (Aldossary et al. 2020; Holmes et al. 2019). Recent data obtained using novel super-resolution imaging techniques suggest that GPCRs are not uniformly distributed but are present in distinct clusters located in specific compartments or “hot spots” in the cell membrane (Sungkaworn et al. 2017). This allows for downstream intracellular signaling to be localized to specific regions within the cell. Different cluster characteristics may modify responses to pharmacological agents (Duke and Graham 2009). Although AT₁Rs are known to be expressed in CB type I cells and the closely associated PC12 cell line, there is currently little informa-

tion regarding the detailed single-molecule spatial organization of these receptors in either of these O₂ sensitive cell types. Furthermore, it is not clear if the single-molecule distribution and cluster characteristics of AT₁Rs can be modified by exposure to other stimuli, such as sustained hypoxia.

This study therefore utilized PC12 cells to determine (1) if AT₁Rs are observed in clusters in O₂ sensitive cells and (2) if the AT₁R cluster characteristics are modified by the exposure to 24 h of hypoxia.

19.2 Methods

19.2.1 PC12 Cell Culture, Hypoxic Protocol, and Immunocytochemistry

PC12 cells are a rat pheochromocytoma cell line that share many similarities with CB type I cells including acute sensitivity to hypoxia. PC12 cells were grown in suspension in RPMI media (1X) Gluta MAX+, supplemented with 10% horse serum, 5% fetal bovine serum, penicillin 50 µg/ml, and streptomycin 50 µg/ml, incubated at 37 °C and equilibrated with 5% CO₂, 21% O₂, pH 7.35–7.45. The experiments started when the cell growth reached steady state at around passage number 35, where cell count was approximately 7.5×10^7 cells/ml.

A subset of cells was taken from the suspension media and plated on 10 mm microwell imaging dishes (MatTek Corporation, Ashland, USA) containing 400 µg/ml human placental collagen (Sigma-Aldrich, Gillingham, UK). Cells were allowed to adhere to the coverslip in normoxia (21% O₂) at 37 °C, for 1 h. Cells were then incubated in either normoxia (Nx; 21% O₂) or hypoxia (Hx; 1% O₂) for 24 h. After 24 h, cells were immediately fixed in 4% paraformaldehyde (Alfa Aesar, Lancashire, UK) for 90 min to ensure maximal immobilization of cellular proteins. Cells were permeabilized with a 0.1% Triton (VWR, Lutterworth, UK) in phosphate-buffered saline (PBS) solution for 5 min and blocked in a

5% BSA in PBS solution for 60 min. The primary rabbit anti-AT₁R antibody (Abcam, Cambridge, UK) (1:500) was diluted in blocking solution and incubated overnight at 4 °C. Cells were washed three times in PBS, blocked again for 30 min, and incubated in secondary antibody Alexa Fluor 647 F(ab')₂ fragment of goat anti-rabbit IgG (H + L), 1:2000 (ThermoFisher Scientific, Waltham, MA, USA), for 90 min at room temperature.

19.2.2 Direct Stochastic Optical Reconstruction Microscopy (dSTORM) Imaging and Cluster Analysis

dSTORM experiments were performed on a NIKON N-STORM microscope equipped with a Nikon × 100 1.49 NA total internal reflection fluorescence (TIRF) oil objective, Perfect Focus Ti-E stand, Agilent MLC400 laser bed, and Andor iXon Ultra EM-CCD camera. Laser illumination was provided using a fully motorized TIRF combiner. Immunolabelled samples were imaged in 0.5 mg/ml glucose oxidase, 40 µg/ml catalase, 10% wt/vol glucose, and 100 mM MEA in PBS, pH 7.4, to induce Alexa 647 blinking. During dSTORM acquisition, the sample was continuously illuminated at 640 nm for 20,000 frames (256 × 256 pixels, 9.2 ms exposure time). For the image sequence, single molecules were localized using the density estimation approach, and an initial reconstructed image was generated as an average shifted histogram. The image sequence was then drift corrected and compensated for multiple blinking. After merging, a normalized 2D Gaussian image was produced, and a color from a predefined table (LUT) was applied. This process was performed using the ThunderSTORM plugin in FIJI (ImageJ) (Fig. 19.1).

A density-based spatial clustering of applications with noise (DBSCAN) algorithm was used to detect and quantify AT₁R clusters (Ester et al. 1996; Pagoon et al. 2016). DBSCAN is an unsupervised learning method, whereby points are

classified as clustered according to two parameters: epsilon or the radius of search and minPts or the minimum number of points required to be classified as a cluster (Ester et al. 1996; Pagoon et al. 2016). This process was performed using MATLAB software, and epsilon and minPts were set to 20 nm and 10, respectively.

19.2.3 Statistical Analysis

Data is presented in the text as mean ± SEM. In figures, data is presented as box-whisker plots with the median, a box representing the interquartile range (IQR), and the whiskers extending to outliers. Single points represent mean data from an individual cell. Significance was taken as $P < 0.05$ using an unpaired two-tailed Student's t-test. Distribution figures were presented as 95th percentile, to eliminate outliers.

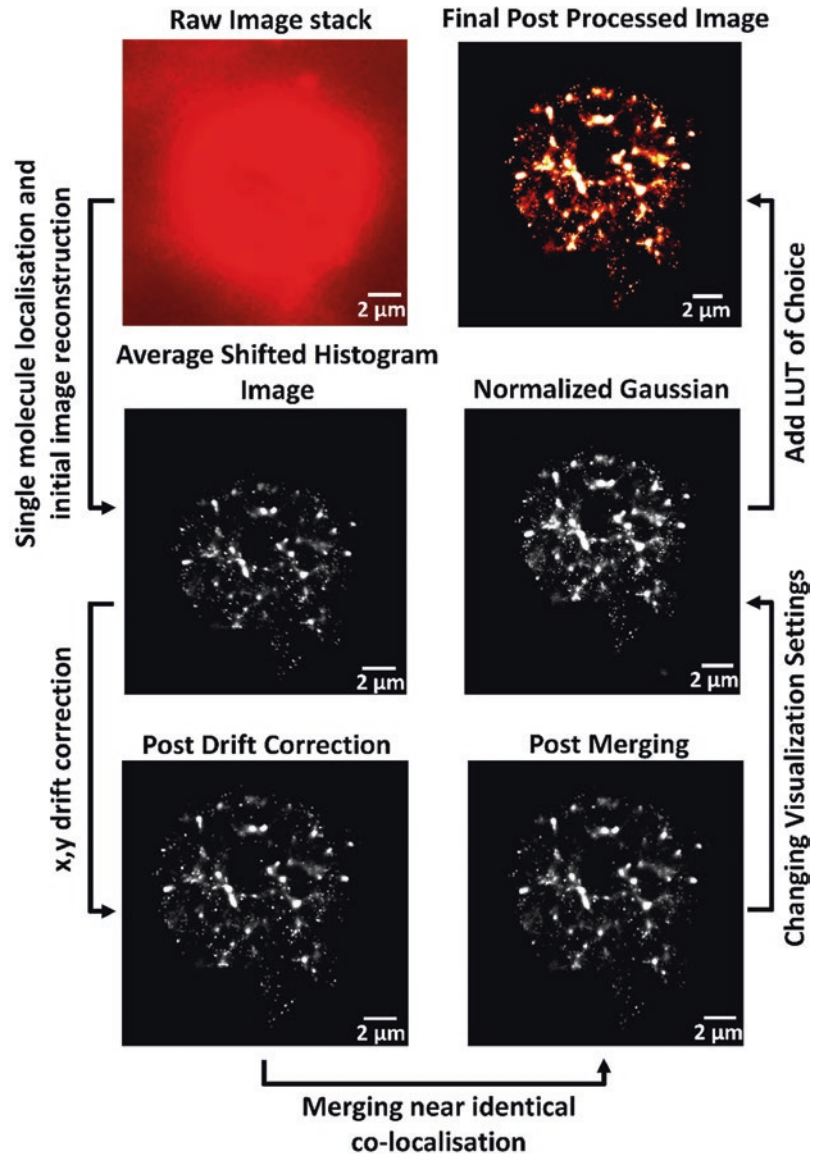
19.3 Results

19.3.1 AT₁Rs Are Clustered on the Cell Membrane of PC12 Cells with Measurable Characteristics

The initial aim was to determine if AT₁Rs were randomly distributed on the cell membrane of PC12 cells or if they were found in clusters. An example reconstructed super-resolution image demonstrating the spatial organization of AT₁Rs across the entire PC12 cell surface is presented in Fig. 19.2a along with a magnified region of interest in Fig. 19.2c.

There are regions on the cell surface with an increased local density of AT₁R, while there are other areas where AT₁R expression is absent. DBSCAN analysis confirmed the presence of distinct AT₁R cluster formation (Fig. 19.2b, d). Identification of AT₁R clustering was apparent in every cell tested ($n = 10$). Analysis revealed a mean of 2.8 ± 0.7 AT₁R clusters/µm² cell membrane when averaged across the entire cell surface, although there was some variation between

Fig. 19.1 Summary of image processing used to generate super-resolution images of angiotensin II receptor type 1 distributions across the cell membrane of PC12 cells. The left top image shows a single raw preprocessed PC12 cell. Left middle image shows the same cell after the localization of single molecules and the generation of an average shifted histogram image. Left bottom image shows the cell after drift correction. Merging near identical coordinates was done next, and the post merging image is shown in right bottom. After merging, a normalized 2D Gaussian image was produced right middle. A color was applied as shown in the right top image. Processing was performed using the ThunderSTORM plugin in FIJI (ImageJ)



cells (range $0.8\text{--}6.8$ AT₁R clusters/ μm^2 ; Fig. 19.2e). Mean AT₁R cluster area was $9.8 \pm 0.6 \times 10^{-3} \mu\text{m}^2$ (range 1.1×10^{-4} to $43.9 \times 10^{-2} \mu\text{m}^2$), with more than 50% of clusters being less than $3.7 \times 10^{-3} \mu\text{m}^2$ (Fig. 19.2f). More than 50% of clusters contained fewer than 100 localizations (range, 10–1041; mean, 252 ± 15 ; median, 45 ± 15 localizations; Fig. 19.2g). The cluster density (a measure of how tightly packed together molecules are within the cluster) identified by DBSCAN showed a range of 1.5×10^4 to 3.6×10^4 localizations/ μm^2 , mean of

$2.5 \pm 0.01 \times 10^4$ localizations/ μm^2 , and median of $2.4 \pm 0.01 \times 10^4$ localizations/ μm^2 (Fig. 19.2h).

19.3.2 Maximum AT₁R Cluster Area Is Increased by Hypoxia

A comparison of the normoxic (Nx, 21% O₂) data was made against PC12 cells subjected to 24 h of 1% O₂ (Hx) to evaluate whether any of the AT₁R cluster parameters would change in response to hypoxia. In terms of the spatial arrangement of

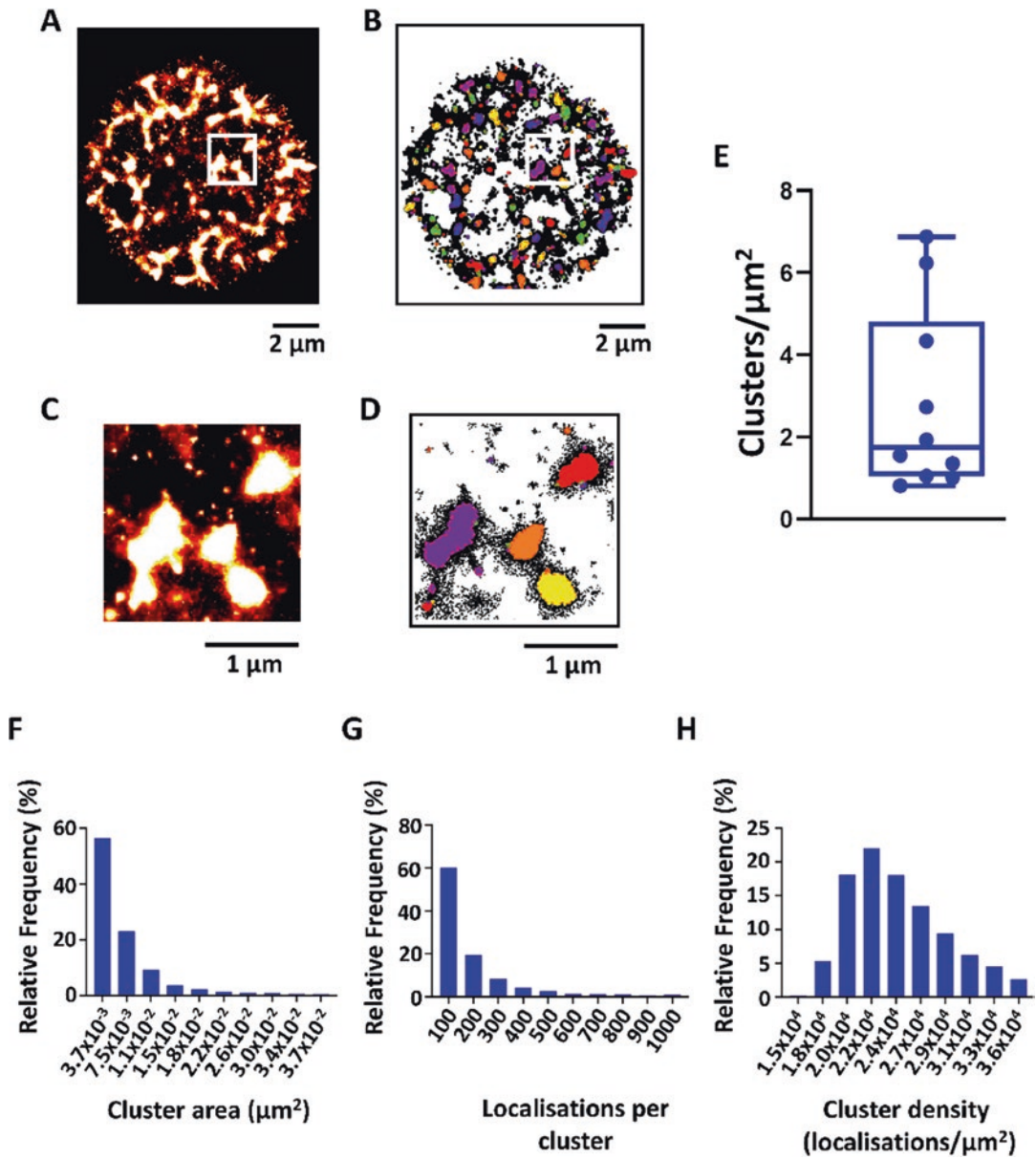


Fig. 19.2 Quantification of angiotensin II receptor type 1 (AT₁R) cluster parameters on the cell surface membrane of PC12 cells. (a–d) Direct stochastic optical reconstruction microscopy (dSTORM) images (a, c) of AT₁R clustering on the cell surface membrane of PC12 cells along with corresponding cluster maps (b, d). (e) The number of AT₁R clusters detected per μm² when averaged across the entire cell surface membrane for ten individual PC12 cells. Box-whiskers denote IQR and max-min values,

respectively. Horizontal line is the median. Individual dots denote data from a single cell. (f–h) Relative frequency distribution plots of cluster area (f), the number of localizations per cluster (g), and the number of localizations per μm² within the cluster (cluster density) (h). For (f–h), data has been distributed into ten equally sized bins. For (f–h), data is from *N* = 3219 clusters taken from *n* = 10 PC12 cells

AT₁R, an initial reflection seen in the examples in Fig. 19.3a suggested that AT₁R clusters were still apparent following 24 h of hypoxia with no obvious differences in the single-molecule organization.

The mean spacing of AT₁R clusters throughout the entire cell membrane surface was consistent between Nx (2.8 ± 0.7 clusters per μm^2 , $n = 10$ cells) and Hx (2.3 ± 0.3 clusters per μm^2 , $n = 10$ cells, $p > 0.5$). The mean and minimum cluster area was similar between groups (Fig. 19.3b, c). However, the maximum cluster area was significantly increased by hypoxia (Fig. 19.3d).

19.3.3 Maximum AT₁R Cluster Area Is Increased by Hypoxia

Based on the previous findings, which indicates that the maximum cluster size is significantly increased after hypoxia, a comparison between Nx ($N = 3219$) and Hx ($N = 2430$) AT₁R cluster distributions was performed. For cluster area, the distribution follows a negative exponential for both Nx and Hx, with the majority of clusters being $7.5 \times 10^{-3} \mu\text{m}^2$ or less (Fig. 19.4a). However, there does appear to be a slightly greater proportion of clusters with particular large areas in the Hx group compared to the Nx group (Fig. 19.4b). Similarly, Hx slightly elevates the proportion of clusters with a particularly high number of localizations when compared to Nx (Fig. 19.4c, d).

Hypoxia did not significantly modify the distribution of cluster densities suggesting that hypoxia does not modify how tightly packed together AT₁R receptors are within the cluster (Fig. 19.4e). This data is indicative of an increased generation of large area superclusters in response to hypoxia, which is dependent on an increase in AT₁R number rather than augmented spacing between the receptors.

19.4 Discussion

The present study showed that AT₁Rs are found in clusters rather than being randomly distributed on the cell membrane of PC12 cells. This data

implies that there are likely to be specific Ang II signaling microdomains within PC12 cells. The identification and quantification of AT₁Rs across the entire cell surface membrane was measured using a DBSCAN analysis and MATLAB algorithm. This study establishes the baseline characteristics of AT₁R clusters in PC12 cells, which can help with identifying alterations in AT₁R cluster distributions in response to pathophysiological stimuli. We have shown that 24 h of Hx slightly alters the single-molecule arrangement of AT₁Rs with an increase in the proportion of very large area clusters.

Alterations in Ang II signaling in response to chronic hypoxia (CH), chronic intermittent hypoxia, and heart failure have been implicated in mediating CB plasticity and hyperactivity (Kumar and Prabhakar 2012). It has been reported that CH increases AT_{1a} and AT_{1b} receptor mRNA expression in type I cells (Leung et al. 1998) as well as enhancing chemoafferent sensitivity to exogenous Ang II (Lam et al. 2004; Leung et al. 2000). Given the link between the CB and augmented vascular sympathetic nerve activity in COPD patients (Iturriaga et al. 2016; Phillips et al. 2018), selective targeting of the Ang II signaling pathway in the CB could be a novel approach to treat neurogenic hypertension of this etiology.

In the current study, when a comparison was made between Nx and Hx groups, the results showed that Hx increased the maximum AT₁R cluster area and altered the cluster distribution, slightly increasing the proportion of large area clusters and the number of clusters with a very high number of localizations. These findings are consistent with CH increasing AT₁R gene expression. In addition, our findings open up the possibility of CH inducing a more intense local Ang II microdomain signal. AT₁R activation is suggested to promote IP₃ dependent release of Ca²⁺ from intracellular stores (Leung et al. 2003), as well as increasing the activity of NADPH oxidase (Garrido and Griendling 2009; Peng et al. 2011) both of which account for acute and sustained type I cell activation. An interesting next step would be to explore the nanoscale relationship between AT₁Rs and IP₃ receptors on the endoplasmic reticulum as well as with NADPH oxidases. This may underpin

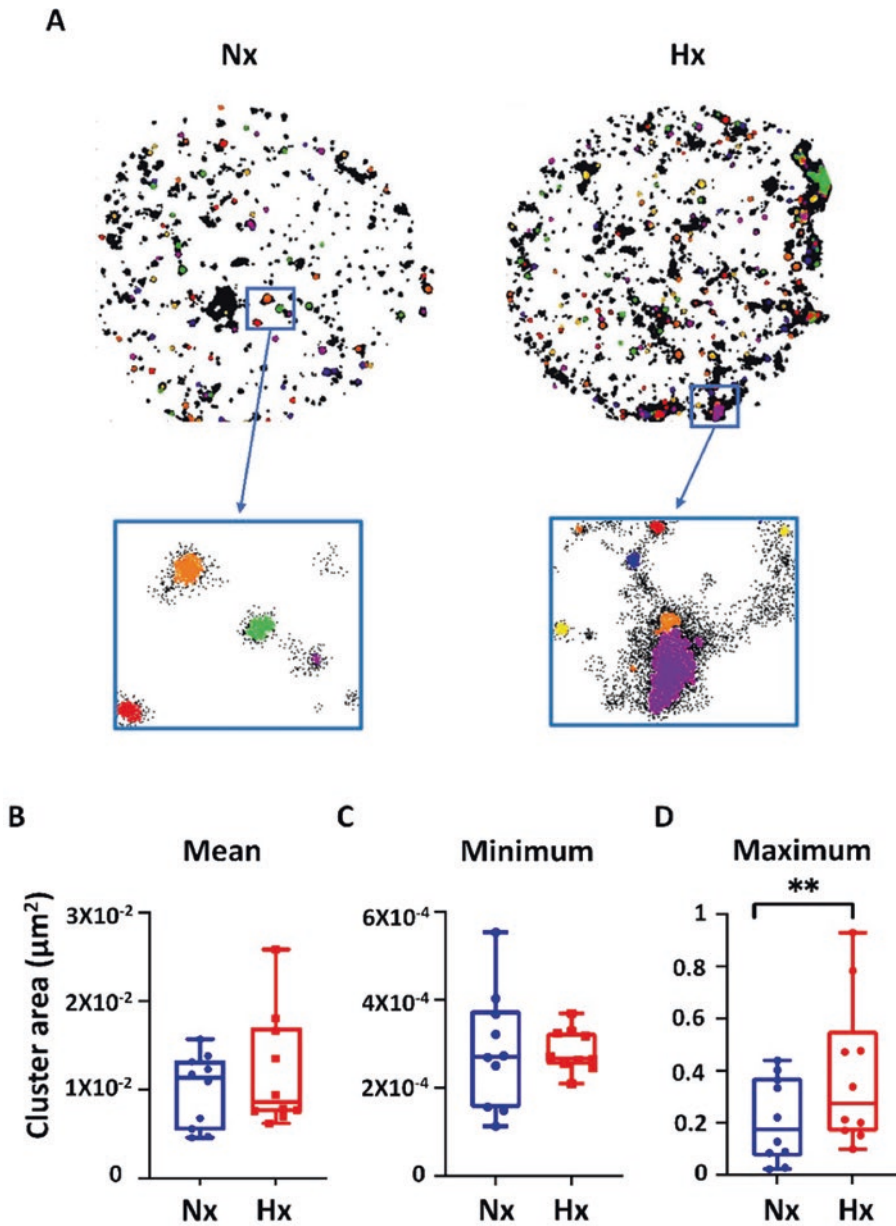


Fig. 19.3 Hypoxia increases the maximum angiotensin II receptor type 1 (AT_1R) cluster area in PC12 cells. (a) Example single-molecule AT_1R cluster maps created by MATLAB using DBSCAN algorithm, for cells exposed to 24 h of normoxia (Nx, 21% O_2 , left) and hypoxia (Hx, 1% O_2 , right). Insets: magnified ROIs showing individual clusters. (b–d) Box-whisker plots comparing the mean

(b), minimum (c), and maximum (d) cluster area between Nx and Hx groups. Box-whiskers denote IQR and maximum values, respectively. All data points (representing individual cells, $n = 10$ cells Nx, $n = 10$ cells Hx) are shown as well as the median. **denotes $p < 0.01$, unpaired two-tailed Student's t-test

local Ang II mediated Ca^{2+} and ROS signaling microdomains within the PC12 cell which could be enhanced in response to CH.

CH has been shown to have a significant influence upon many aspects of the CB type I cell, which shares a number of similar properties to

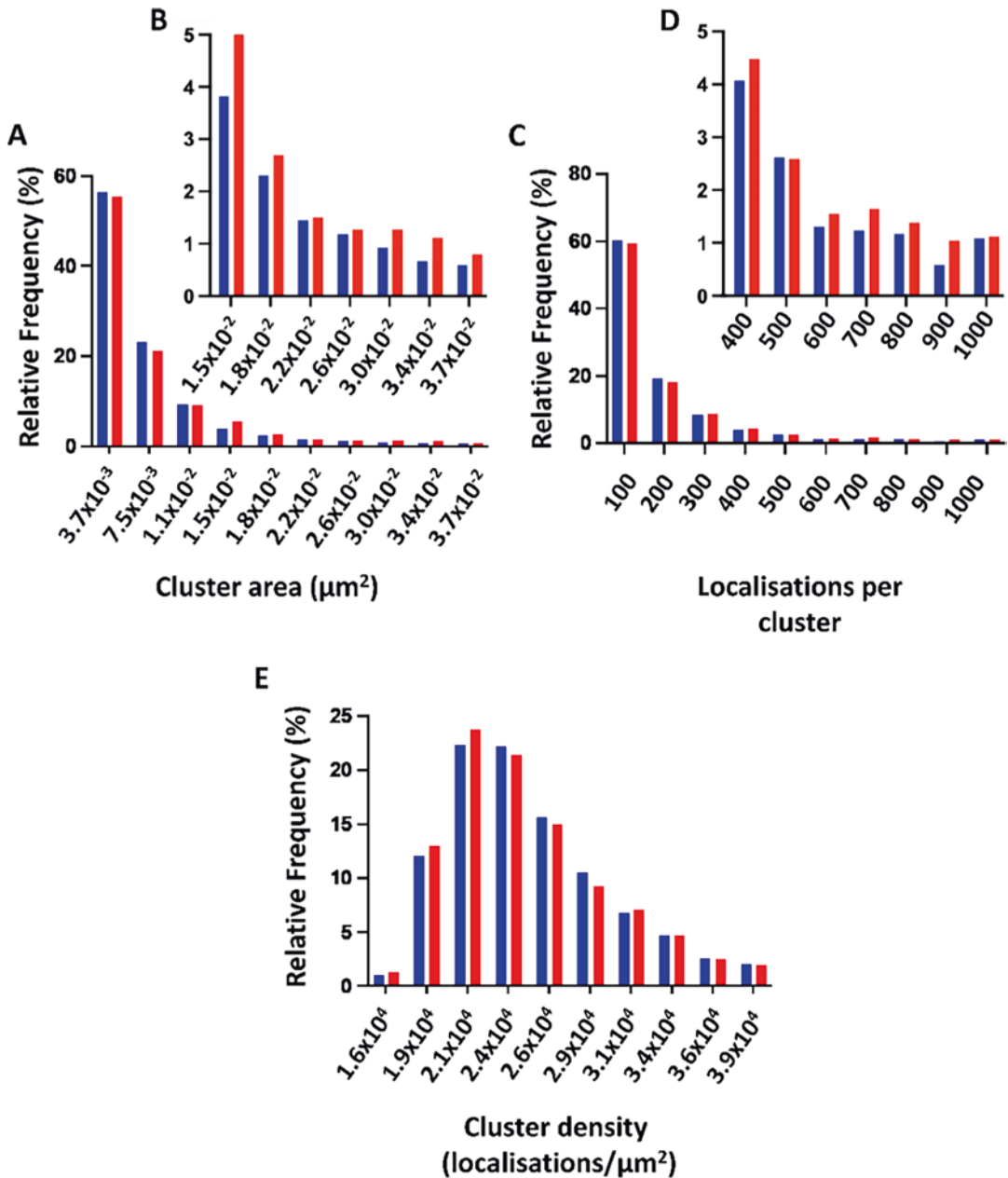


Fig. 19.4 Hypoxia increases the proportion of large area angiotensin II receptor type 1 (AT₁R) clusters. (a–e) Relative frequency distribution plots of AT₁R cluster area (a, b), the number of localizations per cluster (c, d), and the number of localizations per μm² within the cluster

(cluster density) (e) for PC12 cells exposed to either 24 h of normoxia (Nx, $N = 3219$ clusters) or hypoxia (Hx, $N = 2430$ clusters). Data has been distributed into ten equally sized bins. The y-axis has been confined in (b) and (d) to magnify data in the final seven bins

PC12 cells, including acute and specialized O₂ sensitivity. CH can impact on ion channel mRNA expression, enhancing cell excitability, alter neurotransmitter (NTM) secretion (Powell 2007),

and increase the action of neuromodulators, which collectively will facilitate afferent activity (Powell 2007). These changes are associated with an increase in hypoxia-inducible factor 1 α

(HIF-1 α) expression (Powell 2007; Soulage et al. 2004). In addition to changes in gene expression, there is the possibility that hypoxia and HIF-1 α related signaling may modify AT₁R degradation, trafficking, or internalization (Collingridge et al. 2004; Drake et al. 2006). Understanding such modifications would help to explain the increase of AT₁R cluster size and supercluster formation in PC12 cells after CH.

A limitation of this study was performing the experiments on PC12 cells rather than isolated CB type I cells. Similar work performed on type I cells would help extend our understanding of how changes in AT₁R clustering correlate against CB hyperactivity. It would be interesting to observe if the AT₁R clustering seen here in PC12 cells resembles that of the type I cell and if the responses to hypoxia are consistent. A more extensive understanding of the single-molecule distribution of other GPCR and ion clustering in PC12 cells and isolated type I cells is also needed. Furthermore, in the current study, cells were only exposed to single level of hypoxia for 24 h. It is probable that the extent of cluster re-modeling is dependent on both the intensity and duration of the hypoxic stimulus. In vivo cellular/tissue normoxia varies between different organs, but it is estimated that the majority of cell types are exposed to somewhere between 2% and 5% O₂ (Lee et al. 2020). Cell lines which have been cultured over many generations, often in 21% O₂, may well have adapted to survive and grow at much higher O₂ levels. For most cells, cellular hypoxia ranges between 0.5% and 2% (Lee et al. 2020). However, for specialized O₂ sensing cells such as the PC12 cell and CB type I cell, acute responses to hypoxia are initiated at much higher levels, possibly as high as 5% O₂. However, even in these cells, long-term adaptation to hypoxia is likely to be dependent on an alternative O₂ sensing mechanism involving HIF stabilization and alterations in gene expression. Prolyl hydroxylase inhibition and HIF stabilization occur at a lower O₂ level estimated to be between 0.5% and 2% (Lee et al. 2020). Thus, we do accept that the level of O₂ used in this study (1% O₂) can be considered as a relatively severe hypoxic stimulus but was used to initiate considerable HIF stabiliza-

tion which we hypothesized would lead to more long-term changes in AT₁R gene and protein expression. Indeed, in a previous study using PC12 cells, 1% O₂ was shown to cause the maximum increase in HIF2 α stabilization (Seta et al. 2002). That said, it would be interesting to see if alterations in AT₁R cluster characteristics are still observed under more mild hypoxic conditions.

In conclusion, this work demonstrates that AT₁Rs are present in distinct clusters located in specific compartments or “hot spots” in the cell membrane of O₂ sensitive PC12 cells. Exposure to hypoxia augments the maximum cluster area and elevates the proportion of large area clusters. Stronger Ang II microdomain signaling is therefore likely to be apparent in response to hypoxia although this needs to be verified.

References

- Aldossary HS, Alzahrani AA, Nathanael D, Alhuthail EA, Ray CJ, Batis N et al (2020) G-protein-coupled receptor (GPCR) signaling in the carotid body: roles in hypoxia and cardiovascular and respiratory disease. *Int J Mol Sci* 21(17). <https://doi.org/10.3390/ijms21176012>
- Allen AM (1998) Angiotensin AT₁ receptor-mediated excitation of rat carotid body chemoreceptor afferent activity. *J Physiol* 510(Pt 3):773–781
- Andreas S, Herrmann-Lingen C, Raupach T, Luthje L, Fabricius J, Hruska N et al (2006) Angiotensin II blockers in obstructive pulmonary disease: a randomised controlled trial. *Eur Respir J* 27(5):972–979
- Atanasova DY, Dandov AD, Dimitrov ND, Lazarov NE (2018) Immunohistochemical localization of angiotensin AT₁ receptors in the rat carotid body. *Acta Histochem* 120(2):154–158. <https://doi.org/10.1016/j.acthis.2018.01.005>
- Collingridge GL, Isaac JT, Wang YT (2004) Receptor trafficking and synaptic plasticity. *Nat Rev Neurosci* 5(12):952–962
- Drake MT, Shenoy SK, Lefkowitz RJ (2006) Trafficking of G protein-coupled receptors. *Circ Res* 99(6):570–582
- Duke T, Graham I (2009) Equilibrium mechanisms of receptor clustering. *Prog Biophys Mol Biol* 100(1–3):18–24
- Ester M, Kriegel H-P, Sander J, Xu X (1996) A density-based algorithm for discovering clusters in large spatial databases with noise. *KDD Proc* 96:226–231
- Fung ML, Lam SY, Chen Y, Dong X, Leung PS (2001) Functional expression of angiotensin II receptors in type-I cells of the rat carotid body. *Pflugers Arch* 441(4):474–480

- Garrido AM, Griendling KK (2009) NADPH oxidases and angiotensin II receptor signaling. *Mol Cell Endocrinol* 302(2):148–158
- Holmes AP, Ray CJ, Thompson EL, Alshehri Z, Coney AM, Kumar P (2019) Adrenaline activation of the carotid body: key to CO₂ and pH homeostasis in hypoglycaemia and potential pathological implications in cardiovascular disease. *Respir Physiol Neurobiol* 265:92–99. <https://doi.org/10.1016/j.resp.2018.05.008>
- Iturriaga R, Del Rio R, Idiaquez J, Somers VK (2016) Carotid body chemoreceptors, sympathetic neural activation, and cardiometabolic disease. *Biol Res* 49:13. <https://doi.org/10.1186/s40659-016-0073-8>
- Kumar P, Prabhakar NR (2012) Peripheral chemoreceptors: function and plasticity of the carotid body. *Compr Physiol* 2(1):141–219
- Lam SY, Fung ML, Leung PS (2004) Regulation of the angiotensin-converting enzyme activity by a time-course hypoxia in the carotid body. *J Appl Physiol* 96(2):809–813, 00684.2003 [pii]. <https://doi.org/10.1152/japplphysiol.00684.2003>
- Lee P, Chandel NS, Simon MC (2020) Cellular adaptation to hypoxia through hypoxia inducible factors and beyond. *Nat Rev Mol Cell Biol* 21(5):268–283. <https://doi.org/10.1038/s41580-020-0227-y>
- Leung PS, Yao XQ, Chan HC, Fu LX, Wong PY (1998) Differential gene expression of angiotensin II receptor subtypes in the epididymides of mature and immature rats. *Life Sci* 62(5):461–468. [https://doi.org/10.1016/s0024-3205\(97\)01140-5](https://doi.org/10.1016/s0024-3205(97)01140-5)
- Leung PS, Lam SY, Fung ML (2000) Chronic hypoxia upregulates the expression and function of AT(1) receptor in rat carotid body. *J Endocrinol* 167(3):517–524, JOE03924 [pii]. <https://doi.org/10.1677/joe.0.1670517>
- Leung PS, Fung ML, Tam MS (2003) Renin-angiotensin system in the carotid body. *Int J Biochem Cell Biol* 35(6):847–854, S1357272502001802 [pii]. [https://doi.org/10.1016/s1357-2725\(02\)00180-2](https://doi.org/10.1016/s1357-2725(02)00180-2)
- Opie LH, Sack MN (2001) Enhanced angiotensin II activity in heart failure: reevaluation of the counterregulatory hypothesis of receptor subtypes. *Circ Res* 88(7):654–658. <https://doi.org/10.1161/hh0701.089175>
- Pageon SV, Nicovich PR, Mollazade M, Tabarin T, Gaus K (2016) Clus-DoC: a combined cluster detection and colocalization analysis for single-molecule localization microscopy data. *Mol Biol Cell* 27(22):3627–3636. <https://doi.org/10.1091/mbc.E16-07-0478>
- Peng Y-J, Raghuraman G, Khan SA, Kumar GK, Prabhakar NR (2011) Angiotensin II evokes sensory long-term facilitation of the carotid body via NADPH oxidase. *J Appl Physiol* 111(4):964–970
- Phillips DB, Steinback CD, Collins SE, Fuhr DP, Bryan TL, Wong EYL et al (2018) The carotid chemoreceptor contributes to the elevated arterial stiffness and vasoconstrictor outflow in chronic obstructive pulmonary disease. *J Physiol Lond* 596(15):3233–3244. <https://doi.org/10.1113/jp275762>
- Powell FL (2007) The influence of chronic hypoxia upon chemoreception. *Respir Physiol Neurobiol* 157(1):154–161, S1569-9048(07)00014-6 [pii]. <https://doi.org/10.1016/j.resp.2007.01.009>
- Seta K, Kim HW, Ferguson T, Kim R, Pathrose P, Yuan Y et al (2002) Genomic and physiological analysis of oxygen sensitivity and hypoxia tolerance in PC12 cells. *Ann N Y Acad Sci* 971:379–388. <https://doi.org/10.1111/j.1749-6632.2002.tb04500.x>
- Soulage C, Pascual O, Roux J-C, Denavit-Saubié M, Pequignot J-M (2004) Chemosensory inputs and neural remodeling in carotid body and brainstem catecholaminergic cells. *Adv Exp Med Biol* 551:53–58
- Sungkaworn T, Jobin ML, Burnecki K, Weron A, Lohse MJ, Calebiro D (2017) Single-molecule imaging reveals receptor-G protein interactions at cell surface hot spots. *Nature* 550(7677):543–547. <https://doi.org/10.1038/nature24264>
- van de Wal RM, Plokker HW, Lok DJ, Boomsma F, van der Horst FA, van Veldhuisen DJ et al (2006) Determinants of increased angiotensin II levels in severe chronic heart failure patients despite ACE inhibition. *Int J Cardiol* 106(3):367–372. <https://doi.org/10.1016/j.ijcard.2005.02.016>



The Carotid Body “Tripartite Synapse”: Role of Gliotransmission

20

Erin M. Leonard and Colin A. Nurse

Abstract

In mammals, cardiorespiratory reflexes originating in the carotid body (CB) help maintain homeostasis by matching oxygen supply to oxygen demand. CB output to the brainstem is shaped by synaptic interactions at a “tripartite synapse” consisting of chemosensory (type I) cells, abutting glial-like (type II) cells, and sensory (petrosal) nerve terminals. Type I cells are stimulated by several blood-borne metabolic stimuli, including the novel chemoexcitant lactate. During chemotransduction, type I cells depolarize and release a multitude of excitatory and inhibitory neurotransmitters/neuromodulators including ATP, dopamine (DA), histamine, and angiotensin II (ANG II). However, there is a growing appreciation that the type II cells may not be silent partners. Thus, similar to astrocytes at “tripartite synapses” in the CNS, type II cells may contribute to the afferent output by releasing “gliotransmitters” such as ATP. Here, we first consider whether type II cells can also sense lactate. Next, we review and update the evi-

dence supporting the roles of ATP, DA, histamine, and ANG II in cross talk among the three main CB cellular elements. Importantly, we consider how conventional excitatory and inhibitory pathways, together with gliotransmission, help to coordinate activity within this network and thereby modulate afferent firing frequency during chemotransduction.

Keywords

Carotid body · Lactate · Angiotensin II · Dopamine · Chemoreceptor Type I cells · Glial-like Type II cells · Petrosal neurons

20.1 Introduction

The mammalian carotid body (CB) is now viewed as a versatile metabolic sensor that initiates cardiorespiratory reflexes in response to changes in blood chemicals (Kumar and Prabhakar 2012). Stimulation of the CB by metabolic signals such as low O₂ (hypoxia), elevated CO₂/H⁺, acid hypercapnia, low glucose (hypoglycemia), and elevated lactate leads to an increase in CB sensory afferent discharge that is relayed to the brainstem and helps restore homeostasis (Kumar and Prabhakar 2012; Chang et al. 2015; Ortego-Sáenz and López-Barneo 2020; Iturriaga et al. 2021; Torres-Torrel et al. 2021). However, because CB hyperactivity can be maladaptive in

E. M. Leonard (✉)
Department of Biology, Wilfrid Laurier University,
Waterloo, Canada
e-mail: eleonard@wlu.ca

C. A. Nurse
Department of Biology, McMaster University,
Hamilton, ON, Canada

certain pathophysiological conditions such as cardiovascular disorders, e.g., congestive heart failure and hypertension (Fung 2014; Schultz et al. 2015; Zera et al. 2019; Iturriaga et al. 2021), there is a need for a mechanistic understanding of how sensory information is processed by the CB. While significant progress has been made in understanding the transduction pathways in chemoreceptor (type I or glomus) cells (reviewed in Buckler 2015; Ortego-Sáenz and López-Barneo 2020), elucidation of the role of neurotransmitters in synaptic integration has lagged behind (Nurse 2010, 2014; Leonard et al. 2018).

Morphologically, a rich vascular network aids in the delivery of chemical signals to the CB sensory apparatus comprising clusters of type I cells in synaptic contact with afferent (petrosal) nerve terminals and in intimate association with glial (type II) cells (Kumar and Prabhakar 2012). According to the classical paradigm, CB chemosensory signaling is dependent solely on synaptic transmission between presynaptic type I cells and postsynaptic petrosal nerve endings. However, the emerging view is that the type II cells may not be silent partners but, rather, active participants in the integrated CB sensory output (Tse et al. 2012; Nurse 2014). This role is similar to the one commonly accepted for glial cells of the CNS, where brain function is thought to depend on coordinated activity at a “tripartite synapse” comprising presynaptic, postsynaptic, and astrocytic glial cells (Eroglu and Barres 2010; Parpura et al. 2012). Our previous studies using a coculture model of the CB provided evidence for a “tripartite synapse” involving purinergic cross talk among type I cells, type II cells, and petrosal neurons during chemotransduction (Zhang et al. 2012; reviewed in Leonard et al. 2018). Here, we first consider whether or not in addition to type I cells, type II cells can also sense the novel CB chemoexcitant lactate, since they are known to express low levels of the lactate monocarboxylic transporter (MCT4). In addition, we update the evidence highlighting the pivotal role of excitatory and inhibitory pathways in helping to fine tune the integrated CB sensory output. We also review some of the evidence supporting the role of glial type II cells in shaping the neurotransmit-

ter pool at the sensory synapse during chemotransduction.

20.2 Methods

20.2.1 Cell Culture

Dissociated rat CB cells from juvenile (P9-P14) rats were cultured using established techniques (Zhang et al. 2012). Procedures for animal handling conformed to the guidelines of the Canadian Council on Animal Care (CCAC) and McMaster University’s Animal Research and Ethics Board. Excised CBs were cleaned of surrounding tissue, placed in an enzyme solution for 1 h, prior to mechanical dissociation in supplemented F-12 growth medium. Following trituration, the dissociated cells were plated into culture dishes and incubated in a humidified 95% air:-5% CO₂ atmosphere. For cocultures, dissociated neurons from P9-P14 rat petrosal ganglia were added to a preexisting monolayer of CB cells ~3 days later.

20.2.2 Fura-2 Ratiometric Ca²⁺ Imaging

Ratiometric intracellular Ca²⁺ measurements were obtained using established procedures (Murali et al. 2014; Leonard and Nurse 2020). Cell cultures were loaded with 2.5–5 μM fura-2 diluted in standard bicarbonate-buffered solution (BBS) for 20 min at 37 °C. The culture dish was placed on the stage of a Nikon inverted microscope and perfused with BBS bubbled with 95% air-5% CO₂ at 37 °C during recordings of intracellular Ca²⁺ responses.

20.2.3 Solutions and Drugs

The standard BBS contained (in mM) NaHCO₃, 24; NaCl, 115; glucose, 5; KCl, 5; CaCl₂, 2; and MgCl₂, 1, at 37 °C; the pH was kept at 7.4 by bubbling the solution with a 95% air-5% CO₂ gas mixture. For a hypoxic stimulus, the perfusate

was bubbled with a 95% N₂-5% CO₂ gas mixture (PO₂ ~ 15–20 mmHg); for hypercapnia, the perfusate was bubbled with a 10% CO₂ gas mixture.

20.3 Results

20.3.1 Selective Chemoexcitants for Carotid Body Type I Versus Type II Cells

It is well established that certain CB chemoexcitants such as low O₂ (hypoxia), high CO₂/H⁺ (acid hypercapnia), and high K⁺ (hyperkalemia) have direct effects on type I cells, leading to an elevation of intracellular Ca²⁺ via voltage-gated Ca²⁺ entry and neurotransmitter release (Buckler 2015; Kumar and Prabhakar 2012; Piskuric and Nurse 2013; Ortego-Sáenz and López-Barneo 2020). However, though type II (glial) cells do not respond directly to these stimuli, they may do so indirectly, due to cross talk from neighboring type I cells within chemoreceptor cell clusters (Tse et al. 2012; Murali and Nurse 2016; Leonard et al. 2018). More recently, lactate, considered a metabolic fuel as well as a signaling molecule, has been identified as a novel CB chemostimulus that increases ventilation by acting directly on type I cells (Chang et al. 2015; Torres-Torrelo et al. 2021). The first step in this signaling pathway involves transport of lactate into type I cells via monocarboxylic acid transporters (MCT2/4), expressed in type I cells (Torres-Torrelo et al. 2021). However, it is unknown whether lactate can also be sensed by type II cells, though they express low levels of MCT4 (Torres-Torrelo et al. 2021). Typically, isolated chemoreceptor cell clusters *in vitro* consist of type I cells and a smaller population of abutting type II cells (Zhang et al. 2012; Murali and Nurse 2016). Type II cells can be readily identified within these clusters since they uniquely express G-protein coupled P2Y2 receptors (P2Y2R) which can be selectively activated using the agonist UTP (Tse et al. 2012; Zhang et al. 2012). As illustrated in Fig. 20.1a, b, perfusion of CB cultures with lactate (5–10 mM) induced intracellular Ca²⁺ elevations in type I cells as expected, however,

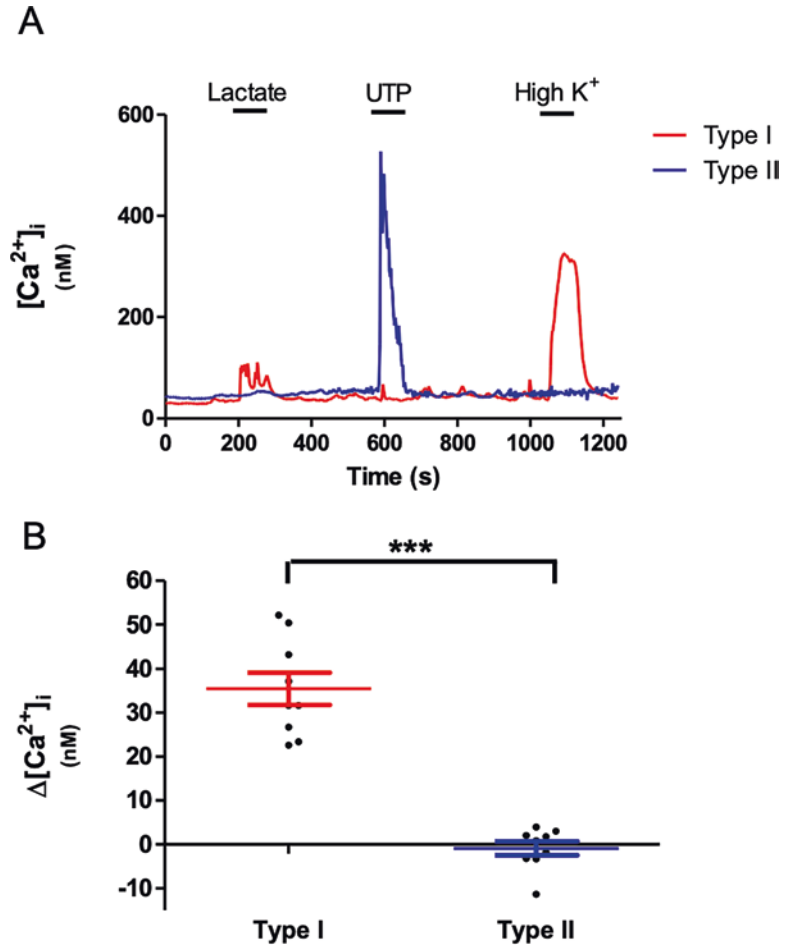
neighboring type II cells were unresponsive. These data confirm the sensitivity of CB type I cells to lactate (Torres-Torrelo et al. 2021), and suggest that the low expression of MCT4 in type II cells is unlikely to be associated with a signaling role.

20.3.2 Crosstalk from Type I to Type II Cells During Chemotransduction: Paracrine Roles for ATP and Angiotensin II

Glial cells are typically non-excitabile and commonly signal via intracellular Ca²⁺ elevations when stimulated by neurotransmitters at tripartite synapses (Parpura et al. 2012). Because type II glial cells express G-protein coupled receptors for several CB neurotransmitters and neuromodulators (reviewed in Leonard et al. 2018), the question arose whether these receptors become activated during chemotransduction. Here we briefly review the case for ATP which, when applied exogenously, elicits intracellular Ca²⁺ responses in type II cells via G-protein coupled P2Y2 receptors (Tse et al. 2012; Murali et al. 2014; Murali and Nurse 2016). Consistent with the role of ATP as a major CB excitatory neurotransmitter during chemotransduction (reviewed in Nurse 2014; Leonard et al. 2018), previous studies from this laboratory demonstrated that cross talk from type I to type II cells was inhibited following blockade of P2Y2 receptors (P2Y2R) on type II cells (with suramin) or degradation of extracellular ATP with apyrase (Murali and Nurse 2016). However, in the latter study, suramin had no effect on cross talk in ~10% of the cases, and the mean peak Ca²⁺ response in type II cells was reduced by ~84% in the presence of suramin. These data suggest other CB neurotransmitters or neuromodulators may contribute to cross talk, albeit to a lesser extent than ATP.

To address this possibility, we considered the potential role of the renin-angiotensin system (RAS) since it is expressed in CB type I cells and is significantly upregulated in conditions of

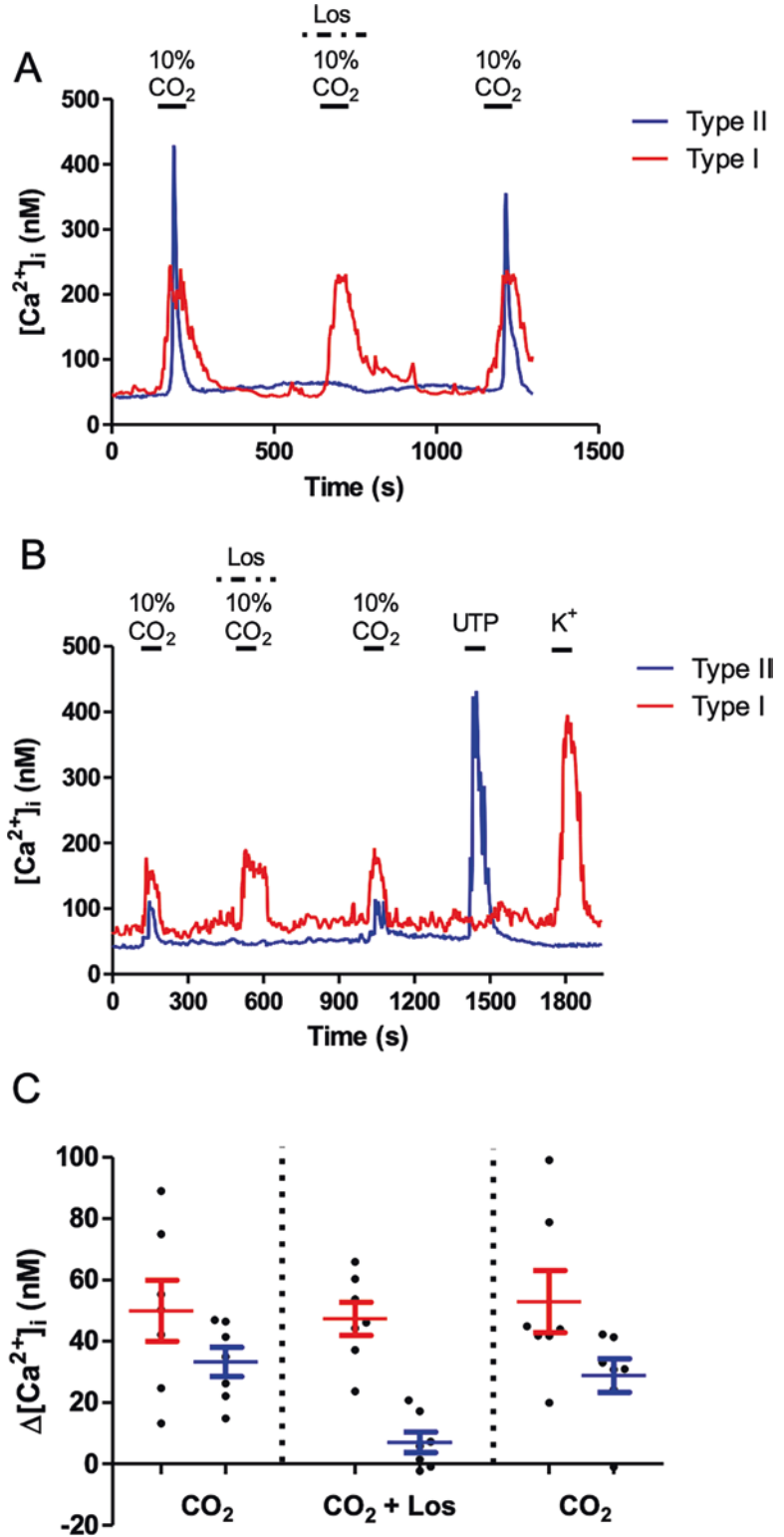
Fig. 20.1 Effects of lactate on intracellular Ca^{2+} responses in carotid body type I versus type II cells. (a) Example showing that application of 5 mM lactate causes a rise in intracellular Ca^{2+} in type I, but not type II, cells. Note, type I cells were identified by a Ca^{2+} response to high K^+ (30 mM) but not to the P2Y2R agonist UTP (100 μM); conversely, type II cells were identified by a Ca^{2+} response to UTP, but not high K^+ . (b) Summary data comparing the effects of lactate on the intracellular Ca^{2+} elevation in type I vs type II cells ($n = 9$ dishes; *** $p < 0.0001$). (Unpublished data from S. Murali and C.A. Nurse)



chronic hypoxia (Fung 2014). Moreover, type II cells were previously shown to be exquisitely sensitive to angiotensin II (ANG II), which interacted with G-protein coupled AT1 receptors (AT1R) to generate robust intracellular Ca^{2+} elevations with an EC_{50} of ~ 8 nM (Tse et al. 2012; Murali et al. 2014). As exemplified in Fig. 20.2a, we encountered a few cases where blockade of AT1 receptors with losartan reversibly inhibited type I to type II cross talk during application of high CO_2 in CB cultures grown under normoxic conditions. In order to optimize the potential for ANG II-AT1R cross talk, CB cultures were exposed to chronic hypoxia (2% O_2) for ~ 48 h. In one experimental series illustrated in Fig. 20.2b–c, losartan caused a similar inhibition of type I to type II

cross talk during application of high CO_2 . Note in Fig. 20.2a–b that high CO_2 triggered intracellular Ca^{2+} elevations in the type I cells, followed by delayed or indirect Ca^{2+} responses in the type II cells. In the presence of losartan (1 μM), the delayed type II cell responses were strongly inhibited, whereas the type I cell responses were largely unaffected (Fig. 20.2a, b). These data suggest that ANG II, released from type I cells during application of high CO_2 , was sufficient to activate nearby type II cells by a paracrine mechanism. Given that type I cells also express excitatory AT1R (Fung et al. 2001; Murali et al. 2014), it appears that in these cases any potential autocrine or paracrine actions of ANG II on type I cells within the cell cluster were negligible.

Fig. 20.2 Effects of the AT1 receptor antagonist, losartan, on cross talk between type I and type II cells during hypercapnia. In a normoxic CB culture (a), hypercapnia (10% CO₂) caused an intracellular Ca²⁺ elevation in a type I cell and a delayed Ca²⁺ response in a "follower" type II cell, identified by sensitivity to UTP. This type I to type II cross talk was reversibly inhibited in the presence of the angiotensin II receptor (AT1R) blocker, losartan (los; 1 μM). In (b), (c), losartan caused a similar inhibition of type I to type II cross talk in CB cultures exposed to chronic hypoxia (Chox; 2% O₂) for 48 h to enhance angiotensin II AT1R signaling. Note that while the type II cell responses were abolished in (a), (b), the type I cell responses were unaffected. Summary data from Chox experiments (n = 7) are shown in (c); in some cases, residual type II cell Ca²⁺ responses persisted in the presence of losartan. (Unpublished data from E.M. Leonard, S. Murali and C.A. Nurse)



20.3.3 Inhibitory Roles of Dopamine and Histamine in Type I to Type II Cross Talk

Dopamine (DA) is the best characterized inhibitory CB neurotransmitter that is released during chemoexcitation (Kumar and Prabhakar 2012; Ortego-Sáenz and López-Barneo 2020). In addition to its presynaptic and postsynaptic inhibitory functions (reviewed in Leonard et al. 2018; Ortego-Sáenz and López-Barneo 2020), recent evidence suggests DA may also inhibit cross talk from type I to type II cells (Leonard and Nurse 2020). For example, in some cases, cross talk during hypoxia or hypercapnia was potentiated in the presence of the D2 receptor antagonist, sulpiride (10 μ M) (Fig. 20.3a, b).

In Fig. 20.3a, hypoxia, when applied alone, evoked an intracellular Ca^{2+} response in the type I cell, accompanied by a negligible or weak Ca^{2+} response in a neighboring type II cell. However, in the presence of sulpiride, the same hypoxic stimulus evoked a dramatic increase in the type II cell intracellular Ca^{2+} response (Fig. 20.3a). These data suggest that DA released during chemotransduction may inhibit type I to type II cross talk via paracrine activation of D2-like receptors (D2R). The mechanism appears to involve cross inhibition between G-protein coupled D2R and P2Y2R signaling pathways in type II cells following co-activation by released DA and ATP, respectively. This posit is supported by the following observations: (i) the frequency and magnitude of cross talk events recorded in type II cells were enhanced in the presence of sulpiride or following DA depletion using reserpine; (ii) the intracellular Ca^{2+} responses in type II cells evoked by the P2Y2R agonist UTP were inhibited during co-application with DA; and (iii) this inhibition was reversed when sulpiride was also present (Leonard and Nurse 2020).

However, less well-studied histamine, which is released from the carotid body during acute hypoxia (Koerner et al. 2004), may also be involved in cross inhibition, at least in a subpopulation (~18%) of type II cells (Nurse et al. 2018). As exemplified in Fig. 20.3c, d, exogenous histamine may inhibit intracellular Ca^{2+} elevations

evoked by UTP in some type II cells, though the underlying histamine receptor subtype remains to be determined. The notion that such inhibitory pathways may be restricted to subgroups of type I/II cell clusters is of interest in the context of the “ribbon cable” hypothesis proposed to explain how specific reflex components of the CB chemoreflex become activated depending on the stimulus type (Zera et al. 2019).

20.3.4 Evidence for ATP as a Type II Cell “Gliotransmitter”

Glial cells in the CNS typically release “gliotransmitters” such as ATP, glutamate, and GABA in response to elevations in intracellular Ca^{2+} (Eroglu and Barres 2010; Parpura et al. 2012). To explore the role of gliotransmission in the CB, we reconstructed “tripartite synapses” in vitro using a coculture model of isolated chemoreceptor (type I/type II) cell clusters and juxtaposed sensory (petrosal) neurons (Zhang et al. 2012; Leonard and Nurse 2020). Our previous studies demonstrated that selective stimulation of type II cells in such cocultures using the P2Y2R agonist UTP sometimes led to membrane depolarization and excitation of nearby petrosal neurons (Zhang et al. 2012). This excitation was attributable to the delayed release of the gliotransmitter ATP from type II cells followed by stimulation of ATP-sensitive (but UTP-insensitive) ionotropic P2X2/3 receptors expressed in petrosal neurons, since it was sensitive to P2X2/3R blockers. Further, in similar cocultures, UTP induced a rapid increase in intracellular Ca^{2+} in type II cells, followed by a delayed Ca^{2+} response in nearby petrosal neurons (Leonard and Nurse 2020), as exemplified in Fig. 20.4b.

Similarly, we attribute the latter response to the release of ATP from type II cells followed by stimulation of nearby petrosal P2X2/3 receptors. The following observations, together with inhibitory effect of P2X2/3 receptor blockers described above, support a model for ATP acting as a CB gliotransmitter. First, UTP activated an inward current in type II cells that was inhibited by ATP-permeable pannexin-1 (Panx-1) channel

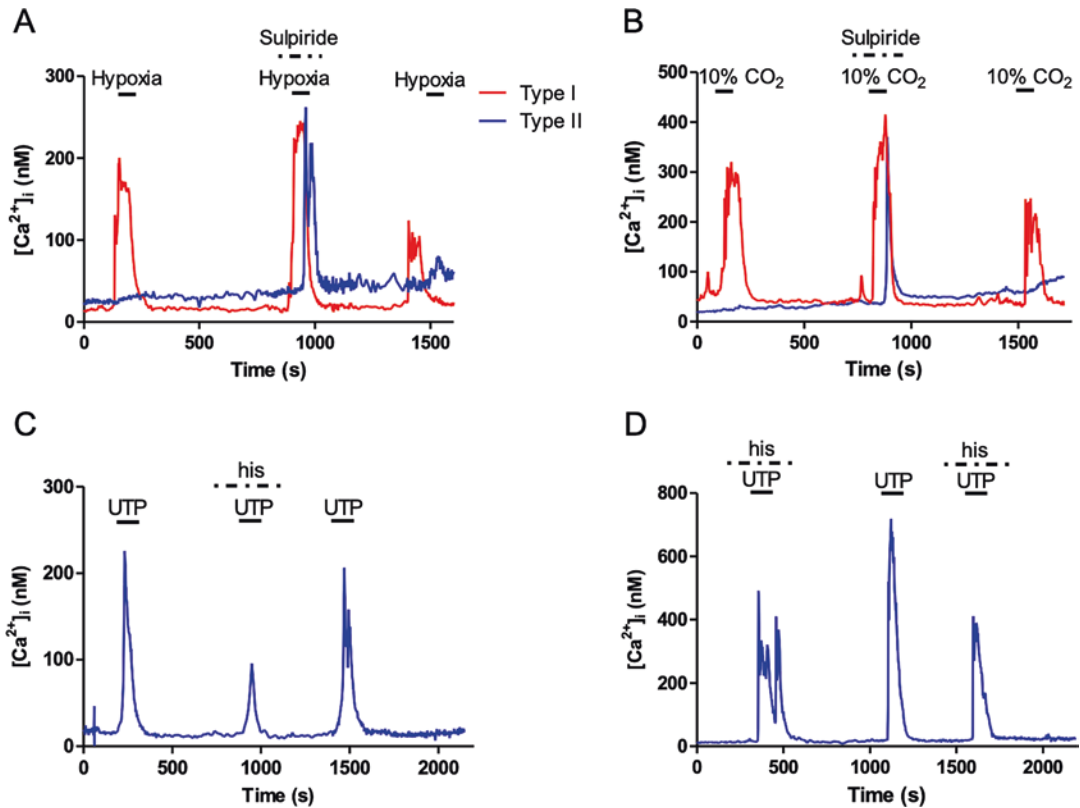


Fig. 20.3 Dopaminergic inhibition of type I to type II cross talk during chemotransduction and histaminergic inhibition of purinergic signaling in type II cells. In (a), hypoxia elicited an intracellular Ca^{2+} elevation in a type I cell, but a negligible Ca^{2+} response in a neighboring type II cell. However, when the D2 receptor antagonist, sulpiride (10 μM), was present, there was a dramatic potentiation of the Ca^{2+} response in the same type II cell. In (b),

a similar pattern was observed in a different type I/type II cell pair during application of a hypercapnic (10% CO_2) stimulus. In (c), (d), exogenous histamine (his; 10 μM) reversibly inhibited the excitatory effects of UTP (acting via P2Y2R; 100 μM) on type II cells, regardless of the sequence of application of the two agents. (Data in (c), (d), from Nurse et al. 2018)

blockers, i.e., 10Panx peptide and carbenoxolone (Zhang et al. 2012; Murali et al. 2014, 2017). Second, this inward current was also sensitive to chelation of intracellular Ca^{2+} with BAPTA (Murali et al. 2014, 2017), suggesting a link to P2Y2R-mediated intracellular Ca^{2+} elevations in type II cells. Third, the UTP-induced depolarization of petrosal neurons in coculture was inhibited by blockers of Panx-1 channels (Zhang et al. 2012). Taken together, these experiments provided the basis for a model whereby type II cells act as an amplifier of the excitatory neurotransmitter ATP during chemotransduction, via the mechanism of “ATP-induced ATP release”

(Zhang et al. 2012; Leonard et al. 2018). Accordingly, ATP released from type I cells would lead to paracrine stimulation of P2Y2R on nearby type II cells, followed by the Ca^{2+} -dependent recruitment of ATP-permeable Panx-1 channels coupled to the further release of ATP.

In the above scenario, the effect of gliotransmission at the CB tripartite synapse (Fig. 20.4a) is to modulate sensory transmission postsynaptically. However, presynaptic modulation of type I cell function is also possible. For example, as exemplified in Fig. 20.4b, stimulation of type II cells with UTP can also lead to intracellular Ca^{2+} elevations in neighboring type I cells (Murali and

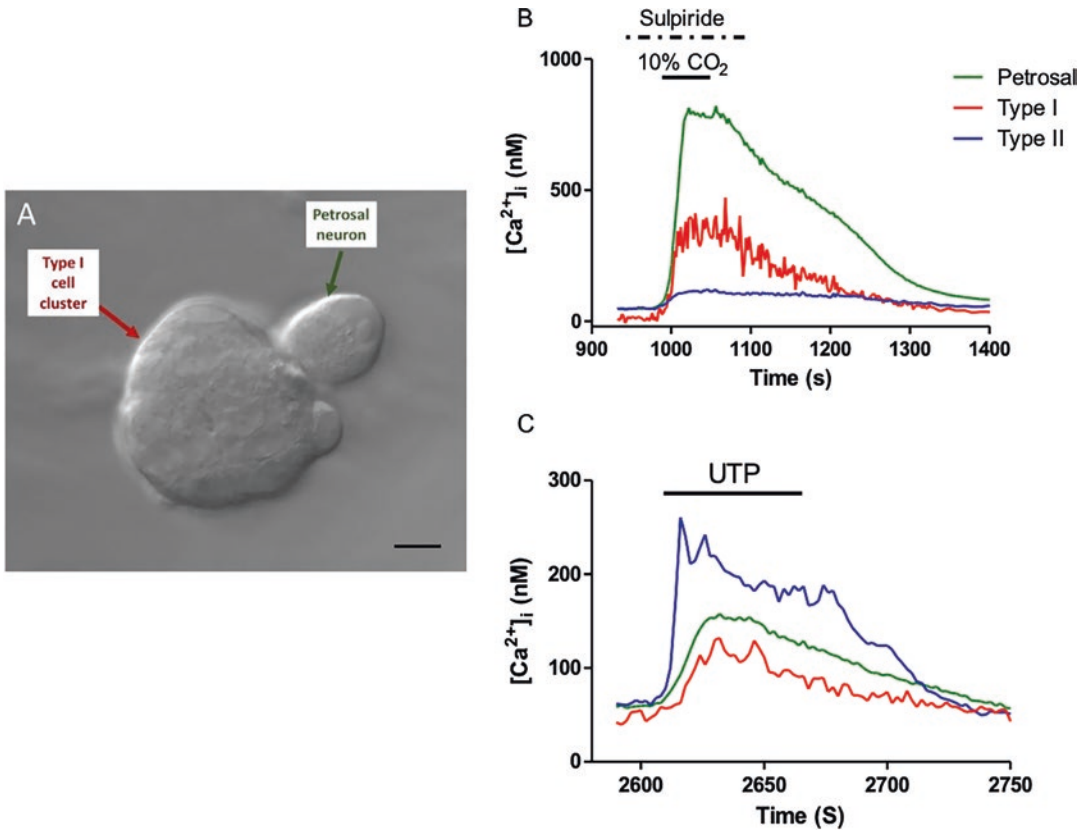


Fig. 20.4 Synaptic interactions and gliotransmission at the carotid body “tripartite synapse” in coculture. In cocultures of carotid body chemoreceptor (type I/type II) cell clusters and adjacent petrosal neurons (PN), intracellular Ca^{2+} transients were monitored in all three cell types simultaneously. (a) Typical DIC image of a coculture showing a petrosal neuron adjacent to a type I/type II cell cluster. (b) An example where application of a hypercapnic (10% CO_2) stimulus elicited an intracellular Ca^{2+} elevation in a type I cell, followed by Ca^{2+} elevations in both

the adjacent PN and a type II cell; in this example, sulpiride was present to suppress DA inhibition. In a different coculture (c), selective stimulation of type II cells using the P2Y2R agonist UTP (100 μM) led to “follower” responses in both the PN and a type I cell that were dependent on the release of the “gliotransmitter” ATP from type II cells via pannexin-1 channels (reviewed in Leonard et al. 2018). Scale bar in A = 10 μm . (Data in (c); adapted from Leonard and Nurse 2020)

Nurse 2016; Leonard and Nurse 2020). These presynaptic responses are further delayed, relative to the postsynaptic responses in petrosal neurons, because they are attributable to two time-dependent processes: (i) the enzymatic and extracellular breakdown of ATP, released from type II cells, to adenosine via a series of nucleotidases (Murali and Nurse 2016; Leonard et al. 2018) and (ii) the effect of adenosine on G-protein coupled A2a receptors on type II cells, leading to membrane depolarization and voltage-gated Ca^{2+} entry (Tse et al. 2012; Murali and Nurse 2016). Additionally, adenosine generated in this way

may also act postsynaptically on A2a receptors to enhance petrosal firing frequency via regulation of HCN cation channels (Zhang et al. 2018).

20.4 Discussion

In this paper, we review and update the evidence supporting the role of carotid body (CB) cells, i.e., chemoreceptor type I and glial type II cells, and their neurotransmitter output in shaping the integrated sensory output during chemotransduction. First, we confirm that the novel chemoexci-

tant lactate is sensed by type I cells (Torres-Torrelo et al. 2021); however, we further show that type II cells are unresponsive to lactate. Second, we discuss how excitatory neurotransmitters and neuro-modulators, such as ATP and angiotensin II, influence intracellular Ca^{2+} signaling in type II cells as a consequence of cross talk from neighboring type I cells. Third, we discuss how inhibitory type I cell neurotransmitters, such as dopamine (DA) and histamine (His), can regulate purinergic cross talk from type I to type II cells. Fourth, using the coculture model of the CB, consisting of type I/type II cell clusters and neighboring sensory (petrosal) neurons, we discuss the role of the “tripartite synapse” in determining the final CB sensory output, including the potential contribution of the “gliotransmitter” ATP, released from type II cells. In this model, the excitatory neurotransmitter ATP, released from type I cells during chemotransduction, activates P2Y2R in neighboring type II cells, leading to Ca^{2+} -dependent opening of ATP-permeable pannexin I (Panx-1) channels and the further release of ATP (Nurse 2014; Nurse et al. 2018; Leonard et al. 2018). Interestingly, other CB neurotransmitters and neurotransmitters such as ACh, 5-HT, and ET-1 are also capable of eliciting a rise in intracellular Ca^{2+} and activation of Panx-1 channels in type II cells via G-protein coupled signaling pathways (Murali et al. 2014; Leonard et al. 2018). Thus, it is likely that these pathways also lead to ATP release from type II cells and therefore purinergic regulation of the tripartite synapse. There is emerging evidence that glutamate, acting at both ionotropic and metabotropic receptors, also plays a role in CB chemoreception (Li et al. 2020, 2021); however, further studies are required to determine whether glutamate can affect Ca^{2+} signaling in type II cells. Of note, in another chemosensory organ, i.e., the taste bud, purinergic signaling and gliotransmission at a “tripartite synapse” have recently been proposed to regulate afferent firing during taste transduction (Rodriguez et al. 2012).

It is noteworthy that during chemoexcitation by both hypoxia and hypercapnia, purinergic type I to type II cross talk is strongly counteracted by concurrent DA-mediated inhibition

(Fig. 20.3a, b; Leonard and Nurse 2020). Consequently, some type II cells that did not respond initially to the chemostimulus showed a dramatic elevation in intracellular Ca^{2+} in the presence of sulpiride, a D2R antagonist. These, and other supporting data, suggest that during chemotransduction, type I cells release ATP and DA which have antagonist actions on Ca^{2+} signaling in nearby type II cells via P2Y2R and D2R, respectively (Leonard and Nurse 2020). Similarly, histamine appears to have a similar inhibitory action as DA, at least in a subpopulation of type II cells. It remains to be determined whether other inhibitory CB neurotransmitters, e.g., GABA, can similarly modulate type I to type II cross talk.

A new finding was the demonstration that angiotensin II (ANG II) can mediate cross talk from type I to type II cells during hypercapnia. This was more readily seen in CB cultures exposed to chronic hypoxia, a condition known to upregulate the renin angiotensin system (RAS) in CB type I cells during whole animal exposure in vivo (Fung 2014). In successful cases, hypercapnia caused a rapid rise in intracellular Ca^{2+} in type I cells followed by a delayed rise in neighboring type II cells due to cross talk. Interestingly, the type II cell responses were abolished or markedly inhibited by the AT1R blocker, losartan. By contrast, the type I cell responses were unaffected even though they express functional AT1R (Fung 2014; Fung et al. 2001; Murali et al. 2014). This is consistent with previous observations that type II cell Ca^{2+} responses to exogenous ANG II occurred more frequently and were more robust than type I cell responses (Murali et al. 2014). These data raise the possibility that in pathological conditions known to increase circulatory levels of ANG II, e.g., obstructive sleep apnea and congestive heart failure (Fung 2014; Schultz et al. 2015), the CB chemoreflex may become activated by direct stimulation of type II cells which display nanomolar sensitivity to ANG II (Murali et al. 2014). Other type I cell neurotransmitters such as endothelin-1 and 5-HT can also function as circulatory hormones. These may also directly stimulate type II cells acting alone or in combination with ANG II (Murali et al.

2017; Leonard and Nurse 2020). Thus, a broad repertoire of neurotransmitters and neuromodulators may act on multiple receptors at the CB tripartite synapse, providing a finely tuned network for regulating synaptic transmission in both normal and pathophysiological conditions.


Acknowledgments This work was supported by an operating grant from the Canadian Institutes of Health Research (CIHR) to C.A.N. and a NSERC Discovery Grant to E.M.L. (05466). We thank Sindy Murali for contributions to Figs. 20.1 and 20.2.

References

- Buckler KJ (2015) TASK channels in arterial chemoreceptors and their role in oxygen and acid sensing. *Pflugers Archiv Eur J Physiol* 467(5):1013–1025
- Chang AJ, Ortega FE, Riegle J et al (2015) Oxygen regulation of breathing through an olfactory receptor activated by lactate. *Nature* 527:240–244
- Eroglu C, Barres BA (2010) Regulation of synaptic connectivity by glia. *Nature* 468(7321):223–231
- Fung M-L (2014) The role of local renin-angiotensin system in arterial chemoreceptors in sleep-disordered breathing disorders. *Front Physiol* 5:336
- Fung M-L, Lam S-Y, Chen Y, Dong X, Leung PS (2001) Functional expression of angiotensin II receptors in type-I cells of the rat carotid body. *Pflugers Arch* 441(4):474–480
- Iturriaga R, Alcayaga J, Chappelle MW et al (2021) Carotid body chemoreceptors: physiology, pathology, and implications for health and disease. *Physiol Rev* 101(3):1177–1235
- Koerner P, Hesslinger C, Schaefermeyer A et al (2004) Evidence for histamine as a transmitter in rat carotid body sensor cells. *J Neurochem* 91(2):493–500
- Kumar P, Prabhakar NR (2012) Peripheral chemoreceptors: function and plasticity of the carotid body. *Compr Physiol* 2(1):141–219
- Leonard EM, Nurse CA (2020) Expanding role of dopaminergic inhibition in hypercapnic responses of cultured rat carotid body cells: involvement of type II glial cells. *Int J Mol Sci* 21:5434
- Leonard EM, Salman S, Nurse CA (2018) Sensory processing and integration at the carotid body tripartite Synapse: Neurotransmitter Functions and Effects of Chronic Hypoxia. *Front Physiol* 9. <https://doi.org/10.3389/fphys.2018.00225>
- Li C, Huang L, Jia X et al (2020) Functional glutamate receptors are expressed in the carotid chemoreceptor. *Respir Res* 21:208
- Li C, Zhao B, Zhao C et al (2021) Metabotropic glutamate receptors I regulates rat carotid body response to acute hypoxia via presynaptic mechanism. *Front Neurosci* 15:741214
- Murali S, Nurse CA (2016) Purinergic signalling mediates bidirectional crosstalk between chemoreceptor type I and glial-like type II cells of the rat carotid body. *J Physiol* 594(2):391–406
- Murali S, Zhang M, Nurse CA (2014) Angiotensin II mobilizes intracellular calcium and activates pannexin-1 channels in rat carotid body type II cells via AT1 receptors. *J Physiol* 592(21):4747–4762
- Murali S, Zhang M, Nurse CA (2017) Evidence that 5-HT stimulates intracellular Ca²⁺ signalling and activates pannexin-1 currents in type II cells of the rat carotid body. *J Physiol* 595(13):4261–4277
- Nurse CA (2010) Neurotransmitter and neuromodulatory mechanisms at peripheral arterial chemoreceptors. *Exp Physiol* 95(6):657–667
- Nurse CA (2014) Synaptic and paracrine mechanisms at carotid body arterial chemoreceptors. *J Physiol* 592(16):3419–3426
- Nurse CA, Leonard EM, Salman S (2018) Role of glial-like type II cells as paracrine modulators of carotid body chemotransmission. *Physiol Genomics* 50(4):255–262
- Ortego-Sáenz P, López-Barneo J (2020) Physiology of the carotid body: from molecules to disease. *Annu Rev Physiol* 82:127–149
- Parpura V, Heneka MT, Montana V et al (2012) Glial cells in (patho) physiology. *J Neurochem* 121(1):4–27
- Piskuric NA, Nurse CA (2013) Expanding role of ATP as a versatile messenger at carotid and aortic body chemoreceptors. *J Physiol* 591(2):415–422
- Rodriguez YA, Roebber JK, Dvoryanchikov G et al (2012) “Tripartite synapses” in taste buds: a role for type I glial-like taste cells. *J Neurosci* 41(48):9860–9871
- Schultz HD, Marcus NJ, Del Rio R (2015) Mechanisms of carotid body chemoreflex dysfunction during heart failure. *Exp Physiol* 100(2):124–129
- Torres-Torrel H, Ortega-Saenz P, Gao L et al (2021) Lactate sensing mechanisms in arterial chemoreceptor cells. *Nat Commun* 12:4166
- Tse A, Yan L, Lee AK et al (2012) Autocrine and paracrine actions of ATP in rat carotid body. *Can J Physiol Pharmacol* 90(6):705–711
- Zera T, Moraes DVA, da Silva MP et al (2019) The logic of carotid body connectivity to the brain. *Physiology* 43:264–282
- Zhang M, Piskuric NA, Vollmer C et al (2012) P2Y2 receptor activation opens pannexin-1 channels in rat carotid body type II cells: potential role in amplifying the neurotransmitter ATP. *J Physiol* 590(17):4335–4350
- Zhang M, Vollmer C, Nurse CA (2018) Adenosine and dopamine oppositely modulate a hyperpolarization-activated current I_h in chemosensory neurons of the rat carotid body in co-culture. *J Physiol* 596(15):3101–3117



Carotid Body-Mediated Chemoreflex Function in Aging and the Role of Receptor-Interacting Protein Kinase

Esteban Díaz-Jara, Karla G. Schwarz, Angelica Ríos-Gallardo, Camilo Toledo, Julio A. Alcayaga, Felipe A. Court, and Rodrigo Del Rio 

Abstract

Ventilatory impairment during aging has been linked to carotid body (CB) dysfunction. Anatomical/morphological studies evidenced CB degeneration and reductions in the number of CB chemoreceptor cells during aging. The mechanism(s) related to CB degeneration in

aging remains elusive. Programmed cell death encompasses both apoptosis and necroptosis. Interestingly, necroptosis can be driven by molecular pathways related to low-grade inflammation, one hallmark of the aging process. Accordingly, we hypothesized that necrotic cell death dependent on receptor-interacting protein kinase-3 (RIPK3) may contribute, at least in part, to impair CB function during aging. Adult (3 months) and aged (24 months) wild type (WT) and RIPK3^{-/-} mice were used to study chemoreflex function. Aging results in significant reductions in both the hypoxic (HVR) and hypercapnic ventilatory responses (HCVR). Adult RIPK3^{-/-} mice showed normal HVR and HCVR compared to adult WT mice. Remarkable, aged RIPK3^{-/-} mice displayed no reductions in HVR nor in HCVR. Indeed, chemoreflex responses obtained in aged RIPK3^{-/-} KO mice were undistinguishable from the ones obtained in adult WT mice. Lastly, we found high prevalence of breathing disorders during aging and this was absent in aged RIPK3^{-/-} mice. Together our results support a role for RIPK3-mediated necroptosis in CB dysfunction during aging.

E. Díaz-Jara · K. G. Schwarz · C. Toledo
Laboratory of Cardiorespiratory Control, Pontificia Universidad Católica de Chile, Santiago, Chile

A. Ríos-Gallardo · R. Del Rio (✉)
Laboratory of Cardiorespiratory Control, Pontificia Universidad Católica de Chile, Santiago, Chile

Centro de Excelencia en Biomedicina de Magallanes (CEBIMA), Universidad de Magallanes, Punta Arenas, Chile
e-mail: rdelrio@bio.puc.cl

J. A. Alcayaga
Laboratorio de Fisiología Celular, Facultad de Ciencias, Universidad de Chile, Santiago, Chile

F. A. Court
Center for Integrative Biology, Faculty of Sciences, Universidad Mayor, Santiago, Chile

FONDAP Geroscience Center for Brain Health and Metabolism, Santiago, Chile

Buck Institute for Research on Aging, Novato, USA

Keywords

Carotid body · Hypoxia · RIPK3 · Aging · Necroptosis

21.1 Introduction

Aging is a natural process characterized by a chronic, low-grade inflammation and reduction in physiological functions, which represents the primary risk factor in the pathogenesis of multiple diseases (Kennedy et al. 2014). Indeed, gradual decline in cardiorespiratory function associated with the loss of precise arterial gases sensing by chemoreceptors and progressive deteriorations in the structure and function of the heart are hallmarks of aging (Chan and Welsh 1998; Chiao and Rabinovitch 2015; Knapowski et al. 2002; Sorbini et al. 1968). Moreover, evidence shows that elderly display reduced ventilatory responses to both hypercapnia and hypoxia (Peterson et al. 1981), high apnea-hypopnea index and arrhythmia index compared to younger subjects (Arnardottir et al. 2016; Curtis et al. 2018). Importantly, alterations in the arterial PO₂ sensing during aging is a matter of growing interest due to the high incidence of cardiorespiratory disorders. However, the precise molecular mechanisms involved in the loss of O₂ sensing during aging are not known.

The carotid body (CB), located in the bifurcation of the common carotid artery, is the main O₂ sensor (Iturriaga et al. 2021). Sensory transduction in the CB is a cell-autonomous process performed by oxygen-sensitive cells (glomus cells) that generate a neurosecretory response (i.e. catecholamine release) under acute hypoxemia and hypercapnia. Activation of CB increases neural discharge toward brainstem cardiorespiratory nuclei to elicit reflex hyperventilation and secondary modulation of cardiac autonomic function (Iturriaga et al. 2021).

Aging causes marked changes in CB morphology and function (Di Giulio et al. 2003) and reduces CB catecholamine release in response to hypoxic stimulus (Conde et al. 2006). Indeed, histological studies showed significant increase of connective tissue within the CB tissue in elderly

subjects compared to young ones (Hurst et al. 1985). Furthermore, a reduction in neurotransmitter content and loss of glomus cells have also been observed in aged animals (Conde et al. 2006). However, the precise molecular mechanisms that contribute to loss of CB function during aging have not been previously studied.

Inflammaging plays an important role in the underlying mechanisms of physiological and pathological aging (Royce et al. 2019) given the progressive increase of circulating proinflammatory cytokines, including tumor necrosis factor α (TNF α), interleukin 1 β (IL1 β), and IL (Ferrucci et al. 2005). Interestingly, necroptosis is an inflammatory cell death pathway associated with the release of damage-associated molecular patterns (DAMPs), which has been proposed as a main mechanism linked to the development of several age-related diseases (Pinti et al. 2014). One of the key activators of the necroptosis pathway is the receptor-interacting protein kinase-3 (RIPK3) (Royce et al. 2019; Wang et al. 2021). Indeed, it has been shown that loss of RIPK3 reduced the physiological consequences of necroptosis activation (Cao et al. 2022). However, the contribution of RIPK3 and necroptosis in CB function decline during aging has not been previously addressed. Accordingly, we aimed to determine whether the loss of RIPK3 during aging may improve chemoreflex/breathing function in aged mice.

21.2 Methodology**21.2.1 Animals**

Adult (3–6 months old) and aged (≥ 24 months old) C57BL6 wild-type (WT) mice and knockout RIPK3 mice (RIPK3^{-/-}) were used in this study. All experiments were performed in accordance with the National Institutes of Health (NIH) Guide for the Care and Use of Laboratory Animals. Experimental protocols were approved by the Bioethical Committee for Animal Experiments of the Universidad Mayor. All the animals were kept at controlled room temperature under a 12-h light/dark cycle with ad libitum access to food and water. At the end of the experiments, all animals

were humanely euthanized with sodium pentobarbital injection (100 mg/kg i.p.).

21.2.2 Breathing and Chemoreflex Function

Resting breathing (RB) and chemoreflex function were recorded using whole-body plethysmography (EMKA Technologies, France) in freely behaving mice. The recording chamber was flushed with input and output flow rates set at 0.75 ml/min. Ventilatory parameters as tidal volume (VT), respiratory frequency (Rf), and minute ventilation (VE: VT × Rf) were analyzed using ecgAUTO software (EMKA Technologies, France). Peripheral and central chemoreflex were evaluated by allowing the mice to breath hypoxic (FiO₂ 10%) and hypercapnic (FiCO₂ 7%) gas mixtures for 2 min. The hypercapnic ventilatory response (HCVR) and hypoxic ventilatory response (HVR) were obtained by calculating the slope of the VE gain and FiCO₂ 0.03% and 7% or FIO₂ 21% and 10%, respectively. For RB analysis, 1 h of recording was used to quantify apnea-hypopnea index. Apnea was defined as breathing cessation and hypopnea as reductions of VT > 50% for at least three continuous ventilatory cycles.

21.2.3 Statistical Analysis

Data is presented as mean ± standard error mean (SEM). Comparisons were evaluated using T-Student between group (adult and aged). The level of significance was set at $p < 0.05$. All the statistical analysis was performed with GraphPad Prism 7.0 software (La Jolla, USA).

21.3 Results

21.3.1 Resting Ventilatory Physiological Parameters

We found no differences in resting ventilatory variables in adult RIPK3^{-/-} mice and aged-matched WT mice. Indeed, values obtained in

VT, Rf, and VE in adult RIPK3^{-/-} mice were undistinguishable from the ones obtained in adult WT mice (Table 21.1). On the contrary, RIPK3^{-/-} aged mice displayed a higher resting ventilation compared to aged WT mice (Table 21.1).

21.3.2 Loss of RIPK3 Signaling Improves Peripheral and Central Chemoreflex Function in Aged Animals

We found no significant difference in the hypoxic ventilatory response (HVR) between adult RIPK3^{-/-} mice and adult WT animals (Fig. 21.1a, b). Contrarily, aged WT mice displayed a diminished peripheral chemoreflex drive compared to aged RIPK3^{-/-} animals (Fig. 21.1a, b) (0.99 ± 0.17 vs. 2.18 ± 0.49 ml/min/10 g, WT aged vs. RIPK3^{-/-} aged, respectively). Indeed, aged RIPK3^{-/-} mice showed similar peripheral chemoreflex drive values compared to adult WT mice (1.77 ± 0.7 vs. 2.18 ± 0.49 ml/min/10 g, WT adult vs. RIPK3^{-/-} aged, respectively) (Fig. 21.2a, b).

In addition, we found no difference in the central chemoreflex drive and hypercapnic ventilatory response (HVCR) between adult RIPK3^{-/-} and adult WT animals (Fig. 21.2a, b). However, aged RIPK3^{-/-} mice displayed no reductions in central chemoreflex drive compared to aged WT animals (Fig. 21.2a, b). Indeed, RIPK3^{-/-} aged mice showed a sixfold higher HCVR compared to aged WT mice (0.34 ± 0.27 vs. 2.03 ± 0.39 ml/min/10 g, WT aged vs. RIPK3^{-/-} aged, respectively). Accordingly, we found that aged RIPK3^{-/-} mice showed similar central chemoreflex responses compared to adult WT mice (1.70 ± 0.29 vs. 2.03 ± 0.39 ml/min/10 g, WT adult vs. RIPK3^{-/-} aged, respectively) (Fig. 21.2a, b).

21.3.3 Absence of RIPK3 Decreased the Incidence of Breathing Disorders in Aged Mice

We aimed to determine if RIPK3^{-/-} contributes to breathing disorders during aging. Interestingly, both adult and aged RIPK3^{-/-} mice display a

Table 21.1 Physiological ventilatory variables in adult and aged mice

	Sham		CBD	
	WT (<i>N</i> = 4)	RIPK3 ^{-/-} (<i>N</i> = 4)	WT (<i>N</i> = 4)	RIPK3 ^{-/-} (<i>N</i> = 4)
BW (g)	31.20 ± 1.93	34.79 ± 1.58	33.08 ± 1.03	35.41 ± 2.43
VT (ml/10 g)	0.02 ± 0.00	0.02 ± 0.00	0.03 ± 0.00	0.02 ± 0.00
Rf, breath/min	195.40 ± 43.18	209.58 ± 17.27	122.10 ± 14.23	195.80 ± 27.76*
VE (ml/min/10 g)	4.73 ± 0.49	5.29 ± 0.20	3.62 ± 0.09	4.57 ± 0.29*

Data is presented as mean ± SEM. BW body weight, VT tidal volume, RF respiratory frequency, VE minute volume. Unpaired T-test. **P* < 0.05 vs. WT

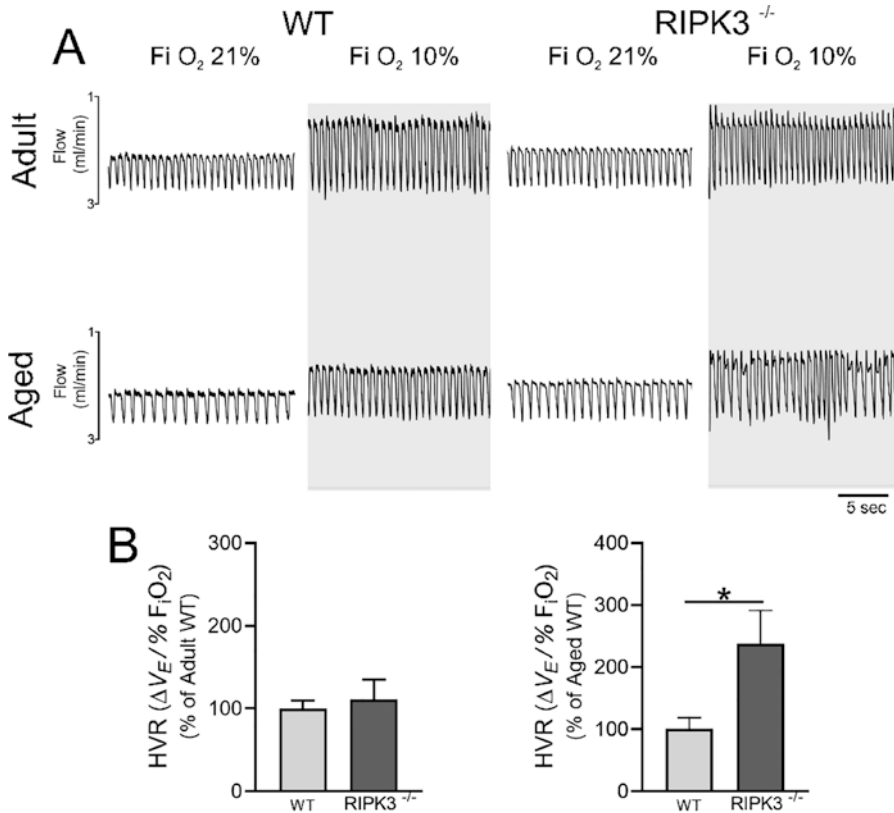


Fig. 21.1 Enhanced peripheral chemoreflex drive in aged RIPK3^{-/-} mice. (a) Representative recordings of ventilatory flow during gas challenges with normoxia (FiO₂ 21%, top panel) and hypoxia (FiO₂ 10%, bottom panel) obtained in one adult WT, aged WT, adult RIPK3^{-/-}, and aged

RIPK3^{-/-}. (b) Summary data showing changes in the gain of the hypoxic ventilatory response (HVR) normalized by WT group (adult or aged). Data is presented as mean ± SEM and analyzed by unpaired t-test, **p* < 0.05, *n* = 4 mice per group

lower incidence of hypopneas at rest compared to adult and aged WT mice (Fig. 21.3a). Indeed, compared to the aged WT group, aged RIPK3^{-/-} mice showed a significant decrease in the apnea hypopnea index (WT adult and aged with

9.75 ± 1.25 and 10.50 ± 1.22 events/h vs. RIPK3^{-/-} adult and aged mice with 4.00 ± 0.91 and 3.25 ± 0.62 events/h) (Fig. 21.3b). No changes were found in apnea/hypopnea duration nor in the total numbers of sigh between groups.

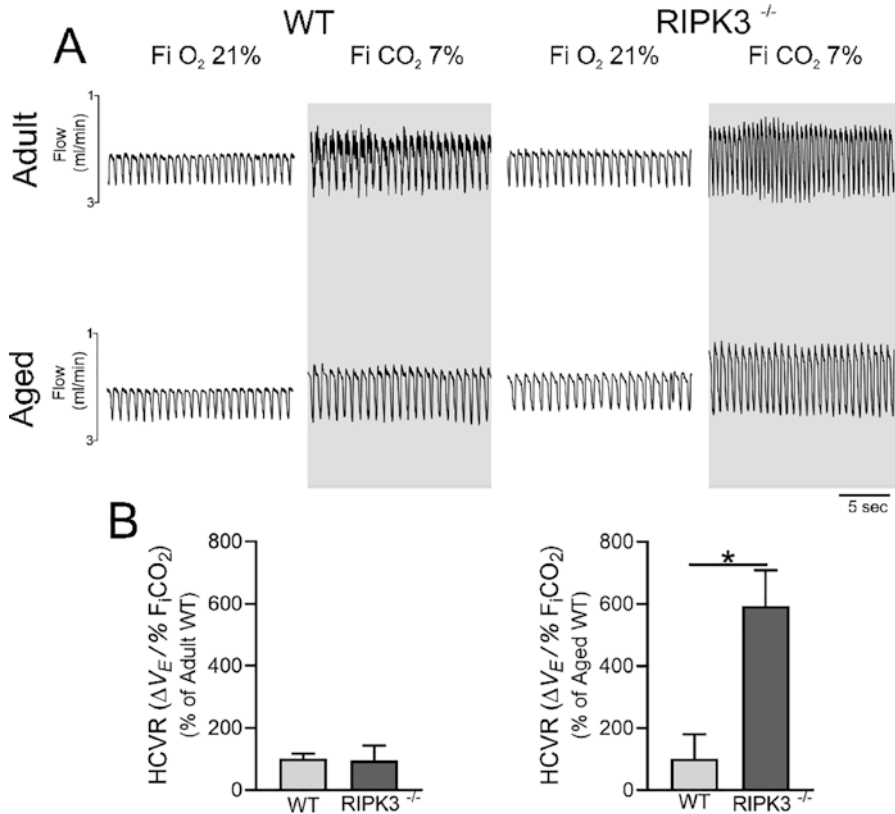


Fig. 21.2 Enhanced central chemoreflex drive in aged RIPK3^{-/-} mice. (a) Representative recordings of ventilatory flow during chemoreflex testing with normoxia (FiO₂ 21%, top panel) and hypercapnia (FiCO₂ 7%, bottom panel) obtained in one adult WT, aged WT, adult RIPK3^{-/-},

and aged RIPK3^{-/-}. (b) Summary data showing changes in the gain of the hypercapnic ventilatory response (HCVR) normalized by WT group (adult or aged). Data is presented as mean \pm SEM and analyzed by unpaired t-test, * $p < 0.05$, $n = 4$ mice per group

21.4 Discussion

The main aim of the present study was to determine the contribution of RIPK3, a key necroptosis mediator, on CB-mediated chemoreflex function during aging in mice. The major findings of this study were as follows: (i) RIPK3^{-/-} rescues chemoreflex in aged mice, and (ii) loss of RIPK3 signaling decreases the incidence of breathing disorders (i.e., apnea/hypopnea index) in both adult and aged mice. Together, these results suggest that RIPK3-mediated necroptosis contributes to the progressive decline in chemoreflex function during aging in mice.

Aging is an irreversible and inevitable physiological process that is characterized by time dependent cellular and functional decline, result-

ing in the deterioration of several physiological functions (Campisi et al. 2019). In this regard, aging is one of the main risk factors in the occurrence of many aging-related disorders, including neurodegenerative diseases, cardiovascular diseases, cancer, and other diseases (Kronenberg and Drage 1973). One of the main systems affected by aging is the cardiorespiratory system, mainly due to the gradual loss of ventilatory response to hypoxic challenge (Janssens et al. 1999; Peterson et al. 1981). The latter has also been linked to the increased frequency of obstructive sleep apnea in humans (Behan et al. 2002; Guénard and Marthan 1996). Some age-related deficits in cardiorespiratory regulation have been associated to a decline in the functionality of the CBs. Here we showed for the first time that

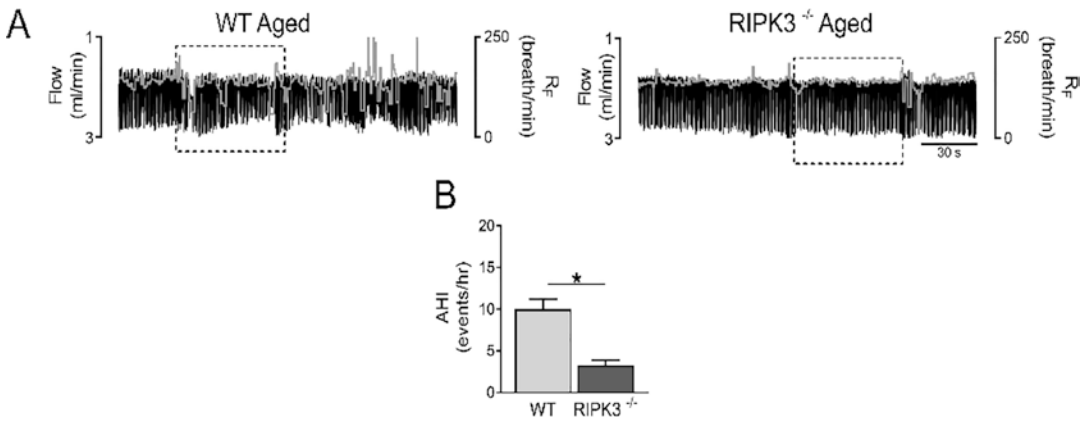


Fig. 21.3 Loss of RIPK3 blunts incidence of hypopneas in mice. (a) Representative traces of resting ventilatory flow and respiratory frequency from one aged WT and one aged RIPK3^{-/-} KO mice. Note that aged RIPK3^{-/-} KO

displays a regular breathing pattern compared with aged WT. (b) Summary data for AHI index. Data is presented as mean \pm SEM and analyzed by unpaired t-test, * $p < 0.05$, $n = 4$ mice per group

necroptosis, via RIPK3, is involved in the decline of CB function in aged mice. Indeed, our results showing that loss of RIPK3 signaling results in normal ventilatory response to hypoxia in aged mice compared to age-matched WT mice support the notion that RIPK3-mediated necroptosis is required to the decline in CB function in aging.

Our results confirm and extend previous reports showing a loss of HVR in aged rodents and are in line with reports showing decreased HVR also in humans. Interestingly, the latter has been associated with a loss of O₂ sensing cell within the CB tissue. Whether these declines in HRV during aging are a cause or consequence of cell death of CB chemoreceptor cells through necrosis remains to be determined. However, our results showing that RIPK3 KO aged mice display normal HVR compared to aged WT mice support the notion that RIPK2-mediated necroptosis is needed to decrease CB-mediated chemoreflex function in aging.

Contrarily to HVR, previous data obtained in humans indicate no changes in PCO₂ in older people compared to young subjects. Therefore, it could be suggested that the loss of HCVR during aging could be mediated, at least in part, to the loss-of-function of aged CBs. Therefore, it is possible to hypothesize that blunted HCVR in old mice may be related to degeneration of central chemoreceptor, degeneration of CB, or both.

Future studies are needed to fully determine the mechanism associated with reduced HCVR in aged mice.

In summary, our results show that RIPK3, the master regulator of necroptosis, contribute to the decline in CB-mediated chemoreflex function during aging. Also, we identified that loss of RIPK3 markedly reduced the incidence of breathing disorders. Together, our results support the notion that necroptosis may play a role in the alteration of breathing control during aging.

Acknowledgments This work was supported by Fondo de Desarrollo Científico y Tecnológico (FONDECYT #1220905) to RDR Geroscience Center for Brain Health and Metabolism, FONDAP-15150012, and FONDECYT #1150766 to FC. We thank Mr. Fidel Flores and Paulina Arias for their help in managing the animal facility.


References

- Arnardottir ES, Bjornsdottir E, Olafsdottir KA, Benediktsdottir B, Gislason T (2016) Obstructive sleep apnoea in the general population: highly prevalent but minimal symptoms. *Eur Respir J* 47(1):194–202. <https://doi.org/10.1183/13993003.01148-2015>
- Behan M, Zabka AG, Mitchell GS (2002) Age and gender effects on serotonin-dependent plasticity in respiratory motor control. *Respir Physiol Neurobiol* 131(1–2):65–77. [https://doi.org/10.1016/s1569-9048\(02\)00038-1](https://doi.org/10.1016/s1569-9048(02)00038-1)

- Campisi J, Kapahi P, Lithgow GJ, Melov S, Newman JC, Verdin E (2019) From discoveries in ageing research to therapeutics for healthy ageing. *Nature* 571(7764): 183–192. <https://doi.org/10.1038/s41586-019-1365-2>
- Cao J, Zhang J, Qian J, Wang X, Zhang W, Chen X (2022) Ca²⁺/calmodulin-dependent protein kinase II regulation by RIPK3 alleviates necroptosis in transverse arch constriction-induced heart failure. *Front Cardiovasc Med* 9:847362. <https://doi.org/10.3389/fcvm.2022.847362>
- Chan ED, Welsh CH (1998) Geriatric respiratory medicine. *Chest* 114(6):1704–1733. <https://doi.org/10.1378/chest.114.6.1704>
- Chiao YA, Rabinovitch PS (2015) The aging heart. *Cold Spring Harb Perspect Med* 5(9):a025148. <https://doi.org/10.1101/cshperspect.a025148>
- Conde SV, Obeso A, Rigual R, Monteiro EC, Gonzalez C (2006) Function of the rat carotid body chemoreceptors in ageing. *J Neurochem* 99(3):711–723. <https://doi.org/10.1111/j.1471-4159.2006.04094.x>
- Curtis AB, Karki R, Hattoum A, Sharma UC (2018) Arrhythmias in patients ≥80 years of age: pathophysiology, management, and outcomes. *J Am Coll Cardiol* 71(18):2041–2057. <https://doi.org/10.1016/j.jacc.2018.03.019>
- Di Giulio C, Cacchio M, Bianchi G, Rapino C, Di Ilio C (2003) Selected contribution: carotid body as a model for aging studies: is there a link between oxygen and aging? *J Appl Physiol* (Bethesda, Md.: 1985) 95(4):1755–1758. <https://doi.org/10.1152/jappphysiol.00406.2003>
- Ferrucci L, Corsi A, Lauretani F, Bandinelli S, Bartali B, Taub DD, Guralnik JM, Longo DL (2005) The origins of age-related proinflammatory state. *Blood* 105(6):2294–2299. <https://doi.org/10.1182/blood-2004-07-2599>
- Guénard H, Marthan R (1996) Pulmonary gas exchange in elderly subjects. *Eur Respir J* 9(12):2573–2577. <https://doi.org/10.1183/09031936.96.09122573>
- Hurst G, Heath D, Smith P (1985) Histological changes associated with ageing of the human carotid body. *J Pathol* 147(3):181–187. <https://doi.org/10.1002/path.1711470306>
- Iturriaga R, Alcayaga J, Chappelle MW, Somers VK (2021) Carotid body chemoreceptors: physiology, pathology, and implications for health and disease. *Physiol Rev* 101(3):1177–1235. <https://doi.org/10.1152/physrev.00039.2019>
- Janssens JP, Pache JC, Nicod LP (1999) Physiological changes in respiratory function associated with ageing. *Eur Respir J* 13(1):197–205. <https://doi.org/10.1034/j.1399-3003.1999.13a36.x>
- Kennedy BK, Berger SL, Brunet A, Campisi J, Cuervo AM, Epel ES, Franceschi C, Lithgow GJ, Morimoto RI, Pessin JE, Rando TA, Richardson A, Schadt EE, Wyss-Coray T, Sierra F (2014) Geroscience: linking aging to chronic disease. *Cell* 159(4):709–713. <https://doi.org/10.1016/j.cell.2014.10.039>
- Knapowski J, Wieczorowska-Tobis K, Witowski J (2002) Pathophysiology of ageing. *J Physiol Pharmacol* 53(2):135–146
- Kronenberg RS, Drage CW (1973) Attenuation of the ventilatory and heart rate responses to hypoxia and hypercapnia with aging in normal men. *J Clin Invest* 52(8):1812–1819. <https://doi.org/10.1172/JCI107363>
- Peterson DD, Pack AI, Silage DA, Fishman AP (1981) Effects of aging on ventilatory and occlusion pressure responses to hypoxia and hypercapnia. *Am Rev Respir Dis* 124(4):387–391. <https://doi.org/10.1164/arrd.1981.124.4.387>
- Pinti M, Cevenini E, Nasi M, De Biasi S, Salvioli S, Monti D, Benatti S, Gibellini L, Cotichini R, Stazi MA, Trenti T, Franceschi C, Cossarizza A (2014) Circulating mitochondrial DNA increases with age and is a familiar trait: implications for “inflammaging”. *Eur J Immunol* 44(5):1552–1562. <https://doi.org/10.1002/eji.201343921>
- Royce GH, Brown-Borg HM, Deepa SS (2019) The potential role of necroptosis in inflammaging and aging. *GeroScience* 41(6):795–811. <https://doi.org/10.1007/s11357-019-00131-w>
- Sorbini CA, Grassi V, Solinas E, Muiesan G (1968) Arterial oxygen tension in relation to age in healthy subjects. *Respiration* 25(1):3–13. <https://doi.org/10.1159/000192549>
- Wang L, Zhou L, Zhou Y, Liu L, Jiang W, Zhang H, Liu H (2021) Necroptosis in pulmonary diseases: a new therapeutic target. *Front Pharmacol* 2497. <https://doi.org/10.3389/fphar.2021.737129>



Chronic Metformin Administration Does Not Alter Carotid Sinus Nerve Activity in Control Rats

Joana F. Sacramento, Bernardete F. Melo, Jesus Prieto-Lloret, and Silvia V. Conde 

Abstract

Metformin is a glucose-lowering, insulin-sensitizing drug that is commonly used in the treatment of type 2 diabetes (T2D). In the last decade, the carotid body (CB) has been described as a metabolic sensor implicated in the regulation of glucose homeostasis, being CB dysfunction crucial for the development of metabolic diseases, such as T2D. Knowing that metformin could activate AMP-activated protein kinase (AMPK) and that AMPK has been described to have an important role in CB hypoxic chemotransduction, herein we have investigated the effect of chronic metformin administration on carotid sinus nerve (CSN) chemosensory activity in basal and hypoxic and hypercapnic conditions in control

animals. Experiments were performed in male Wistar rats subjected to 3 weeks of metformin (200 mg/kg) administration in the drinking water. The effect of chronic metformin administration was tested in spontaneous and hypoxic (0% and 5% O₂) and hypercapnic (10% CO₂) evoked CSN chemosensory activity. Metformin administration for 3 weeks did not modify the basal CSN chemosensory activity in control animals. Moreover, the CSN chemosensory response to intense and moderate hypoxia and hypercapnia was not altered by the chronic metformin administration. In conclusion, chronic metformin administration did not modify chemosensory activity in control animals.

Keywords

Carotid body · Carotid sinus nerve · Hypercapnia · Hypoxia · Metformin

J. F. Sacramento · B. F. Melo · S. V. Conde (✉)
iNOVA4Health, NOVA Medical School, Faculdade de Ciências Médicas, Universidade NOVA de Lisboa, Lisbon, Portugal
e-mail: silvia.conde@nms.unl.pt

J. Prieto-Lloret
NOVA Medical School/Faculdade de Ciências Médicas, NMSIFCM, Universidade Nova de Lisboa, Lisboa, Portugal

Instituto de Biología y Genética Molecular (IBGM), Consejo Superior de Investigaciones Científicas, Universidad de Valladolid, Valladolid, Spain

Departamento de Bioquímica, Biología Molecular y Fisiología, Universidad de Valladolid, Valladolid, Spain

22.1 Introduction

Metformin, a biguanide, is one of the most used oral glucose-lowering drugs in the treatment of type 2 diabetes (T2D) worldwide. This antidiabetic drug is used as first-line therapy for T2D in individuals that do not achieve a glycemic target despite lifestyle and diet interventions (Inzucchi et al. 2015). The antihyperglycemic action of

metformin is mainly due to the inhibition of liver gluconeogenesis, which leads to a decrease in liver glucose output (Shaw et al. 2005). Additionally, in skeletal muscle, metformin improves insulin sensitivity by promoting glucose uptake (McIntyre et al. 1991). At the cellular level, metformin acts primarily in mitochondria by inhibiting complex I of the mitochondrial electron transport chain, which leads to the suppression of ATP production and promotes AMP accumulation (Owen et al. 2000). Metformin is also recognized as an AMP-activated protein kinase (AMPK) activator (Zhou et al. 2001). AMPK is an energy sensor, and its activation by metformin could occur directly or due to AMP accumulation (Hawley et al. 2002). In insulin sensitive tissues, such as the muscle, adipose tissue, and liver, AMPK activation promotes insulin sensitivity (Entezari et al. 2022). Besides its role in glucose homeostasis and insulin sensitivity, AMPK could also have different functions. In the carotid body (CB), a peripheral chemoreceptor, AMPK induced an increase in the carotid sinus nerve (CSN) basal discharges and elicited transmembrane Ca^{2+} influx in CB type I cells (Evans et al. 2005; Wyatt et al. 2007). Moreover, AMPK inhibition attenuates the CSN activity in response to hypoxia (Wyatt et al. 2007).

In the last decade, the CB has also been described as a metabolic sensor involved in the genesis of metabolic disorders. In fact, several metabolic mediators, such as insulin (Ribeiro et al. 2013; Cracchiolo et al. 2019), glucagon-like peptide-1 (GLP-1) (Pauza et al. 2022), and leptin (Ribeiro et al. 2018; Caballero-Eraso et al. 2019), act on the CB. In accordance with the role of CB in the setting of metabolic diseases, its activity is augmented in prediabetes patients (Cunha-Guimaraes et al. 2020) and in prediabetes and T2D animal models (Ribeiro et al. 2013, 2018). Moreover, our group has demonstrated that the modulation of CB activity through the resection of its sensitive nerve, the CSN, or through its bio-electronic neuromodulation is capable of preventing and reversing dysmetabolic pathological features in prediabetes and T2D animal models (Ribeiro et al. 2013; Sacramento et al. 2017, 2018). Considering that the CB is involved in metabolic diseases and that AMPK is present in

the CB and is one of the mechanisms of metformin action, herein we investigated the effect of chronic administration of metformin on basal CSN chemosensory activity and in response to hypoxia and hypercapnia in control animals. We found that metformin consumption for 3 weeks in control animals did not modify CSN basal activity and the hypoxic and hypercapnic CB chemosensory activity.

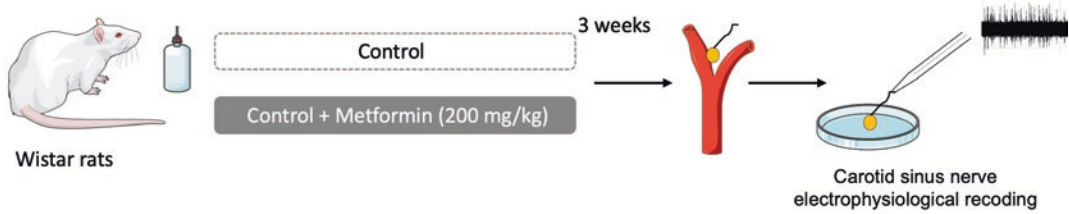
22.2 Methods

22.2.1 Ethical Approval

All animal experimental and care procedures were approved by the Ethics Committee of the NOVA Medical School-Faculdade de Ciências Médicas (NMSIFCM), Universidade Nova de Lisboa, NMS-FCM Animal Welfare Office (ORBEA), and Direcção-Geral de Veterinária (DGAV), Portugal. Principles of laboratory care were followed in accordance with the European Union Directive for Protection of Vertebrates Used for Experimental and Other Scientific Ends (2010/63/EU).

22.2.2 Animal Procedures

Experiments were performed in *Wistar* adult rats (300–380 g) obtained from *vivarium* of the NOVA Medical School-Faculdade de Ciências Médicas (NMS-FCM), Universidade Nova de Lisboa. Animals were kept under temperature and humidity control (21 ± 1 °C; $55 \pm 10\%$ humidity) with a 12-h light/dark cycle. Two groups of control animals that fed a standard diet (14.5% protein, 10% fat, 55.1% carbohydrates; RM3, Special Diet Services, Witham, Essex, UK) were used: a group that drank water and a second group that drank water with metformin (200 mg/kg) for 3 weeks (Fig. 22.1). At the end of 3 weeks on metformin treatment, animals were anesthetized with sodium pentobarbital (60 mg/kg) and tracheostomized, and the carotid arteries were dissected past the carotid bifurcation. At the end of the procedure, animals were killed by intracardiac overdose of sodium pentobarbital.



Electrophysiology CSN recordings protocol:

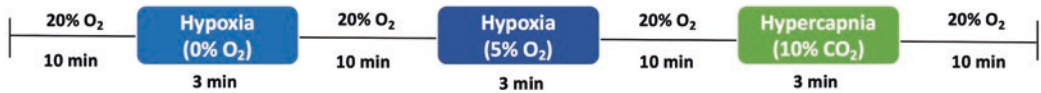


Fig. 22.1 Schematic illustration of the protocol of the study

22.2.3 CSN Electrophysiological Recordings

Extracellular recording from a single (or a few) fiber of CSN was performed using a suction electrode, as previously described by Conde et al. (2012). The pipette potential was amplified (Neurolog Digimiter, Hertfordshire, UK), filtered with low pass (5 kHz) and high pass (10 Hz) filters, digitized at 5 kHz (Axonscope, Axon Instruments, Molecular Devices, Workingham, UK), and stored on a computer. CSN chemosensory activity was identified (spontaneous generation of action potentials at irregular intervals) and confirmed by its increase in response to hypoxia (0% O₂ equilibrated with 5% CO₂ and N₂). CSN unit activity was converted to logic pulses, which were summed every second and converted to a voltage proportional to the sum. The effect of chronic metformin consumption on CSN activity was investigated while perfusing the preparations with normoxic (20% O₂ equilibrated with 5% CO₂ and N₂), hypoxia (0% and 5% O₂ equilibrated with 5% CO₂ and N₂), and hypercapnic (10% CO₂ equilibrated with 20% O₂ and N₂) solutions (Fig. 22.1).

22.2.4 Statistical Analysis

Data was evaluated using Prism version 9 (GraphPad Software Inc., La Jolla, CA, USA) and was presented as mean \pm SEM. The significance of the differences between the mean values

was calculated by Student's *t* test and two-way ANOVA with Bonferroni's multicomparison test. Differences were considered significant at $p < 0.05$.

22.3 Results

Figure 22.2 shows the impact of metformin, an antidiabetic drug used for the treatment of T2D, administered for 3 weeks, on spontaneous and hypoxic and hypercapnic-evoked CSN chemosensory activity in control animals. Typical recordings of CSN chemosensory activity in basal conditions and in response to intense hypoxia (0% O₂) and hypercapnia (10% CO₂) are illustrated in Fig. 22.2a. Chronic metformin administration for 3 weeks did not modify mean basal CSN chemosensory activity in control animals (control = 2.03 ± 0.33 impulses/s; control + metformin = 1.89 ± 0.42 impulses/s) (Fig. 22.2b).

Figure 22.2a, c depict the effect of metformin administration on CSN activity in response to different stimulus in control animals. To correct the CSN activity in response to hypoxia and hypercapnia, the CSN chemosensory activity was expressed as times over basal. Chronic metformin administration for 3 weeks did not alter the CSN response to intense (N₂) and moderate (5% O₂) hypoxia (Fig. 22.2c). Moreover, the increase in the CSN activity evoked by hypercapnia (10% O₂) is not modified by chronic metformin administration for 3 weeks (Fig. 22.2c).

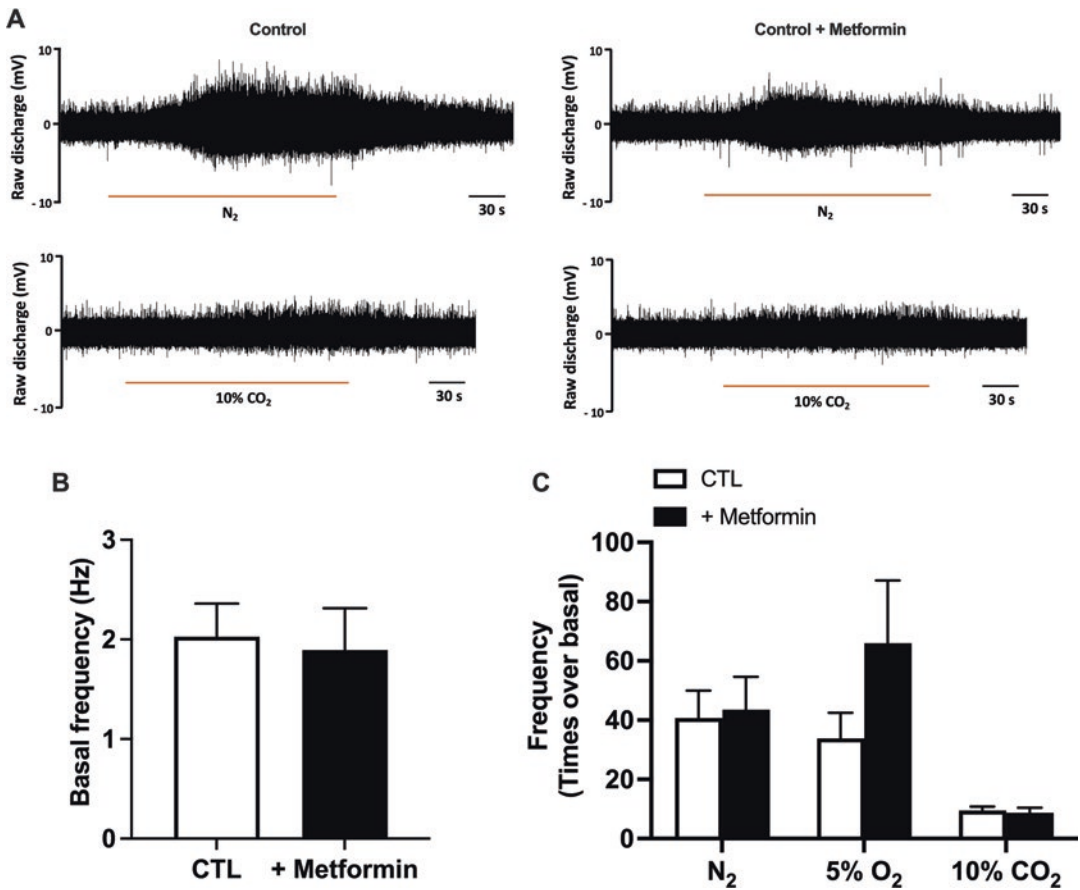


Fig. 22.2 Effect of chronic metformin administration on basal and carotid sinus nerve (CSN) chemosensory activity elicited by hypoxia and hypercapnia in control animals. (a) Typical recordings of the effect of chronic metformin administration on the frequency of action potentials of CSN during superfusion with hypoxia (N₂) (above panel) and hypercapnia (10% CO₂) (below panel). (b) Effect of chronic metformin administration on CSN

basal activity. (c) Effect of chronic metformin administration on CSN activity in response to intense (N₂) and moderate (5% O₂) hypoxia and hypercapnia (10% CO₂). Metformin (200 mg/kg) was administered in the drinking water for 3 weeks. Normoxic and hypoxic solutions were equilibrated with 5% CO₂ and N₂. Hypercapnic solution was equilibrated with 20% O₂ and N₂. Data represent means ± SEM

22.4 Discussion

The present study demonstrates that chronic administration of metformin, a biguanide used as an antidiabetic drug, did not modify basal CSN chemosensory activity and the CSN chemosensory response to intense and moderate hypoxia and to hypercapnia.

Metformin has been widely used as a first-line therapy for the treatment of T2D. The concentration of metformin tested in the present work (200 mg/kg) has been used in several animal studies, being effective in normalizing glucose

homeostasis and insulin sensitivity in animals submitted to hypercaloric diets (Yasmin et al. 2021). Several mechanisms of action have been proposed for metformin, with one being the activation of AMPK (Rena et al. 2017). In the CB, AMPK was initially pointed as being involved in the response to hypoxia. Wyatt and collaborators (2007) described that CSN basal discharge was increased by 5-aminoimidazole-4-carboxamide riboside (AICAR), an activator of AMPK, being this effect diminished with the application of an AMPK antagonist, the compound C. Moreover, AMPK inhibition with compound C attenuated

the CSN chemosensory activity elicited by hypoxia (Wyatt et al. 2007). However, contrasting with these results, in the present study, chronic metformin administration did not change CSN basal chemosensory activity and the CSN frequency of discharge in response to hypoxia and hypercapnia. The discrepancy in the results may be related with off-target effects of the drugs, AICAR and compound C, that have been used in the previous studies (Evans et al. 2005; Wyatt et al. 2007, 2008) and/or acute vs. chronic effect of AMPK activation/metformin consumption. In fact, our results are in agreement with recent studies performed in mice with conditional deletion of the AMPK in catecholaminergic cells (Mahmoud et al. 2016; MacMillan et al. 2022). In these recent studies, *ex vivo* recordings of the CSN showed that basal CSN electrical activity and chemosensory CSN response to hypoxia and hypercapnia were not altered in mice with conditional deletion of AMPK in catecholaminergic cells, suggesting that AMPK in CB type I cells is not necessary for CB activation by hypoxia or hypercapnia (Mahmoud et al. 2016; MacMillan et al. 2022), this being in line with the results obtained herein.

In conclusion, chronic metformin administration did not affect basal and hypoxia and hypercapnia-evoked CSN chemosensory activity, suggesting that the action of metformin on the CB does not contribute to its action as antidiabetic drug. However, herein we only tested a control/healthy state, and therefore the action of chronic metformin in the CB of dysmetabolic animals remains to be established.

Acknowledgments This work was funded with a grant from the Portuguese Foundation for Science and Technology (FCT) with the reference EXPL/MED-NEU/0733/2021. JFS is supported by a contract from FCT with the reference CEEC IND/02428/2018.

References

Caballero-Eraso C, Shin MK, Pho H et al (2019) Leptin acts in the carotid bodies to increase minute ventilation during wakefulness and sleep and augment the hypoxic ventilatory response. *J Physiol* 597:151–172

- Conde SV, Monteiro EC, Rigual R et al (2012) Hypoxic intensity: a determinant for the contribution of ATP and adenosine to the genesis of carotid body chemosensory activity. *J Appl Physiol* (1985) 112:2002–2010
- Cracchiolo M, Sacramento JF, Mazzoni A et al (2019) Decoding neural metabolic markers from the carotid sinus nerve in a type 2 diabetes model. *IEEE Trans Neural Syst Rehabil Eng* 27:2034–2043
- Cunha-Guimaraes JP, Guarino MP, Timóteo AT et al (2020) Carotid body chemosensitivity: early biomarker of dysmetabolism in humans. *Eur J Endocrinol* 182:549–557
- Entezari M, Hashemi D, Taheriazam A et al (2022) AMPK signaling in diabetes mellitus, insulin resistance and diabetic complications: a pre-clinical and clinical investigation. *Biomed Pharmacother* 146:112563
- Evans AM, Mustard KJW, Wyatt CN et al (2005) Does AMP-activated protein kinase couple inhibition of mitochondrial oxidative phosphorylation by hypoxia to calcium signaling in O₂-sensing cells? *J Biol Chem* 280:41504–41511
- Hawley SA, Gadalla AE, Olsen GS, Grahame Hardie D (2002) The antidiabetic drug metformin activates the AMP-activated protein kinase cascade via an adenine nucleotide-independent mechanism. *Diabetes* 51:2420–2425
- Inzucchi SE, Bergenstal RM, Buse JB et al (2015) Management of hyperglycemia in type 2 diabetes, 2015: a patient-centered approach: update to a position statement of the American Diabetes Association and the European Association for the study of diabetes. *Diabetes Care* 38:140–149
- MacMillan S, Holmes AP, Dallas ML et al (2022) LKB1 is the gatekeeper of carotid body chemosensing and the hypoxic ventilatory response. *Commun Biol* 5:1–15
- Mahmoud AD, Lewis S, Juričić L et al (2016) AMP-activated protein kinase deficiency blocks the hypoxic ventilatory response and thus precipitates hypoventilation and apnea. *Am J Respir Crit Care Med* 193:1032–1043
- McIntyre HD, Paterson CA, Ma A et al (1991) Metformin increases insulin sensitivity and basal glucose clearance in type 2 (non-insulin dependent) diabetes mellitus. *Aust NZ J Med* 21:714–719
- Owen MR, Doran E, Halestrap AP (2000) Evidence that metformin exerts its anti-diabetic effects through inhibition of complex I of the mitochondrial respiratory chain. *Biochem J* 348:607
- Pauza AG, Thakkar P, Tasic T et al (2022) GLP1R attenuates sympathetic response to high glucose via carotid body inhibition. *Circ Res* 130:694–707
- Rena G, Hardie DG, Pearson ER (2017) The mechanisms of action of metformin. *Diabetologia* 60:1577
- Ribeiro MJ, Sacramento JF, Gonzalez C et al (2013) Carotid body denervation prevents the development of insulin resistance and hypertension induced by hypercaloric diets. *Diabetes* 62:2905–2916
- Ribeiro MJ, Sacramento JF, Gallego-Martin T et al (2018) High fat diet blunts the effects of leptin on ventilation and on carotid body activity. *J Physiol* 596:3187–3199

- Sacramento JF, Ribeiro MJ, Rodrigues T et al (2017) Functional abolition of carotid body activity restores insulin action and glucose homeostasis in rats: key roles for visceral adipose tissue and the liver. *Diabetologia* 60:158–168
- Sacramento JF, Chew DJ, Melo BF et al (2018) Bioelectronic modulation of carotid sinus nerve activity in the rat: a potential therapeutic approach for type 2 diabetes. *Diabetologia* 61:700–710
- Shaw RJ, Lamia KA, Vasquez D et al (2005) The kinase LKB1 mediates glucose homeostasis in liver and therapeutic effects of metformin. *Science* 310:1642–1646
- Wyatt CN, Mustard KJ, Pearson SA et al (2007) AMP-activated protein kinase mediates carotid body excitation by hypoxia. *J Biol Chem* 282:8092–8098
- Wyatt CN, Pearson SA, Kumar P et al (2008) Key roles for AMP-activated protein kinase in the function of the carotid body? *Adv Exp Med Biol* 605:63–68
- Yasmin T, Rahman MM, Khan F et al (2021) Metformin treatment reverses high fat diet- induced non-alcoholic fatty liver diseases and dyslipidemia by stimulating multiple antioxidant and anti-inflammatory pathways. *Biochem Biophys Rep* 28:101168
- Zhou G, Myers R, Li Y et al (2001) Role of AMP-activated protein kinase in mechanism of metformin action. *J Clin Invest* 108:1167

Concluding Remarks

Rodrigo Iturriaga  and Rodrigo Del Rio 

It is a pleasure for us to write the concluding remarks for the ISAC XXI entitled “Arterial Chemoreceptors – Mal(adaptive) Responses: O₂ Dependent and Independent Mechanisms” held at Nova Medical School, Universidade Nova de Lisboa, Portugal, from June 27 to 30, 2022, and hosted by Profs Silvia V. Conde and Emilia Monteiro. The meeting in the beautiful, cultural, and historic city of Lisbon was a reunion of colleagues and friends after struggling with the worldwide COVID-19 pandemic. The meeting allows senior and young researcher working in the field of arterial chemoreceptors to share new and exciting discoveries and concepts in the field of chemoreception.

The ISAC XXI meeting was organized around the topic “Mal(adaptive) Responses of Peripheral Chemoreceptors: O₂ Dependent and Independent Mechanisms.” The conference included plenary lectures, oral communications, and scientific poster sessions. We would like to highlight that during the welcome session, ISAC recognized the pioneer and continuous contribution to the carotid body physiology of Dr. Robert Fitzgerald

(1932–2022, Baltimore, USA) and Dr. Chris Peers (1963–2018, Leeds, UK).

The chapters included in the present ISAC proceedings book are the result of the contribution of several groups from different laboratories around the world including the work performed by Paton and colleagues from Auckland, New Zealand; Pardal and colleagues from Sevilla, Spain; Machado from Riberao Preto, Brasil; Pimpao and colleagues from Lisbon, Portugal; Marulo and O’Halloran from Cork, Ireland; Castillo-Galan and Iturriaga from Santiago, Chile; Gagnon and Kinkead from Laval, Canada; Valverde and Perez Olea from Valladolid, Spain; Maxwell and O’Halloran from Cork, Ireland; Valverde, Perez Olea, and Rocher from Valladolid, Spain; Bravo and colleagues from Santiago, Chile; Pereyra and colleagues from Santiago, Chile; Cabral and colleagues from Lisbon, Portugal; Schwarz and Del Rio from Santiago, Chile; Sacramento and colleagues from Lisbon, Portugal; Capucho and Conde from Lisbon, Portugal; Moreno, Colinas-Miranda, and Lopez-Barneo from Sevilla, Spain; Evans from

R. Iturriaga
Facultad de Ciencias Biológicas, Pontificia
Universidad Católica de Chile, Santiago, Chile

Centro de Investigación en Fisiología y Medicina de
Altura (FIMEDALT), Facultad de Ciencias de la
Salud, Universidad de Antofagasta,
Antofagasta, Chile

R. Del Rio
Department de Physiology, Pontificia Universidad
Católica de Chile, Santiago, Chile

Centro de Excelencia en Biomedicina de Magallanes
(CEBIMA), Universidad de Magallanes,
Punta Arenas, Chile

Edinburg, UK; Aldossary and Holmes from Birmingham, UK; Leonard and Nurse from Hamilton, Canada; and Diaz-Jara and colleagues from Santiago, Chile.

It is worth to mention and emphasize the participation of numerous young undergraduate students, PhD students, and postdoctoral trainees in the ISAC XXI meeting. As usual in the ISAC meeting, the Heymans-De Castro-Neil prizes for outstanding young researchers in the field were awarded. Selection committee included Profs. Ana Obeso (Valladolid, Spain), Camilo Di Giulio (Chieti, Italy), and Ken O'Halloran (Cork, Ireland). The awardees for the Heymans-De Castro-Neil outstanding research were Adriana Capucho (Portugal), Aoife Slyne (Ireland), and António Pimpão (Portugal). In addition, the Best Poster Presentation Award went to Audrys G. Pauza (UK/New Zealand). The Machiko Shirahata Travel Grants to PhD and postdoc students were selected by Estelle Gauda (Baltimore, USA) and were awarded to Pratik Thakkar (New Zealand), Marianne Gagnon (Canada), Demitris Nathanael (UK), Katherin Pereyra (Chile), Agnieszka Swiderska (UK), and Igor Felipe (New Zealand). Also, a new award was included at this meeting, the ISAC Pipeline Award for

undergraduate student, which highlights the contribution of outstanding undergraduate students to the field of carotid body research and encourages them to continue to perform research in this field. This time, Liena Bravo (Chile) was awarded with ISAC Pipeline Award. We would like to thank the panels for their commitment with these activities and all the young scientists who participated in the meeting. Undoubtedly, this is quite important for the future development of the chemoreceptor field in health and disease.

Finally, during the ISAC business meeting, participants showed their most grateful appreciation for Dr. Silvia Conde and Dr. Emilia Monteiro as former President of ISAC and approved the name of Dr. Rodrigo Del Rio to take leadership of the society for the 2023–2025 period. Dr. Del Rio makes a brief presentation to highlight and propose Chile as the next future venue for the ISAC 2025 meeting. All participants approved Chilean Patagonia to held ISAC 2025.

As the new organizing committee, we would like to kindly invite all of you to the next ISAC 2025 and to continue to encourage young scientist to get involved in ISAC activities.

We deeply expect to see you all back in Chile!